Developmental abnormalities associated with the hypopigmented retina

Marc Samuel Tibber, B.Sc.

Supervisor; Dr. Glen Jeffery

Submitted for the degree of Doctor of Philosophy, 2004

Institute of Ophthalmology

University College London

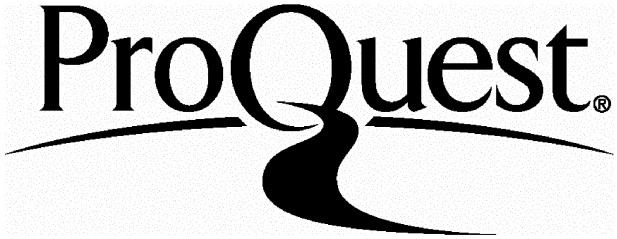


INSTITUTE OF OPHTHALMOLOGY
LIBRARY

Abstract

The albino visual system is characterised by a range of abnormalities including a severe rod deficit, an underdevelopment of the central retina and a misprojection of a portion of the temporal ganglion cells. During development of the retina levels of proliferation and apoptosis are elevated, and the maturational gradient is delayed.

There is evidence from *in vitro* studies to suggest that L-DOPA, a precursor in both the melanin and catecholamine synthesis pathways, is able to regulate these abnormal patterns of cell proliferation in a manner which is consistent with its role in the regulation of retinal development.

The aims of this thesis were; (1) to further characterise the developmental abnormalities associated with albinism, (2) to examine the effects of L-DOPA on patterns of cell division and neurogenesis within an *in vivo* context, and (3) to determine the mechanisms by which L-DOPA mediates its effects. Using both *in vivo* and *in vitro* methods, patterns of cell division and retinal differentiation were examined in pigmented and albino rat tissue.

Results demonstrate that coincidental with abnormal levels of proliferation, the early postnatal albino retina is characterised by; a thickening of the neuroblastic layer, an excess of cells in the cell cycle, defects in the distribution of cleavage orientations within the apical-basal plane and elevations in gap junction expression. Furthermore, the vast majority of these parameters could be regulated by the introduction of L-DOPA to the retina and -preliminary experiments would suggest- through the addition of dopamine.

These findings are consistent with a model in which reduced levels of L-DOPA in the albino retina lead to spatiotemporal defects in patterns of cell division, potentially as a result of secondary consequences on concentrations of retinal dopamine.

List of Figures

Abbreviations used

Cdk	Cyclin dependent kinase;
CdkI	Cyclin dependent kinase inhibitor
DA	Dopamine
D.A.	Dark Agouti
DCC	DOPA decarboxylase
DHICA	5,6-Dihydroxylindole-2-Carboxylic acid
DIC	Differential interference contrast
DMSO	Dimethyl sulphoxide
DOPA	Dihydroxyphenylalanine
E*(n)*	Embryonic day n
EF	Electric field
GCL	Ganglion cell layer
HPLC	High performance liquid chromatography
INL	Inner nuclear layer
IPL	Inner plexiform layer
KS-test	Kolmogorov Smirnov test
LE	Lens epithelium
NBL/NBR	Neuroblastic layer / retina
NGF	Nerve growth factor
OA	Ocular albinism
OCA	Oculocutaneous albinism
ONL	Outer nuclear layer
OPL	Outer plexiform layer
P	Postnatal day
PBS	Phosphate buffer saline
PCD	Programmed cell death
pINL	Presumptive inner nuclear layer
RPE	Retinal pigment epithelium
TH	Tyrosine hydroxylase
VM	Ventricular margin
VZ	Ventricular zone

Declaration

I declare that this thesis, submitted for the degree of Doctor of Philosophy, is of my own composition, and the data presented herein is my own original work, unless otherwise stated.

A list of collaborations, with details of experiments undertaken by/in conjunction with others is provided on the following page.

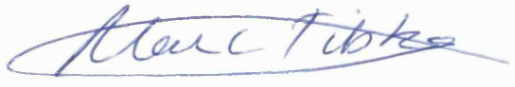

Marc Samuel Tibber, B.Sc.

List of collaborations

(1) Tissue preparation and cell-counts/retinal measurements for the historesin study were undertaken in conjunction with Rachel Peasley, BSc student, chapter 1.

(2) Tissue was prepared for electron microscopy by Peter Munro, (chapter 5).

(3) Connexin-43 labelling of retinal sections was performed by David Becker, (chapters 5 and 7).

(4) The study of cleavage orientations within the plane of the avian retina was undertaken in conjunction with Janet Savage, BSc student, (chapter 6).

(3) All live-imaging of retinal tissue was undertaken by Ines Kralj-Hans, (chapter 7).

Dedicated to my parents....

"I have yet to see any problem, however complicated, which, when you looked at it in the right way, did not become still more complicated."

Poul Anderson

" Clouds are not spheres, mountains are not cones, coastlines are not circles, and bark is not smooth, nor does lightning travel in a straight line."

Benoit Mandelbrot

Acknowledgements

I would like to thank Glen Jeffery, my supervisor, for providing constant supervision throughout all stages of the project, in addition to inspiring giggles and tears of frustration in nearly equal proportions. Thanks to Lynda Erskine for technical advice unequalled by any; Juliet Parry for answering a ceaseless barrage of questions and Jim Bowmaker for providing the jovial face of academia.

I am equally grateful to the following people for their collaboration and technical assistance; David Becker, Ines Kralj-Hans, Peter Mobbs and Peter Munro, as well as Wendy and Nicki from the BRU and Claire from administration. I would also like to express my gratitude to Fight for Sight for funding the research and providing me with this opportunity.

I am especially grateful to Alan Whitmore and Juliet Dukes, though to pin down in which field they have been of help would be to do them an injustice. I am indebted to them for both technical assistance and excessive discussion (of a varied nature), as well as endless personal support. Similarly, I am grateful to Tony Halfyard, David Malkin and Jay Sangha, without whom the institute would have been a much less colourful place.

Finally, I'd like to thank my family, which though small, is incredibly supportive and comparatively devoid of the usual dysfunctions. Thanks especially to my cousin Andrew for putting up with me over the last year, and to my parents, to whom this thesis is dedicated, and to whom I cannot even begin to express the extent of my gratitude.

Abbreviations used

Cdk	Cyclin dependent kinase;
CdkI	Cyclin dependent kinase inhibitor
DA	Dopamine
D.A.	Dark Agouti
DCC	DOPA decarboxylase
DHICA	5,6-Dihydroxylindole-2-Carboxylic acid
DIC	Differential interference contrast
DMSO	Dimethyl sulphoxide
DOPA	Dihydroxyphenylalanine
E*(n)*	Embryonic day n
EF	Electric field
GCL	Ganglion cell layer
HPLC	High performance liquid chromatography
INL	Inner nuclear layer
IPL	Inner plexiform layer
KS-test	Kolmogorov Smirnov test
LE	Lens epithelium
NBL	Neuroblastic layer
NGF	Nerve growth factor
OA	Ocular albinism
OCA	Oculocutaneous albinism
ONL	Outer nuclear layer
OPL	Outer plexiform layer
P	Postnatal day
PBS	Phosphate buffer saline
PCD	Programmed cell death
pINL	Presumptive inner nuclear layer
RPE	Retinal pigment epithelium
TH	Tyrosine hydroxylase
VM	Ventricular margin
VZ	Ventricular zone

Chapter 1:
General introduction

1.1 Early phases of vertebrate optic development

The vertebrate eye primordium is derived from a secondary bulge of the diencephalic neural tube which branches out laterally and grows towards the non-neural surface ectoderm. The distal end of the outgrowth (the optic vesicle) invaginates to form a bi-layered optic cup. Contact with the surface ectoderm induces the development of the lens placode, a localised thickening of the tissue which pinches off from the surface and transforms into the lens (Chow and Lang, 2001). The proximal region of the optic vesicle constricts to form the optic stalk, along which the axons of the ganglion cells will eventually grow and develop into the retinofugal projections of the adult visual system. Vascular mesenchyme grows through the optic fissure, a regional deficiency of the inferior optic cup, and gives rise to the hyaloid artery. Providing temporary nourishment to the lens, the hyaloid artery regresses postnatally. The sclera, choroid and ocular muscles are formed from a condensation of the surrounding mesenchyme, whilst the cornea is generated from the surface ectoderm and cells of the neural crest under the inductive influence of the lens and optic cup. See Barishak (1992) for a comprehensive review.

1.2 Development of the retina

Retinal histogenesis involves a transition from an undifferentiated layer of stem cells to a highly organised and stratified tissue (see Figure 1.2.1). The entire

process can be divided into three distinct though over-lapping phases; (1) proliferation, during which the retina thickens and the cell population expands; (2) differentiation, during which cells exit the cell cycle, migrate to the appropriate layer and adopt a specific identity; (3) cell death and synaptogenesis, during which the circuitry of the retina is established and refined; see Young (1983) for a comprehensive review. Each stage progresses in a crude centre-to-periphery gradient of development, such that at any time-point the central retina is developmentally more mature than the periphery, (see Polley *et al.* (1989)). The one exception to this paradigm however is the retinal pigment epithelium (RPE). The RPE cell is the only cell type in the retina which follows a periphery-to-centre gradient of development.

Cell proliferation

As development progresses both surfaces of the optic cup become closely coupled and the remnant of the neural tube lumen collapses. The outer (medial) surface of the cup is composed of 2-3 layers of columnar cells and will form the retinal pigment epithelium (RPE). The inner (lateral) surface thickens through multiple rounds of replication and forms the prospective neural retina. During cell proliferation, retinal progenitors undergo a stereotypical pattern of cell migration back and forth through the depth of the neuroblastic layer (NBL) known as interkinetic nuclear migration (INM) (Young, 1983). This movement reflects the cell's progression through the various phases of the cell cycle, and is thought to play a critical role in regulating the pace of neurogenesis (Murciano *et al.*, 2002). Cell division (M-phase) occurs at the outer surface of the NBL (the ventricular margin (VM)), whilst DNA replication (S-phase) occurs at the innermost stratum of the NBL. In between these two phases cells migrate from the outer to the inner surface of the NBL and vice versa, intervals known as G1- and G2- phase respectively, (see Figure 1.2.2). These represent the cell cycle checkpoints during which a complex series of interacting signals mediate cell cycle progression, arrest and/or exit. At the heart of this regulatory system are the cyclin dependent kinase (Cdk) proteins and their activating subunits, the

cyclins, which together phosphorylate and thereby regulate a wide range of target proteins (Galderisi *et al.*, 2003).

The number of cells finally generated within the retina is dependent on a multitude of parameters of cell division. The rate of cell cycle progression, the number of mitotic cycles a progenitor completes before undergoing terminal differentiation, as well as the nature of the division (i.e. proliferative vs. differentiative; symmetric vs. asymmetric) all play a role in defining final cell numbers. Hence, the diversity of factors which influence patterns of cell proliferation in the developing retina is great. Of particular significance however are the growth factors (Baker and Yu, 2001), cyclin-dependent kinase inhibitors (Dyer and Cepko, 2000; Dyer and Cepko, 2001a), neurotransmitters (Pearson *et al.*, 2002) and transcription factors, (Estivill-Torrus *et al.*, 2002). See Dyer and Cepko (Dyer and Cepko, 2001b) for a review.

Cell birth and differentiation

As development continues, there is a gradual transition from a period of proliferation to one of differentiation, reflected in a progressive decrease in the proportion of cycling cells (Alexiades and Cepko, 1996). When a cell exits the cell cycle (a state known as G0-phase), it migrates to the layer that is appropriate for its prospective fate and undergoes terminal differentiation. However, studies have shown that cell cycle exit and cell differentiation are not synonymous. Thus, whilst ganglion cells differentiate immediately upon exiting the cell cycle (Waid and McLoon, 1995), there is a considerable delay between the two events with respect to rod photoreceptor genesis (Ezzeddine *et al.*, 1997).

Tritiated thymidine labelling studies indicate that retinal cells are generated in a stereotypic sequence, so that a strong correlation exists between the day on which a cell exits the cell cycle and the ultimate fate it will adopt (see Figure 1.2.3 and Cepko *et al.* (1996)). Though there is considerable divergence between species in the precise order of cell type generation, several

fundamental rules have been conserved across the phylogeny. Thus, in all species studied to date, the ganglion cell and bipolar cell are the first and last cells respectively to be generated. (See Cepko (1993) for discussion). The relationship between the birth date of a cell and its eventual fate has been explored experimentally by advancing and delaying cell cycle exit through the misexpression of cell cycle regulatory proteins in the Xenopus retina (Ohnuma *et al.*, 2002). Results indicate that factors which promote early cell cycle exit enhance the activity of those which promote an early cell fate.

In the mammalian retina there are two overlapping waves of neurogenesis. During the first (peaking at ~E14) cone photoreceptors, horizontal cells, amacrine cells and ganglion cells are born. The second phase of cell production (peaking at ~P0) gives rise to the Müller glia and bipolar cells. Rod photoreceptor generation spans the entire period of retinal histogenesis, but reaches a maximum on the day of birth (Carter-Dawson and LaVail, 1979). Waves of differentiation are initiated in the central retina and progress towards the periphery. In addition, there is a crude inner-to-outer pattern of layer establishment. These sequential waves of development running through the tissue axes overlap so that gradients exist with respect to distinct retinal layers and cell types. The phases of proliferation and differentiation overlap, so that mitotic and post-mitotic cells co-exist both spatially and temporally. Consequently, changes in the extra-cellular environment are insufficient to account for the sequential generation of distinct cell types. The regulation of cell fate is mediated through a complex interplay between local environmental signals and epigenetic factors.

The regulation of cell fate

Clonal analyses demonstrate that retinal progenitors are multipotential. Even during the later phases of cell generation individual cell clones may contain multiple cell types (Turner and Cepko, 1987; Wetts and Fraser, 1988; Turner *et al.*, 1990). However, over time, retinal progenitors undergo a progressive restriction of competence so that towards the end of development cell clones

give rise to a narrower spectrum of cell types (Turner *et al.*, 1990). Subsets of progenitors may be biased towards the generation of specific cell classes. Thus, in the rat, a distinct group of retinal progenitors exhibit a prejudice towards the production of amacrine and horizontal cells as well as a correlated expression pattern of early identity markers associated with these fates (Alexiades and Cepko, 1997).

These studies point to the existence of an intrinsic cell program. However, local environmental signals also play an essential role in cell fate specification. One extremely sophisticated experiment using a disaggregated retinal cell culture system highlights this interaction beautifully. When E15 and P1 rat cells were cultured separately, the latter began to express opsin antigens several days earlier than the former, reflecting the normal developmental time-course found *in vivo.* However, when embryonic cells were cultured in an excess of postnatal cells, whilst the time-course of opsin expression remained the same, the number of rod photoreceptors generated was significantly elevated (Watanabe and Raff, 1990). Thus, although E15 cells exhibited intrinsic differences to those found later during development, the presence of postnatal cells was conducive to the late born cell fate. Conversely, the presence of early embryonic cells was found to inhibit the adoption of a late born cell fate (Belliveau *et al.*, 2000). These studies emphasise the significance of cell-cell interactions and/or diffusible signals in cell fate determination.

A model of retinal progenitor division thus emerges in which progressive changes in an intrinsic program alter a cell's competence to respond to a signal-rich environment which is it self dynamic, (see Edlund and Jessell (1999) for a review). This is reflected in a stage-specific expression pattern of genes that are part of a complex genetic hierarchy. Thus, stem cells, progenitor cells and even cells within distinct retinal laminae exhibit a specific and distinct pattern of neurogenic and proneural gene expression (Perron *et al.*, 1998). Furthermore, misexpression and knock-out studies of these genes, many of which encode transcription factors with a wide range of downstream targets, result in changes in the relative proportion of distinct cell types, reflecting their role in cell fate specification. Thus overexpression of *Hes1* (a bHLH transcription factor) in the

mouse retina using a recombinant retrovirus resulted in an increase in Müller cell numbers (Furukawa *et al.*, 2000; Hojo *et al.*, 2000). In addition, cell-cell interactions have been shown to regulate the expression of these genes, further reenforcing the intricate relationship between intrinsic and extrinsic cell fate determinant mechanisms. (See Edlund and Jessell (1999) for a review). Below are listed some of the fundamental mechanisms of cell fate specification in the retina.

1. *Auto-regulation*

Several cell types of the vertebrate retina have been shown to regulate their own population density through the release of a signal which inhibits further generation of their own cell type. Thus, toxicological ablation of retinal ganglion cells in the developing chick retina led to a consequential repopulation of the ganglion cell layer (GCL) during a phase of cell generation in which ganglion cells are not normally born (Gonzalez-Hoyuela *et al.*, 2001). A candidate signalling molecule in this response is nerve growth factor (NGF). Exclusively expressed by the RGC's, NGF was able to reverse the effects of RGC ablation upon exogenous application. Similarly, addition of dopamine (DA) (which is produced by a subset of tyrosine hydroxylase-positive (TH+) amacrine cells *in vivo*) to dissociated cell cultures from the E11 chick retina led to a 55% reduction in the number of TH+ cells (Guimaraes *et al.*, 2001).

2. *Cell cycle/cell fate coordination*

The cell cycle has been linked to cell fate determination in two distinct though potentially linked ways. First, early cell cycle exit is conducive to the adoption of an early cell fate. This has been shown experimentally by inducing early cell cycle exit through the misexpression of $p27^{Xic1}$ (a Cdk inhibitor; CdkI) in the *Xenopus* retina, resulting in an increase in RGC numbers (Ohnuma *et al.*, 2002). In addition, a number of cell cycle regulators have been shown to influence cell fate directly. Thus, whilst $p57^{Kip2}$ (a CdkI) is upregulated in a subset of retinal cells exiting the cell cycle, $p57^{Kip2}$ deficient mice show changes in amacrine cell population levels, (Dyer and Cepko 2000). Similarly, in addition

to inhibiting cell proliferation, $p27^{Xic1}$ induces Müller cell differentiation as determined by over-expression studies in the *Xenopus* retina (Ohnuma *et al.*, 1999). Interestingly, the molecular domain of $p27^{Xic1}$ responsible for its gliogenic function is located at the N-terminus, and is distinct from the moeity that interacts with the CdK system of cell cycle control.

3. Lateral inhibition

Cell-cell contact is also known to affect cell fate through a process known as lateral inhibition. A highly studied example of this system is the *Notch/Delta* signalling pathway. Activation of Notch (a transmembrane receptor) by Delta (its membrane-associated ligand) has been implicated in a wide range of cell fate decision processes. Thus misexpression of Notch or one of its downstream targets led to an increase in Müller cell numbers in the postnatal rodent retina (Furukawa *et al.*, 2000), and a decrease in ganglion cell numbers in the early embryonic retina (Austin *et al.*, 1995). Similarly, retroviral infection of chick neural crest cells with a constitutively active form of the Notch intracellular domain lead to an up-regulation of glia markers in the dorsal root ganglia (DRG) (Morrison *et al.*, 2000).

4. Asymmetric division

Asymmetric division is a process by which distinct cell fate potentials are assigned to the daughter cells of a mitotic division. In the invertebrate nervous system, this is at least partially mediated through the asymmetric localisation of cell fate determinants within the cell membrane, and a coordinated re-alignment of the mitotic spindle, such that there is an asymmetric pattern of protein inheritance between the two daughter cells. This system has been shown to interact with the *Notch/delta* system of lateral inhibition. Thus Numb, a membrane-associated cytoplasmic protein, antagonises *Notch/delta* signalling (Spana and Doe, 1996), and has been shown to localise asymmetrically within a range of developing tissues. Disruption of this process results in abnormalities in cell fate determination, and more specifically, a reduction in the diversity of

cell types generated (Uemura *et al.*, 1989; Rhyu *et al.*, 1994; Spana and Doe, 1996; Buescher *et al.*, 1998).

Recent studies of the developing vertebrate nervous system have shown that progenitor cells divide with a range of cleavage orientations relative to tissue axes (Chenn and McConnell, 1995; Kornack and Rakic, 1995; Cayouette *et al.*, 2001; Estivill-Torrus *et al.*, 2002; Silva *et al.*, 2002; Cayouette and Raff, 2003; Das *et al.*, 2003). Furthermore, asymmetric localisation patterns of Numb and Notch have been reported (Chenn and McConnell, 1995; Kornack and Rakic, 1995; Zhong *et al.*, 1996; Wakamatsu *et al.*, 1999; Cayouette *et al.*, 2001; Estivill-Torrus *et al.*, 2002; Silva *et al.*, 2002; Cayouette and Raff, 2003; Das *et al.*, 2003). This raises the possibility that a similar mechanism of asymmetric division plays a role in regulating cell fate within the vertebrate nervous system. However, current debate over its putative role in the vertebrate retina is both unresolved and highly controversial (Cayouette *et al.*, 2001; Silva *et al.*, 2002; Cayouette and Raff, 2003; Das *et al.*, 2003; Tibber *et al.*, 2004).

Cell death and synaptogenesis

Programmed cell death (PCD) is an essential developmental mechanism by which cell numbers and tissue size are regulated. In the post-natal rat retina ~50% of cells in the inner nuclear layer (INL) and GCL degenerate. Cell death in the ONL is much lower; only 4% of photoreceptors are lost during an equivalent period (Voyvodic *et al.*, 1995). The process of PCD is under complex regulatory control; each cell possessing an intrinsic program of cell death which may be triggered or blocked by a range of factors including extracellular matrix proteins, trophic factors, neurotransmitters and growth factors. Other important factors include levels of cAMP and target tissue availability; see (Linden, 2000) for a review.

In the rodent retina, the vast majority of cell death occurs during the post-natal period. However, the temporal progression of cell death is cell-type specific (see Figure 1.2.3). Thus, two waves of cell death occur in the GCL, the first involving

a degeneration of the ganglion cells, and the second corresponding to the death of displaced amacrine cells. The peak in cell death occurs at ~P2 with respect to the ganglion cell population, ~P7 in the amacrine population and ~P10 in the bipolar population (Horsburgh and Sefton, 1987). Amacrine and bipolar synapses do not differentiate until ~P11 and ~P13 respectively so that synaptogenesis occurs after the peak in cell death. This would suggest that in the rodent retina survival of these two cell types is largely independent of their post-synaptic targets. This can also be demonstrated by optic nerve transection in the neonatal rat; the cells of the INL are relatively unaffected despite the rapid degeneration of the GCL (Beazley *et al.*, 1987). In support of this physiological divide in the response patterns of distinct cell types ganglion cell death and target refinement are temporally coincidental in the rodent (Jeffery, 1984). A study of the ferret retina however highlights the existence of phylogenetic variation with respect to this paradigm; severance of the ferret optic nerve results in increased cell death within the GCL, INL as well as the NBL (Cusato *et al.*, 2001).

Schematic diagram of the adult retinal structure in cross-section

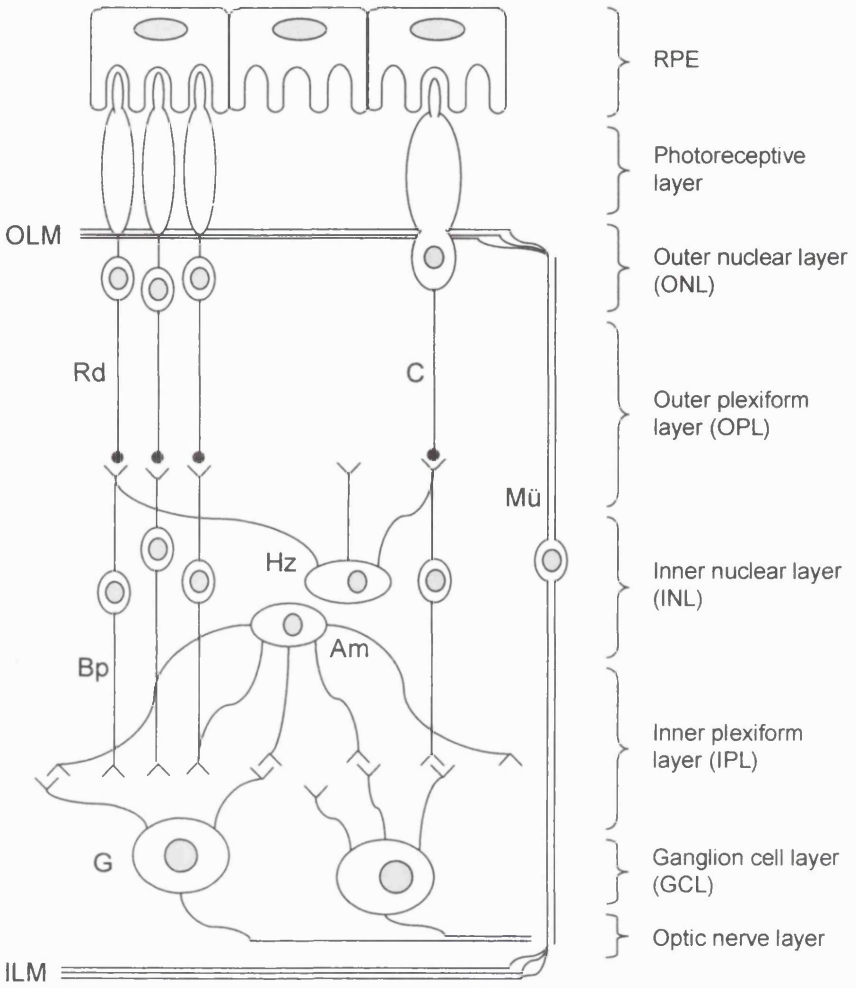

Figure 1.2.1 The adult vertebrate retina is a highly specialised, stratified tissue with distinct nuclear and plexiform layers. Light is absorbed by the outer segments of the rods (Rd) and cones (c) of the photoreceptive layer, the cell bodies of which lie in the outer nuclear layer (ONL). The signal is then transduced to the ganglion cells of the ganglion cell layer (GCL) via bipolar cell interneurones (Bp) which sit in the inner nuclear layer (INL). The retinofugal projections of the eye are mediated by ganglion cells axons which exit the eyeball at the optic nerve head and project to various visual areas/nuclei of the brain. In between the three nerve cell layers lie the outer plexiform layer (OPL) and inner plexiform (IPL), which constitute the sites of synaptic connectivity between the various retinal neurones. In addition, the retina is host to two further types of neurone; the horizontal cell (Hz) and amacrine cell (Am), which mediate horizontal signal transmission within the retina. Müller cells (Mü) are the radial glia of the retinae. They have multiple functions including the regulation of extracellular ionic balance, and contribute to the formation of the outer limiting membrane (OLM) and inner limiting membrane (ILM). The RPE is involved in the turnover of photoreceptor outer segments and absorption of light.

The mitotic cell cycle and interkinetic nuclear migration

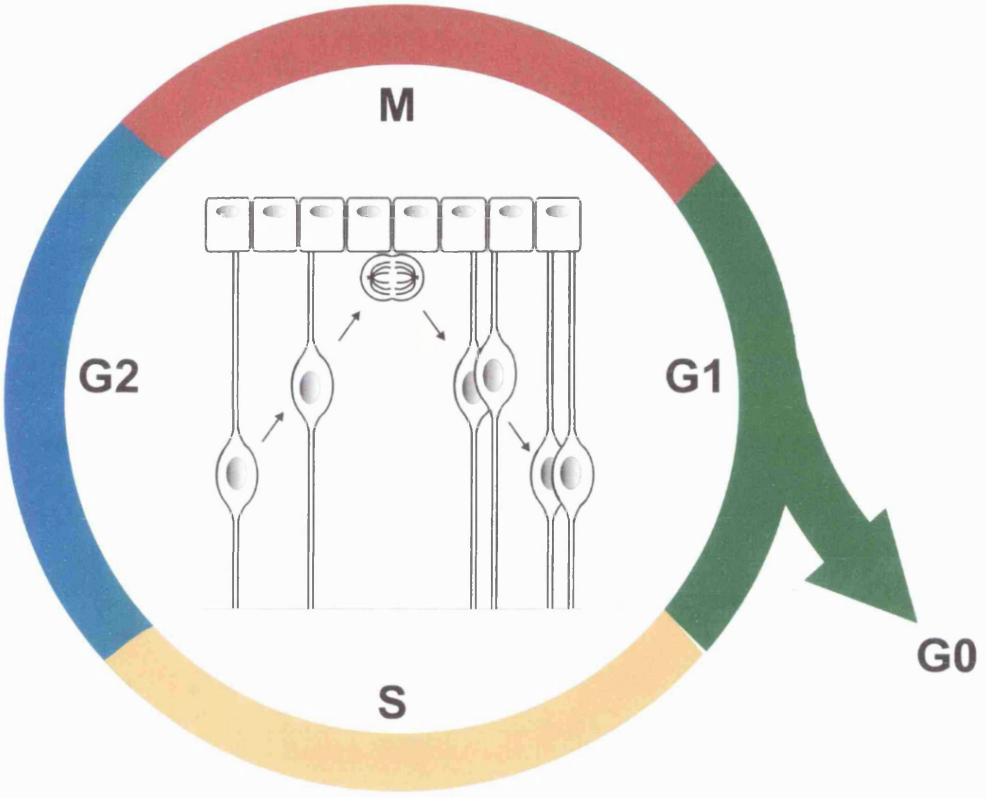

Figure 1.2.2 The early phases of retinal histogenesis are characterised by a stage of prolific cell division during which the cell population rapidly increases in size. Cells undergo division through the mitotic cell cycle, which can be broken down into 4 composite phases. Cells replicate their DNA during S-phase at the innermost stratum of the NBL. They then migrate radially through the depth of NBL during G2-phase, and actively divide (cytokinesis) at the VM during M-phase. If the cell remains proliferative it will subsequently migrate back to the inner limit of the NBL and reenter S-phase anew. Alternatively, the cell may exit the cell cycle (G0-phase) and migrate to the appropriate layer according to its fate where it will undergo terminal differentiation. Thus, retinal progenitors undergo a stereotyped pattern of cell migration back and forth through the depth of the neuroblastic layer (NBL) known as interkinetic nuclear migration (INM), which reflects their progression through the phases of the cell cycle. During G1-, G2- and S-phase, cells in the cell cycle retain processes which span the entire depth of the NBL. These are then retracted during M-phase, although an isolated study has claimed that to the contrary, the basal process persists throughout M-phase (Das *et al.*, 2003).

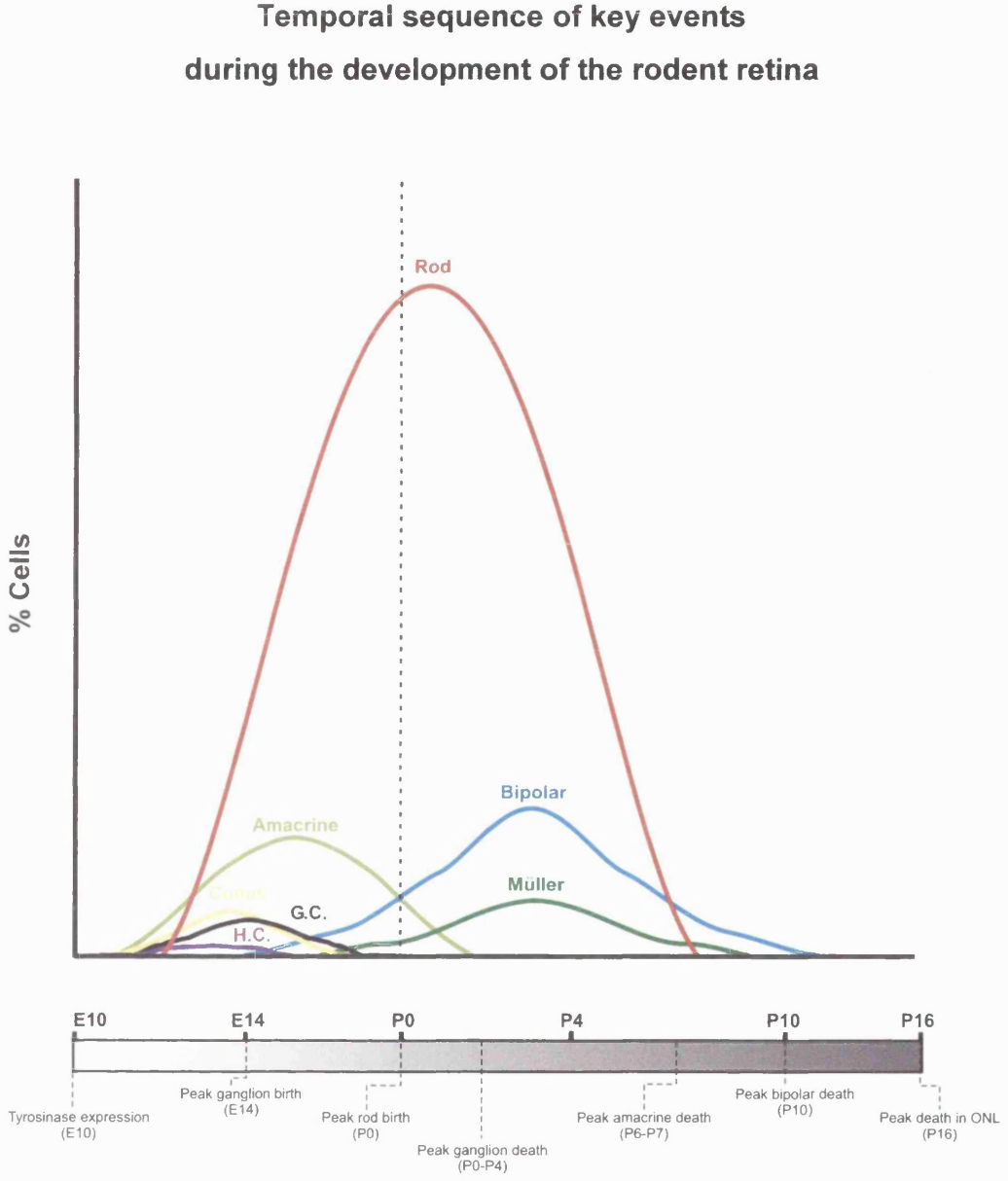

Figure 1.2.3 The successive generation of distinct cell types of the retina follows a highly conserved temporal sequence. There are two main waves of cell generation. The first -which peaks around E14-E15- gives rise to the ganglion (G.C.), horizontal (H.C.) and amacrine cell populations. The second -peaking postnatally- gives rise to the bipolar and Müller cell populations. Rod photoreceptor generation spans the entire period of retinal neurogenesis, peaking around the day of birth. Levels of apoptosis in each cell type population follow a similar temporal sequence in the postnatal retina. Though slight differences exist in the relative timing of developmental events between different rodent species, all data provided in the figure is from the rat or the mouse, which differ by ~24 hours with respect to their gestation periods. The figure has been adapted from Cepko *et al.* (1996). In addition, data has been taken from Horsburgh and Sefton (1987) and Gimenez *et al.* (2003).

The role of the RPE in regulating development

The differentiation of the RPE largely precedes that of the neural retina (Barishak 1992) and has been shown to mediate essential regulatory control over the formation of the neural retina. The RPE is essential for the correct structural organisation of the photoreceptors and outer limiting membrane (Pinzon-Duarte *et al.*, 2000), the regulation of opsin protein expression levels (Jablonski *et al.*, 2000), the formation of photoreceptor outer segments (Caffe *et al.*, 1989), as well as apical localisation of cell division and retinal lamination (Jensen *et al.*, 2001). In addition, genetic ablation experiments in mice have shown that in the absence of the RPE, the entire eye fails to develop (Raymond and Jackson, 1995).

The major pathway for communication between the RPE and neural retina is mediated via a dense network of gap junctions (Becker *et al.*, 1998; Janssen-Bienhold *et al.*, 1998; Pearson *et al.*, 2004a). Formed from two connexon hemi-channels, one contributed by each cell, the gap junction couples tissues both electrically and metabolically, allowing the passage of small molecules up to ~1kDalton in size (Alberts *et al.*, 1994). See Becker *et al.* (1998) for a review of gap junction function in the retina. Transitory gap junctions have been demonstrated between retinal neuroblasts and cells of the RPE during development, presenting a pathway for the transfer of signalling molecules which may influence the cell cycle and/or cell fate (Hayes, 1976; Hayes, 1977). Upon blocking gap junction communication in the chick retina using an antisense gel specific to connexin-43, levels of proliferation in the NBL fell significantly (Becker and Mobbs, 1999). In addition, recent studies would suggest that connexin hemi-channels may exist in the RPE during development, providing a pathway by which chemicals can be released into the subretinal space (Pearson *et al.*, 2004b).

In vitro studies using RPE-conditioned media would suggest that the RPE releases a variety of soluble factors involved in the regulation of retinal development, though very few have been characterised to date (Tombran-Tink *et al.*, 1991; Jablonski *et al.*, 2000; Mitchell, 2001). Recent interest in the field has focused on the role of neurotransmitters (Mitchell, 2001; Pearson *et al.*, 2002; Kubrusly *et al.*, 2003) and calcium transients (Pearson *et al.*, 2004a), and the role they play in the regulation of cell cycle progression in the retina.

1.3 Albinism

Background

Albinism refers to a group of genetic disorders characterised by a disruption of the melanin pigmentation system. Albinism affects approximately 1 in 10,000 humans within Western Europe. The disorder is divided into two distinct forms on the basis of phenotypic similarities rather than common causes. Oculocutaneous albinism (OCA) is characterised by hypopigmentation of the eyes, skin and hair; in ocular albinism (OA) the pigmentation deficit is limited to the eyes alone (Spencer, 1985). In addition to a predisposition to skin carcinomas, albinos suffer from reduced visual acuity and in severe cases, photophobia. Despite the many different forms of albinism all are characterised by abnormalities in visual system development, suggesting a direct regulatory role for melanin or one of its metabolites, as opposed to distinct pleiotropic effects of key genes (Kinnear *et al.*, 1985; King and Summers, 1988).

Melanosome differentiation and melanin synthesis

Both cutaneous and ocular melanin is synthesised in a specialised cell called the melanocyte. Those of the skin, hair and iris are of neural crest origin. The melanocytes of the RPE however are derived from the outer lip of the optic cup, and are thus of neural tube origin. Melanin synthesis takes place within a highly

specialised intra-cellular organelle called the melanosome, which is actively transferred to keratinocytes within the skin, but retained within the cell body of melanocytes in the eye. Despite these differences, melanin synthesis and the differentiation of the melanosome is believed to follow a similar pathway within the RPE and non-ocular melanocytes. As a result, much of our knowledge of these processes has been extrapolated from the study of skin melanocytes.

The melanosome follows a stereotypic differentiation pathway which is reflected in four distinct phases of developmental maturity. The stage I melanosome is a simple intracellular vacuole resembling the endoplasmic reticulum, from which it is derived. In stage II, tyrosinase and associated enzymes involved in the biosynthesis of melanin are transported from the golgi complex to the melanosome (Jimbow *et al.*, 2000). The organelle now exhibits an organised internal structure. During stage III melanin is formed, and by stage IV, pigment deposition is so dense that the internal structure of the melanosome is obscured in a light or electron micrograph.

The enzyme responsible for the rate limiting step in the melanin synthesis pathway is tyrosinase. Possessing two copper-binding sub-units tyrosinase catalyses the hydroxylation of tyrosine into L-DOPA and subsequent oxidation of L-DOPA into DOPA quinone (see Figure 1.3.1). At this stage the synthesis pathway bifurcates, corresponding to the synthesis of two distinct forms of melanin. Eumelanin, which is black/brown in colour, is formed from the metabolites of DOPAchrome, whilst the pheomelanins, which are red/yellow, are derived from the metabolites of 5-S-cysteinylDOPA. The later stages of eumelanin synthesis depend on further enzymatic catalysis by 5,6-dihydroxylindole-2-carboxylic acid (DHICA) oxidase (tyrosinase-related protein1) and Dopachrome tautomerase (tyrosinase-related protein 2).

The melanin biosynthesis pathway

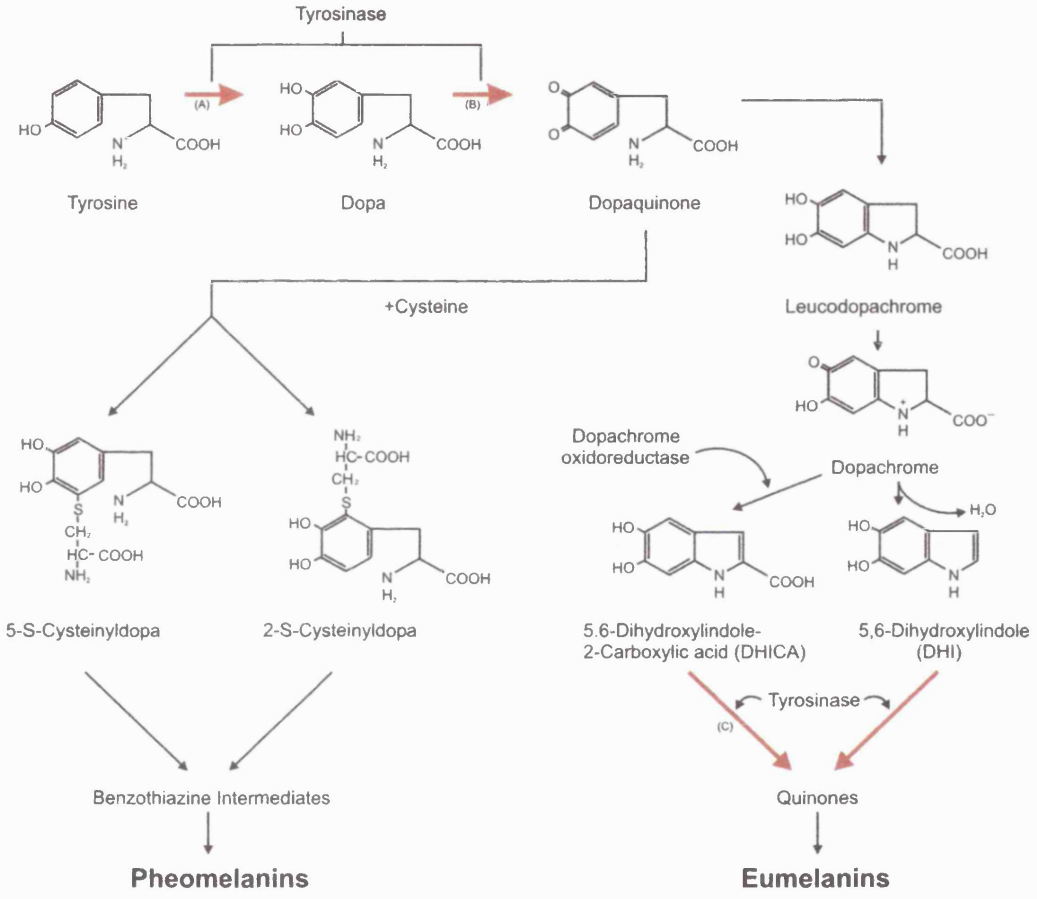

Figure 1.3.1 The rate limiting step in the biosynthesis of eumelanin and pheomelanin involves the oxidation of tyrosine into DOPA and the latter's subsequent conversion into Dopaquinone under the catalytic effects of tyrosinase. Tyrosinase acts at a third point in the pathway, specific to the production of eumelanin. Stages of the pathway which are catalysed by tyrosinase are indicated by red arrows. Tyrosinase is a membrane-bound glycosylated enzyme which uses DOPA as a co-factor and has two copper-binding subunits. Though many of the chemical intermediates in the pathway have been characterised, the precise molecular structure of the melanins are unknown. Eumelanins are black/brown in colour, whilst the pheomelanins are red/yellow. The figure has been adapted from King and Summers (1988).

Subtypes of albinism

Twelve different loci in the human genome have been shown to underlie the multiple forms of albinism documented to date (see Table 1.1). These encode a diverse array of proteins involved in the melanin synthesis pathway, ranging from tyrosinase itself to melanosomal protein transporters and ionic pumps. In addition, multiple syndromes associated with hypopigmentation have been described. Listed below are some of the more common forms of albinism. See the following references for comprehensive reviews; Kinnear *et al.* (1985), King *et al.* (1988), King and Summers (1988).

1. Oculocutaneous albinism

Oculocutaneous albinism is an X-linked autosomal recessive condition that is characterised by reduced levels of pigmentation in the eyes, skin and hair. This group of conditions can be further divided into OCA1 and OCA2, reflecting distinct implicated loci. Localised to chromosome 11 in the human, OCA1 is caused by mutations of the gene encoding tyrosinase (Oetting, 2000; Oetting *et al.*, 2003). OCA1 can itself be further subdivided into OCA1A and OCA1B reflecting mutations that lead to an inactive form of tyrosinase (a null mutation) or a form of tyrosinase with reduced activity (a leaky mutation) respectively. OCA2 is the most common form of OCA and is caused by mutations of the P gene which encodes a melanosomal transmembrane receptor. The precise function of the p-protein has not yet been determined, although several studies have implicated its role as an ion transporter necessary for the regulation of pH levels (Brilliant, 2001).

1. Ocular albinism

Ocular albinism (OA) is characterised by normal to slightly reduced levels of skin pigmentation and a varying degree of ocular hypopigmentation as a function of genetic/racial background. OA can be subdivided into an X-linked

form (OA1), and an autosomal recessive form. The target gene underlying the X-linked form has been mapped, though its function is unclear. Its potential role in melanosome maturation has been suggested however, as OA1 melanosomes are typically enlarged, a feature of premelanosomes that fail to segregate from the endoplasmic reticulum (Oetting, 2002). Of those diagnosed with autorecessive OA, 50% have been found to harbour mutations at the *TYR* or *P* locus. The remaining 50% harbour as yet unidentified mutations (Hasanee and Ahmed, 2001).

Gene	*Protein encoded*	*Function*	*Phenotype*
TYR	Tyrosinase	Oxidation of tyrosine	OCA1
P gene	P protein	pH regulation*	OCA2
TYRP1	Tyrosine related protein 1	DHICA oxidation	OCA3
MATP	Membrane-associated transporter protein	Protein transporter	OCA4
HPS1-HPS6	Membrane-associated protein*	Regulation of organelle biogenesis and size	HPS
CHS1	Cytosolic protein	Vesicular trafficking	CHS
OA1	G-protein coupled receptor	Melanosome maturation*	OA (X-linked)

Table1.3.1 Genes associated with albinism in humans. The primary genes which when mutated lead to distinct forms of albinism are shown above along with the proteins encoded, their predicted functions and associated diseases. As can be seen from the nature of the proteins encoded, albinism can be caused by a direct disruption of the enzymatic conversion of precursors into melanin, or through mutations that disrupt the structure/environment of the melanosome. *Denotes entries for which data is inconclusive. **OCA** = oculocutaneous albinism, **OA** = ocular albinism, **DHICA** = 5,6-Dihydroxylindole-2-Carboxylic acid, **HPS** = Hermansky-Pudlak syndrome, **CHS** = Chediak-Higashi syndrome. Data have been gathered and adapted from Oetting *et al.* (2003) and the albinism database of the international albinism centre (Oetting and Bennett, 2004).

The hypopigmented visual system

Albinos commonly suffer from congenital visual impairment. Iris translucency and a high level of back-scatter as a result of fundus hypopigmentation both contribute to a generalised reduction in visual acuity and in extreme cases photophobia. This is often accentuated by the effects of horizontal nystagmus (an involuntary wandering of the eyes in the horizontal plane), strabismus (squint), as well as a range of anatomical defects associated with the architecture of the retina and defects in the pattern of retinofugal projections (Kinnear *et al.*, 1985; King *et al.*, 1988).

The albino retina is characterised by abnormalities in specific cell populations that are not limited to a single temporal window with respect to their generation. Thus, rod photoreceptors (one of the last cell types to be born in the retina) are reduced by approximately 25-30% in the albino relative to age-matched pigmented controls. In the albino ferret this was detected as a reduction in both rod photoreceptor densities (Jeffery *et al.*, 1994) and ONL thickness, (Jeffery and Kinsella, 1992). Reduced rod counts have also been reported in the albino mouse with a concurrent reduction in rhodopsin levels (Donatien and Jeffery, 2002). Similarly, abnormally low levels of rhodopsin were reported in the early post-natal albino rat (Grant *et al.*, 2001).

An isolated study of the adult hypopigmented cat and rodent retina would suggest that a sub-population of amacrine cells, which are born during the earlier phase of cell production, is also affected in the hypopigmented retina. Thus a higher density of cholinergic amacrine cells were detected within the INL and GCL of the albino retina relative to pigmented controls (Mitrofanis and Stone, 1988).

The ganglion cell, the first to leave the cell cycle, is also severely affected in the albino retina. In the mammal there is a gradient of cell density which reaches its peak in a central retinal specialisation associated with high acuity diurnal vision; the *area centralis* or visual streak (Provis *et al.*, 1998). In the hypopigmented cat

this region is abnormal, with a reduced ganglion cell density, a shift in the distribution of ganglion cell sizes, as well as a disruption of the normal blood vessel patterning (Stone *et al.*, 1978). Similarly, within the central retina of the albino rabbit and ferret, the peak ganglion cell density is significantly reduced (Jeffery and Kinsella, 1992; Donatien *et al.*, 2002).

In the simian primates and many species of fish, reptile and bird the central retina reaches a higher order of specialisation. Known as the *foveola*, the region represents the peak in cone photoreceptor density and is uniquely characterised by the displacement of ganglion cell bodies. In the human and subhuman albino primate this region fails to form completely (Elschnig, 1913; Guillery *et al.*, 1984). There is some debate in the literature as to whether the surrounding (perifoveal) vasculature is abnormal in the human albino retina (Gregor, 1978; Spedick and Beauchamp, 1986).

Albinos exhibit chiasmatic and geniculate abnormalities associated with a misprojection of ganglion fibres from the temporal retina. In a normally pigmented animal, the size of the ipsilateral projection is roughly correlated with the extent to which the eyes are forwards-facing and hence the size of the binocular visual field. This gives rise to a naso-temporal division in the retina with respect to the origin of ipsilaterally and contralaterally projecting ganglion cells, although complete spatial segregation of the two populations would appear to be unique to the primates (Jeffery, 2001).

In the albino, the naso-temporal division is shifted towards the temporal retina such that there is a reduced ipsilateral projection; a feature which has been demonstrated using anatomical, electrophysiological and functional imaging techniques. This pattern would appear to be true of all mammalian albinos studied to date, including the human (Creel *et al.*, 1978; Morland *et al.*, 2002), rat (Chan *et al.*, 1993), mouse (LaVail *et al.*, 1978), cat (Ault *et al.*, 1995) and ferret (Morgan *et al.*, 1987). The size of the misprojection is roughly correlated to the level of pigmentation in the RPE (LaVail *et al.*, 1978; Balkema and Drager, 1990; Rice *et al.*, 1999). As a result of the abnormal decussation patterns there may also be secondary effects on the organisation of the striate

cortex and higher cortical areas (Ault *et al.*, 1995; Hoffmann *et al.*, 2003). See Guillery (Guillery, 1986) for a discussion of patterns of cortical reorganisation as a consequence of abnormal decussation patterns.

In view of the wide variety of cell-type specific defects that have been described in the albino retina (outlined above), secondary repercussions on patterns of retinal circuitry and synapse formation remain to be addressed. An isolated study of neurotransmitter levels in the adult pigmented and albino rat retina highlights the existence of subtle perturbation in the ratio of GABA to glutamate in the albino (Blaszczyk *et al.*, 2004). It is likely, that with future studies of this kind, and developments in cellular and molecular biology techniques, the list of abnormalities associated with the albino visual system will continue to grow.

Albinism across the phylogeny

Several reports suggest that the abnormalities associated with the albino visual system are unique to the mammal, although studies of hypopigmentation in lower vertebrates are scarce. Anterograde labelling of the axolotl retinofugal pathway highlighted no differences between the contribution of ipsilateral and contralateral projections in pigmented and albino animals (Guillery and Updyke, 1976). Similarly, histological analysis of pigmented and albino budgerigar retinae highlighted no differences with respect to layer thickness, cell density or cell size between the phenotypes (Jeffery and Williams, 1994), and the rhodopsin content of pigmented and albino *Xenopus* frog retinae did not differ (Grant *et al.*, 2001). Although the reason for this phylogenetic divide remains unclear, an interesting possibility was raised by histological examination of the squirrel retina, one of the few cone-dominated mammals. In the albino squirrel, the ganglion cell deficit of the central retina was greatly reduced (Esteve and Jeffery, 1998), raising the possibility that rod-dominated and cone-dominated retinae differ fundamentally with respect to patterns of development.

Developmental abnormalities of the albino visual system

Recent studies suggest that visual system anomalies in the albino are retinal-based in origin, and a direct consequence of a disruption of the pigmentation pathway, as opposed to the pleiotropic effects of key genes. Evidence to support this comes from the fact that visual deficits are common to all albinos irrespective of the genetic basis of their condition, (see table 1.3.1). Even the misprojection of retinal axons at the optic chiasm can be traced back to patterns of cell production in the developing neuroblastic retina (Cronin *et al.*, 2003). When mice retinal axons were cultured on chiasm explants, they exhibited no differential growth as a function of the pigmentation type of their source (Marcus *et al.*, 1996). Thus, in the albino, a sub-set of ganglion cells in the temporal retina adopt an inappropriate identity, as opposed to midline cells of the albino and pigmented chiasm being inherently different.

The developing albino retina is characterised by an excessive level of proliferation, and/or an extension of the proliferative phase. This has been demonstrated both *in vivo* and *in vitro* in the rat (Ilia and Jeffery, 1999; Webster and Rowe, 1991), as well as in histological sections of the developing albino mouse retina (Donatien and Jeffery, 2002). Maximum differences were found to occur around the day of birth/during the early post-natal period and were coincidental with a transient thickening of the albino retina, as well as elevations in levels of cell death (Ilia and Jeffery, 1999). This led the authors to speculate that abnormally high levels of mitosis in the albino retina may lead to tissue hypoxia and a subsequent wave of excessive cell death, thus accounting for the rod photoreceptor deficit. In support of this theory, exposing newborn mice to hyperoxic conditions for 24 hours had a differential effect on cell death within the two pigmentation types, reducing levels of apoptosis by ~60% and 80%, in the pigmented and albino retina respectively (Semo *et al.*, 2001).

In a separate study of the albino mouse, elevated levels of retinal proliferation (relative to pigmented controls) were detected in the temporal periphery at E11-E12; a window of development corresponding to the early phase of ganglion cell generation (Rachel *et al.*, 2002). This pattern may have been overlooked in the

rat however, as data were pooled from temporal and nasal sections. In addition, the earliest phase of development studied in the rat was E12, so that subtle differences in developmental timing between the mouse and rat retina could explain the discrepancy (Ilia and Jeffery, 1999). Thus, there are two phases of development during which levels of proliferation are perturbed; ~E11 and ~P0. These temporal windows coincide with the generation of ganglion cells and rod photoreceptors, the two primary cell types which are affected in the albino. The precise mechanisms by which abnormalities during development are translated into the stereotypic deficits associated with the adult cell populations of the retina are unclear.

The albino retina is also characterised by a delay in the centre-to-periphery gradient of development. This was first demonstrated in the hypopigmented rat, in which the processes of OPL and inner plexiform layer (IPL) formation as well as the onset of apoptosis were delayed by approximately 30 hours in the albino relative to pigmented controls (Webster and Rowe, 1991). Using tritiated thymidine-labelling, a similar delay was detected in the formation of all three nuclear layers of the albino rat retina relative to the pigmented (Ilia and Jeffery, 1996; Ilia and Jeffery, 2000). This delay was also detected in patterns of retinal proliferation (Ilia and Jeffery, 1999).

The regulatory role of melanin and its metabolites

It is has been clearly demonstrated that the visual deficits associated with albinism are a direct manifestation of a disruption in the melanin synthesis pathway. Thus, introduction of a functional tyrosinase gene into an albino mouse and rabbit retina lead to a complete phenotypic rescue with respect to the ganglion cell and rod photoreceptor deficits (Jeffery *et al.*, 1997). However, it is unclear whether the developmental defects reported in the albino retina are a direct manifestation of reduced levels of melanin in the RPE, or one of its metabolites/precursors. Traditional hypothesis have tended to favour the former. The discovery that melanin may function as a calcium buffer (an ion heavily implicated in the control of developmental processes) and has strong

antioxidant properties leant credence to this view (Drager, 1985; Drager and Balkema, 1987; Salceda and Sanchez-Chavez, 2000).

Recent studies suggest that L-DOPA, a precursor in both the melanin and catecholamine synthesis pathways, may mediate critical regulatory control over a range of developmental processes. L-DOPA is formed by the oxidation of tyrosine (see Figure 1.3.1), a reaction which is primarily catalysed by tyrosinase in the melanocytes and tyrosine hydroxylase (TH) within neural tissues, and is generated at reduced levels in the albino eye and skin (Gaudin and Fellman, 1967; Ilia and Jeffery, 1999). Recent evidence has come to light that tyrosinase-mediated tyrosine oxidation in the RPE may provide a source of L-DOPA for catecholamine synthesis in the neural retina (Kubrusly *et al.*, 2003). The authors became interested in the possibility upon discovery that D_1-receptors (activated by dopamine (DA)) and DOPA decarboxylase (DDC; the second enzyme in the catecholamine synthesis pathway) were expressed in the neural retina prior to TH expression (Lankford *et al.*, 1988; Gardino *et al.*, 1993; Kubrusly *et al.*, 2003).

Incubation of retinal segments in L-DOPA led to an accumulation of DA and an increase in cyclic AMP (cAMP) levels, (a measure of dopaminergic stimulation via D_1-like DA receptors). Furthermore, exposure of retinal segments to RPE-conditioned media triggered a 3-fold increase in the rate of cAMP accumulation (Kubrusly *et al.*, 2003). This raises the possibility that the production of L-DOPA in the RPE during the early phases of development may provide a key substrate source for catecholamine synthesis, as well as the initial step in the generation of melanin. Further evidence to support this possibility arose from studies of peripheral DA levels in TH null mice on pigmented and albino backgrounds. In the E15 pups, levels of DA were reduced in the albino TH null mice, but were relatively unaffected in the pigmented transgenics, suggesting the existence of a secondary tyrosinase-mediated source of L-DOPA in the peripheral nervous system (Eisenhofer *et al.*, 2003).

There is also a growing body of evidence to suggest that L-DOPA has endogenous neurotransmitter/neuromodulatory properties, which are

independent of its conversion to DA (Misu *et al.*, 2002). In support of this hypothesis, several nuclei of the rhombencephalon and mesencephalon produce L-DOPA as an end-product (Smeets and Gonzalez, 2000). In addition, L-DOPA has been directly implicated in cell cycle regulation. It has been used as an anti-tumour agent, arresting cell cycle progression selectively during S-phase (Wick, 1977; Akeo *et al.*, 1994). When added to the albino rat retina in culture, L-DOPA reduced levels of proliferation and apoptosis to a level comparable with age-matched pigmented controls (Ilia and Jeffery, 1999). L-DOPA has recently received attention in the field of glaucoma research. Transgenic mice exhibiting defects in the structure of Schlemm's canal (a drainage system of the anterior chamber) exhibited a more severe phenotype on a hypopigmented background than on a pigmented (Libby *et al.*, 2003). Furthermore, this differential response was eradicated when embryos and neonates were administered L-DOPA during the period of ocular development.

Finally, a recent study suggests that L-DOPA may be needed for the correct folding and stabilisation of the tyrosinase protein, without which it is susceptible to proteolytic degradation (Halaban *et al.*, 2001). These findings suggest that RPE-derived L-DOPA represents a critical regulator of visual system development, potentially independent of its conversion into other bioactive products. See Hornykiewicz (2002) for a comprehensive review of the history of research into the biological properties of L-DOPA.

Aims of the thesis

1. *To elucidate the nature of abnormalities in patterns of cell division, cell cycle control and neurogenesis in the albino retina.*

   Several studies have documented defects in patterns of proliferation, retinal maturation, cell localisation and cell cycle control in the developing albino retina. However, no single study has correlated all these parameters within a single albino model. Furthermore, recent progress in the understanding of vertebrate retinal development has highlighted other potential areas of relevance to the pathogenesis of albinism. Consequently, the orientation of cell division and the nature of RPE/NBR interactions were also examined in the albino retina.

2. *To characterise the effects of L-DOPA on patterns of retinal cell division and neurogenesis within an in vivo context.*

   Evidence from *in vitro* studies would suggest that exogenously applied L-DOPA is capable of regulating abnormal patterns of proliferation and apoptosis in the developing albino retina. However, data from an *in vivo* model is lacking. Consequently, a comprehensive series of studies into the effects of L-DOPA on critical parameters of division (identified from point 1 above) were undertaken in the newborn rat.

3. *To determine the mechanisms by which L-DOPA mediates its effects.*

   Finally, in an attempt to correlate the results generated whilst addressing points 1 and 2 above, an hypothesis as to the potential mechanisms by which L-DOPA mediates regulatory control over the processes of retinal development was explored. Recent studies of the chick retina have highlighted a putative link between the melanin and catecholamine biosynthesis pathways of the developing retina.

General methodology

Throughout the course of these studies a comparative approach was taken using a tyrosinase-negative rodent model of albinism, the Wistar rat, and a pigmented control, the Dark Agouti (D.A.). All experiments were focused on the second phase of cell generation, corresponding to the peak in rod photoreceptor birth.

The majority of studies to date that have addressed the development of the albino retina deal exclusively with the ganglion cell layer and associated chiasmatic abnormalities. Consequently, the rod photoreceptor deficit has been largely overlooked, despite the fact that it constitutes the single largest population of cells in the mammalian retina.

By focusing on the neonatal period, DOPA and its metabolites could be administered to pups directly as opposed to *in utero*, facilitating their delivery with a higher degree of accuracy with respect to dosage.

All use of animals was carried out in accordance with regulations defined by the Animals (Scientific Procedures) Act, 1986. Specific experimental methods and protocols will be dealt with at the start of each experimental chapter.

Chapter 2:
Cell proliferation and the cell cycle

2.1 Introduction

The albino retina is characterised by a range of developmental abnormalities that point to the existence of perturbations in the process of cell cycle regulation. Repeated studies have shown that mitotic levels are significantly elevated in the developing hypopigmented retina (Webster and Rowe, 1991; Ilia and Jeffery, 1999; Donatien and Jeffery, 2002; Gimenez *et al.*, 2004). Furthermore, studies of the YRT4 mouse (a tyrosinase transgenic exhibiting a regional distribution of pigmentation) have demonstrated the existence of localised regions of elevated proliferation which accurately map to patches of low pigmentation in the over-lying RPE (Gimenez *et al.*, 2004). In addition, by blocking melanin formation in cultured E10-11 mouse eyecups, an increase in the neuroblastic cell population was induced (Rachel *et al.*, 2002).

Delays in the processes of development have also been documented in the albino visual system. Thus, in a study of the rat retina, outer plexiform layer (OPL) formation, inner nuclear layer (INL) cell differentiation and patterns of cell death were all delayed in the albino retina by approximately 30 hours relative to the pigmented (Webster and Rowe, 1991). Similarly, thymidine studies of the developing albino rat retina highlighted the existence of a temporal lag in patterns of cell production (Ilia and Jeffery, 1996) and cell proliferation (Ilia and Jeffery, 1999). Finally, intraocular injections of an anterograde label in the Siamese cat highlighted the existence of a delay in the formation of the retinogeniculate pathway (Kliot and Shatz, 1985).

L-DOPA is a melanin precursor present at reduced concentrations in the developing albino retina (Ilia and Jeffery, 1999). When introduced into developing eyecup preparations *in* vitro, L-DOPA suppressed the abnormal proliferation to a level comparable with age-matched pigmented animals (Ilia and Jeffery, 1999). When added to dissociated RPE cells, L-DOPA arrested cell cycle progression during S-phase in a dose-dependent manner (Akeo *et al.*, 1994). In addition, it has been developed as an anti-tumour agent (Wick, 1977). Recent findings suggest that L-DOPA may have an endogenous role as a neurotransmitter in the CNS (Misu *et al.*, 2002). Furthermore, its generation in the RPE may provide a substrate for catecholamine synthesis in the neural retina prior to the expression of tyrosine hydroxylase (Kubrusly *et al.*, 2003).

These findings point to the existence of abnormalities in cell cycle progression and/or cell cycle exit in the developing albino retina. In view of the fact that L-DOPA is present at lower levels in the albino retina (Ilia and Jeffery, 1999), is generated at a reduced rate in hypopigmented skin (Gaudin and Fellman, 1967) and has been implicated in the regulation of cell cycle progression (Akeo *et al.*, 1994), L-DOPA represents a likely candidate molecule to mediate cell cycle regulation in the wildtype eye. In addition, L-DOPA may provide the critical link between defects in the melanin synthesis pathway and the developmental/anatomical abnormalities associated with albinism.

2.2 Experimental aims

Initial *in vivo* experiments were conducted to replicate previous studies, and determine whether abnormalities in patterns of cell generation could be detected in the chosen model of albinism; the Wistar rat. In addition to quantifying levels of proliferation using two different staining methods measurements were made to determine the relative thickness of the various cell layers.

Patterns of cell cycle exit were explored using antibodies against a marker of cells within the cell cycle (Ki67). The level of developmental maturity was then gauged using two distinct indices of tissue differentiation. First, the extent of OPL formation was analysed and expressed as a proportion of the total retinal length. Second, the frequency of horizontal cells per mm of retina was calculated.

The effects of L-DOPA on levels of proliferation and tissue differentiation were then assessed *in vivo*, its *in vitro* effects having been previously documented using both organotypic (Ilia and Jeffery, 1999) and single cell (Wick, 1980; Akeo *et al.*, 1994) culture methods.

2.3 Methods

Levels of proliferation

E18, P1 and P4 pigmented (D.A.) and albino (Wistar) rat litters were examined to determine patterns of proliferation over time. In addition, levels of mitosis were quantified in P4 albino rats following administration of L-DOPA or D-DOPA (a biologically inactive isoform). Six eyes (each from a different animal) were analysed per pigmentation type/developmental stage, (three for each method of data analysis; see below). Similarly, three L-DOPA and three D-DOPA-treated eyes were included in the analysis.

DOPA administration

P3.5 albino rats were administered subcutaneous injections of L-DOPA (Sigma) in conjunction with a decarboxylase inhibitor (carbidopa), or D-DOPA (Roche), at a concentration of 15μg per gram of body weight in phosphate buffer saline (PBS), (3mM). Eighteen hours later (~P4), the animals were killed and the tissue processed as described below.

Histology and immunohistochemistry

Following decapitation the eyes were removed, fixed in 4% formalin overnight at room temperature and cryoprotected in 20% sucrose. The cornea and lens were removed and the tissue bathed in a 2:1 mixture of 20% sucrose/OCT for 30 minutes. Eyecups were embedded in OCT and quickly frozen by submersion in dry ice. Twenty-micron sections were taken in the horizontal plane, transferred to poly-lysine coated glass slides (BDH Laboratory Supplies) and left to dry overnight. Slides were then stored at -20°C in a tightly sealed container with anhydrous calcium sulphate, (a desiccant).

On the day of staining slides were defrosted over a 2 hour period at room temperature, soaked in PBS for 60 seconds and left to dry. They were then perfused with proteinase K (6.6μg/ml in 10mM tris/1mM EDTA at pH7.6; Sigma) for 20 minutes at 4°C. The tissue was washed in PBS and post-fixed in pre-cooled 70% ethanol for 10 minutes at -20 °C. Epitopes were blocked in 10% goat serum with 1% Triton X-100 (Sigma). Slides were incubated overnight at 4°C in rabbit anti-γ-tubulin antibodies, (diluted 1:500 in 1% Triton /5% goat serum).

Primary antibodies were detected using the biotin-Streptavidin detection system which both amplifies the signal and reduces the signal to noise ratio by minimising the level of unspecific binding. Slides were incubated for 2 hours in a biotinylated goat anti-rabbit IgG antibody (1:100; Vector Laboratories), and subsequently for 1 hour in Streptavidin-Cy2 (1:100; Amersham Pharmacia Biotech). After a series of washes the tissue was counterstained with propidium iodide (5μg/ml in PBS; Sigma) to visualise the nuclei of dividing retinal progenitors. The slides were then washed in distilled water and coverslipped in Vectashield fluorescent mounting medium (Vector laboratories).

In parallel, slides were stained with an antibody against phosphohistine-H3, a marker of cells in late G2- and M-phase. Tissue was dissected, fixed, cryoprotected, embedded, stored and sectioned as described above. Tissue was blocked in 10% goat serum (Vector laboratories) with 1% Triton X-100 in

PBS, and incubated overnight at room temperature in rabbit anti-phosphohistone-H3 antibodies, (1:100; Upstate Technologies). After washing in PBS the slides were perfused for 2 hours in an Alexa 488nm goat anti-rabbit IgG, (1:200; Molecular Probes). The tissue was counterstained with propidium iodide and coverslipped in Vectashield fluorescent mounting medium.

Imaging and analysis

Serial sections of the eye exhibiting a clear C-shape morphology were examined using a Zeiss laser scanning confocal microscope (LSM 500). Multiple regions of interest (ROI's) were scanned from both central and peripheral locations and serial sections taken in the z-plane. Resulting sampled volumes had dimensions of 115x56x20μm in the x-, y- and z-planes respectively, with potential variation in the z-plane thickness. All cells passing through the central most slice within the z-plane were studied, and the number of mitotically active cells (i.e. in prophase, metaphase, anaphase or telophase) were counted. Mitotic cells were identified by the presence of associated centrosome pairs (positive for γ-tubulin) and condensed chromatin. Counts per unit length were then standardised per mm of retina. A minimum of 34 regions were sampled per time-point/pigmentation type.

In addition, a second mitotic index was calculated using tissue stained for phosphohistone-H3, a marker of actively dividing cells. Counts were made from digital fluorescent images taken using an upright Olympus light microscope with fluorescent unit attached to a Nikon digital camera DXM1200. Counts were made along the VM per 300μm of retina and standardised per mm. Thirty, sixty and sixty regions were sampled at E18, P1 and P4 respectively for each pigmentation type.

Statistical analyses were performed using SPSS 10.1 (SPSS Inc.). The single-sample Kolmogorov-Smirnov test confirmed that the data were normally distributed. Pair-wise independent sample t-tests were then used to make both inter- and intra-pigmentation type comparisons. *P* values quoted do not assume

equality of variance. Comparison of data between DOPA-treated retinae was undertaken using the ANOVA test with Tukey HSD *post hoc* analysis.

Cell cycle exit

Pigmented (D.A.) and albino (Wistar) P1 and P4 rat litters were analysed for patterns of Ki67 localisation. Three eyes (each from a different animal) were studied per time-point/pigmentation type.

Histology and immunohistochemistry

Heads were removed and fixed in 4% formalin for 3 hours at room temperature. The eyes were enucleated and the cornea and lens removed. Eyecups were left in fix for a further 3 hours, washed in PBS and cryoprotected in 20% sucrose overnight, and bathed in a 2:1 mixture of 20% sucrose/OCT for 30 minutes. Eyecups were embedded in OCT and quickly frozen by submersion in dry ice. Five micron sections were taken in the horizontal plane, transferred to poly-lysine coated glass slides and left to dry overnight. On the day of staining slides were defrosted over a 2 hour period, soaked in PBS for 60 seconds and left to dry.

The slides were heated in 0.01 M sodium citrate buffer (2.1g citric acid /1g sodium hydroxide in 1 litre of distilled water, adjusted to pH 6.0) in a pressure cooker for 5 minutes (timed from the point of steam release). After washing in PBS the tissue was blocked in 10% horse serum in PBS with 1% Triton X-100 for 90 minutes and incubated overnight at room temperature in mouse anti-Ki67 antibodies (1:100; Novocostra), washed in PBS and incubated for 2 hours in fluorescein horse anti-mouse (1:100; Vector laboratories). Tissue was then counterstained with propidium iodide and coverslipped in Vectashield fluorescent mounting medium.

Imaging and analysis

Fluorescent images were gathered using an upright Olympus light microscope with fluorescent unit attached to a Nikon digital camera DXM1200. Images were cropped in Photoshop 7.0.1 (Adobe) to a standardised size (100μmx100μm), creating a region of interest (ROI) that encompassed the ventricular zone (VZ) and a large portion of the NBR. These were then imported into ImageTool Version 3.0 (UTHSCSA), and analysed using a built-in count and tag function.

The percentage of cells that were (a) Ki67-positive and (b) Ki67-negative were calculated. These values represent the proportion of cells that were in the cell cycle (the proliferative or p-fraction) and the proportion that were post-mitotic (the quiescent or q-fraction) respectively. Twelve regions of interest of the afore-mentioned dimensions were analysed per pigmentation type/developmental stage. Data were gathered from both central and peripheral regions of the retina.

Statistical analyses were performed using SPSS 10.1 (SPSS Inc.). The KS-test confirmed that the data were normally distributed. Pair-wise independent samples t-tests were then used to make comparisons between retinal locations and between pigmentation types. Equality of variance was not assumed.

Retinal lamination and differentiation

Pigmented (D.A.) and albino (Wistar) P1 and P4 rat litters were examined for patterns of retinal differentiation. In addition, the study was extended to P4 albino retinae following administration of L-DOPA or PBS (a negative control). Shown in brackets are the number of eyes (each from a different animal) analysed from each experimental group; pigmented P1 (4), pigmented P4 (6), albino P1 (3), albino P4 (3), L-DOPA-treated albino (3), saline-treated albino (3).

DOPA administration

P3.5 albino rats were administered subcutaneous injections of L-DOPA (3mM in PBS; Sigma) in conjunction with a decarboxylase inhibitor (carbidopa), or PBS (a negative control). Eighteen hours later (~P4), the animals were killed and the tissue processed as described below.

Histology and immunohistochemistry

Postnatal rats were killed by decapitation and their heads fixed in 4% formalin overnight. The eyes were enucleated and the cornea and lens removed. Tissue was dehydrated through a series of graded ethanol concentrations; 50%, 70%, 90% and 100% (each at 30 minutes), followed by three changes of fresh 100% ethanol (each at 15 minutes). Eyecups were then embedded in Historesin (Leica). Four micron sections were taken in the horizontal plane and transferred to poly-lysine coated glass slides. Tissue was then stained with cresyl violet.

Imaging and analysis

The three largest non-sequential sections were selected from each eye and examined under a light microscope using a x20 magnification objective. The outline of the retina was traced through a drawing tube and the following features calculated; the length of the OPL (expressed as a proportion of the total retinal length) as well as the thickness of the entire retina, the NBL and presumptive inner nuclear layer (pINL). Five separate measurements were taken of each layer per section/retinal region and the average taken. In this way local variance due to tissue compression/stretching was minimised. In addition, the density of mitotic cells and the density of horizontal cells were calculated per unit area.

Statistical analyses were performed using SPSS 10.1 (SPSS Inc.). The KS-test was used to check for a normal distribution. Data was then subjected to an ANOVA test with Tukey HSD *post hoc* analysis.

2.4 Results

Levels of mitosis

Levels of proliferation were examined in E18, P1 and P4 pigmented and albino rat retinae using two different methods of analysis (Figure 2.4.1). First, mitotic cell counts were made from confocal micrographs of the VZ. They were identified by the presence of condensed chromatin and a pair of associated centrosomes. In parallel mitotic counts were made from fluorescent micrographs of tissue stained with antibodies against phosphohistone-H3, an antigen which is exclusively expressed during late G2- and M-phase.

In Figures 2.4.2 & 2.4.3 mitotic cell counts (standardised per unit area) are plotted for E18-P4 retinae. Error bars represent the standard deviation. Samples were taken from both central and peripheral locations. Finally, data from both central and peripheral retina at P4 were compared between pigmented, albino, L-DOPA-treated albino and D-DOPA-treated albino retinae (Figure 2.4.4.).

In accordance with previous reports (Alexiades and Cepko, 1996), levels of mitosis in the pigmented rat peaked around the day of birth in both the central and peripheral retina (Figure 2.4.2). At E18 and P1, central counts were higher than in the periphery (approximately 16-17% higher) though these differences were not statistically significant (p=0.207 and 0.39). This reflects a temporal lag between the regions; developmental processes of the retina typically occurring within a centre-to-periphery gradient. By P4 however, mitotic levels had dropped off in the central retina, and were approximately 75% lower than in the periphery, a difference which was statistically significant (p= 0.001). In the albino retina there was a similar relative shift in mitotic levels over time. Peak levels were reached by P1 (Figure 2.4.2). Initial counts were higher in the central retina (p=0.108 and 0.45 at E18 and P1 respectively) confirming the existence of a centre-to-periphery gradient of development in the albino,

although differences were not statistically significant. By P4 however, patterns of cell generation in the albino were clearly abnormal. Mitosis failed to drop off in the periphery, such that levels were significantly higher in the central retina (p=0.005).

This pattern of mitosis was confirmed in data generated from the phoshohistone-H3 study (Figure 2.4.3). Thus, in the pigmented rat levels of proliferation were found to peak around the day of birth both in the central and peripheral retina. Similarly, in the albino retina, levels of proliferation rose between E18 and P1, and abnormalities could be detected by P4. The severity of the abnormality seen in the peripheral albino retina was even more marked in this dataset. In the peripheral retina of the albino, levels of proliferation increased between P1 and P4 (Figure 2.4.3B).

Comparisons drawn between corresponding regions of the pigmented and albino retina highlight several significant differences (Figure 2.4.2). In both central (Figure 2.4.2A) and peripheral (Figure 2.4.2B) regions of the retina mitotic levels were indistinguishable between the pigmented and albino at E18 (p=0.967 and 0.744 in the centre and periphery respectively). By P1 however, mitotic levels were elevated by approximately 18% and 28% in the central and peripheral retina respectively relative to age-matched pigmented controls, though this had not yet reached a significant level (p=0.109 and 0.173). This difference was further amplified and reached statistical significance by P4, with mitotic levels 100% and 48% higher in the central and peripheral regions of the albino retina relative to the pigmented, (p=0.028 and 0.014). The general pattern of these findings was also confirmed from the studies using the phosphohistone-H3 marker (Figure 2.4.3). At P4, levels of mitosis were significantly elevated in the albino central and peripheral retina relative to pigmented controls (p=0.038 and 0.027).

Finally, the effects of L-DOPA and D-DOPA on mitotic levels were examined in the P4 albino retina. Again, data was separated into central and peripheral groups. Figure 2.4.4 demonstrates that application of L-DOPA significantly reduced mitotic levels in both the central and peripheral albino retina by

approximately 50% (p=0.006 and 0.003 respectively). Application of D-DOPA however, had no effect (p=0.542 and 0.325 in the central and peripheral retina respectively). It is interesting to note that in the central retina levels of proliferation were indistinguishable between the pigmented and L-DOPA treated albino tissue, implying that the treatment reduced levels of proliferation in the albino to a level comparable with the wildtype. In the peripheral albino retina however, L-DOPA-treatment suppressed proliferation to a level below that found in the wildtype. This effect was reflected in a significant difference between levels of proliferation in pigmented and L-DOPA-treated albino tissue (p=0.032).

Cell cycle exit

The proportion of cells that had left the cell cycle (the q-fraction) and the complementary fraction that remained proliferative (the p-fraction) were determined in the pigmented and albino retina at P1 and P4 using an antibody against Ki67, a marker of all cells within the cell cycle, i.e. in M-, G1-, S- or G2-phase in contrast to G0-phase (Gerdes *et al.*, 1984). Data is presented qualitatively (in the form of a series of fluorescent micrographs; Figure 2.4.5), and quantitatively (Figure 2.4.6). In the latter, the proportion of cells that were positively labelled for Ki67 is plotted. Error bars represent the standard deviation.

In the pigmented retina, the proportion of cells within the cell cycle dropped between P1 and P4 by approximately 53% and 26% in the central and peripheral retina respectively (p=0.003 and 0.001; Figure 2.4.6). By this stage of development the majority of cells are exiting the cell cycle and undergoing terminal differentiation, a reflection of the transition from a proliferative to a differentiative phase of organogenesis (Takahashi *et al.*, 1996). This pattern was further reflected in a comparison of data from central and peripheral retina. At both P1 and P4, the proportion of cells within the cell cycle was greater in the peripheral retina relative to the centre as the centre was developmentally more mature (p=0.029 and 0.002 at P1 and P4 respectively).

In the albino retina there was also a decrease in the proportion of cells within the cell cycle between P1 and P4; levels dropping by approximately 13% and 19% in the central and peripheral retina respectively (p=0.024 and 0.004; Figure 2.4.6). Though this is indicative of a centre-to-periphery gradient of development and the usual reduction in proportion of cycling cells as development progresses (Alexiades and Cepko, 1996), the differences between time-points were less marked than in the pigmented control. This was supported by comparisons of data from central and peripheral retina. At P1 in the albino retina the p-fraction was higher in the central retina (p=0.006), but not at P4 (p=0.099). Thus, differences in the p-fraction between retinal regions were significant for all time-points/pigmentation types examined, except the P4 albino retina. Once again these findings highlight the existence of abnormalities in the albino cell cycle focused around P4, and/or a flattening of the centre-to-periphery gradient of development.

At P1 the proportion of cells within the cell cycle did not differ between pigmentation types; p=0.762 and 0.684 in the central (Figure 2.4.6A) and peripheral (Figure 2.4.6B) retina respectively. However, at P4 a significantly higher proportion of cells remained in the cell cycle in the albino retina relative to the pigmented. This pattern was true of data from both central and peripheral retinal regions, (p=0.003 and 0.028 respectively).

Retinal lamination and differentiation

Patterns of retinal lamination, differentiation and growth were examined at P1 and P4 in thin histological sections of albino and pigmented rat retinae (Figure 2.4.7). In addition, P4 albino retinae were examined following administration of L-DOPA in conjunction with a decarboxylase-inhibitor (carbidopa). In parallel, a number of pups were injected with PBS as a negative control. The thickness of the entire retina, NBL and presumptive inner nuclear layer (pINL) are presented in the form of a series of grouped frequency histograms for central and peripheral retinal regions. In addition, two indices of tissue differentiation were

calculated; the density of horizontal cells per cm of retina and size of the developing OPL.

Patterns of lamina thickness varied within pigmentation types as a function of both retinal location and age, though these differences did not always reach statistical significance. Thus, all layers of the retina were found to increase in size between P1 and P4 (11±6% in the pigmented and 14±9% in the albino) reflecting normal retinal development and growth. In addition, this pattern could be detected as differential layer sizes in the central and peripheral retina. The retina and its composite layers were consistently thicker in the central retina relative to the periphery, reflecting the centre-to-periphery gradient of development (Figure 2.4.8). Similarly, between P1 and P4 the density of horizontal cells per unit area increased in both the albino and pigmented retina, (by 4.6% and 69.5% respectively). Likewise, the outer plexiform layer extended by 96.3% and 240% in the pigmented and albino retina respectively between P1 and P4. These findings imply a progressive differentiation of the nuclear and plexiform layers.

Differences between pigmentation types could also be detected. Though differences did not always reach statistical significance, patterns were consistent between regions and developmental stages. Thus, at P1 and P4 (central and peripheral retina), the thickness of the entire retina as well as the NBL were greater in the albino than they were in the pigmented (22±17% greater, Figure 2.4.8). In contrast, the presumptive inner nuclear layer (pINL) did not differ between pigmentation types. Thus, there is evidence for a delay in the process of retinal development, and/or a prolongation of the proliferative phase as a result of delayed cell cycle exit.

At both stages examined the density of horizontal cells per unit area was greater in the pigmented retina than it was in the albino, though the difference was only significant at P1 ($p<0.05$, Figure 2.4.9A). Finally, at equivalent stages of development the OPL occupied a significantly larger proportion of the retina in the pigmented than it did in the albino ($p<0.05$, Figure 2.4.10A). These findings would suggest that retinal development is delayed in the albino, and

can be detected as a prolongation of the proliferative state, as well as a delay in the processes of retinal lamination and cell differentiation.

Next, the effects of L-DOPA administration on patterns of retinal differentiation were explored. Whilst L-DOPA did not affect the density of horizontal cells in the retina (Figure 2.4.9B) it did promote maturation of the OPL ($p<0.05$, Figure 2.4.10B). Though the albino phenotype was not completely rescued with respect to OPL formation, this study provides the first evidence that L-DOPA promotes retinal differentiation. The majority of studies to data have focused on its documented antimitotic properties.

Cell proliferation

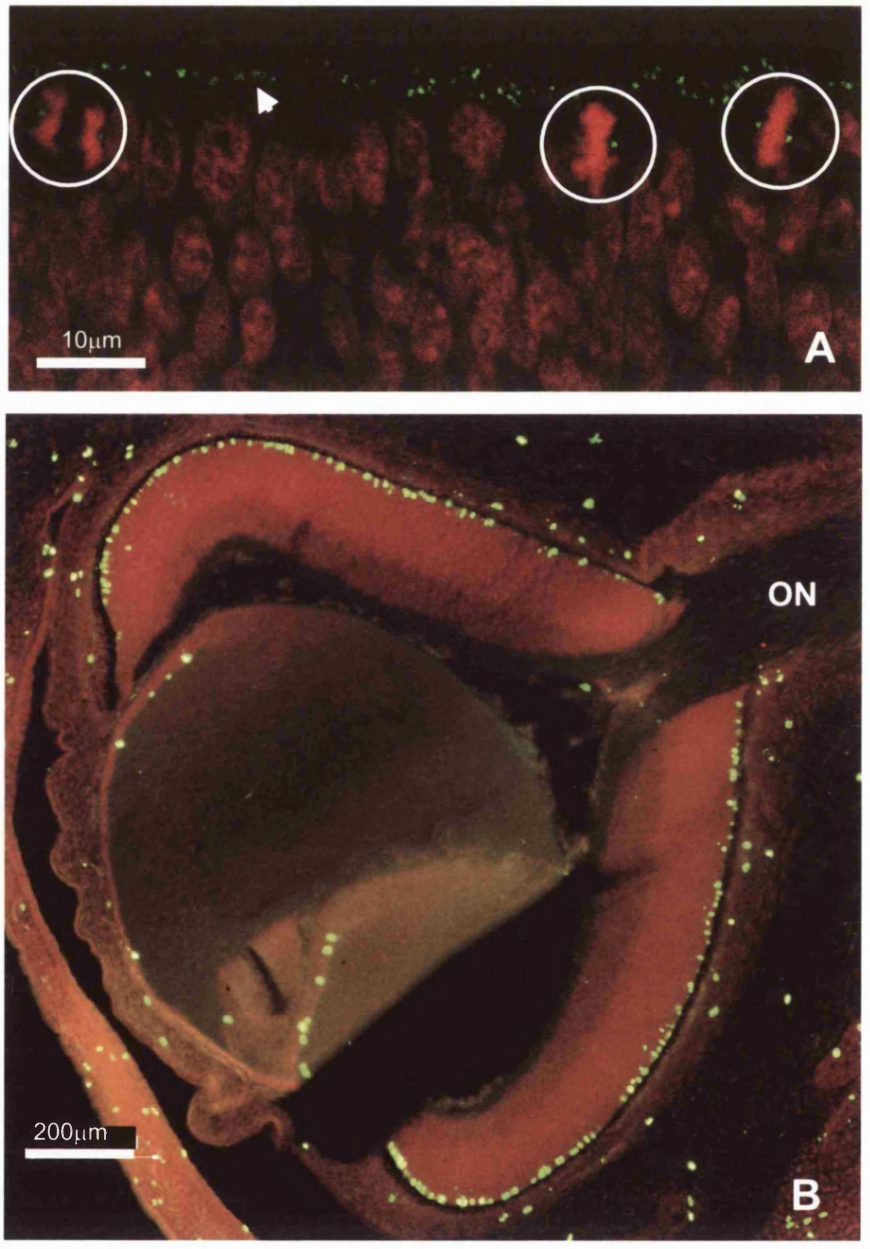

Figure 2.4.1 Mitotic indexes were calculated in the pigmented and albino retina at E18, P1and P4. Two different staining methods were employed to visualise cells undergoing cell division. (A) Tissue was stained for γ-tubulin (green). Dividing cells (encircled) were detected by the presence of condensed chromatin and associated chromosome pairs. (B) In parallel, tissue was stained for phosphohistone-H3 (yellow/green), a late G2-/M-phase marker. Within the neuroblastic retina cell proliferation was localised exclusively to the ventricular margin. ON=optic nerve.

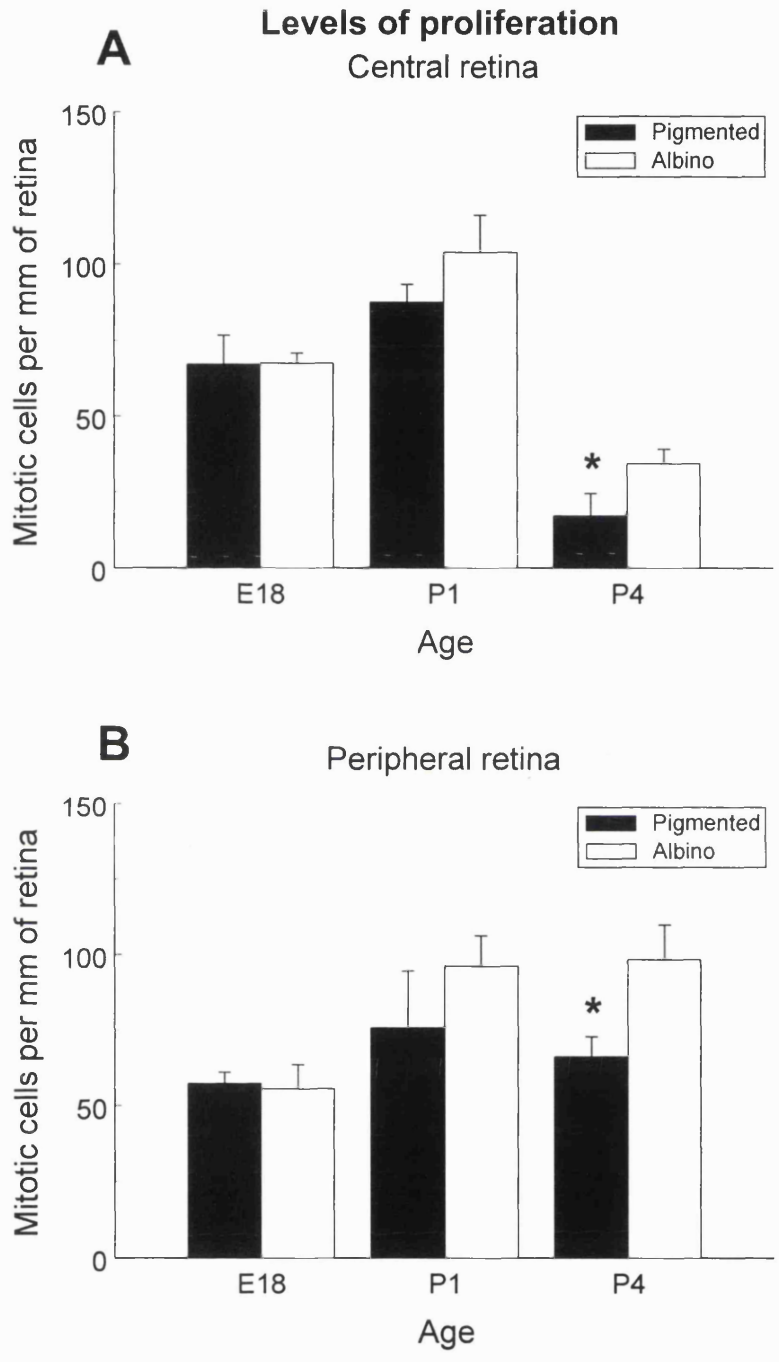

Figure 2.4.2 Mitotic levels are plotted in the (A) central and (B) peripheral retina for pigmented (black) and albino (white) tissue at E18, P1 and P4. Error bars represent the standard deviation. Dividing cells were identified by the presence of condensed chromatin and an associated pair of centrosomes. Three retinae were sampled and a minimum of 34 regions analysed per time-point/pigmentation type. At P4 levels of proliferation were significantly elevated in both the central and peripheral albino retina relative to pigmented controls. * $p<0.05$.

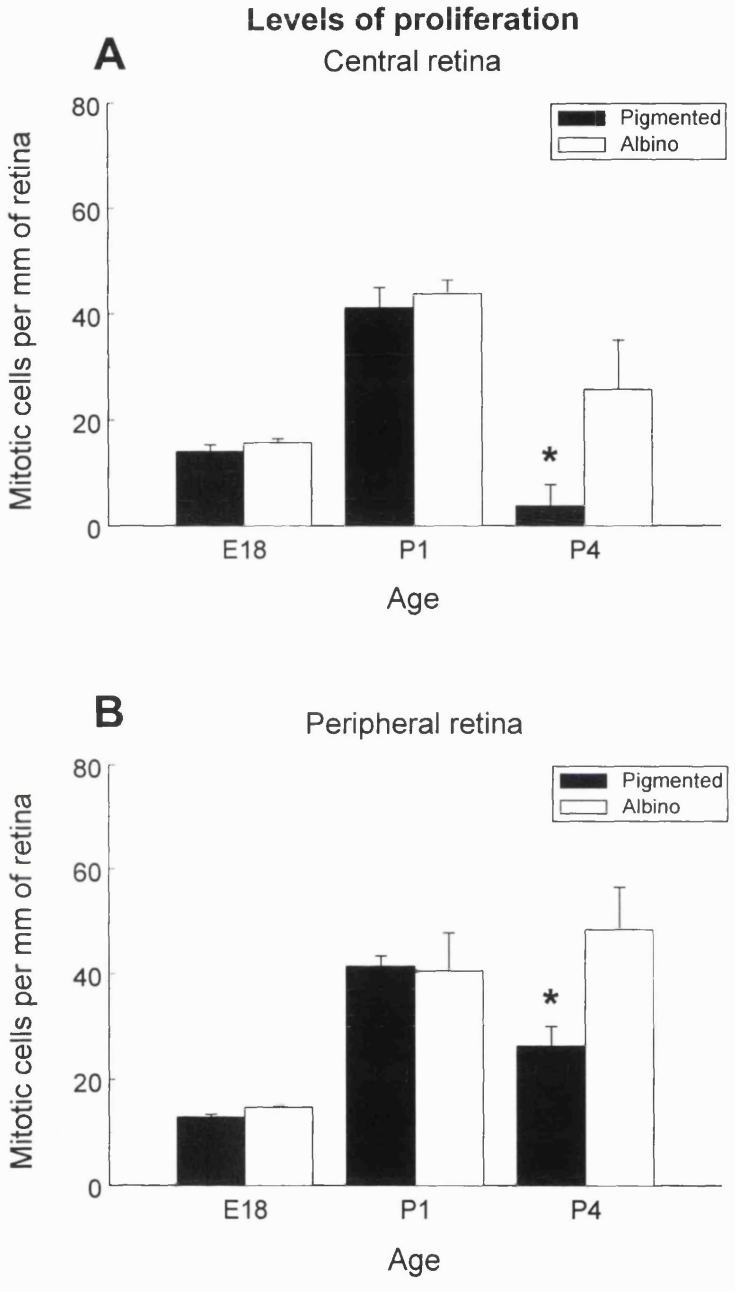

Figure 2.4.3 Cell division in the pigmented and albino retina was visualised using a second detection method; tissue was stained for phosphohistone-H3, a marker of cells in late G2- and M-phase. Mitotic levels are plotted in the (A) central and (B) peripheral retina for pigmented (black) and albino (white) tissue at E18, P1 and P4. Error bars represent the standard deviation. Three retinae were examined per time-point/pigmentation type. 30, 60 and 60 regions were sampled at E18, P1 and P4 respectively per pigmentation type/retinal location. The data follows the same pattern presented in Figure 2.4.2, indicating that by P4 levels of proliferation were significantly elevated in both the central and peripheral albino retina relative to pigmented controls. No differences were found at earlier time points. * $p<0.05$.

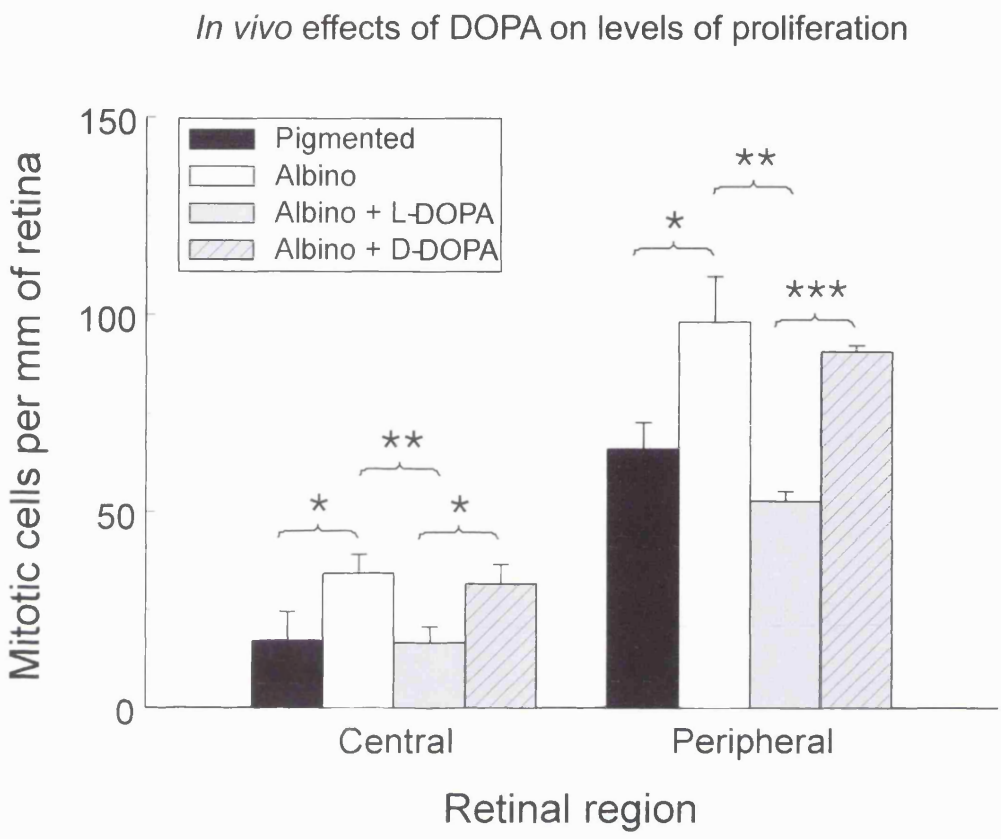

Figure 2.4.4 Mitotic levels are plotted for pigmented, albino and DOPA-treated (L- and D-) albino rat retinae. Separate results are provided for central and peripheral retinal locations. Error bars represent the standard deviation. Three retinae were examined and a minimum of 34 regions sampled per time-point/pigmentation type. Introduction of DOPA to the albino retina was found to reduce mitosis in an L-isoform-specific manner, irrespective of retinal location. * $p<0.05$, ** $p<0.01$, *** $p<0.001$.

Ki67 localisation

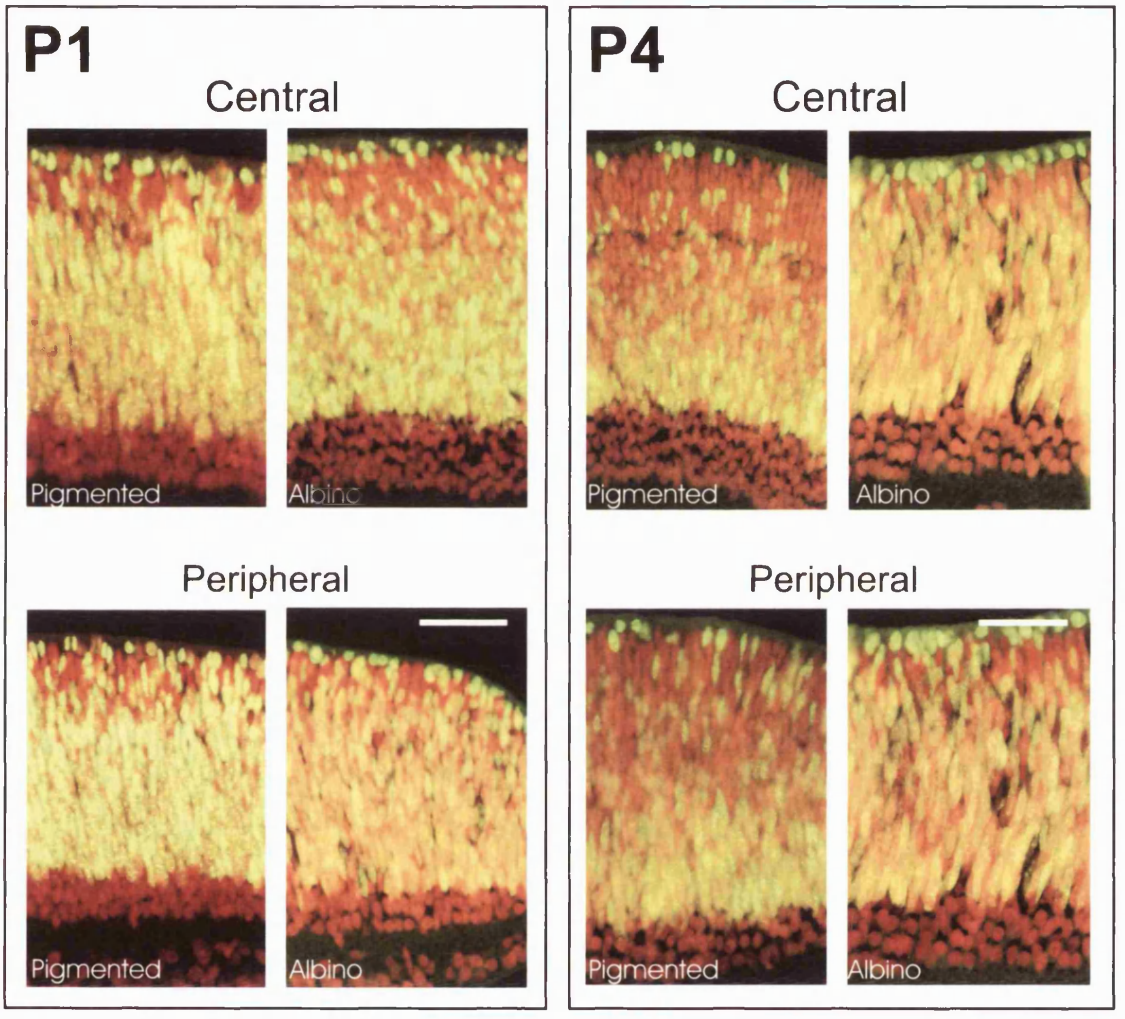

Figure 2.4.5 P1 and P4 pigmented and albino retinal tissue was stained with antibodies against Ki67, a cell cycle marker (yellow) and counterstained with propidium iodide (red) to visualise nucleic acid. Sections were taken in the horizontal plane at the level of the optic nerve. Images are oriented with the VM at the top. Ki67 staining is restricted to a subset of cells within the active neuroblastic layer. A higher proportion of Ki67-positive cells can be seen in the albino relative to the pigmented at P4. Quantitative results are presented in Figure 2.4.6 to support these findings. Scale bar=~50μm.

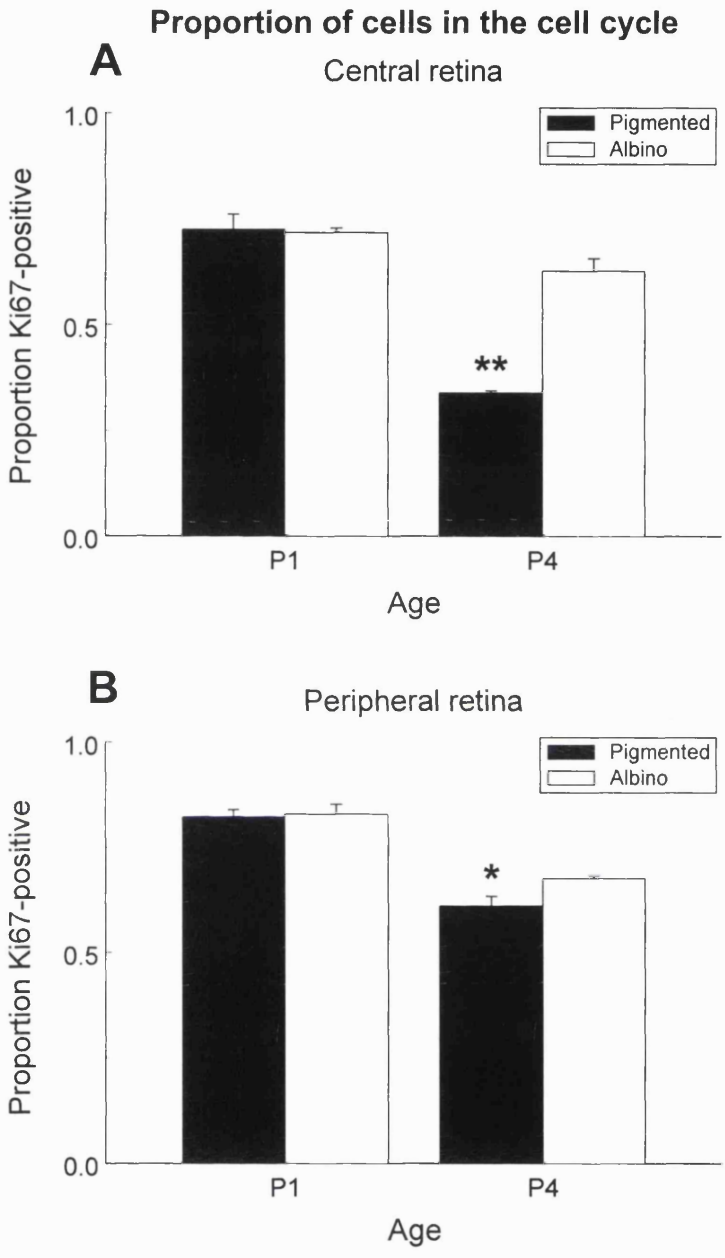

Figure 2.4.6 The proportion of Ki67-positive cells (the p-fraction) in the neuroblastic layer is plotted for the (A) central and (B) peripheral pigmented and albino rat retina at P1 and P4. Error bars represent the standard deviation. Data were gathered from 3 retinae per time-point/pigmentation type/retinal region. At P4 the p-fraction was significantly higher in the albino relative to the pigmented in both the central and peripheral retina. * $p<0.05$, ** $p<0.01$.

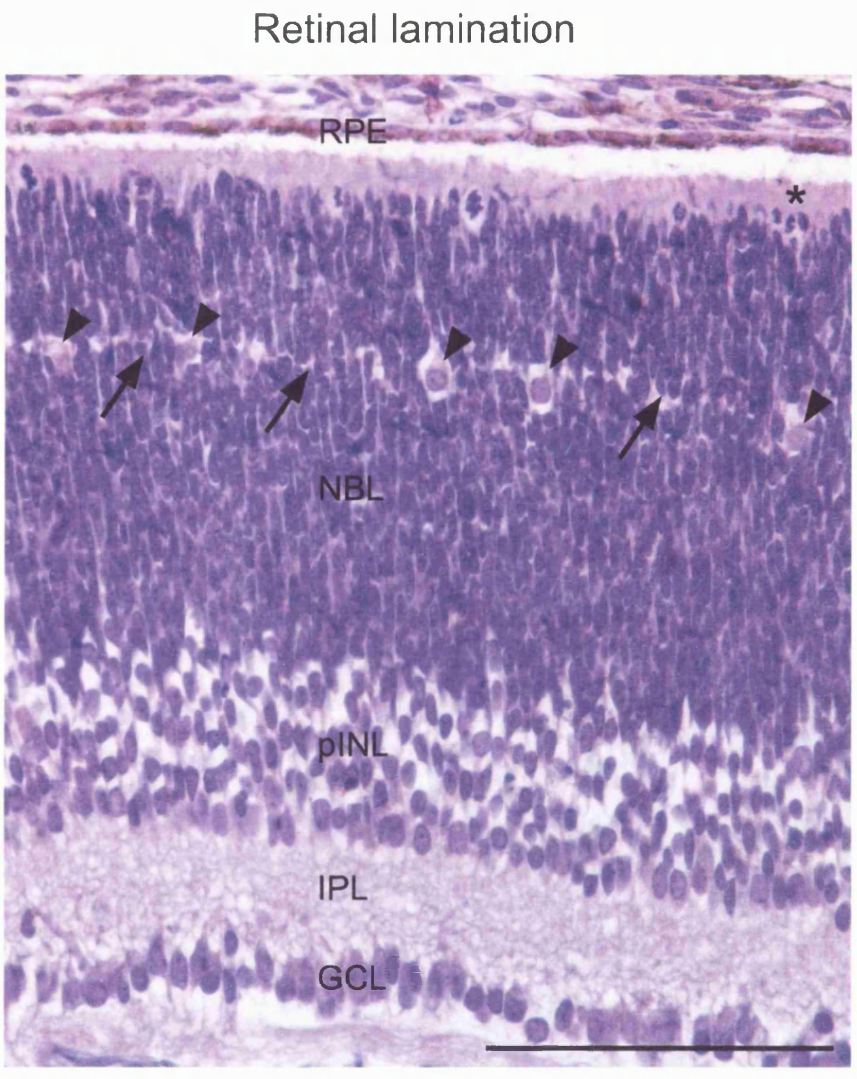

Figure 2.4.7 Pigmented and albino P1 and P4 tissue were analysed with respect to a range of different developmental parameters. L-DOPA-treated and saline-treated P4 albino retinal sections were also included in the study. The level of tissue differentiation was quantified using two different indices. The density of horizontal cells (black arrowheads) was calculated and expressed as a frequency per unit area. In parallel, the length of the developing OPL (black arrows) was determined and expressed as a proportion of the total retinal length. In the early postnatal retina the developing OPL is visible as a small separation of the tissue within the neuroblastic layer. As development progresses this division extends towards the peripheral retina and thickens. Measurements were also made to determine the thickness of the neuroblastic layer (NBL), presumptive inner nuclear layer (pINL) and inner plexiform layer (IPL). A mitotic figure at the ventricular margin is denoted by an overlying asterisk. GCL=ganglion cell layer. RPE=retinal pigment epithelium. Scale bar=100μm.

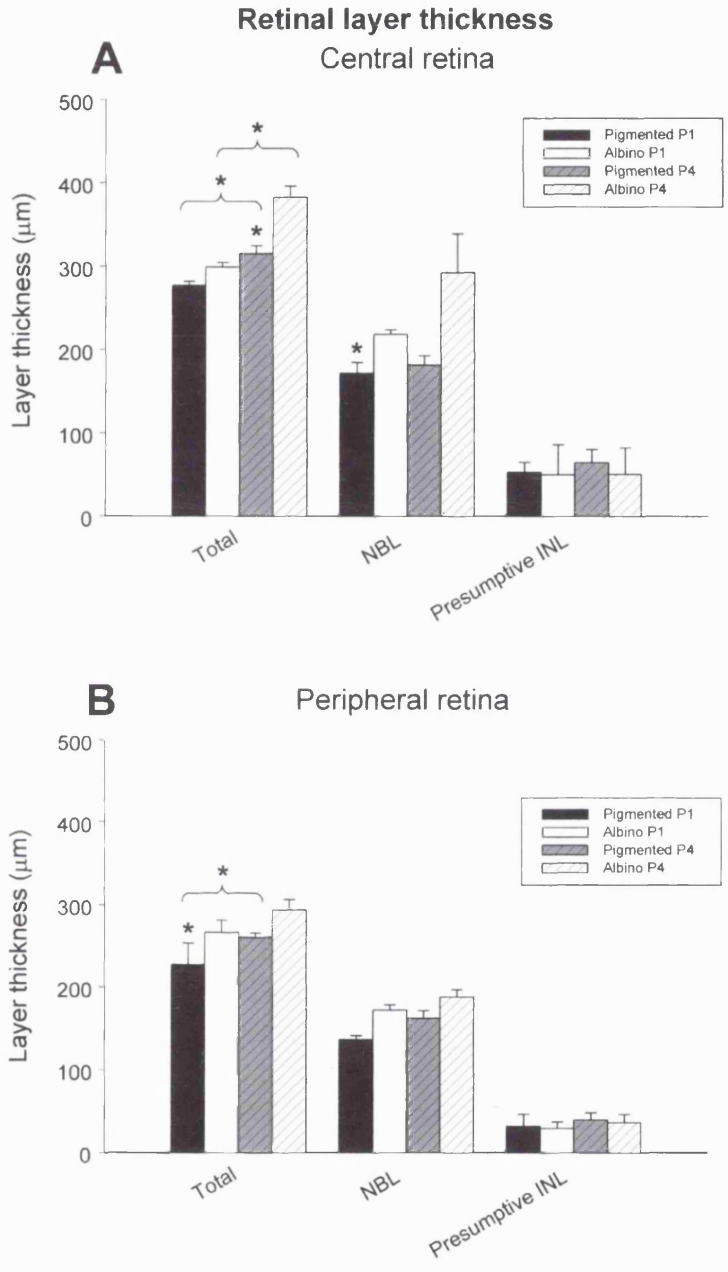

Figure 2.4.8 Measurements of P1 and P4 pigmented and albino tissue were undertaken to determine the thickness of the entire retina, the neuroblastic layer (NBL) and the presumptive inner nuclear layer (INL) at both central (A) and peripheral (B) locations. The entire retina and NBL were consistently thicker in the P4 retina, reflecting normal retinal growth patterns. In addition, the albino retina was consistently thicker than the pigmented, and could be attributed to differences in the size of the NBL rather than the presumptive inner nuclear layer. Though these differences were consistent they did not always reach statistical significance. * Denotes a statistical difference (at least at the 5% level) between data from age-matched pigmentation types. An * with a bracket denotes an intra-pigmentation type difference between time-points. Error bars represent the standard deviation. * $p<0.05$.

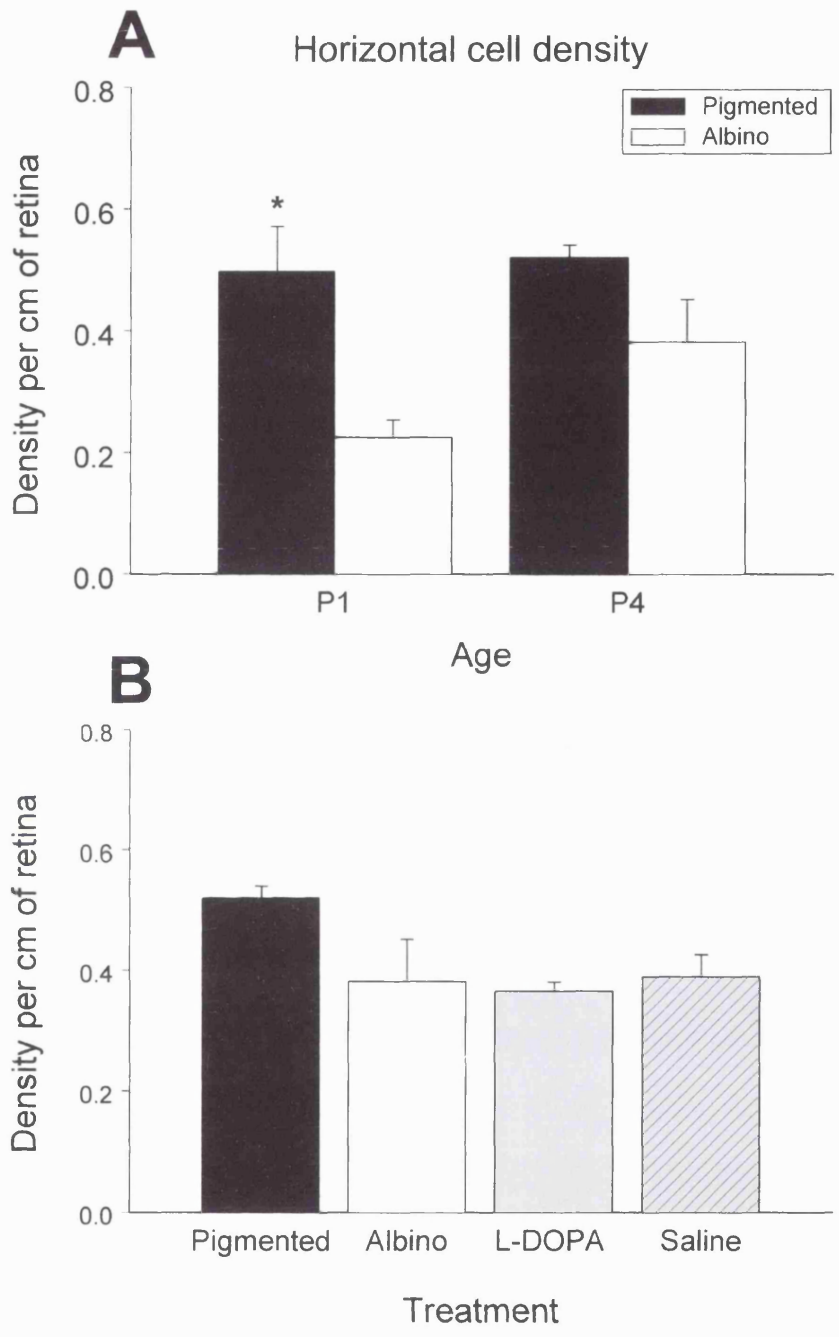

Figure 2.4.9 (A) The number of horizontal cells per centimetre of retina (presumed to reflect the state of tissue differentiation) is presented for pigmented and albino retinae at P1 and P4. (B) The horizontal cell density is also plotted for the P4 albino retina following subcutaneous injection of L-DOPA (with carbidopa) or saline. For reference, data from the pigmented and untreated albino P4 retina are reproduced from (A). Horizontal cell density was significantly higher in the P1 pigmented retina relative to the albino, potentially reflecting a greater level of tissue differentiation. Treatment with L-DOPA did not influence this parameter. * $p<0.05$.

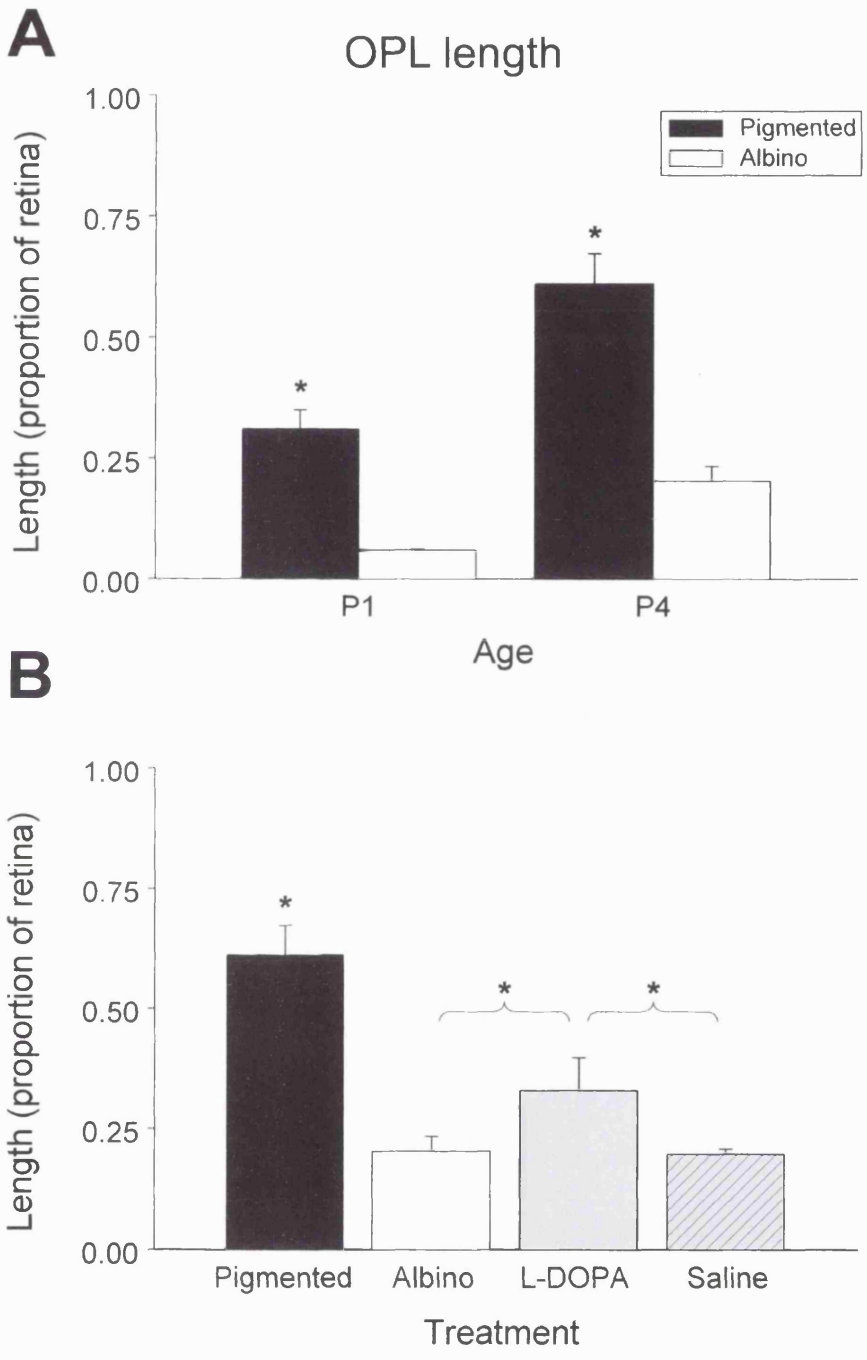

Figure 2.4.10 (A) The length of the developing OPL is presented as a proportion of the entire retina for pigmented and albino P1 and P4 retinae. (B) In addition, data is presented from the P4 albino retina following treatment with L-DOPA and saline. The length of the OPL increased between the two developmental stages and was consistently greater in the pigmented tissue (relative to the age-matched albino tissue). In addition, treatment with L-DOPA reduced the extent of this difference and promoted differentiation of the OPL. Error bars represent the standard deviation. * $p<0.05$.

2.5 Discussion

Using two different immunohistological methods to calculate the mitotic index, results indicate that abnormal levels of proliferation in the albino retina are focused postnatally around P4. In contrast to previous findings, differences could not be detected earlier on during development (Ilia and Jeffery, 1999; Donatien and Jeffery, 2002). Though data is not provided for later time-points, it seems likely that these differences would persist until proliferation ceases. Observation of P6 tissue would suggest that by this late in development proliferation has largely ceased in the central pigmented retina, but persists at relatively high levels in the albino.

It is unlikely that two such robust methods of analysis would generate identical erroneous results, suggesting that there is another reason for the discrepancy between reported findings. This could be due to inherent variation in both the severity of the abnormality as well as its relative timing in different animal models. Indeed a range of values have been quoted to describe the extent to which proliferation is elevated in the albino retina relative to the pigmented. In a pioneer study of the rat retina, small but consistent differences in levels of proliferation were noted between the pigmentation types, though the data never reached statistical significance (Webster and Rowe, 1991). In the Sprague-Dawley (albino) rat, mitotic levels were significantly elevated from E17 through to P6, with peak differences of 50% occurring at P1 (Ilia and Jeffery, 1999). In the hypopigmented NMRI mouse, maximal differences occurred at P4, with mitotic levels being elevated by approximately 147% relative to a transgenic phenotype rescue (Gimenez *et al.*, 2004). In another hypopigmented mouse (the Balb/c) mitotic levels were elevated by 18% and 34% at P1 and P3 respectively relative to a pigmented control (Donatien and Jeffery, 2002). Finally, in a transgenic mouse exhibiting localised variation in pigmentation, levels of mitosis were elevated by ~112% in pigmented regions relative to unpigmented patches (Gimenez *et al.*, 2004).

Results are complicated by the fact that data is not always normalised relative to a pigmented control of the same genetic background, so that absolute levels of proliferation are not directly comparable. However, the results described here fall within the range of previously reported values. In the Wistar rat, levels of proliferation were elevated by 98% and 48% in the central and peripheral retina respectively, relative to pigmented controls. The consistency in the general pattern of these findings, in conjunction with the data gathered from the transgenic models would suggest that the fundamental conclusions of this study are robust. Levels of proliferation are significantly elevated in the albino retina, and are focused primarily in the newborn/early postnatal retina.

Next, the *in vivo* effects of L-DOPA administration on patterns of mitosis were demonstrated, previous studies having highlighted its action *in vitro* (Akeo *et al.*, 1994; Ilia and Jeffery, 1999). L-DOPA reduced cell division in the albino retina to a level comparable with the wildtype. Furthermore, the effect was specific to the L- isoform, raising the possibility that it is of biological relevance. The precise mechanism by which L-DOPA induces a reduction in levels of proliferation has not been resolved however. *In vitro* studies of cultured RPE cells would suggest that L-DOPA arrests cell cycle progression selectively in S-phase (Akeo *et al.*, 1994), whilst live-imaging studies of the developing retina indicate that L-DOPA also acts to prolong prophase (Kralj-Hans, unpublished observations).

The proportion of cells within the cell cycle was then examined in the pigmented and albino retina as levels of proliferation and cell cycle exit are intimately connected. Thus, BrdU studies of the mouse neocortex have shown that application of either GABA or glutamate to organotypic slices *in vitro* leads to increased proliferation and a concerted reduction in cell cycle exit (Haydar *et al.*, 2000). To address this issue the proportion of cells that were proliferative (the p-fraction), as well as the complementary proportion that had left the cell cycle (the q-fraction), were examined using an antibody against the cell cycle marker Ki67. Results indicate that in the albino retina a significantly higher proportion of cells were still in the cell cycle at P4 relative to the pigmented control, both in central and peripheral regions. Interestingly no differences were

found in the proportion of cells in the cell cycle at P1. Thus, the albino retina is characterised by an excessive level of proliferation which is temporally coincidental with an abnormally high proportion of cells within the cell cycle. These findings were also confirmed by histological analysis of retinal laminae in the pigmented and albino retina. At both P1 and P4 the albino retina was thicker than the pigmented, a pattern which could be specifically attributed to a thickening of the NBL. In contrast, the pINL did not differ between pigmentation types. This would strongly suggest that the postnatal albino retina is abnormally thick due to a delay/failure in cell cycle exit, resulting in an over-proliferative state.

In an hypothesis proposed by Ilia and Jeffery (2000), they suggest that as a result of the aberrant thickness of the retinal neuroepithelium during development, the tissue becomes hypoxic and characterised by a period of excessive cell death. Indeed studies have shown that the albino retina is under severe metabolic stress and that exposure to an high oxygen environment reduces levels of apoptosis, an effect which is less marked in the pigmented (Semo *et al.*, 2001). Furthermore, levels of pyknosis are significantly elevated in the albino rat from E17 to P6 and can be regulated by the addition of L-DOPA *in vitro* (Ilia and Jeffery, 1999). In contrast, studies of the pigmented and albino mouse failed to highlight differences in levels of apoptosis (Donatien and Jeffery, 2002). In view of the fact that the developing albino retina is abnormally proliferative, whilst the adult retina is characterised by translaminar deficits (Elschnig, 1913; Jeffery and Kinsella, 1992; Ilia and Jeffery, 2000), one might expect levels of cell death to be elevated perforce. This is not necessarily so however, as differential patterns of eye growth or cell division (with respect to the symmetry or asymmetry of cell fate) could resolve this apparent paradox, (see chapter 3).

If the proliferative phase is prolonged in the albino retina, what are the knock-on effects on the next stage of organogenesis, i.e. differentiation? To address this question (at both the cell and tissue level) the processes of differentiation were examined in histological sections of the postnatal pigmented and albino retina. Two separate indices were used. First, the density of horizontal cells per unit

area of retina was calculated. In parallel, the length of the developing OPL was measured and expressed as a proportion of the total retinal length. On the basis of these measurements the process of tissue differentiation would seem to be delayed in the albino retina and could be detected both in a reduced density of horizontal cells, as well as a delay in OPL formation. Furthermore, this latter parameter could be regulated by the introduction of L-DOPA into the retina. This provides the first evidence to suggest that in addition to its anti-mitotic properties L-DOPA promotes tissue differentiation.

In the absence of further data, solid predictions with respect to the implications of these findings on patterns of cell fate can not be made. By remaining in the cell cycle too long individual retinal progenitors may undergo a higher number of proliferative divisions before undergoing terminal differentiation. This would result in the generation of an excess of late-born cell types, i.e. Müller cells, bipolar cells and/or rod photoreceptors. In a study of the mouse retina premature cell cycle exit induced by the overexpression of $p27^{Kip1}$ resulted in an increase in the relative proportion of clones containing rod photoreceptors (Dyer and Cepko, 2001a). The author suggests that this may reflect a peak in rod cell generation which precedes that of the bipolar and Müller cell. Thus, perhaps in the albino retina, delayed cell cycle exit implies the reverse; an increase in the proportion of clones containing bipolar and Müller cells, potentially at the cost of rod photoreceptors. Studies of bipolar and Müller cell densities in the albino retina may well cast some light on this hypothesis (see chapter 3).

Alternatively, if cells remain in the cell cycle too long they may miss the appropriate cues, and eventually die due to an inappropriate environment for their survival or differentiation. Once again, late-born cell types, i.e. Müller cells, bipolar cells or rod photoreceptors would be selectively affected, potentially leading to deficits in one or more of these cell classes.

Conclusions

These findings demonstrate an elevated level of proliferation in the developing albino retina which is temporally coincidental with an excess of cells that remain in the cell cycle and an abnormal thickening of the NBR. In addition to -and potentially as a result of- this prolongation of the proliferative phase, there is a delay in the differentiation of the retina. This can be detected in the formation of the OPL as well as the birth of horizontal cells, and is in agreement with previous reports of delays in the centre-to-periphery gradient of development in the albino (Webster and Rowe, 1991; Ilia and Jeffery, 1999). Thus, a failure to exit the cell cycle at the correct time point may imply a prolonged state of developmental immaturity and a delay in the normal processes of tissue differentiation. Furthermore, many of these abnormalities can be regulated and/or corrected by the introduction of L-DOPA into the developing albino retina.

Further evidence to support the role of L-DOPA in the regulation of retinal development comes from a series of studies that are currently in progress in a collaborating laboratory. A transgenic mouse model has been generated in which L-DOPA is synthesised in the retina, though its conversion further down the melanin biosynthesis pathway is blocked. A tyrosine hydroxylase construct, driven by a promoter expressed in the RPE, has been introduced onto an albino background (the NMRI mouse). Preliminary unpublished results would suggest that the resulting transgenic mouse is phenotypically normal with respect to the development and anatomy of its visual system, despite a lack of ocular pigmentation (Montoliu, 2004).

Chapter 3:
Cleavage orientations
within the apical-basal plane

3.1 Introduction

In the central nervous system individual stem cell or progenitor lineages are composed of multiple cell types (Turner *et al.*, 1990). Even during its final division, a neuroblast may divide asymmetrically to generate two different cells types (Turner and Cepko, 1987). An asymmetric division is therefore defined as one in which distinct cell fates or developmental potentials are assigned to each of the daughter cells. One way by which this can be achieved is through the asymmetric localisation of cell fate determinants such as Numb and Prospero within the cell membrane, coupled with a tight regulation of the cell's cleavage orientation (Bardin *et al.*, 2004). Thus, alternative cleavage orientations give rise to distinct inheritance patterns, and in the case of an asymmetric division, both daughter cells are able to respond differentially to an identical set of environmental cues (Cayouette and Raff, 2002; Zhong, 2003). In many systems, asymmetric division is a key developmental mechanism in the generation of cellular diversity (Lu *et al.*, 2000; Knoblich, 2001).

In the invertebrate nervous system asymmetric division has been well documented. In Drosophila, sensory organ precursors (SOP's) of the peripheral nervous system; as well as ganglion mother cells (GMC's) and MP2 precursors of the central nervous system follow a stereotypic pattern of asymmetric cell division and Numb inheritance, which is essential for the correct specification of

cell lineage. Disruption of this process results in the generation of abnormal ratios of neuronal to non-neuronal cells and/or a reduction in the diversity of cell types, (Uemura *et al.*, 1989; Rhyu *et al.*, 1994; Spana and Doe, 1996; Buescher *et al.*, 1998).

Recent studies would suggest that patterns of cleavage orientation may also play a role in the process of asymmetric cell division within the vertebrate nervous system. Time-lapse imaging studies of the developing ferret cortex have shown that the distribution of cleavage orientations at the ventricular margin (VM) is tightly regulated over time (Chenn and McConnell, 1995). According to the hypothesis presented by Chenn and McConnell (1995), horizontal divisions expand the progenitor pool, whilst vertical divisions generate one progenitor and one post-mitotic cell, a system which is reminiscent of the invertebrate stem cell division, (see Lin and Schagat (1997) for a review). Thus, as development progresses, a switch from an horizontal to a vertical mode of division is associated with the transition from tissue expansion to morphological differentiation. In addition, several cell fate determinant proteins exhibiting asymmetric distribution patterns have been reported in the developing vertebrate nervous system (Chenn and McConnell, 1995; Zhong *et al.*, 1996; Wakamatsu *et al.*, 1999; Cayouette *et al.*, 2001; Shen *et al.*, 2002; Silva *et al.*, 2002).

The regulation of cleavage orientation may also play an integral role in the generation of cellular diversity in the developing vertebrate retina. In the rat retina, vertical divisions were found to peak around the day of birth, coinciding with the peak in cell generation (Cayouette *et al.*, 2001). In a follow-up study using long-term videomicroscopy of green-fluorescent-protein labelled retinal explants from neonatal rats, the link was made between the adoption of a vertical orientation during division and the generation of two daughter cells with distinct cell fates (Cayouette and Raff, 2003).

A model of asymmetric division in the vertebrate retina has been proposed whereby the peak in vertical divisions around the day of birth is correlated with the generation and specification of Müller cells and/or bipolar cells at the

expense of rod photoreceptors (Cayouette and Raff, 2003). Several lines of reasoning support this hypothesis. First, the peak in proportion of vertical divisions occurs around the day of birth, coinciding with the peak in the generation of these cell types (Cepko *et al.*, 1996). Secondly, cleavage orientations in the vertebrate retina have been shown to regulate Numb inheritance patterns (Zhong *et al.*, 1996; Wakamatsu *et al.*, 1999; Cayouette *et al.*, 2001; Silva *et al.*, 2002; Cayouette and Raff, 2003). In addition, Numb negatively regulates the expression of Notch (Guo *et al.*, 1996; Spana and Doe, 1996), a membrane-bound receptor involved in the process of lateral inhibition and the specification of glial cell fate (Furukawa *et al.*, 2000; Hojo *et al.*, 2000; Morrison *et al.*, 2000). Finally, overexpression of Numb in the rat retina using retroviral vectors led to an increase in the size of the photoreceptor cell population, whilst simultaneously inducing a reduction in Müller glia and interneurons (Cayouette and Raff, 2003).

The albino retina is characterised by abnormalities in patterns of cell generation (Webster and Rowe, 1991; Ilia and Jeffery, 1996; Ilia and Jeffery, 1999; Ilia and Jeffery, 2000; Donatien and Jeffery, 2002) which temporally coincide with the peak in vertical divisions (Cayouette *et al.*, 2001), as well as the peak in rod photoreceptor generation (Cepko *et al.*, 1996). This is of significance as the rod photoreceptor population is severely affected in the albino (Jeffery and Kinsella, 1992; Jeffery *et al.*, 1994; Donatien and Jeffery, 2002), and the specification of its identity has been putatively linked to patterns of asymmetric division in the retina (Cayouette *et al.*, 2001; Cayouette and Raff, 2003). Consequently, a series of studies was undertaken to examine the distribution of cleavage orientations in the albino retina, and hence ascertain whether rod photoreceptor deficits can be correlated to defects in patterns of cleavage orientations during development.

3.2 Experimental aims

Initial experiments were conducted to quantify the proportion of horizontal and vertical divisions in the developing retinal neuroepithelium of pigmented and

albino rats. Tissue from E18-P6 was examined, as previous studies have highlighted this window of development as a critical period of transition with respect to patterns of cell division in the retina (Cayouette *et al.*, 2001). Having demonstrated both quantitative and qualitative abnormalities in the regulation of cleavage orientation in the albino retina, the potential effects of L-DOPA administration were examined. Previous studies have highlighted its role in the regulation of cell division, as well its putative involvement in the pathogenesis of albinism (Wick, 1977; Akeo *et al.*, 1994; Ilia and Jeffery, 1999). (Also, see chapter 2).

In addition to a regulated cleavage orientation, asymmetric division requires a concerted asymmetric distribution pattern of cell fate determinants within the same plane. Perhaps the most heavily documented example is the protein Numb. A plasma-membrane associated cytoplasmic protein, Numb antagonises Notch signalling and is asymmetrically localised to the apical or basal surface of the vertebrate retina during development (Zhong *et al.*, 1996; Wakamatsu *et al.*, 1999; Cayouette *et al.*, 2001; Silva *et al.*, 2002; Cayouette and Raff, 2003) . Consequently, patterns of Numb localisation were examined in the pigmented and albino retina to ascertain; (a) if both components necessary for asymmetric division were present in the retinae of pigmented and albino animals (i.e. an asymmetric distribution pattern of cell fate determinants as well as a regulated cleavage orientation); and (b) whether the regulation of Numb localisation is independent of cleavage orientation in the developing rodent retina.

Finally, a study of Müller cell densities was undertaken in the adult pigmented and albino retina. Current hypotheses as to the function of asymmetric division in the developing vertebrate retina predict its involvement in the process of cell fate specification, and more precisely, the promotion of a photoreceptor cell fate at the expense of a Müller or bipolar cell identity (Cayouette *et al.*, 2001; Cayouette and Raff, 2003). Consequently, the effects of aberrant patterns of cleavage orientation on the adult population of Müller glia were examined in the albino retina.

3.3 Methods

Calculation of cleavage orientation

Pigmented (D.A.) and hypopigmented (Wistar) rat litters were used at stages between E18 and P6. Shown in brackets are the number of eyes (each from a different animal) examined from each experimental group; pigmented E18 (4), P1 (12), P4 (3), P6 (3); albino E18 (4), P1 (5), P4 (4), P6 (3); L-DOPA-treated albino (4), D-DOPA-treated albino (3).

DOPA administration

P3.5 albino rats were administered subcutaneous injections of L-DOPA in conjunction with a decarboxylase inhibitor (carbidopa), or D-DOPA, at a concentration of 15μg per gram of body weight in PBS, (3mM). 18 hours later (~P4), the animals were killed and the tissue processed as described below.

Histology and Immunohistochemistry

To characterise the orientation of dividing cells at the VM the centrosomes and nucleic acid were labelled in pigmented and albino tissue as described by Cayouette *et al.* (2001). Animals were killed by decapitation, the eyes enucleated and fixed in 4% formalin overnight at 4°C. They were then cryoprotected in 20% sucrose, the cornea and lens removed, and transferred to a 2:1 mixture of 20% sucrose/OCT for 30 minutes. They were subsequently embedded in OCT and frozen by submersion in dry ice. Twenty micron sections were taken in the horizontal plane, transferred to poly-lysine coated glass slides (BDH Laboratory Supplies) and left to dry overnight.

Sections were washed in PBS and perfused with Proteinase K (6.6μg/ml in 10mM tris/1mM EDTA at pH7.6; Sigma) for 20 minutes at 4°C. The excess was then rinsed off with PBS and the tissue post-fixed in pre-cooled 70% ethanol for 10 minutes at -20°C. Epitopes were blocked in 10% goat serum with 1% Triton

X-100 (Sigma). Slides were incubated overnight at 4°C in rabbit anti-γ-tubulin antibodies, (diluted 1:500 in 1% Triton /5% normal goat serum; Sigma). Primary antibodies were detected using the biotin-Streptavidin detection system. Sections were incubated for 2 hours in biotinylated goat anti-rabbit IgG antibodies (Vector Laboratories), and subsequently for 1 hour in Streptavidin-Cy2 (1:100; Amersham Pharmacia Biotech). The tissue was then counterstained with propidium iodide (5μg/ml in PBS) to visualise nuclei and coverslipped in Vectashield fluorescent mounting medium (Vector laboratories).

Imaging and analysis

To quantify the orientation of mitotic spindles relative to the plane of the VM serial sections of the retina exhibiting a clear C-shape morphology were studied using the 488nm and 543nm lines of a Zeiss laser scanning confocal microscope (LSM 500). Multiple areas were scanned from both central and peripheral locations and serial sections in the z-plane taken, facilitating three-dimensional reconstruction. Resulting sampled volumes had dimensions of 115x56x20μm in the x-, y- and z- planes respectively, with potential variation in the z-plane thickness. All mitotic cells with visible pairs of centrosomes were then analysed using Zeiss Image Examiner Version 1.8. The three-dimensional coordinate values of each centrosomal pair were recorded by panning through the depth of the image using an in-built tool that simultaneously visualises z-stacks in three orthogonal planes. This was necessary as divisions occurred at all orientations both within the plane of the tissue and within the apical-basal plane, so that it was often necessary to scan back and forth through the z-plane to obtain the coordinates of each centrosome pair. In addition, the central slice within the z-stack was used to gather the coordinates of a minimum of ten reference points defining the outer limit of the NBR.

The orientation of the mitotic spindle was then calculated for individual cells using three-dimensional coordinate geometry in a technique developed by A.V. Whitmore (Cayouette *et al.*, 2001). The coordinates of the centrosomes (which are assumed to be indicative of the mitotic spindle polarity) are plotted relative to a reference plane which is calculated by fitting a regression line to the outer

limit of the NBR. The angle formed at the hypothetical interface between a line connecting the centrosomes of a dividing cell and the reference plane is a measure of the mitotic spindle orientation. This is assumed to be orthogonal to the cleavage plane, so that an angle of 0^{o} represents a horizontal division, and an angle of 90^{o} represents a vertical division. In addition, the program calculates the inter-centrosomal distance (which can loosely be correlated to the stage of mitosis) and the azimuth (rotational orientation within the plane of the epithelium). (See appendix to Cayouette *et al.* (2001) for more details of methods).

Data gathered were then reanalysed using a custom-written Matlab program to calculate the distance from the centre of a dividing retinal neuroblast to the VM (see appendix 4 for code). The program uses the coordinate pairs which describe the position of the centrosomes (gathered as outlined above) and calculates a third coordinate pair which lies midway along a theoretical line connecting both. This point (A) represents the centre of the dividing cell. Next, the linear equation of the reference plane (defined by the outer limit of the NBR) is used to calculate the coordinates of a theoretical point (B) on this line which shares the same value for x as (A). Finally, a third point (C) is defined which lies on the reference plane such that a line A-C is normal to the reference plane. Length A-C is thus a measure of the distance of the cell from the VM and can be calculated using simple trigonometry. (A), (B) and (C) define a right-angled triangle for which one of the angles is known (derived from the gradient of the reference plane) as well as the length of one of the triangle's sides (A-B). The distance A-C can then be calculated using the sine rule.

Statistical analyses were performed using SPSS 10.1 (SPSS Inc.). Pair-wise chi-squared tests were applied to compare the proportion of horizontal ($<45^{o}$) to vertical divisions ($\geq 45^{o}$) between pigmentation types. This particular test was used as it addressed the primary parameter of interest in this study, the relative proportion of vertical divisions being of direct biological relevance. In addition, the three most heavily sampled retinae from each group were used to calculate the mean proportion of vertical divisions per time-point/pigmentation type. Inter-

pigmentation type comparisons were then made using independent samples t-tests, thus eliminating the possibility that data was skewed by extreme outliers.

For the calculation of cleavage orientations, *n*= 161, 71, 290, 123 and 100 cells analysed at E18, E20, P1, P4 and P6 respectively in the pigmented retina; and n=160, 250, 171 and 102 cells analysed at E18, P1, P4 and P6 respectively in the albino. In addition, 181 and 146 cells were analysed from P4 L-DOPA and D-DOPA-treated albino retinae respectively. See start of section for details of the number of animals used per group.

Patterns of Numb localisation

Histology and Immunohistochemistry

Pigmented and albino rat tissue was collected, fixed, cryoprotected and embedded in OCT as outlined above. Twenty micron sections were taken in the horizontal plane, transferred to poly-lysine coated glass slides (BDH Laboratory Supplies) and left to dry overnight. Similarly, the tissue was pre-treated and post-fixed in Proteinase K (Sigma) and 70% ethanol respectively (see above). Epitopes were then blocked in 10% goat serum (Sigma) with 1% Triton X-100 and the slides incubated overnight at room temperature in mouse anti-numb antibodies, (diluted 1:500 in 0.1% Triton /5% goat serum in PBS; BD Biosciences). A secondary biotinylated goat anti-mouse antibody (1:200; Vector Laboratories) was applied for 90 minutes followed by Streptavidin-Cy2 for 3 hours (1:100; Jackson ImmunoResearch). Finally, the tissue was counterstained with propidium iodide for 2.5 minutes (5μg/ml in PBS) and coverslipped in Vectashield fluorescent mounting medium (Vector laboratories).

Imaging and analysis

Retinae were examined using the 488nm and 543nm lines of a Zeiss laser scanning confocal microscope (LSM 500). Reference images from the central retina were then taken from both pigmented and albino tissue. No quantitative

analysis was performed, only the general distribution of staining patterns was noted.

Müller cell density

Müller cell densities were calculated in pigmented (D.A.) and hypopigmented (Wistar) rat retinae from 9 week old animals. Four eyes (each from a different animal) were examined per group.

Histology and immunohistochemistry

Adult animals were killed by CO_2 and perfused transcardially with 0.9% saline (in PBS) followed by 4% formalin. Heads were fixed in 4% formalin for 5 hours, initial experiments having demonstrated the protocol's sensitivity to over-fixation. The eyes were then enucleated, the cornea and lens removed, cryoprotected and embedded as described above. Ten micorn sections were taken in the horizontal plane, and transferred to poly-lysine slides. Endogenous peroxidase activity was blocked with 0.3% H_20_2 in PBS for 20 minutes. Slides were then microwaved in citrate buffer (pH6) for a total period of 5 minutes and left to stand at room temperature for a further 25 minutes. The tissue was blocked in 10% normal horse serum with 1% Triton X-100.

Müller cell specific antigens were detected by incubation over night at room temperature in anti-vimentin antibodies, (1:100, DAKO) and subsequent exposure for 2 hours to peroxidase-coupled horse anti-mouse secondary antibodies (1:100; Vector Laboratories). The reaction was then developed by incubation in Tris-HCL with 0.05% DAB (weight/volume) and 0.005% H_2O_2. The tissue was finally brought to ispopropyl alcohol via a series of alcohol washes of increasing concentrations (5 minutes each at 50%, 70%, 90%, 96% and 100% ethanol) and coverslipped in glycerol.

Imaging and analysis

Sections were visualised under a standard light microscope. In the retina, antibodies against vimentin, an intermediary filament protein, selectively labelled Müller cell trunks (spanning the entire thickness of the retina), as well as side-arms that projected tangentially through the OPL. Counts were made based on observations at a level halfway along the inner portion of the trunk (at the level of the IPL) as this section of the tissue offered the most robust and consistent labelling. Counts were made per graticule (200μm in length) in a series of adjacent, non-overlapping regions spanning from the ON and moving progressively outwards towards the peripheral retina. Four retinae were examined per pigmentation group. For each of these retinae a minimum of 5 non-serial sections were analysed and where possible data gathered at all eccentricities from both nasal and temporal retina. Given that each hemiretina was 19±1 graticules in length (~4mm), a total of 666 and 615 fields were scanned in the pigmented and albino retina respectively.

Statistical analyses were performed in SPSS 10.1 (SPSS Inc.). Data were normally distributed as determined by the KS-test, and comparisons made using the One-Way ANOVA test with Tukey HSD *post-hoc* analysis.

3.4 Results

Localisation of neuroblasts to the ventricular margin

As described in chapter 1, retinal neuroblasts undergo a stereotypic pattern of radial migration back and forth across the thickness of the retina, which reflects the passage of cells through the phases of the cell cycle as well as changes in susceptibility to a range of regulatory signals (Murciano *et al.*, 2002). Thus, whilst DNA replication (S-phase) is restricted to the inner region of the NBR, cell division (M-phase) is restricted to the VM (the apical surface of the NBR). A study of the albino mouse demonstrated abnormalities in the spatial

organisation of migrating neuroblasts during development (Rachel *et al.*, 2002). Consequently, a study was undertaken to ascertain whether dividing cells were correctly localised to the VM in the albino retina, as they are in the pigmented.

Figure 3.4.2 presents frequency distributions of the vertical distance between dividing retinal neuroblasts and the VM for pigmented and albino tissue. Values have been collated from E18, P1 and P4. Data from the pigmented retinae are normally distributed about a mean distance of 5.2 μm, (p=0.558[1], KS-test). The distance from the VM was calculated using the centre of the cell rather than the outer-membrane as a reference point. As a retinal neuroblast is approximately 10μm in diameter (see Figure 3.4.1) a mean distance of 5.2μm would imply that cells undergoing mitosis are tightly apposed to the VM.

In the albino retina however, the data does not fit a Normal or a Poisson distribution (p=0.064, KS-test). Though the mean distance from the VM does not significantly differ between the albino and the pigmented (5.7μm to 5.2μm respectively), the standard deviation is higher (4.1μm to 2.8μm), and so is the range (19.57μm to 14.62μm). In addition, the distribution is skewed; 1.008 compared to 0.439 (values of ≥1 being indicative of an asymmetric distribution). Comparing the overall data distributions for the pigmented and albino retinae using the KS-test highlighted differences that approached statistical significance at the 5% level, p=0.064.

In Figure 3.4.3 cumulative frequency distributions of the distance between dividing cells and the VM are plotted for pigmented (Figure 3.4.3A) and albino (Figure 3.4.3B) retinae at E18, P1 and P4. Pigmented data at all stages examined closely fit a normal distribution (all p values were >0.2, see footnote 1). However, a different pattern emerged in the albino. Data were normally distributed in the P4 albino, but not at E18 or P1 (p=0.09 and 0.06 respectively).

---

[1] In this form of KS-test data is compared to an idealised (e.g. normal) distribution. Hence, the null hypothesis that must be rejected is that the data fits the predicted model. A p value of 0.6 implies that there is a 60% chance that the data is normally distributed.

Having demonstrated differences in the localisation patterns of dividing retinal neuroblasts between the pigmented and albino retina, studies were undertaken to determine whether this has an impact on the orientation of dividing cells. Perhaps cells which are not correctly localised to the VM during cell division are unable to utilise a putative polarity signal (potentially mediated by the RPE or dividing neighbours) as a reference to define apical-basal polarity. In a study of the developing cat retina, a subset of mitotic cells were found to divide in the inner region of the NBL, and exhibited no preferred cleavage orientation (Robinson *et al.*, 1985). Scatter plots are therefore presented plotting cleavage orientation against the distance of the cell from the VM (Figure 3.4.4).

For both pigmented (Figure 3.4.4 A) and albino (Figure 3.4.4 B) data R^2 values were extremely low (<0.01) and the gradient was minimal (<0.01). Hence, within the limits of this study there was no correlation between the orientation and position of a dividing cell relative to the VM. As the regions scanned were only 56μm wide in the y-plane any extreme exogenous divisions outside the ventricular zone would not have been detected in this study. However, it is clear from both personal observation and existing literature that if such divisions occur, it is at an extremely low frequency.

Cleavage orientation and mitotic phase

In the developing rat telencephalon dividing neuroblasts undergo extensive metaphase rotations within the plane of the neuroepithelium, which only cease upon anaphase entry (Adams, 1996). Similarly, in the mouse fore-brain, neural stem cells undergo bidirectional oscillatory movements within the apical-basal plane which are specific to metaphase (Haydar *et al.*, 2003). Consequently, might data on cleavage orientations be biased by the inclusion of data from anaphase cells? If cells rotate within the apical-basal plane, the cleavage orientation of a cell in metaphase might not reflect the final orientation adopted at cytokinesis. If this were true, and the rotations were extensive both in duration and angular displacement, one would expect extreme cleavage

orientations (i.e. ≥45°) and levels of variance to be unequally distributed between metaphase and anaphase cell populations.

Scatter plots are presented plotting the inter-centrosomal distance (i.e. the distance between the two poles of a dividing cell) against the mitotic spindle orientation (Figure 3.4.5). The inter-centrosomal distance is assumed to be correlated with the phase of the mitotic division. Given that retinal neuroblasts are relatively homogenous in size, metaphase is characterised by a comparatively small inter-centrosomal distance, whilst anaphase is characterised by a larger inter-centrosomal distance. By simultaneously noting the inter-centrosomal distance of dividing cells and scoring them as being either in metaphase, early anaphase or late anaphase on the basis of overall morphology and the appearance of their chromatin one can detect this general correlation and even make a rough estimation of the cut-off value. Thus, inter-centrosomal distances <5μm were taken to be indicative of a cell in metaphase, whilst distances ≥5μm were assumed to be indicative of an anaphase cell.

For both pigmented (Figure 3.4.5 A) and albino (Figure 3.4.5 B) data R^2 values were low (<0.01) and the gradient was minimal (<0.01). In addition, the spread and variance of cleavage orientations is independent of inter-centrosomal distance. The data is clumped independently with respect to both the x- and y-axes, indicating that neither of these parameters is randomly distributed. There is clearly no correlation between the two parameters (cleavage orientation and inter-centrosomal distance), suggesting that the data will not be biased by the inclusion of values from cells in anaphase.

Cleavage orientation; patterns over time

The distribution of dividing retinal neuroepithelial cells relative to the plane of the tissue are shown in Figures 3.4.6 – 3.4.9 in a series of frequency distributions. The data have been grouped into 10° bins ranging from 0° to 90°, (representing horizontal and vertical divisions respectively) for both pigmented (A) and albino (B) retinae at E18, P1 and P4. In addition, superimposed are pie-

charts, indicating the proportion of horizontal (dark grey) to vertical (light grey) divisions. Horizontal and vertical divisions were defined as divisions occurring at an angle of $<45^{o}$ or $\geq 45^{o}$ relative to the VM respectively.

In pigmented retinae at all time points studied there was a unimodal preference for divisions occurring at $0\text{-}10^{o}$ relative to the reference plane, i.e. with the mitotic spindle aligned parallel to the plane of the RPE (a horizontal division). The distribution of orientations was found to shift significantly over time, such that the proportion of all divisions exhibiting a vertical orientation was maximal around the day of birth. Levels rose from 1% at E18 to a peak of 9% at P1 (p=0.002, chi-squared test), subsequently falling back to 3% at P4 (p=0.051) and finally, dropping to 0% at P6 (p=0.07). These findings are in accordance with Cayouette *et al.* (2001) with respect to the changing pattern of cleavage orientations over time.

In the albino retina there was also a unimodal preference for horizontal divisions at all time-points studied. However, the shift in proportion of horizontal to vertical divisions over time was abnormal with respect to the pattern observed in the pigmented retina. The proportion of vertical divisions rose from 4% at E18 to 10% at P1, (p=0.026, chi-squared test). However, after P1 the proportion of vertical divisions did not subsequently drop, but rose to 11% at P4, a value which is significantly different from E18 (p=0.011), but not P1 (p=0.615). The proportion of vertical divisions finally began to fall by P6 (p=0.0183). These findings suggest a regulatory failure in the control of cleavage orientation in the albino retina manifested as an excessive level of vertical divisions at P6. This is supported by statistical comparison of data from pigmented and albino retinae at corresponding time-points. Significant differences in the proportion of vertical divisions was detected between pigmentation types at P4 and P6 only (p=0.15, 0.693, 0.013 and 0.007 at E18, P1, P4 and P6 respectively).

As data were compared using a distribution-based, non-parametric test, there was no consideration of potential inter-replicate variation, i.e. inherent variation between individual animals from each time-point and pigmentation group. Consequently, it is possible that data was skewed by extreme outliers, with a

potential to create false positives in a chi-squared test. Hence, data were re-analysed using a completely different method. The proportion of all cell divisions that were vertically oriented was calculated for individual animals, and mean values plotted in the form of a histogram (Figure 3.4.10). Error bars represent the standard errors of the mean. Plotted in this format, the data supports the findings of the alternative analysis. The proportion of vertical divisions is significantly elevated in the albino retina at P1 and P4 (p=0.024 and 0.022 respectively, independent samples t-test). Thus, patterns of cleavage orientation are abnormal in the albino retina, the peak in proportion of verticals being both elevated and delayed relative to the pigmented.

Cleavage orientation; spatiotemporal gradients

To consider the shifting pattern of cleavage orientations within the framework of the centre-to-periphery gradient of retinal development, data was separated into two groups according to the region of origin; central or peripheral. In addition to the four time-points already examined (E18, P1, P4 and P6), further data were gathered from pigmented tissue at E20 (central retina) and albino tissue at P6 (peripheral retina) in an attempt to generate an higher sampling frequency at key stages.

Data has been plotted with developmental stages on the x-axis and the proportion of all divisions that were vertically oriented on the y-axis (Figure 3.4.11A&B). In addition, a second plot is provided, in which results from central retina have been phase-shifted by a 24 hour delay on the x-axis, and the peripheral results have been shifted by a 24 hour advance (Figure 3.4.11A'&B'). Hence, there is a compensation for the reported 48 hour delay between these regions, which is a manifestation of the centre-to-periphery gradient of development within the retina (Young, 1983). Consequently, one can examine the shifting patterns of cleavage orientation over time as they occur within the centre-to-periphery axis as a single developmental event. Essentially, one is standardising data relative to a reference point midway between the central and peripheral retina. If a developmental event occurs within a centre-to-periphery

gradient, at any single time-point, a snapshot of the central retina will theoretically resemble the pattern which will be found in the reference region 24 hours later, (the centre being developmentally more advanced). Conversely, a snapshot of the peripheral retina will resemble the pattern found in the reference region 24 hours prior, (the periphery being comparatively immature).

By connecting sequential values for the phase-shifted pigmented central and peripheral data (combined in a single plot) a curve is generated with a sharp peak around the day of birth (Figure 3.4.11A'). This would suggest that the systematic shift towards an increased prevalence of vertical divisions around P1 occurs within the framework of the centre-to-periphery gradient of development, and as with other developmental processes, is delayed by approximately 48 hours in the periphery relative to the centre.

In the albino however, a very different pattern emerges (Figure 3.4.11B'). In the central retina the proportion of vertical divisions increases at each consecutive time-point, so that by P4 when levels of proliferation are beginning to drop off, vertical divisions constitute 18.3% of the total. In the peripheral retina, the pattern of cleavage orientations does not shift over time, and 6.4±0.6% of all divisions are vertically aligned at all time-points studied. Thus, in the central albino retina the increasing prevalence of vertical divisions continues unchecked postnatally, with no indication that this pattern will be broken before proliferation ceases. In the periphery, the distribution of cleavage orientations does not change over time. Instead, the proportion of vertical divisions fluctuates about a base-line minimum.

Effects of L- and D-DOPA administration

In retinal tissue explants, the RPE (or an RPE-derived factor) influences the orientation of cell division within the NBR and is conducive to the adoption of a vertical orientation (Cayouette *et al.*, 2001). Furthermore, patterns of cleavage orientation are disrupted in the early postnatal albino retina. As the developmental abnormalities of the retina associated with albinism must

ultimately be traced back to the RPE, is it possible that an RPE-derived melanin precursor is involved in the regulation of cleavage orientations? To examine this hypothesis, the effects of L-DOPA on patterns of cleavage orientation were ascertained. Past studies have demonstrated its putative role in regulating cell division (Wick, 1977; Akeo *et al.*, 1994; Ilia and Jeffery, 1999).

Subcutaneous injections of L-DOPA in conjunction with its decarboxylase inhibitor were administered to P3.5 Wistar pups which were subsequently killed and fixed for analysis 18 hours later (~P4). Negative controls were administered D-DOPA, a non-active isoform, at the same concentration. The data are presented in the form of a series of frequency histograms illustrating the distribution of cleavage orientations relative to the VM as well as superimposed pie-charts describing the relative proportion of horizontal to vertical divisions (Figure 3.4.12). Note that half of the data is replicated from Figure 3.4.8 so that direct comparisons can be made with data from DOPA-treated tissue.

L-DOPA administration reduced the proportion of vertical divisions in the albino to a level comparable to that in the pigmented retina (3%), an effect which was significant at the 1% level (p=0.004, chi-squared test). Administration of D-DOPA however did not influence the distribution of cleavage orientations (p=0.882). This would suggest that the effect of L-DOPA on the distribution of cleavage orientations is a biological response as opposed to a cytotoxic effect.

Numb localisation patterns

Having demonstrated the existence of spatiotemporal abnormalities in the regulation of cleavage orientations as well as subtle defects in cell localisation in the albino retina, the issue of cell fate determinant localisation was addressed. A brief study was therefore undertaken to determine patterns of Numb distribution in the early postnatal retina, (when vertical divisions are most abundant). Numb is a cytoplasmic cell fate determinant protein for which distribution patterns have been well characterised in a range of vertebrate and invertebrate systems. In addition, previous studies have highlighted its putative

role in the specification of late-born cell types in the rat retina (Cayouette *et al.*, 2001; Cayouette and Raff, 2003).

Staining was undertaken on P1 and P4 pigmented and albino rat tissue (Figure 3.4.13). These time-points were selected as they coincide with documented abnormalities in levels of proliferation, cell cycle exit and cleavage orientation in the albino retina; see chapter 2 (Ilia and Jeffery, 1999; Donatien and Jeffery, 2002). No quantification was undertaken as the signal was highly variable, even between adjacent regions on a single slice. This would seem to be characteristic of all commercially available antibodies against Numb when applied to rodent retinal tissue (Cayouette, 2003). However, where a strong signal was obtained, staining patterns were consistent.

No gross differences were visible between patterns of Numb staining in the pigmented and albino rat retina. Staining was relatively diffuse and localised to two main regions; the apical surface of the NBR, and a subset of post-mitotic cells in the GCL and pINL (Figure 3.4.13). These findings support previous studies which demonstrate Numb expression in both retinal progenitors, and post-mitotic cells of the vertebrate retina (Dooley *et al.*, 2003), and are consistent with a model of differential inheritance patterns during vertical divisions of the retina (Cayouette *et al.*, 2001; Cayouette and Raff, 2003).

Null mutations in tissue polarity genes such as *frizelled* and *dishevelled* disrupt the mitotic spindle orientation of SOP divisions relative to the anterior-posterior axis in Drosophila, whilst the association between Numb localisation and the cleavage plane of subsequent divisions remains intact. (See Shulman *et al.* (1998) for a review). This would imply the existence of multiple parallel mechanisms which define/maintain axis polarity at the cell and tissue level. Though abnormalities in cleavage orientation have been demonstrated within the developing albino retina, there was no evidence of associated changes in patterns of Numb localisation at the gross level.

Müller cell density

Müller glia were identified in the retina by staining for vimentin (Figure 3.4.14). Cell densities were quantified in the adult (9 week old) pigmented and albino retina at all retinal eccentricities (Figures 3.4.15 & 3.4.16). Data are presented in the form of a series of scatter plots from a randomly selected pigmented and albino retina (Figure 3.4.15) as well as for the averaged data from all 4 retinae (Figure 3.4.16). Statistical analyses were first performed to determine whether Müller cell densities varied according to retinal eccentricity. Only the most peripheral and central counts (corresponding to the regions directly adjacent to the optic nerve head and *orra serrata*) were found to be significantly different at the 5% level (p=0.024; ANOVA test).

Müller cell densities did not vary as a function of retinal eccentricity. This would seem to contradict previous studies which have shown that in the mammalian retina, Müller cell densities largely follow the isodentity lines of neurones, reaching a peak in the central retina; rabbit (Robinson and Dreher, 1990; Reichenbach *et al.*, 1991; Dreher *et al.*, 1992), cat, dog, human, echidna, guinea pig (Dreher *et al.*, 1992). This is in contrast to the retina of "lower vertebrates" which exhibit a uniform distribution of Müller cell densities and a general reduction in number; toad (Gabriel *et al.*, 1993), turtle (Gaur *et al.*, 1988). However, in the rodent retina, cell density gradients are flattened, and elevations in Müller cell numbers are restricted to a small elliptical region of the dorsoventral retina (Dreher *et al.*, 1992). In this study no attempt was made to keep track of nasal/temporal orientation and counts were made from horizontal sections rather than whole-mount preparations. Consequently, it is likely that this specialised area was not sampled, and hence, the subtle centre-to-periphery density gradient was not detected. Similarly, in a comprehensive study of the mouse retina the authors were unable to detect any difference in Müller cell densities between the central and peripheral retina (Jeon *et al.*, 1998). Their results were also based on counts made from horizontal sections rather than whole-mount preparations.

Having demonstrated that Müller cell densities varied minimally across the retina, comparisons were made between pigmented and albino retinae. An extensive ANOVA test was performed on all the data from both pigmented and albino tissue combined. However, the first and last counts (corresponding to regions directly adjacent to the *orra serrata* and optic nerve head) were discarded from both data-sets. The only value found to differ significantly was the third count along in the albino retina corresponding to a region 600µm from the optic nerve head. In this region the density of Müller cells was found to be significantly elevated relative to regions of the pigmented retina in which densities were at a minimum. However, given that this difference was not significant relative to the corresponding region of the pigmented retina and was an isolated example, it would seem to be an artefact of such a wide-ranging statistical comparison. Consequently, there was no evidence to suggest that Müller cell densities differ significantly between the pigmented and albino retina, nor that there is a shift in cell fate postnatally, as current models would predict (Cayouette *et al.*, 2001; Cayouette and Raff, 2003).

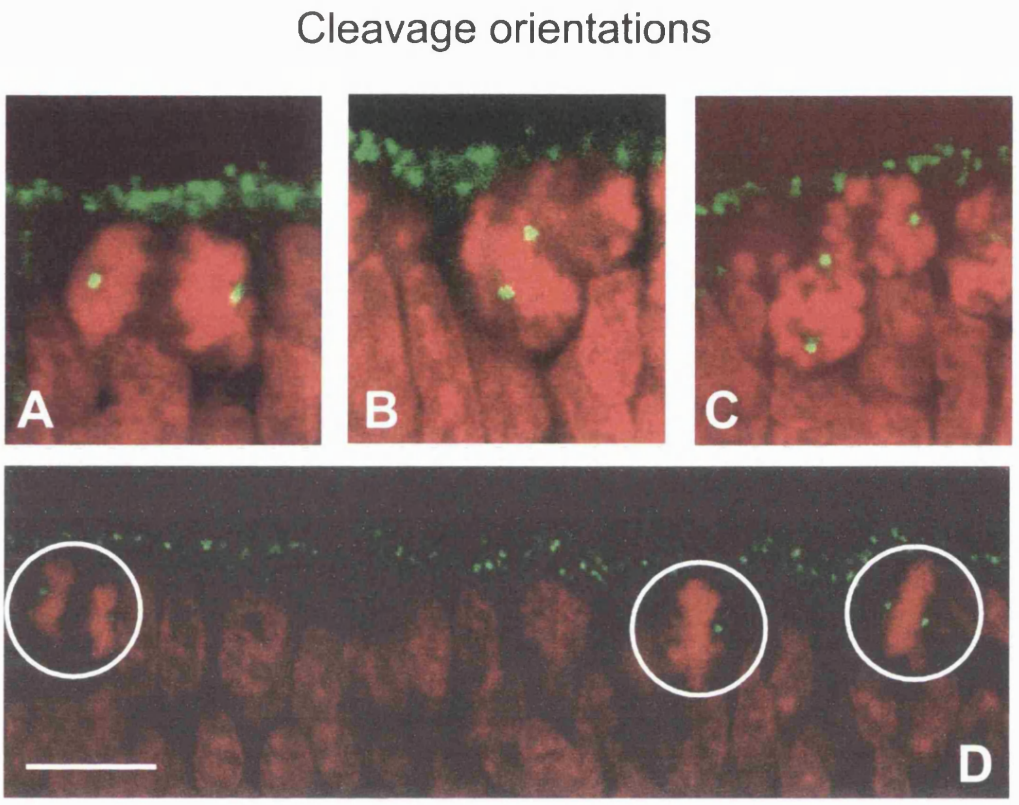

Figure 3.4.1 The orientation of cell division was visualised in the developing pigmented and albino retina using antibodies against γ-tubulin, the primary protein component of the centrosomes. Tissue was counterstained with propidium iodide to visualise nucleic acid. The centrosomes are replicated prior to M-phase and distributed to opposing ends of the cell where they form the mitotic spindle poles. They provide an indication of the orientation of the mitotic spindle, which is perpendicular to the cleavage plane. Orientations were then calculated relative to a reference plane defined by the outer limit of the NBR. High magnification confocal images of cells in (A) anaphase (horizontal orientation), (B) metaphase (intermediary orientation), and (C) early anaphase (vertical orientation) infront of another anaphase cell (horizontal orientation) are presented. (D) Lower magnification image of the NBR showing the relationship between dividing cells and the VM. Note the line of centrosomes that define the outer limit of the NBR. Scale bar=10μm.

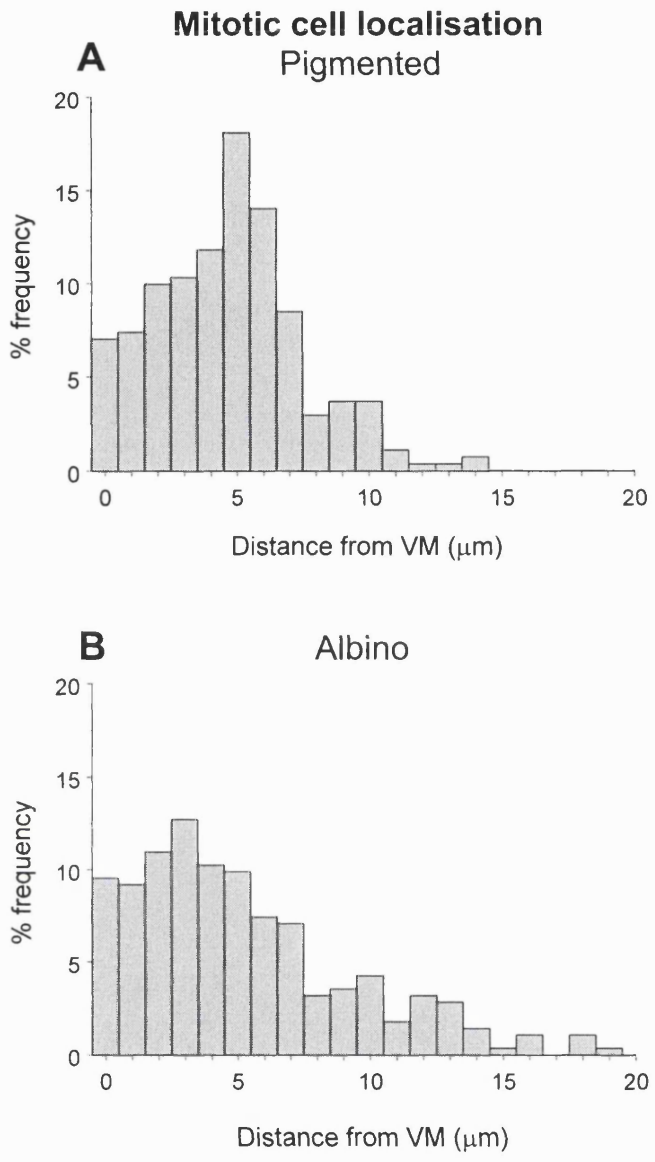

Figure 3.4.2 The distribution of distances between the VM and dividing retinal neuroblasts is presented for (A) pigmented and (B) albino tissue. Data for the pigmented retina is normally distributed about a mean of 5.2μm (p=0.558). Distances in the albino however are non-normally distributed (p=0.001). The null hypothesis in this form of KS-test is that the data is normally distributed, hence, a p value of 0.001 implies that there is only a 0.1% chance that the data fits the predicted model. In addition, data from the albino is heavily skewed with a greater range than the pigmented (19.57μm compared to 14.62μm), as well as a larger standard deviation (4.1μm compared to 2.8μm). A direct comparison of the two distributions highlights a difference which approaches statistical significance at the 5% level (p=0.064, KS-test). Data has been collated from E18, P1 and P4; N=9 eyes examined (each from a different animal) per pigmentation type, and n= 271 and 283 cells analysed from pigmented and albino retinae respectively.

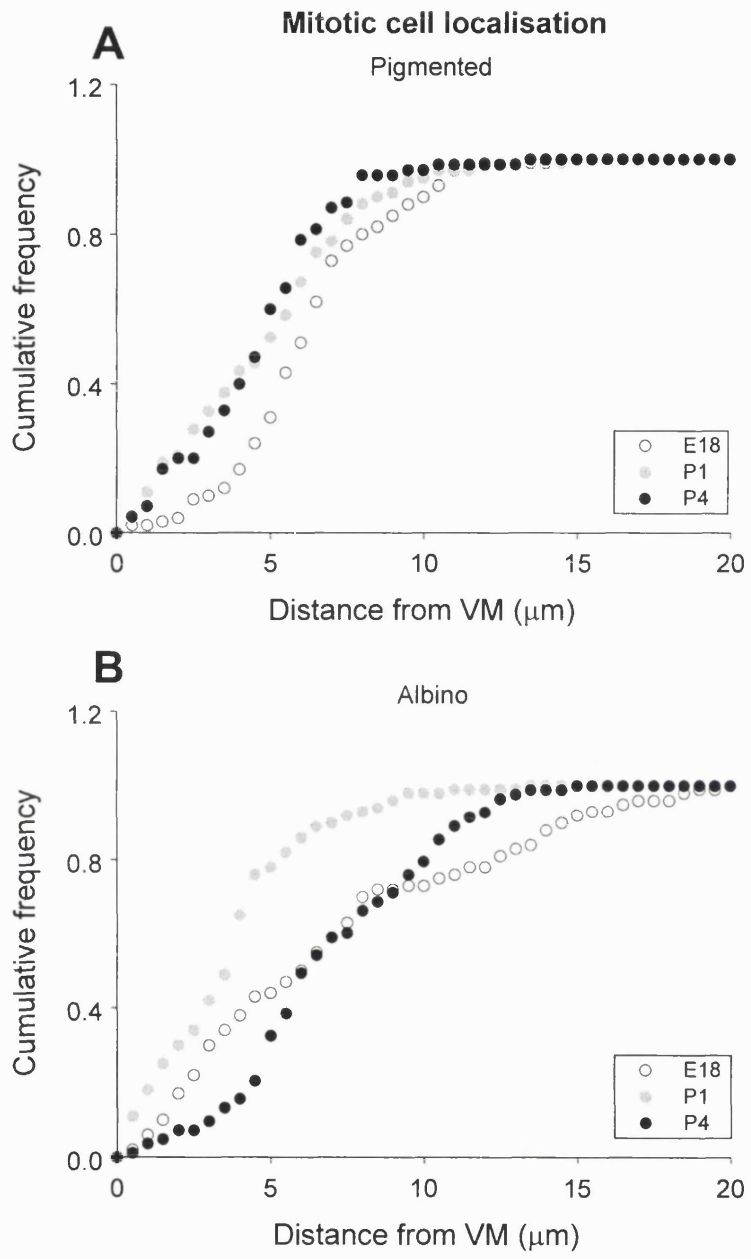

Figure 3.4.3 The distribution of distances between the VM and dividing retinal neuroblasts is presented for (A) pigmented and (B) albino tissue and is broken down into its composite developmental stages; E18, P1 and P4. Tests for normality (KS-test) indicate that in the pigmented retina, data closely fits a normal distribution at all time-points examined, (all p values are >0.2; the null hypothesis being that the data fits the predicted model). In the albino retina data closely fits the idealised distribution at P4 (p=0.5), but not at E18 and P1 (p= 0.09 and 0.06 respectively). The number of cells analysed per time-point = E18(100), P1(101) and P4(70) for the pigmenteds; and E18(100), P1(100) and P4(83) for the albinos. Three retinae (each from a different animal) were examined per group.

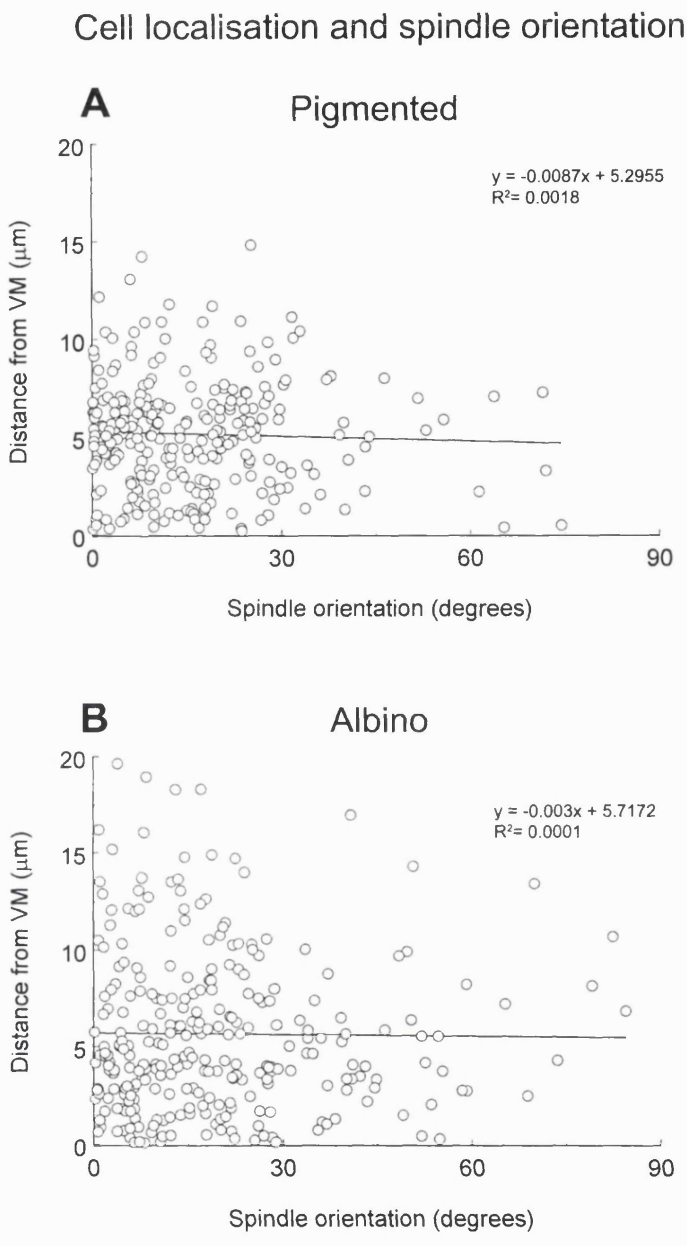

Figure 3.4.4 Correlation between the orientation of a dividing cell and its distance from the VM. Scatter plots are presented for the (A) pigmented and (B) albino retina, with a fitted regression line. Superimposed is the equation of the fitted line and an R^2 value which indicates the fit of the data to the model. There is no detectable relationship between these two parameters. It is interesting to note however that for the albino retina, the spread of data on both the x- and y-axes is greater than for the pigmented, implying a higher number of vertical divisions and subtle abnormalities in cell localisation. Data has been collated from E18, P1 and P4; N=9 animals examined per pigmentation type, n= 271 and 283 cells analysed from pigmented and albino retinae respectively.

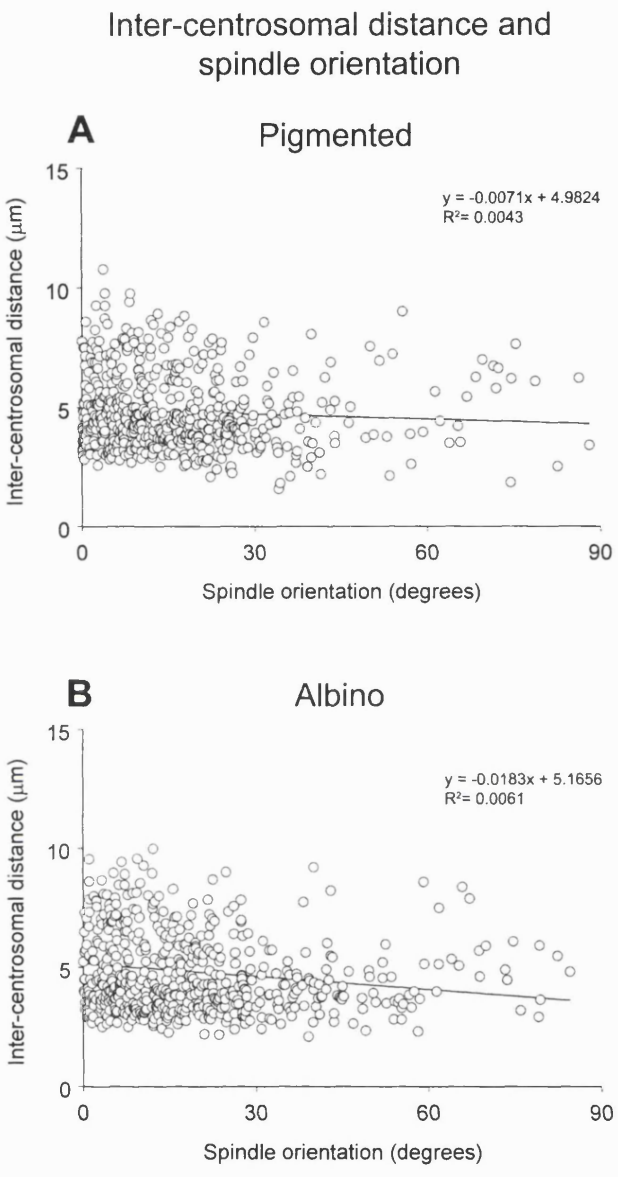

Figure 3.4.5 Correlation between the orientation of a dividing cell and the inter-centrosomal distance. Scatter plots are presented for the (A) pigmented and (B) albino retina, with fitted regression line. Superimposed is the equation of the fitted line as well as an R^2 value which indicates the fit of the data to the model. The inter-centrosomal distance is roughly correlated to the phase of the division, experiments having determined that distances <5µm are indicative of cells in anaphase, whilst distances ≥5µm are indicative of cells in anapahase. There is no detectable relationship between these two parameters, suggesting that the data is not biased by the inclusion of anaphase cells. Data has been collated from E18, P1 and P4; N=9 animals per pigmentation type, n= 271 and 283 cells analysed from pigmented and albino retinae respectively.

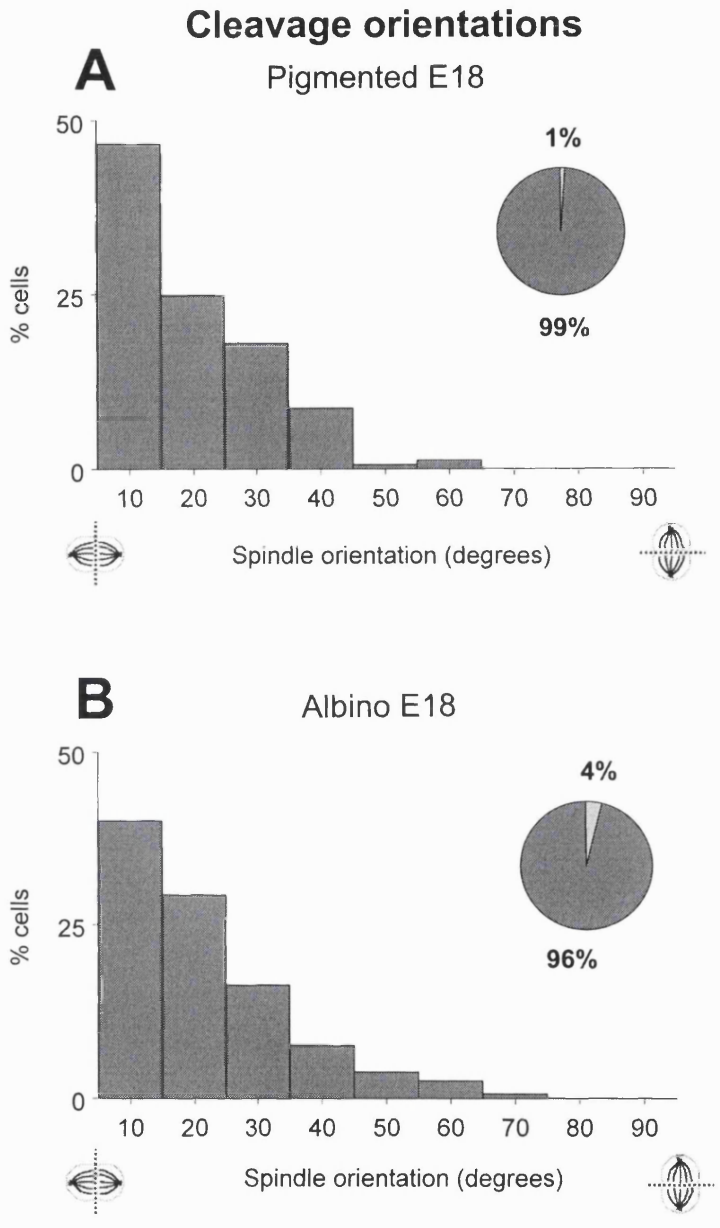

Figure 3.4.6 Frequency histograms of the distribution of cleavage orientations relative to the VM are presented for the (A) pigmented and (B) albino retina at E18. Superimposed are pie-charts describing the relative proportion of horizontal (dark grey) to vertical (light grey) divisions. No difference in the proportion of vertical divisions was found between the pigmented and albino retina at this stage of development (p=0.15, chi-squared test). Data was gathered from 4 retinae (each from a different animal) per pigmentation group, and n=161 and 160 cells analysed from pigmented and albino retinae respectively.

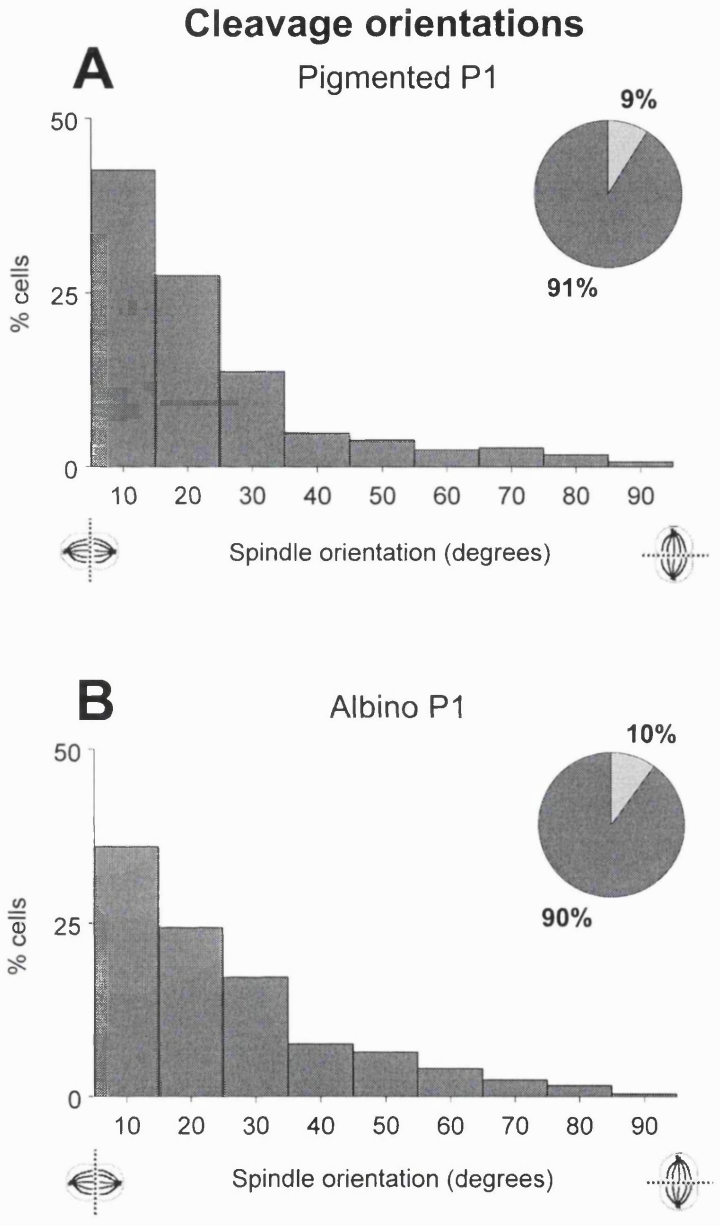

Figure 3.4.7 Frequency histograms of the distribution of cleavage orientations relative to the VM are presented for the (A) pigmented and (B) albino retina at P1. Superimposed are pie-charts describing the relative proportion of horizontal (dark grey) to vertical (light grey) divisions. No difference in the proportion of vertical divisions was found between the pigmented and albino retina at this stage of development (p=0.693, chi-squared test). N=12 pigmented and 5 albino eyes examined (each from a different animal); n=290 and 250 cells analysed from pigmented and albino retinae respectively.

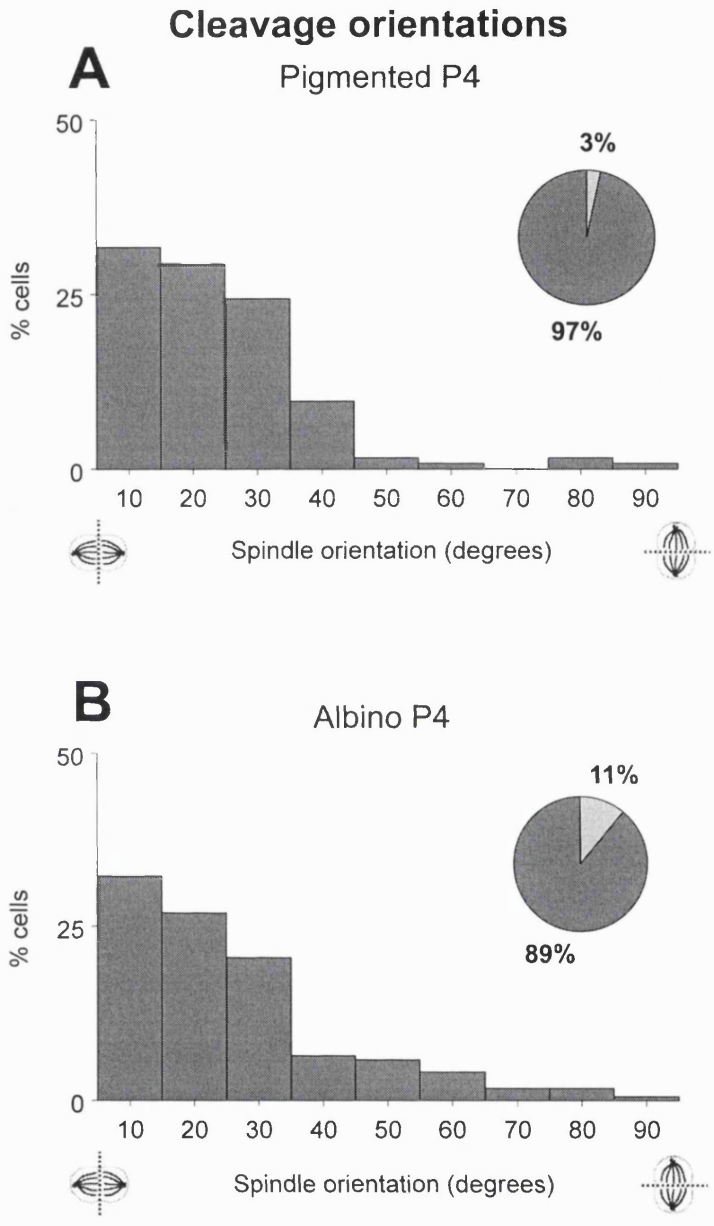

Figure 3.4.8 Frequency histograms of the distribution of cleavage orientations relative to the VM are presented for the (A) pigmented and (B) albino retina at P4. Superimposed are pie-charts describing the relative proportion of horizontal (dark grey) to vertical (light grey) divisions. The proportion of vertical divisions was significantly elevated in the albino retina relative to the pigmented at this stage of development (p=0.013; chi-squared test). N=3 pigmented and 4 albino eyes examined (each from a different animal); n=123 and 171 cells analysed from pigmented and albino retinae respectively.

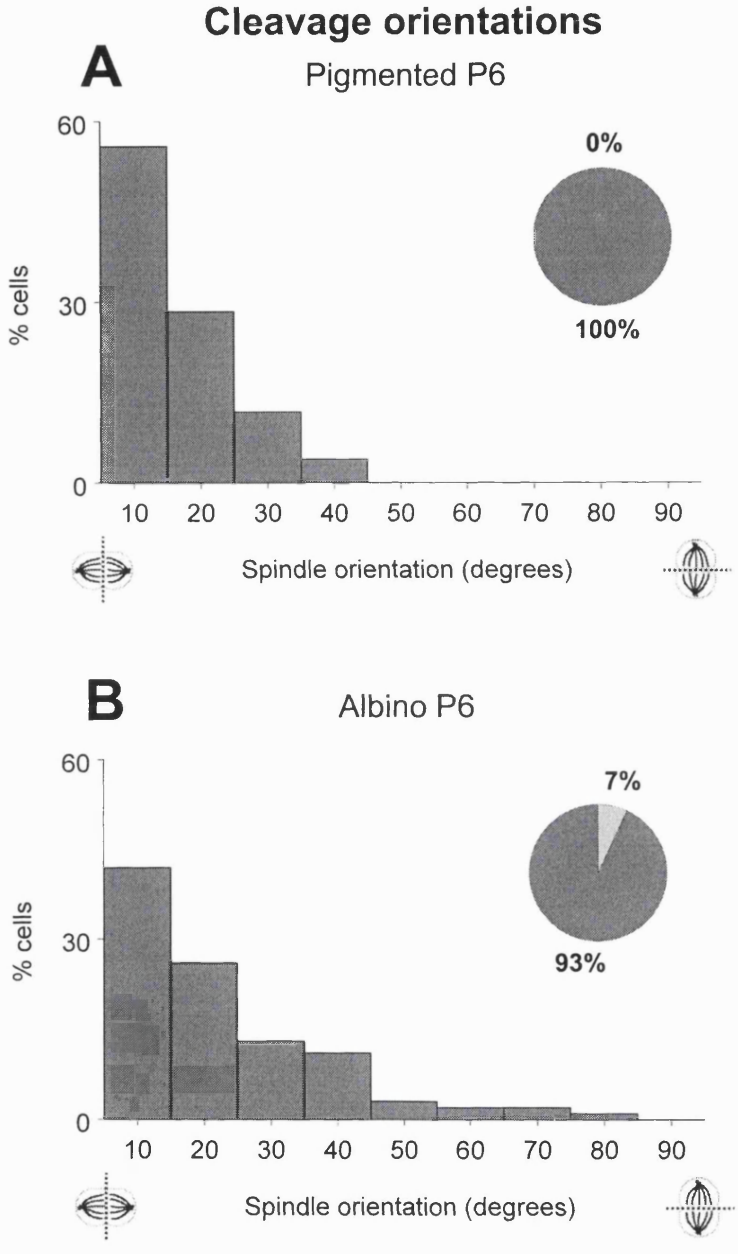

Figure 3.4.9 Frequency histograms of the distribution of cleavage orientations relative to the plane of the tissue are presented for the (A) pigmented and (B) albino retina at P6. Superimposed are pie-charts describing the relative proportion of horizontal (dark grey) to vertical (light grey) divisions. The proportion of vertical divisions was significantly elevated in the albino retina relative to the pigmented at this stage of development (p=0.007; chi-squared test). Data was gathered from 3 retinae (each from a different animal) per pigmentation group, and n=100 and 102 cells analysed from pigmented and albino retinae respectively.

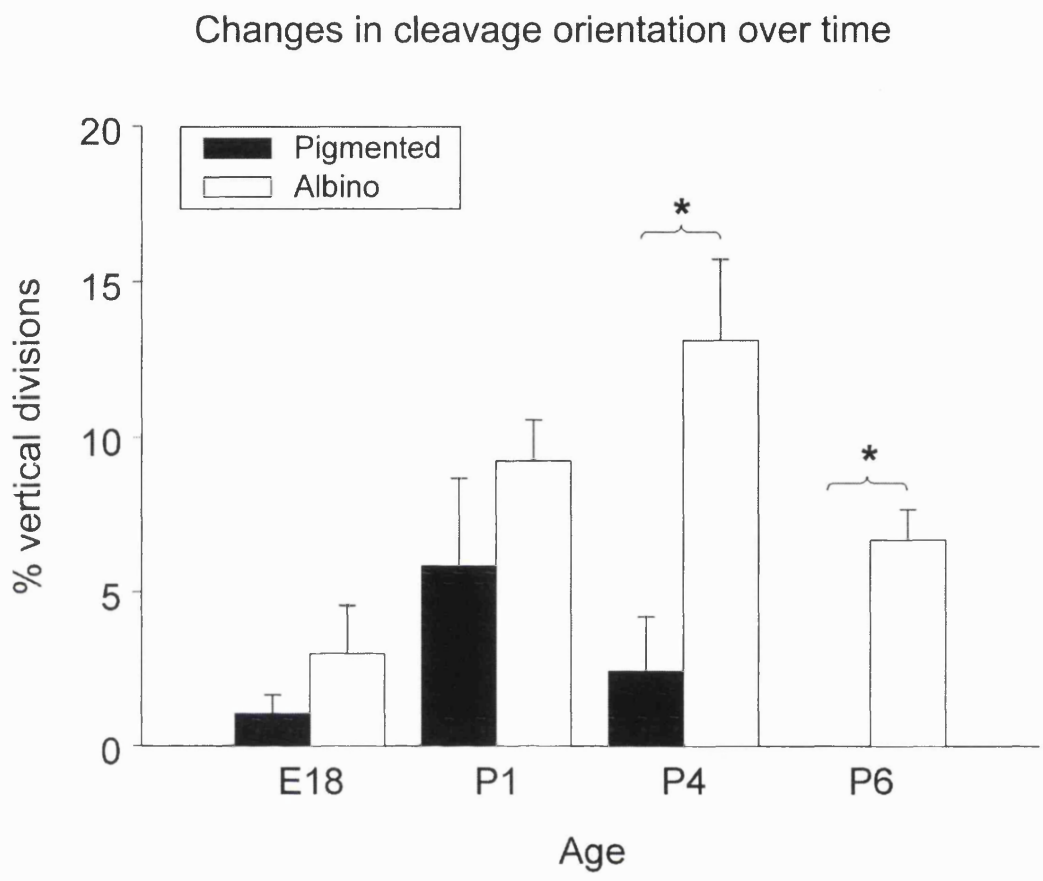

Figure 3.4.10 Data from Figure 3.4.6-3.4.9 has been reanalysed and presented in the form of a bar chart plotting the mean % of divisions that were vertically oriented at each consecutive time-point for both pigmented (black) and albino (white) retinae. Error bars represent the standard error of the mean. In addition to illustrating the shift in patterns of cleavage orientation over time in the wildtype retina, the plot illustrates the nature of the abnormality in the albino.The proportion of vertical divisions is both quantitatively elevated and temporally delayed in the albino. Data was gathered from the three retinae in each group that were most heavily sampled. Pair-wise statistical comparisons were undertaken using the independent samples t-test, and results mirror the results of the chi-squared tests. The number of cells analysed per time-point = E18(118), P1(165), P4(123) and P6(100) for the pigmenteds; and E18(160), P1(210), P4(157) and P6(102) for the albinos.*$p<0.05$.

Cleavage orientation in the central and peripheral retina

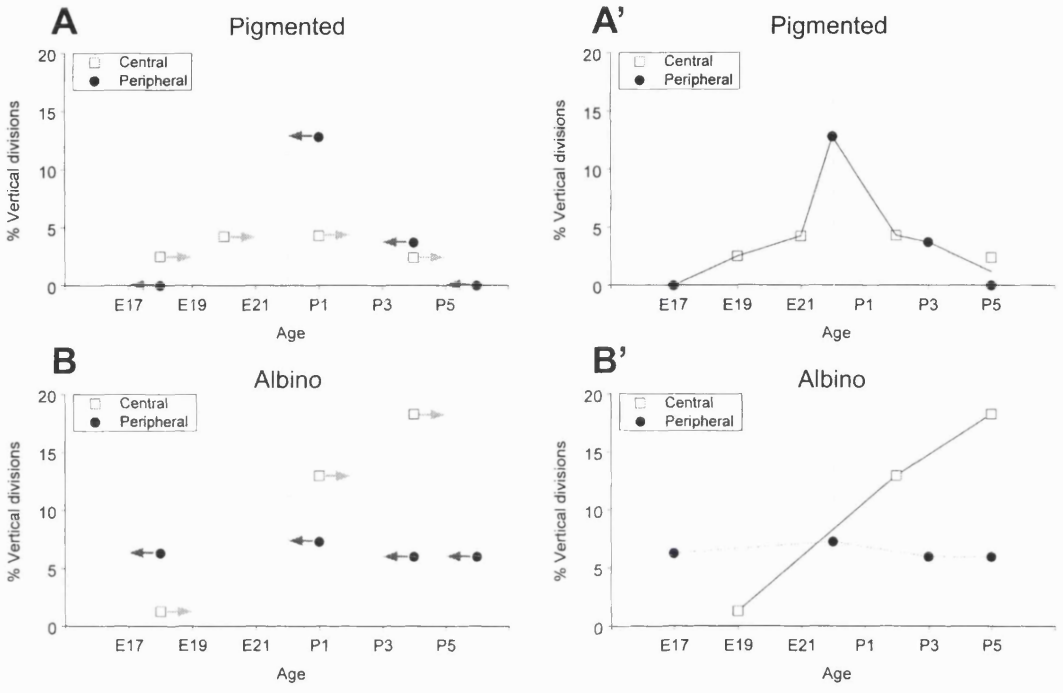

Figure 3.4.11 The proportion of all divisions exhibiting a vertical cleavage orientation (≥ 45° to the plane of the tissue) is presented for the (A) pigmented and (B) albino retina for central and peripheral regions. Developmental stages are represented on the x-axis. In addition, data from the (A') pigmented and (B') albino retina has been replotted such that results from central retina have been phase-shifted by a 24 hour delay, and the peripheral results have been shifted by a 24 hour advance, thus compensating for the reported 48 hour lag between the two regions. Spatiotemporal patterns of cleavage orientation are both quantitatively and qualitatively disrupted in the albino. N=161, 71, 290, 123 and 102 cells analysed at E18, E20, P1, P4 and P6 respectively from the pigmented, and n=160, 250, 171 and 102 cells analysed at E18, P1, P4 and P6 respectively from the albino.

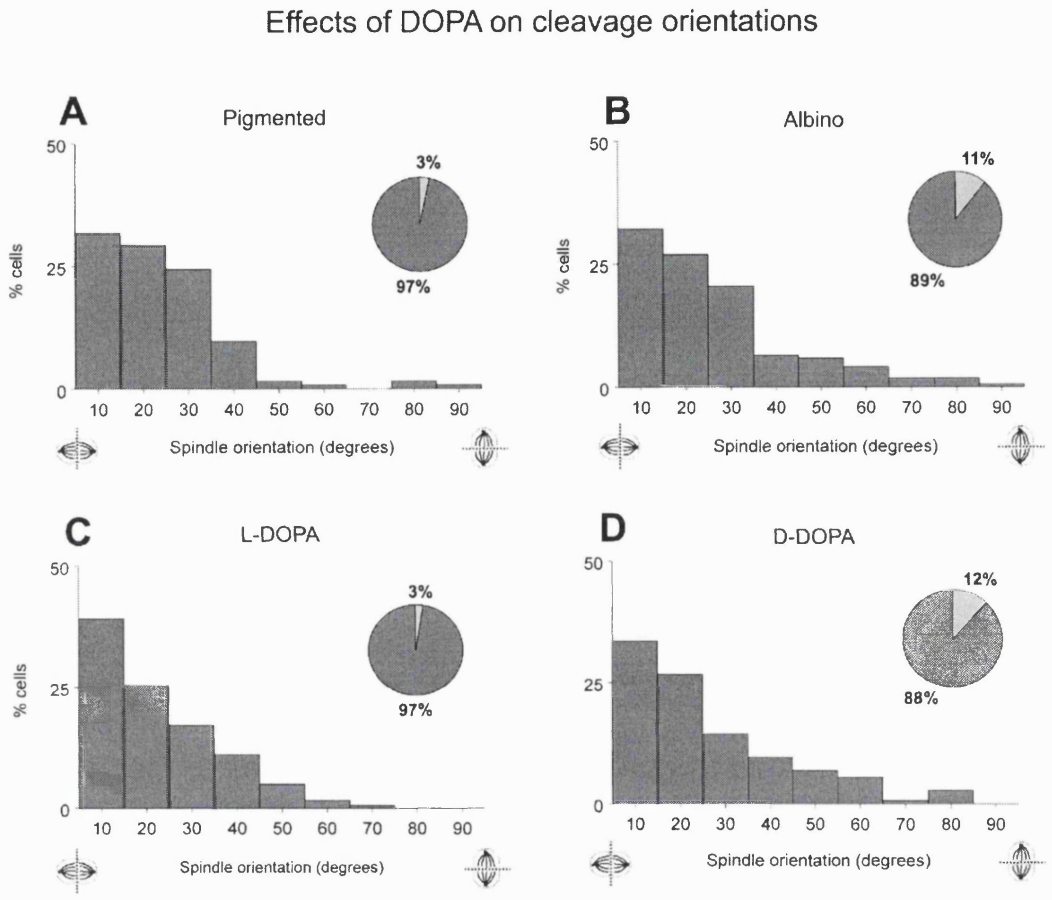

Figure 3.4.12 Frequency histograms of the distribution of cleavage orientations relative to the plane of the tissue are presented for the (A) pigmented, (B) L-DOPA-treated albino, (C) albino and (D) D-DOPA-treated albino retina at P4. Superimposed are pie-charts describing the relative proportion of horizontal (dark grey) to vertical (light grey) divisions. L-DOPA administration was found to significantly reduce the proportion of vertical divisions in the albino retina to a level comparable to age-matched pigmented controls (p=0.004; chi-squared test). D-DOPA, a biologically inactive isoform, had no effect on cleavage orientation, (p=0.882, chi-squared test). Three retinae (each from a different animal) were examined per group, except for the albino control, for which N=4; n=123, 171, 181 and 146 cells analysed from the pigmented, albino, L-DOPA-treated albino and D-DOPA-treated albino retina respectively.

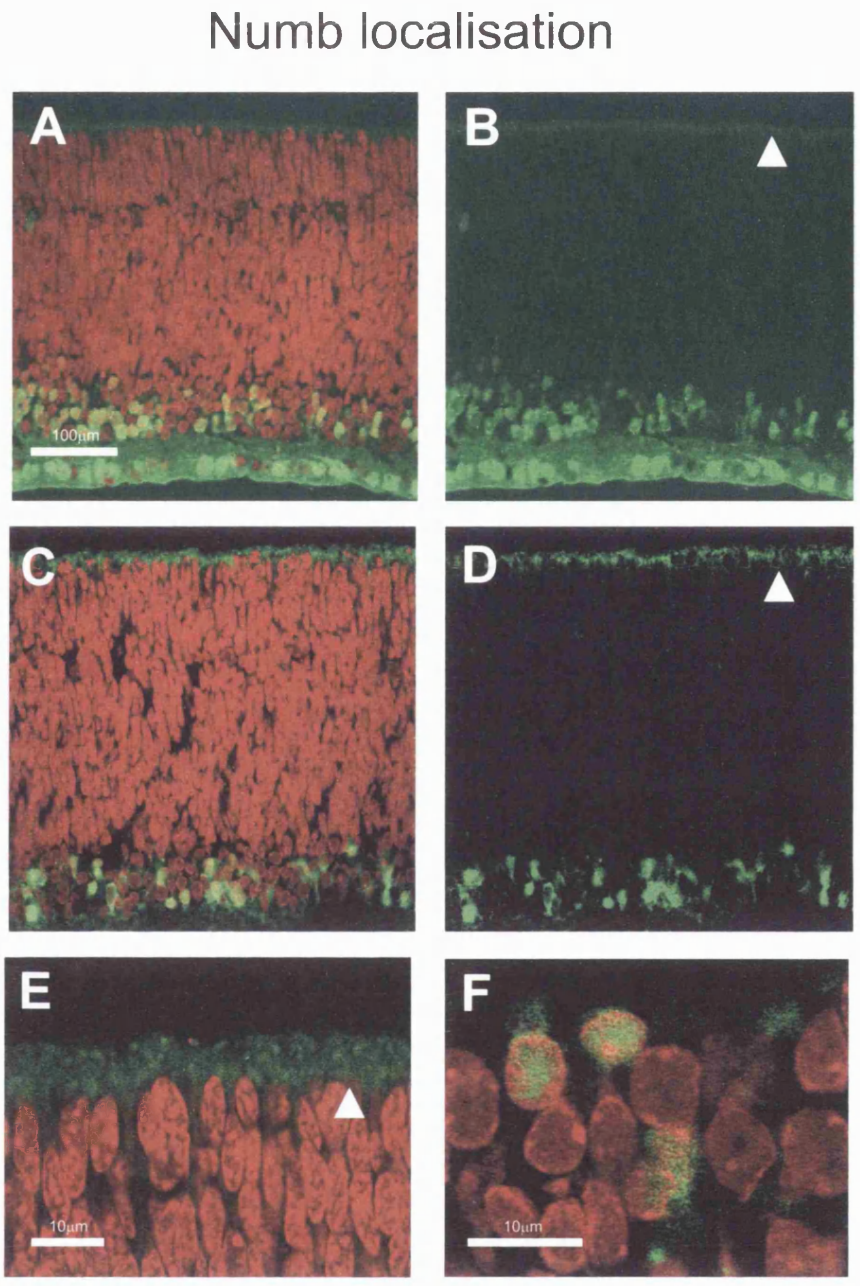

Figure 3.4.13 Confocal micrographs of horizontal retinal sections are presented for the (A-B) pigmented and (C-D) albino retina at P4. Numb, a cell fate determinant which negatively regulates Notch, is labelled in green. The tissue is counterstained with propidium iodide (red). In both phenotypes, Numb is asymmetrically localised to the apical surface of the VM, as well as a subset of differentiated cells in the INL and GCL. This pattern is reinforced in higher magnification images of the (E) VM, and (F) GCL of the albino retina.

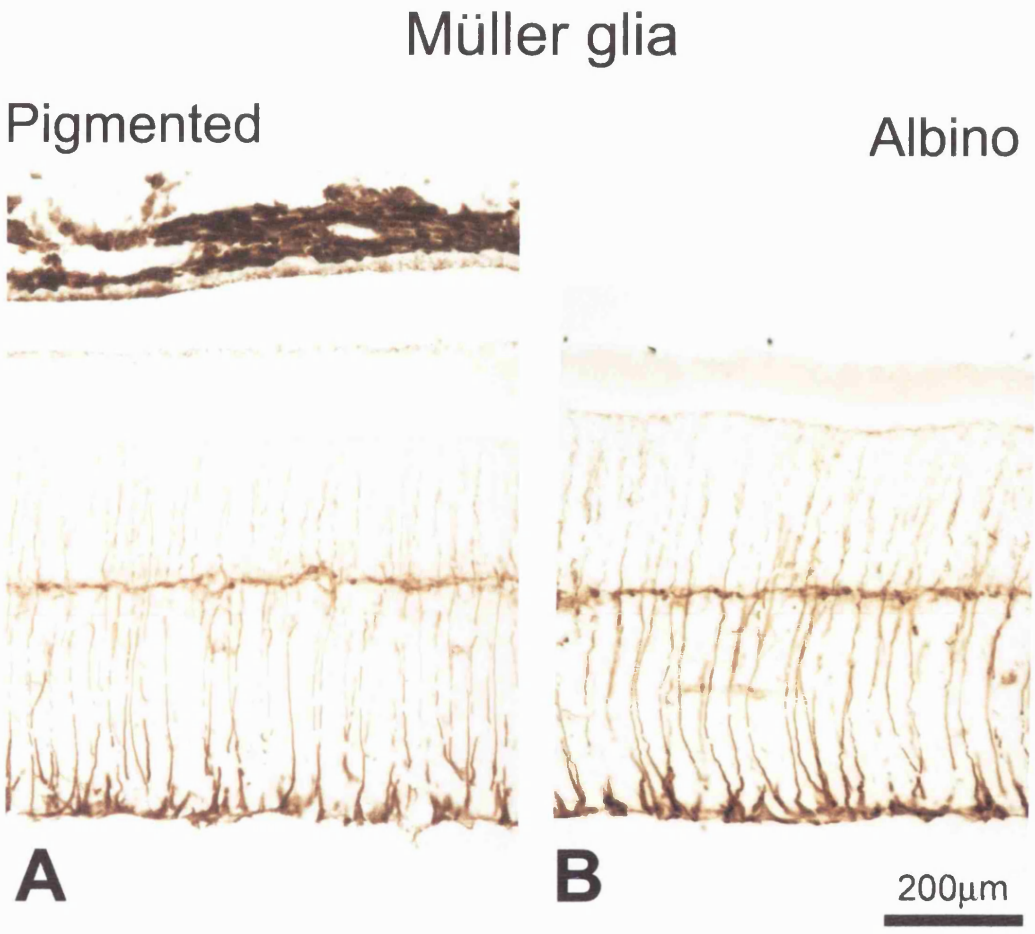

Figure 3.4.14 Light micrographs of horizontal sections passing through the ON in the (A) pigmented, and (B) albino adult rat retina are presented. Antibodies against vimentin, an intermediary filament protein, selectively labelled Müller cell trunks that spanned the thickness of the retina, as well as side-arms that extended tangentially through the OPL.

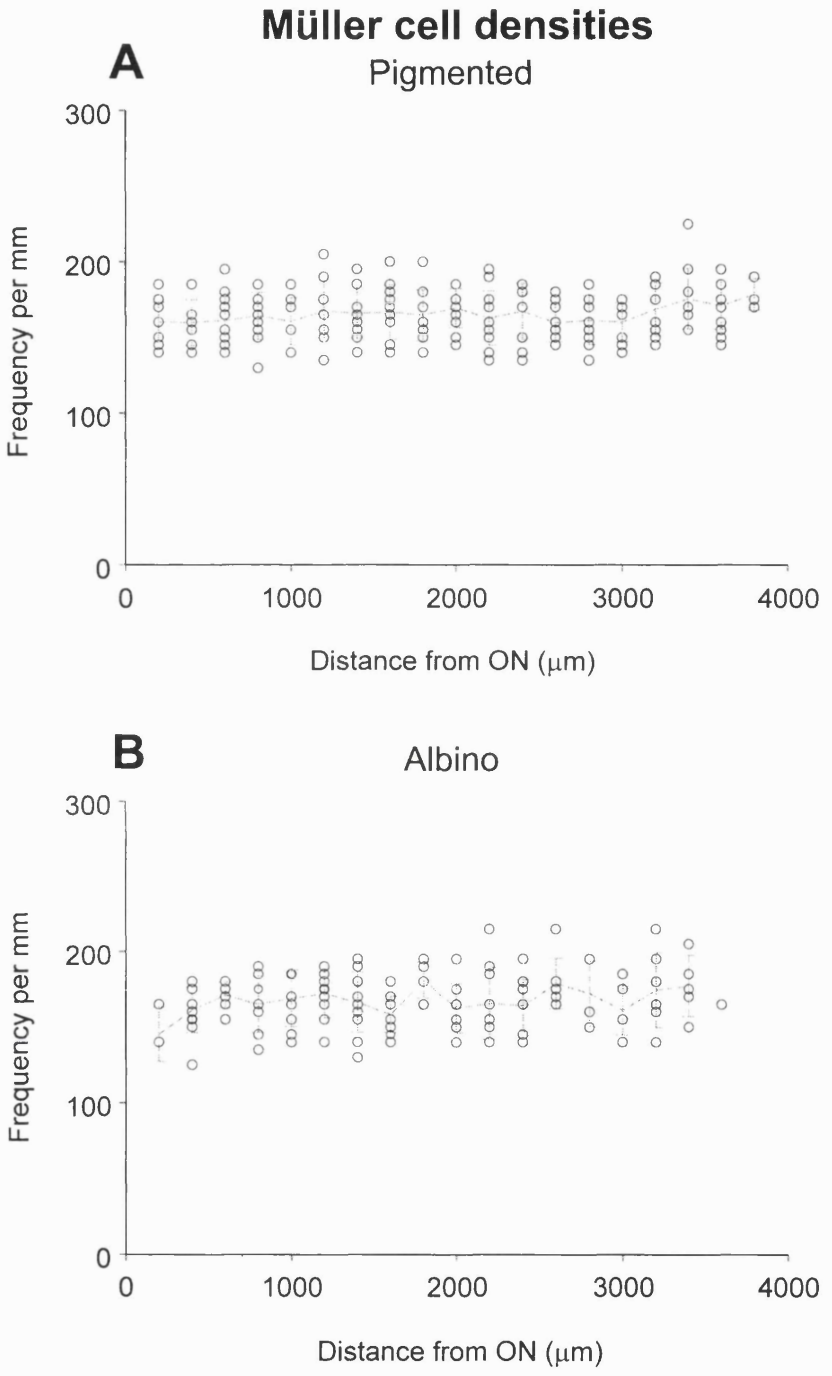

Figure 3.4.15 Müller cell densities are shown in the form of scatter pots with retinal eccentricity running along the x-axis for the (A) pigmented and (B) albino retina. Data is presented for a randomly selected retina from each pigmentation type. For each retina examined a minimum of 5 non-serial sections were analysed. Each hemiretina was 19±1 graticules in length (~4mm).

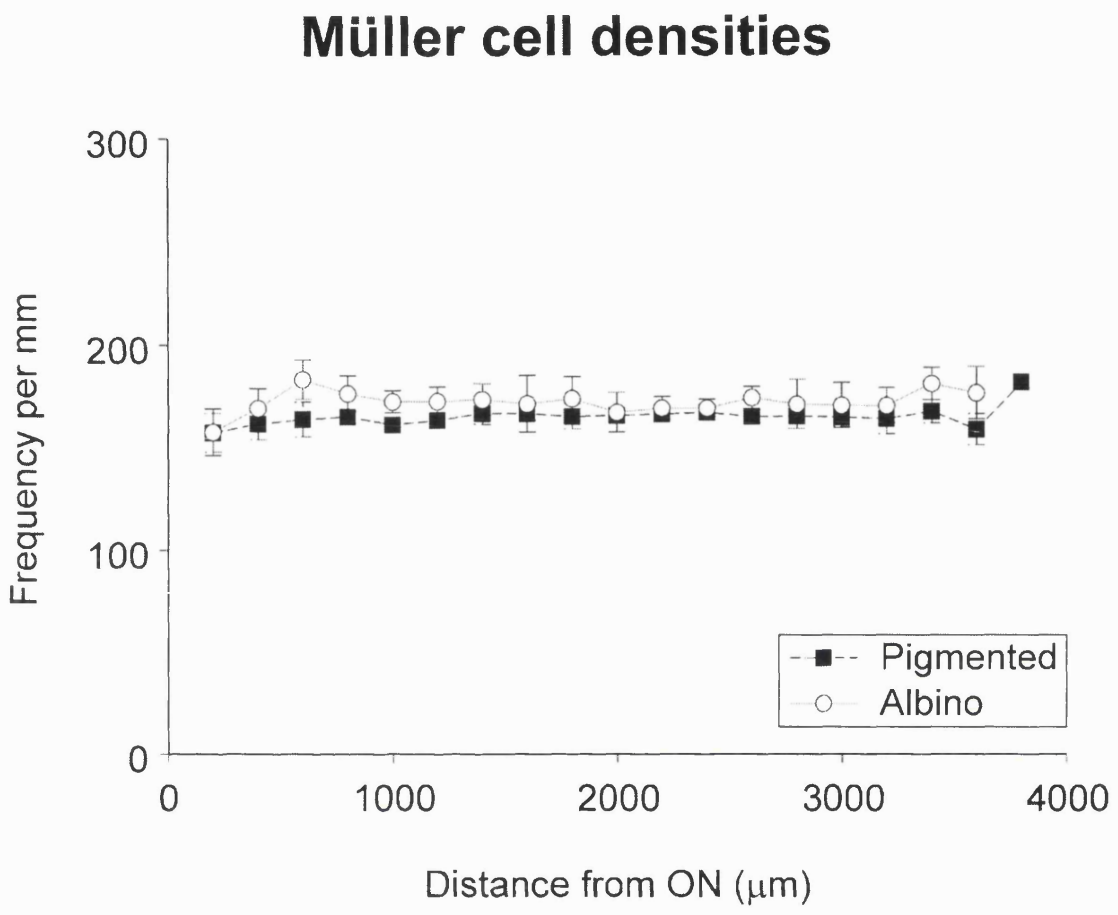

Figure 3.4.16 Müller cell densities are shown in the form of scatter pots with retinal eccentricity running along the x-axis for the (A) pigmented, and (B) albino retina. Data is presented for the entire averaged dataset. Error bars represent the standard deviation. Müller cell densities did not vary significantly as a function of retinal eccentricity, nor as a function of ocular pigmentation levels. 4 retinae were examined per phenotype. For each of these retinae a minimum of 5 non-serial sections were analysed at all retinal eccentricities. Given that each hemiretina was 19±1 graticules in length (~4mm), a total of 666 and 615 fields were scanned from pigmented and albino retinae respectively.

3.5 Discussion

Patterns of cleavage orientation have been analysed in the pigmented and albino rat retina around the time of birth (E18-P6), as previous studies have highlighted this period of development as the peak of cell generation, as well as a critical temporal window with respect to shifting patterns of cleavage orientation. In addition, it corresponds to the period of peak rod cell generation, one of the primary cell types which is affected in the albino retina.

Patterns of cell localisation

In both the pigmented and albino rat, retinal progenitors were closely apposed to the VM during cell division. Though the mean distance between the centre of a dividing cell and the VM did not differ significantly between pigmentation types, the distribution patterns of the data did. Whilst the pigmented data was normally and symmetrically distributed, the albino data was non-Gaussian and heavily skewed, with a broader range. These findings point to subtle abnormalities in the spatial organisation of cells within the cell cycle. Similarly, Rachel *et al.* (2002) demonstrated a spatial disorganisation of retinal neuroblasts and ganglion cells in the E16 albino retina. A broad disorganisation of the fine cytoarchitecture may therefore be a general feature of the albino retina, in conjunction with more specific and cell-type restricted abnormalities.

No relationship was detected between the distance of a dividing cell from the VM and its cleavage orientation. Nor was there any correlation between the distance of a cell from the VM and its inter-centrosomal distance, (an indication of the cell's phase within the mitotic cycle). The latter is an essential point, as one potential criticism of the study is that data has been gathered using histological methods on fixed tissue rather than live-imaging of cultured retinae. In addition, the analysis incorporated measurements taken from cells in metaphase, which have been reported to rotate extensively during development

within both the apical-basal and planar axes of the rodent telencephalon (Adams, 1996; Haydar *et al.*, 2003). However, results would suggest that if cells rotate within the apical-basal plane of the retina movements are largely restricted to an angular band about the horizontal, as the vast majority of cells were found to lie parallel to the RPE (see Figures 3.4.6-3.4.9). This supports the findings of Tibber *et al.* (2004); metaphase rotations within the plane of the developing rat retina were minimal, and restricted to minor oscillations about the orientation finally adopted during anaphase.

Cleavage orientations

In support of Cayouette *et al.* (2001), horizontal divisions predominated at all stages of development examined within the pigmented rat retina, the proportion of vertical divisions never having exceeded 13% of the total. Patterns of cleavage orientation shifted over time so that a peak in the proportion of vertical divisions was detected around the day of birth. This pattern is also in support of Cayouette *et al.* (2001), though absolute levels of vertical divisions reported differed between the two studies. Thus, whilst Cayouette *et al.* (2001) reported a peak of ~20% at P0, analysis of the D.A. rat at P1 would suggest a figure closer to 10%. There are two potential explanations for this discrepancy. First, it may simply reflect a low sampling rate. The study of the D.A. rat was focused on P1 as opposed to P0, so that it is conceivable that the true peak was missed as a result of this 24 hour difference. Alternatively, the discrepancy between datasets may reflect inter-species variation. Changes in patterns of cleavage orientation over time were found to occur within the framework of the centre-to-periphery gradient of development.

In the albino rat retina, both quantitative and qualitative abnormalities were found in patterns of cleavage orientation. Pooling of data from central and peripheral retinal regions highlighted an excessive level of vertical divisions at both P1 and P4. When data from each retinal location were considered independently, the abnormalities were found to be even more severe. In the central retina the number of vertical divisions was found to increase linearly at

each consecutive time-point, whilst in the periphery, the distribution of cleavage orientations did not shift over time. Instead the proportion of vertical divisions fluctuated about a baseline.

These findings suggest a disruption of the regulatory processes that control cleavage orientations in the albino retina. In the wildtype retina, a horizontal division would seem to be the "default" state adopted in the absence of further signalling. Hence, when cultured in the absence of the RPE, retinal neuroblasts are much less likely to adopt a vertical orientation (Cayouette *et al.*, 2001). This hypothesis is supported by *in vitro* tissue culture experiments in chapters 4 and 7; outside of the context of the surrounding tissues, retinal progenitors quickly become oriented so that the long axis of the mitotic spindle lies within the plane of the tissue. Thus, around the day of birth some putative signal must initiate a shift in the likelihood of a specific orientation being adopted. This could either be actively mediated by initiating a cascade of events that induce the adoption of a vertical alignment, or through the removal of some form of inhibition, which restricts the movement of the cell. In the albino central retina it would seem that this hypothetical inductive signal successfully triggers an increase in the proportion of vertical divisions postnatally. However, either the signal is not successfully down-regulated at the appropriate time-point, or a second inhibitory signal is absent so that the proportion of vertical divisions continues to rise un-checked in the central retina. In the periphery however, the proportion of vertical divisions does not shift from a base-line level, potentially indicating that the inductive signal is not correctly propagated along the central/peripheral axis.

There are a multitude of potential candidate molecules that might mediate this signal, the extracellular environment of the subretinal space around the day of birth is rapidly changing, many key developmental events being focused around this time-point. The possibility that L-DOPA (a melanin precursor) is connected to this signalling process -and hence the regulation of cleavage orientations- was explored. There are several lines of reasoning to suggest this putative link. The RPE is essential for the localisation of cell divisions to the VM (Jensen *et al.*, 2001), and plays an integral role in the regulation of cleavage orientations (Cayouette *et al.*, 2001). These two parameters are both disrupted in the

developing albino retina, as demonstrated by the work of Rachel *et al.* (2002) and results outlined above. Furthermore, the RPE is the primary site of the albino condition, and several studies have shown that L-DOPA -which is present at reduced concentrations in the albino RPE (Ilia and Jeffery, 1999)- is able to mediate regulatory control over cell division (Wick, 1977; Akeo *et al.*, 1994; Ilia and Jeffery, 1999).

Subcutaneous injections of L-DOPA were administered to early postnatal albino rats. As a negative control, animals from the same litter were injected with D-DOPA, a biologically inactive isoform. The application of L-DOPA *in vitro* reduced the abnormally high proportion of vertical divisions both in the central and peripheral retina to a level that was either equivalent to or less than those found in time-matched pigmented retinae. In view of the purported link between asymmetric division and a stem cell mode of proliferation (Lin and Schagat, 1997) it is tempting to correlate these dual effects of L-DOPA and draw a causal link between the two. It has been suggested that by this stage of development the majority of horizontal divisions (symmetric with respect to the contemporary paradigm) will generate two post-mitotic cells (Takahashi *et al.*, 1996; Haydar *et al.*, 2003). Vertical divisions on the other hand will either generate two distinct post-mitotic cell types, or one post-mitotic cell and one progenitor. A potential model of the albino condition is thus that in the absence of L-DOPA a higher proportion of cells adopt a vertical orientation and hence an asymmetric mode of division. This would favour the generation of one post-mitotic cell and one progenitor, thus maintaining a larger population of actively dividing cells in the cell cycle which would be manifested as elevated levels of mitosis and a thickening of the NBL (see chapter 1).

It is clear that the effects of L-DOPA on cleavage orientation and levels of proliferation in the retina are not causally linked, at least within the framework of these studies. The average duration of the cell cycle is approximately 30 hours in a neonatal mouse (Young, 1985), and 28 hours in the rat; M-phase (0.8 hours), G1-phase (13 hours), S-phase (12.5 hours), G2-phase (1.5 hours), (Denham, 1967). Consequently, any effects on levels of proliferation (exclusively detected in M-phase by definition) which are mediated through a

shift in the distribution of cleavage orientations would only be noticeable ~30 hours post-treatment when cells have divided, and either passed through to G_0, or all the way through G1-phase, S-phase and G2-phase, having migrated back to the VM for another round of division. In this study, effects on both cleavage orientation and cell proliferation were detected within 18 hours of L-DOPA administration. This period is sufficient for effects occurring as early as the latter period of G1-phase to be apparent, but not any effects that originate during M-phase.

There are two main possibilities to explain these findings. First, the effects of L-DOPA on patterns of proliferation, cell cycle progression, cleavage orientation and apoptosis may be mediated by multiple independent pathways. The alternative model however, in keeping with Occam's razor (the law of parsimony), would suggest that the diverse effects of L-DOPA on the processes of retinal development are secondary to a more fundamental response.

Müller cell densities

The current model of asymmetric division in the vertebrate retina would suggest that a vertical division results in the differential inheritance of apically localised Numb to the apical daughter cell. Consequently, unopposed Notch signalling in the basal cell leads to the up-regulation of Müller cell specific genes (Cayouette *et al.*, 2001; Cayouette and Raff, 2003)[2]. If this model were correct, given the abnormally high proportion of vertical divisions in the albino retina, coupled with a severe rod photoreceptor deficit in the adult (Jeffery *et al.*, 1994; Jeffery *et al.*, 1997), one might expect a corresponding increase in Müller cell densities in the adult retina, i.e. a cell-type specific shift in cell fate.

Upon examination of age-matched adult pigmented and albino rat retinae no differences in Müller cell densities were detected between the two pigmentation

[2] Notch signalling promotes a glial cell fate in the developing retina (Ohnuma *et al.*, 1999; Furukawa *et al.*, 2000), and interestingly, blocks ganglion cell differentiation during early phases of development (Austin *et al.*, 1995; Silva *et al.*, 2003).

types. It is possible that abnormal patterns of Müller cell generation around the time of birth are subsequently masked by differential patterns of cell death postnatally. Indeed, Müller cell morphology and population sizes are extremely robust and would seem to vary little between mammals with respect to their retinal distribution (Dreher *et al.*, 1992). Alternatively, patterns of Müller cell genesis might not be affected by changes in cleavage orientation. Instead, there may be a re-specification of post-mitotic cells towards the photoreceptor cell fate at the expense of the bipolar cell (Cayouette *et al.*, 2001; Cayouette and Raff, 2003). A comprehensive study of the relative densities of bipolar cells in the adult pigmented and albino retina is a crucial next step in understanding the developmental abnormalities associated with albinism, as well as the role of cleavage orientations in the vertebrate retina. Studies are currently underway to address this very question.

3.6 Conclusions

Patterns of cleavage orientation in the developing albino retina are severely disrupted with both quantitative and qualitative abnormalities occurring postnatally. In addition, this process is affected by L-DOPA administration in a manner consistent with it serving an endogenous regulatory function. However, the effects of L-DOPA on cleavage orientation and levels of proliferation do not seem to be causally linked, at least within the framework of these studies. This would suggest either a more fundamental underlying mechanism by which L-DOPA mediates these secondary effects, or the existence of multiple functional roles of L-DOPA in a number of developmental processes. Recent findings which highlight the potential role of L-DOPA as an endogenous neurotransmitter independent of its conversion into dopamine (DA) may eventually cast some light on this issue (Misu *et al.*, 2002). (See chapter 7).

Despite severe abnormalities in the distribution of cleavage orientations in the developing albino retina, Müller cell densities in the adult were stable and comparable to age-matched pigmented retinae. These findings bring in to question the validity of contemporary models of asymmetric division in the

vertebrate retina (Cayouette *et al.*, 2001; Cayouette and Raff, 2003). Indeed, one difficulty in studying the pathogenesis of albinism is the lack of data regarding the fundamental mechanisms of developmental processes involved in normal wild-type organogenesis. Despite the demonstration of severe abnormalities in patterns of cleavage orientation within the developing albino retina, the precise role of asymmetric division in the vertebrate retina remains unresolved and highly controversial (Cayouette *et al.*, 2001; Silva *et al.*, 2002; Cayouette and Raff, 2003; Das *et al.*, 2003; Tibber *et al.*, 2004).

Chapter 4:
Effects of an electric field on cleavage orientations within the apical-basal plane

4.1 Introduction

Having demonstrated both quantitative and qualitative abnormalities in patterns of cleavage orientation in the developing albino retina, the precise nature of its role in the processes of asymmetric division and cell fate specification remain unresolved. Long-term videomicroscopy of green-fluorescent-protein labelled rat retinal explants would suggest that the orientation of cell division is correlated to the symmetry or asymmetry of daughter cell fates. However, this is merely inferred from the early migration patterns of cells as they leave the ventricular zone (Cayouette and Raff, 2003). Studies to date are therefore limited by the relatively low frequency of vertical divisions in the vertebrate retina, and the difficulties involved in following both daughter cells of a single division through to their eventual fate. Consequently, there is a need for the development of an *in vitro* system in which the orientation of division can be manipulated and the resulting effects on patterns of cell birth and relative cell numbers can be determined.

Past studies have demonstrated the existence of endogenous electric fields (EFs) that are capable of orientating cell division at wound margins of the corneal epithelium (Song *et al.*, 2002). Furthermore, the application of an electric field (EF) in a dissociated cell culture system induces a range of vector-specific reorientation responses (Hinkle *et al.*, 1981; Orida and Feldman, 1982;

Luther *et al.*, 1983; Cooper and Keller, 1984; Cooper and Schliwa, 1985), including a reorientation of the cleavage orientation (Zhao *et al.*, 1999). Consequently, the potential to manipulate cleavage orientations through the application of a direct current (DC) EF was assessed in an *in vitro* retinal organ culture system.

4.2 Background

Endogenous biological EFs have been demonstrated in a wide variety of developing structures (Jaffe and Stern, 1979; Hotary and Robinson, 1990; Shi and Borgens, 1995). These EFs usually take the form of a transepithelial potential (TEP); sustained by electrogenic Na^+ uptake at the apical surface of the epithelium (Smith and Benos, 1991), the TEP is typically inwardly positive and in the order of 10-100mV/mm in magnitude. During development, TEPs polarise tissue structures, such that changes in EF properties can often be temporally correlated with key development events. The relevance of EFs to the processes of development can be demonstrated experimentally by suppressing or shunting endogenous EF's so that regional-specific developmental abnormalities are induced (Hotary and Robinson, 1992; Borgens and Shi, 1995).

In the adult, the TEP serves a distinct putative function. Upon damage of the electrically tight epithelium a pathway for current flow is generated that can trigger responses associated with tissue repair and wound healing. One of the most extensively studied models of this process is the bovine corneal epithelium. Upon wounding of the cornea, this TEP –which is ~42mV/mm in magnitude (Chiang *et al.*, 1992)- drives a current flow that is capable of reorienting the plane of cell division and up-regulating levels of proliferation (Zhao *et al.*, 1999; Song *et al.*, 2002).

A wide variety of cell types have been shown to respond *in vitro* to the application of an EF; neural crest cells, macrophages, fibroblasts, epidermal cells, epithelial cells and neurones (Hinkle *et al.*, 1981; Orida and Feldman,

1982; Luther *et al.*, 1983; Cooper and Keller, 1984; Cooper and Schliwa, 1985). EFs have been shown to influence cellular processes as diverse as the orientation of division, levels of proliferation, direction of growth and pseudopodial extension, levels of protein expression as well the spatial distribution of membrane-associated receptors (Robinson, 1985; McCaig and Zhao, 1997). See (Cooper and Schliwa, 1985) for an in-depth discussion of the potential mechanisms involved.

4.3 Experimental aims

The influence of EF application on the distribution of cleavage orientations was determined using an organotypic culture system adapted from a technique described by McCaig *et al.* (1994). The effects of varying culture period duration and voltage magnitude were assessed, as well as the impact of serum-supplemented medium.

4.4 Methods

Pigmented (D.A.) rat litters were used throughout this series of studies. Three retinae (each from a different animal) were cultured under each set of experimental conditions described below.

Tissue preparation

P2 pigmented rats were decapitated and their heads maintained in chilled nutrient media (F-12 minimal essential medium; GIBCO). The eyes were enucleated and the cornea and lens removed. The neural retina was dissected away from the surrounding RPE/choroid/sclera and floated on to an organotypic cell culture insert (Millipore). A series of radial cuts were made and the retina flat-mounted ventricular surface up. Excess media was removed by blotting with tissue paper. The retina was then covered with a thin layer of collagen gel (a

50:50 mix of bovine dermis and rat tail collagen; Collaborative Research) and incubated for 20 minutes at 37°C/5% CO_2/100% humidity to allow the gel to set.

Electric Field application and culture conditions

Retinae were transferred on cell culture inserts to a petri-dish lined with 2% agar (weight/volume in Steinberg's solution) which thus formed a highly conductive gel bed. DC electric fields were then applied to the system using a method adapted from that described by McCaig *et al.* (1994) for the growth of nerve cells within an EF. The EF was generated from a DC power source (EC250-90, Thermo Electron Company) with silver electrodes in beakers of Steinberg's solution and transferred via agar-saline bridges (2% agar weight/volume in Steinberg's solution) to the agar-lined petri-dish. Agar-bridges were used to avoid contamination by electrolysis products. The position of the anode and cathode were reversed for each subsequent trial. (See Figure 4.4.1).

The base of the well insert was made of a low resistance nitrocellulose membrane whilst the bordering rim was formed from a non-conductive plastic. By placing one end of an agar bridge in a pool of excess media directly over the retina, and the other just outside the perimeter of the well insert, a pathway of least resistance was created such that the EF was forced to pass through the retina with a field vector running perpendicular to the plane of the tissue, see Figure 4.4.2. In order to apply an EF with a field vector orthogonal to this plane, the retina was cultured on the opposite side of the well insert, which was then embedded in the agar lined petri-dish, under-side up. The electrodes were then placed on either side of the tissue in an excess of media so that the EF could pass unimpeded across the plane of the retina.

Retinae were cultured for periods of 1-6 hours at 37°C/5% CO_2 /100% humidity in EFs of 50mV/mm, 90mV/mm and 125mV/mm, (minimum recorded). Unless otherwise stated all nutrient medium used was basic F-12 minimal essential medium (GIBCO). For the experimental groups the EF was applied perpendicular to the plane of the tissue, i.e. running along the apical-basal axis.

As negative controls, one group of retinae were cultured without an EF (i.e. the power pack was disconnected), and a second group were cultured within an EF running through the plane of the tissue. The latter control was designed to distinguish general effects of exposure to an EF from those which are specific to the plane of the applied EF. Finally, a group of retinae were cultured in minimal essential medium which was supplemented with 10% foetal calf serum and 0.1% trypsin.

Fixation and staining

Cell culture inserts were removed from the incubator and immersed in 4% formalin overnight. The whole-mounts were then dissected from the nitrocellulose membrane, washed repeatedly in PBS and cryoprotected overnight in 20% sucrose. These were then embedded in a 2:1 mixture of 20% sucrose/OCT for 30 minutes before being transferred to pure OCT and rapidly frozen down on dry ice. Twenty micron sections were taken in the horizontal plane, transferred to super-frost glass slides (BDH Laboratory Supplies) and left to dry overnight. Slides were soaked in distilled water for 60 seconds to remove the OCT and then left to dry. After washing with PBS the sections were stained with propidium iodide for 1 minute (5μg/ml in PBS). The slides were then coverslipped in fluorescent mounting medium (DAKO).

Image analysis

Images were gathered using the 543nm line of a Zeiss laser scanning confocal microscope (LSM 500) using a x60 oil objective lens with 1.5x digital magnification. Eight bit z-stack images were generated with dimensions of approximately 98x98x10μm in the x-, y- and z-planes respectively. These were then used to render three dimensional projections which could be rotated about the y-axis (Figure 4.4.3A). Individual metaphase and anaphase cells were identified by the presence of condensed chromatin in the form of metaphase/anaphase bars and rotated until the plane of the division lay parallel

to the plane of the screen. The orientation of the cleavage plane relative to the ventricular surface was then calculated using a built-in measurement function within Zeiss image examiner Version 2.8 (Figure 4.4.3B). The technique is based on that described by Haydar *et al.* (2003). The orientation of between 137 and 148 cells were studied from 3 retinae per experimental group.

Statistical analyses were performed using SPSS 10.1 (SPSS Inc.). The proportion of cells from each experimental group that exhibited an horizontal, intermediate or vertical orientation were compared using the chi-squared test. In addition, the mean proportion of cells falling into each category were compared between treatment groups using the one-way ANOVA test.

Electric field delivery

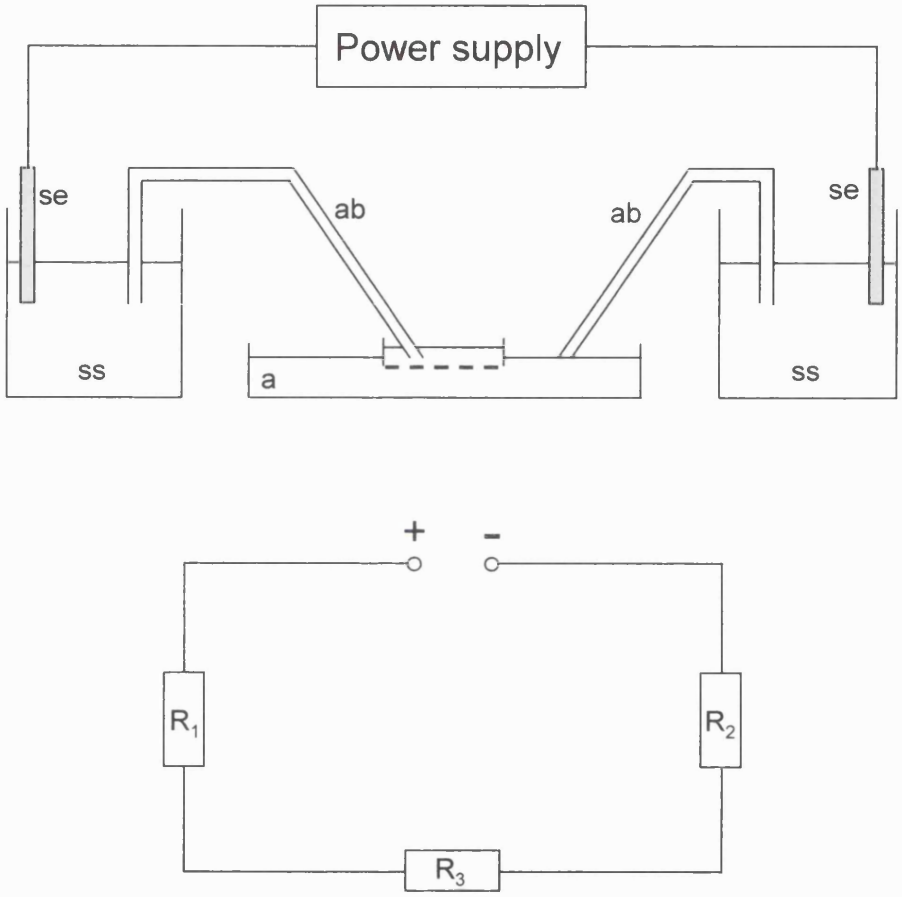

Figure 4.4.1 Retinae were cultured on a Millipore well insert embedded in a petri-dish lined with 2% agar (thus forming a highly conductive gel bed (a)). The electrodes were connected to a DC power supply (maximum output 250V) and submerged in beakers of Steinberg's solution (ss). The resulting EF was transferred to the petri-dish via agar-saline bridges (ab), the tips of which were submerged in excess media to ensure good contact. There were 3 main points of resistance in the system, (R1, R2 and R3). R1 and R3 represent the resistances formed by the agar bridges (~65kΩ each). R3 represents the combined resistances of the area of gel bed traversed by the current and the resistance of the retina/over-lying collagen and was equal to ~300Ω. When 100V was passed through the system, the current equalled ~700μA and the voltage across the retina was in the order of 50mV/mm.

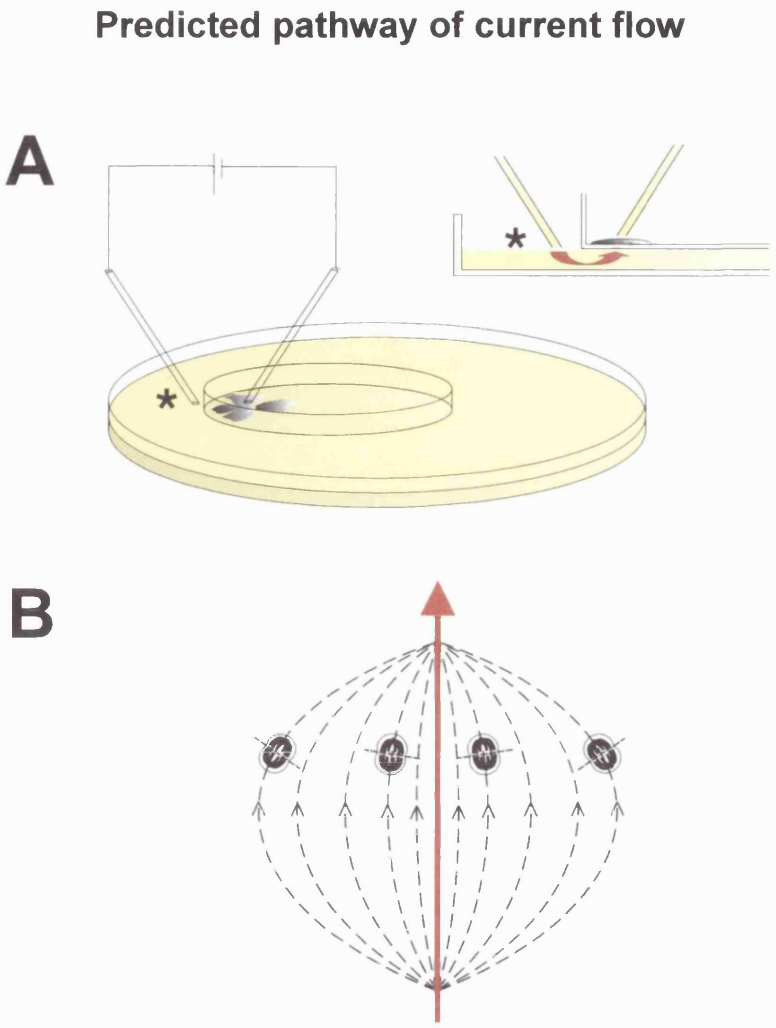

Figure 4.4.2 Schematic diagram illustrating the predicted pathway of current flow through the experimental system. (A) As shown in Figure 4.4.1 the DC EF is delivered to the petridish via agar-saline bridges to avoid contamination with electrolysis products. Inset is a diagram in which the predicted pathway of least resistance is shown (red arrow). (B) The net EF vector is shown as it passes through the NBR (red arrow). The dotted lines represent the field lines of the EF, which may be diffuse and/or distorted as a result of regional variations in tissue resistance. If dividing retinal neuroblasts were reoriented by the application of an EF cells would be shifted from the horizontal pattern of cell division which predominates in the vertebrate retina. In order to distinguish the general effects of exposure to an EF from those which are specific to the plane of the applied EF, retinae were cultured in parallel with an EF running through the plane of the tissue.

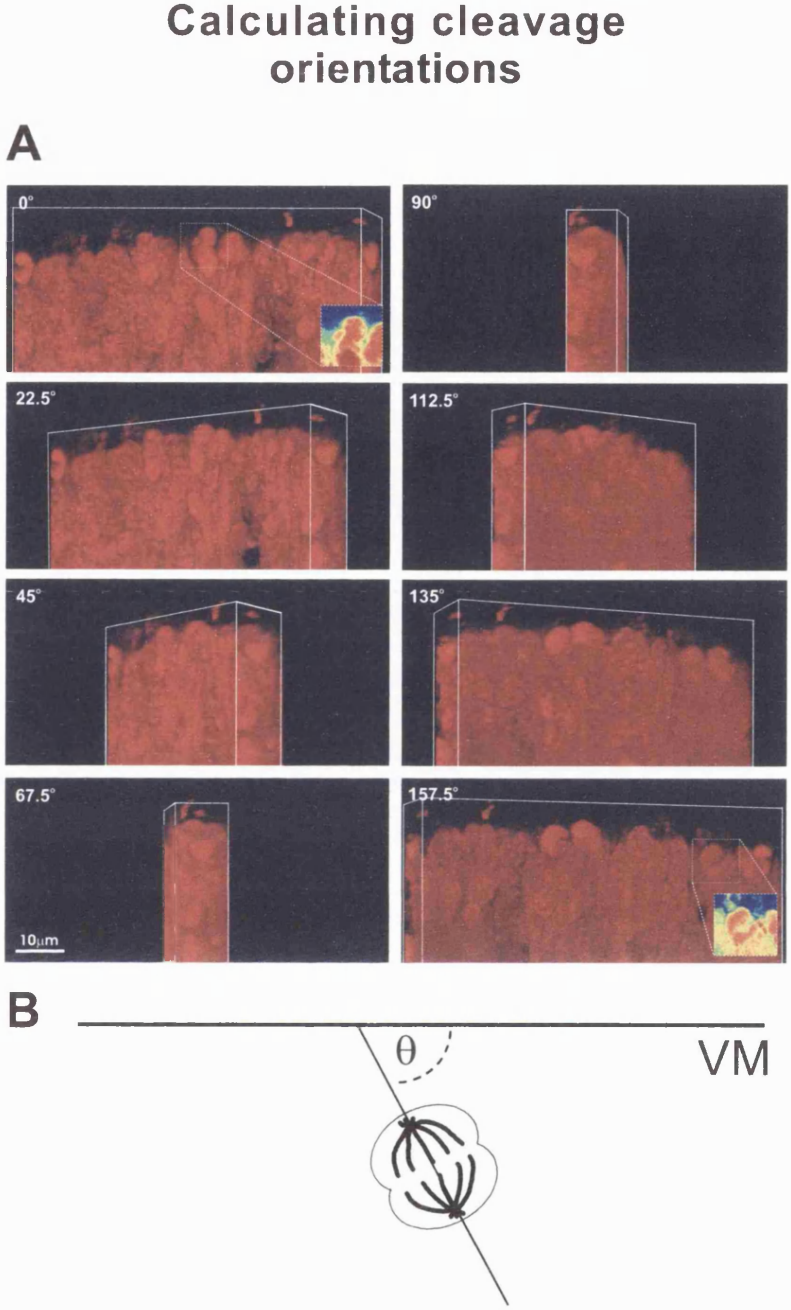

Figure 4.4.3 Cleavage orientations were calculated from z-stack projections of the retina. (A) Images were rotated about the y-axis until the dividing cell of interest (a metaphase or anaphase profile) was oriented such that the division fell within the plane of the screen. (B) The orientation of division (θ) relative to the plane of the VM was then calculated from the angle between two plotted, intersecting lines; the first defining the plane of the VM, and the second lying parallel to the mitotic spindle axis. Higher magnification images of metaphase and anaphase profiles are inset in (A). They have been converted into intensity plots to maximise contrast between the cells and surrounding tissue. The dimensions of the z-stack are 98x47x12μm in the x-, y- and z-planes respectively. In each sequential panel the projected image has been rotated 22.5° clockwise about the y-axis.

4.5 Results

P2 pigmented (D.A.) rat retinae were cultured within an EF under a series of experimental conditions in which the duration, magnitude and vector of EF application were varied. In addition, a group of retinae were cultured in medium which was supplemented with foetal calf serum and trypsin in an attempt to overcome any bonds that may have restricted cell motility, and to promote a reorientation response. For each group examined tissue appeared healthy as determined by the presence of actively dividing cells and the integrity of the GCL, as well as overall gross morphology (Figure 4.5.1A). However, certain restricted regions of each retina appeared abnormal as determined by the presence of a high density of apoptopic nuclei (Figure 4.5.1B). These were common in areas of the retina where the tissue had become folded over and were consequently excluded from analysis.

Cleavage orientations were calculated relative to the plane of the VM using a technique described by Haydar *et al.* (2003), (see Figure 4.4.3). The distribution of cleavage orientations is presented in the form of a bar chart, Figure 4.5.3. The percentage of divisions exhibiting a horizontal (0-30°) and intermediate (30-60°) orientation relative to the VM is shown for each experimental group. Cells exhibiting a vertical orientation (60-90°) are not presented visually as only 1 cell out of the 831 studied throughout the series of experiments fell into this category. Error bars represent the standard deviation.

EFs were applied for 1 hour at 50mV/mm, 90mV/mm and 125mV/mm. Cleavage orientations did not vary as a function of EF magnitude within the voltage range examined. Data for the 90mV/mm was not analysed quantitatively, although a limited sampling of the tissue would suggest that cleavage orientations were still predominantly horizontally aligned. Similarly, increasing the culture period to 2 hours had no effect on the distribution of cleavage orientations. Finally, an EF was applied to the developing retina at

125mV/mm for a total duration of 6 hours. In addition, the media was supplemented with foetal calf serum as past studies suggest that EF-mediated responses may be serum dependent (Zhao *et al.*, 1996). Trypsin, an amino acid-specific proteolytic enzyme, was also added to the media at a concentration of 0.1%, in an attempt to degrade any protein scaffolding that might have restricted cell motility through cell-cell or cell-extracellular matrix interactions. As can be seen from Figure 4.5.3, none of these factors influenced the cells' responsiveness to an EF with respect to cleavage orientation. Data were compared using the chi-squared test (p=0.15). The proportion of dividing cells that were intermediately, horizontally and vertically aligned were then compared independently between experimental groups using the one-way ANOVA test (p=0.53, 0.5 and 0.46 respectively).

As cleavage orientations did not differ between experimental groups, data were pooled and presented in the form of a single frequency histogram, Figure 4.5.3. In addition, the distribution of cleavage orientations *in vivo* within the P1 DA retina is reproduced from chapter 3 for comparison. The data have been grouped into 10^{o} bins ranging from 0^{o} to 90^{o}, (representing horizontal and vertical divisions respectively). Superimposed are pie-charts, indicating the proportion of horizontal (dark grey) to vertical (light grey) divisions. Horizontal and vertical divisions were defined as divisions occurring at an angle of $<45^{o}$ or $\geq 45^{o}$ relative to the VM respectively.

Similar to the pattern found *in vivo* there was a strong unimodal preference for horizontal divisions in the neonatal rat retina following short-term culture. However, in the *in vitro* system the proportion of vertical divisions was as low as 1.7%, and no cells were aligned at orientations greater than the 62^{o} relative to the VM, despite the fact that a total of 831 cells were sampled throughout the study. This would suggest that when the neural retina is removed from its physiological surroundings, cells either return to a "default" horizontal alignment, or alternatively, become restricted in this orientation. These findings support the role of the RPE or an RPE-derived factor in the regulation of cleavage orientations (Cayouette *et al.*, 2001).

Tissue morphology

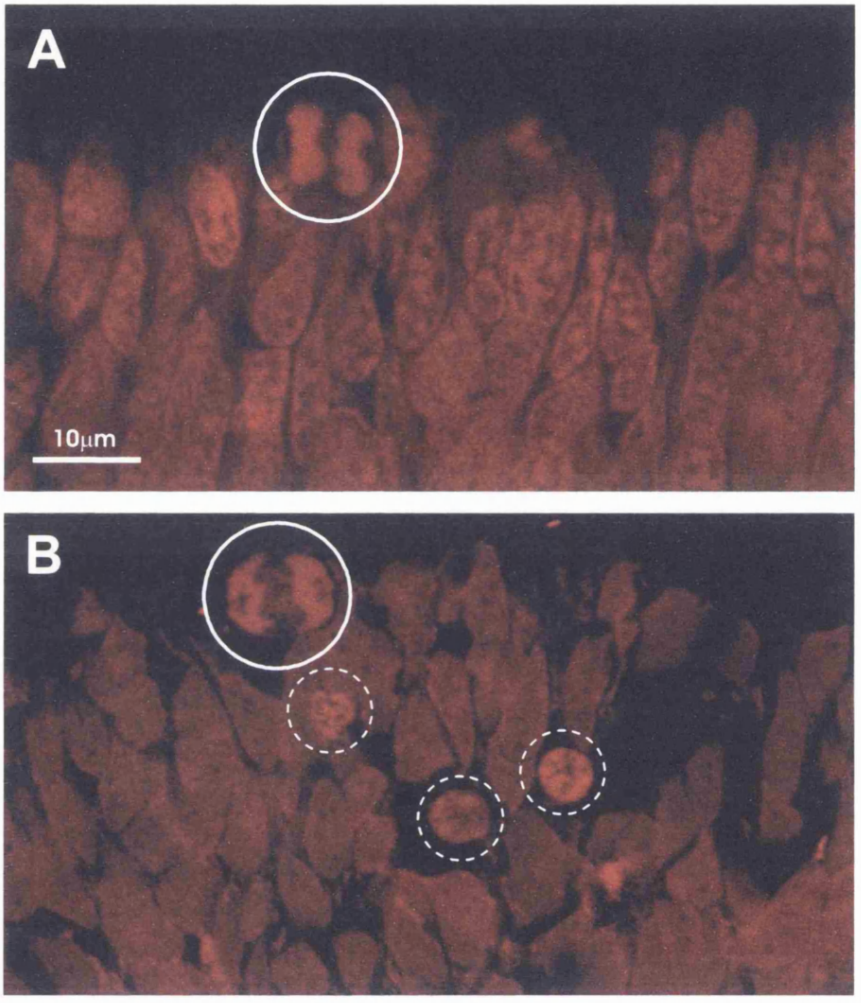

Figure 4.5.1 For all treatments studied sections of cultured retinae appeared healthy as determined by the gross morphology of the GCL and presence of actively dividing cells at the VM (A). Restricted regions of the tissue appeared abnormal however (independent of treatment) and were characterised by high levels of apoptosis (B). These were common around the borders of the tissue and in regions that had become folded over during preparation. These regions were consequently excluded from the analysis. Anaphase profiles are encircled by solid white lines. Apoptopic nuclei are encircled by dotted white lines. Tissue was stained with propidium iodide (red) to visualise the nucleic acid and facilitate calculation of cleavage orientations.

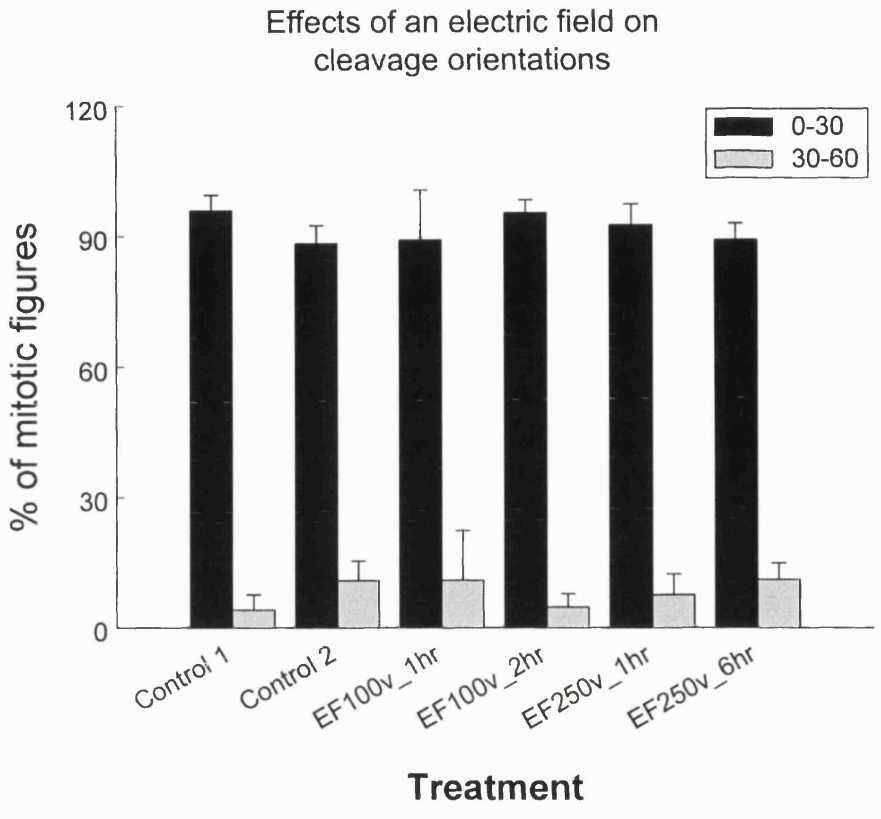

Figure 4.5.2 Cultured P2 pigmented rat retinae were exposed to a range of EF conditions (see text). The EF was applied perpendicular to the plane of the tissue (i.e. along the apical-basal axis) for a duration of 1 hour by default. Two negative controls were employed; the tissue was cultured in the absence of an EF (during which the power source was disconnected, control1), and in the presence of an equivalent field that ran through the plane of the tissue (i.e. orthogonal to the field vectors used in other treatments, control 2). Bar charts are presented illustrating the percentage of all divisions exhibiting a horizontal (0-30°) and intermediate (30-60°) orientation. Error bars represent the standard deviation. Cells exhibiting a vertical alignment (60-90°) are not shown as only one cell out of 813 fell into this category. Statistical analysis using the chi-squared test indicates that the proportion of horizontal, intermediate and vertical divisions did not differ between treatments (p=0.15).

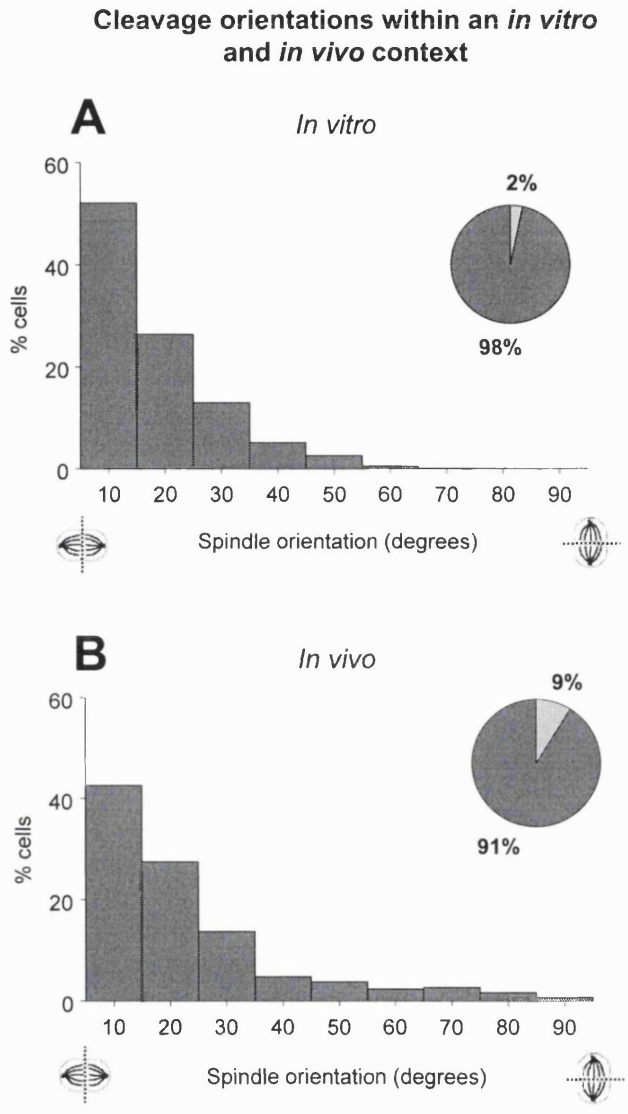

Figure 4.5.3 (A) The frequency distribution of cleavage orientations is shown for pooled data from EF-treated and control pigmented P2 retinae, (no significant differences having been found between groups). As can be seen there is a strong unimodal preference for horizontal divisions and despite the fact that the plot incorporates the analysis of 831 cells no divisions exceeded an orientation of 62° relative to the VM. Only 1.7% of all divisions were vertically aligned relative to the plane of the tissue, (≥45°). 831 cells were analysed from a total of 18 retinae. (B) For comparison, data is also reproduced from chapter 3, presenting the distribution of cleavage orientations in the P1 D.A. rat *in vivo*. Similarly, there is a unimodal preference for horizontal divisions. However, in the *in vivo* retina there is a broader distribution of cleavage orientations and a much higher proportion of vertical divisions (9%). 171 cells were analysed from a total of 3 retinae.

4.6 Discussion

The effects of EF field application on cleavage orientations were examined within the developing retinal neuroepithelium using an *in vitro* organotypic culture system. Whilst a range of parameters of cell division/cell motility are affected by the application of an EF (Robinson, 1985; McCaig and Zhao, 1997), this study only addressed its potential effects on cleavage orientations. If retinal neuroblasts could be re-oriented through the application of an EF, the technique might be developed as a tool to examine the relationship between patterns of cell division and the processes of asymmetric division/cell fate determination (Cayouette and Raff, 2003).

No changes in patterns of cell orientation were induced upon application of an EF up to 125mV/mm in magnitude (minimum recorded), even following exposure periods of 6 hours in duration. In addition, supplementation of foetal calf serum and trypsin to the minimal medium did not alter the cells' responsiveness, past studies having demonstrated serum-dependency (Zhao *et al.*, 1996). Though one cannot rule out the possibility that cellular responses may be induced at higher voltages or using a different experimental set-up, the series of voltages used through out this study were well within the range reported to elicit an array of cellular responses, both *in vivo* and *in vitro. In vitro* studies of cultured human and bovine corneal epithelial cells routinely induce a re-orientation of both cell division and cell migration through the application of DC EFs of less than100mV/mm (Zhao *et al.*, 1996; McCaig and Zhao, 1997; Zhao *et al.*, 1997; Zhao *et al.*, 1999). Furthermore, re-orientation responses can be detected within 30 minutes of EF application (Zhao *et al.*, 1997).

Thresholds for EF-induced responses in other disaggregated cell culture systems (e.g. myoblasts, neurones, neural crest cells and fibroblasts) are generally in the order of 0.1-0.3mV per cell diameter (Robinson, 1985). If a typical retinal neuroblast is assumed to be ~20μm in diameter, the range of EFs used throughout this study were in the order of 1-2.5mV/cell diameter,

approximately an order of magnitude greater than the minimum necessary to induce a re-orientation response in other cell types.

Why were patterns of cleavage orientation in the developing retina unaffected by the application of an EF? The first possibility is that the experimental design was flawed. In all reported studies to date the effects of an EF on cleavage orientation were such that the cleavage plane was aligned perpendicular to the field vector (Zhao *et al.*, 1999; Song *et al.*, 2002). By extrapolation one would predict that an EF passing through the apical-basal axis of the retina might increase the probability of a cell adopting a vertical orientation, i.e. such that its cleavage plane lies parallel to the VM. However, to ensure that an effect was not overlooked as a result of a distinct response pattern in the retina, EFs were also applied through the plane of the tissue. Results from both experimental set-ups suggest that EF application elicited no response, and cells retained a strong propensity to align themselves within the plane of the tissue irrespective of the orientation of EF application.

Is it possible that the EF was not delivered effectively? The power supply used (designed for electrophoresis) was programmed to cut out if the circuit was broken. During none of the experimental runs was this contiguity interrupted. In addition, though precise voltages were found to vary slightly over time and between replicates values quoted for each experimental group were the minimum recorded. Consequently, constant DC fields were delivered with voltages of a relevant magnitude, i.e. within the range reported to elicit a response. Finally, there is the possibility that the path taken by the EF differed from the prediction. The rim of the cell culture insert was made of a non-conductive plastic. Hence, with the second electrode placed directly over the collagen gel, the current had to pass through the nitrocellulose basement membrane and up through the retina to complete the circuit. However it is possible, indeed likely, that the field was diffuse, and whilst the overall vector of the field lay perpendicular to the plane of the tissue the actual field lines may have been distorted by variations in tissue resistance. Even so, if the EF had elicited a response one would expect a broader distribution of cleavage orientations than seen in Figure 4.5.3A. (See Figure 4.4.2).

The second possibility is that retinal neuroblasts are intrinsically unresponsive to an EF. This would suggest that galvanotropism rather than being a ubiquitous property of the eukaryotic cell is unique to a certain subset of cell-types. Indeed many cells reported to date as being responsive to an EF are highly motile and migratory, e.g. fibroblasts (Hinkle *et al.*, 1981), macrophages (Orida and Feldman, 1982), and neural crest cells (Cooper and Keller, 1984). In addition, not all EF-sensitive cells exhibit a vector specific re-alignment response. The only example of an EF-triggered re-orientation of a cell's cleavage plane is to be found in the wounded corneal epithelium, for which an endogenous physiological role has been strongly implicated (Zhao *et al.*, 1999; Song *et al.*, 2002). In addition, the majority of *in vitro* studies of EF-induced responses have been limited to a handful of model systems (e.g. neurite outgrowth) which have traditionally been used due to their documented responsiveness and may thus not reflect widespread phenomena.

The third possibility is that retinal neuroblasts are responsive to an EF, but are physiologically constrained by their surroundings within the tissue. It is likely that the effects of EF application will vary significantly depending on whether they are studied *in vivo*, *in situ*, or in disaggregated cell culture systems. Though an individual cell may respond to an EF in isolation, other factors including mechanical constraints, guidance/polarisation cues, cell-cell interactions and the influence of the extracellular matrix scaffold will affect its potential motility within the context of the entire tissue.

In the corneal epithelium several potential mechanisms underlying EF-mediated re-orientation of the cleavage plane have been suggested. These primarily revolve around an asymmetric re-localisation of membrane associated receptors (specifically the EGF) and lipid domains at the cathodal-facing side (Zhao *et al.*, 2002). These may be capable of sequestering aster microtubules and hence re-orientating the mitotic spindle. In the cultured retinal neuroepithelium, an asymmetric re-localisation of membrane-associated receptors may be induced by the presence of an EF, though the machinery necessary for the re-orientation of the cleavage plane within the apical-basal

axis may be absent. Indeed there is considerable evidence to suggest that retinal progenitors require either the presence of the over-lying RPE or an RPE-derived factor to adopt an orientation that deviates from the horizontal.

In an *in vitro* organotypic culture system, the proportion of dividing retinal neuroblasts exhibiting a vertical orientation dropped by half from 19% to 11% when cultured in the absence of the RPE (Cayouette *et al.*, 2001). In all studies to date of the vertebrate retina, neuroblasts exhibit a strong unimodal preference for divisions within the plane of the tissue (Cayouette *et al.*, 2001; Silva *et al.*, 2002). Thus, vertical divisions are found in the vertebrate retina during a limited temporal window around the day of birth, and would thus appear to represent a temporary shift from the "default" pattern of division. Taken together these findings would suggest that dividing cells within the developing retinal neuroepithelium either actively "seek" a horizontal orientation or are physiologically restrained in this position during M-phase.

4.7 Conclusions

Within the range of voltages and exposure times explored throughout this series of studies no effects on the distribution of cleavage orientations could be detected in the developing retinal neuroepithelium upon application of an EF. Though one cannot dismiss the possibility that responses may be induced at higher voltages or using a different experimental set-up, field strengths and exposure times used were in the range of those previously reported to elicit a response. Interest in galvanotropism was rooted in its potential to be exploited for the development of a model system in which the effects of cleavage orientation on asymmetric division and cell fate specification could be examined. However, if extremely high voltages or extensive programs of tissue pre-treatment are needed to facilitate a response, one might question the physiological relevance and/or experimental value of such a model.

Chapter 5:
RPE/neural retina interaction

5.1 Introduction

A disruption in melanin synthesis at any stage of the pathway results in a stereotypical pattern of retinal defects including a severe rod deficit and an underdevelopment of the central retina (Jeffery and Kinsella, 1992; Jeffery *et al.*, 1994; Grant *et al.*, 2001; Donatien and Jeffery, 2002). Furthermore, both these aberrancies can be corrected by the introduction of a functional tyrosinase gene (Jeffery *et al.*, 1997). Thus, the root of these abnormalities must ultimately be traced back to the pigmented tissues of the eye, i.e. the RPE and/or choroid. The mechanisms by which these defects of the RPE are transduced to the neural retina are unclear. This is perhaps unsurprising given that relatively little is known about the nature of RPE /neural retina interaction during development within the wildtype eye. However, several key studies have highlighted the essential regulatory role that the RPE plays in the formation of a fully functional and morphologically intact neural retina (Raymond and Jackson, 1995; Jablonski *et al.*, 2000; Pinzon-Duarte *et al.*, 2000; Jensen *et al.*, 2001).

The primary pathway for communication between the RPE and neural retina during development is via gap junctions. Formed from two connexon hemi-channels, the gap junction couples cells both electrically and metabolically, allowing the passage of molecules up to ~1kDalton in size (Alberts *et al.*, 1994). Each connexon is composed of six identical protein subunits called connexins which encompass a central aqueous pore. Different types of connexins are

characterised by subtle differences in their properties and exhibit distinct and specific patterns of expression, both spatially and temporally. Thus, connexin-43 (Cx43) is most abundant in epithelial tissues, and is found extensively in the RPE and at the RPE/NBR interface in the adult and embryonic retina respectively (Becker *et al.*, 1998; Janssen-Bienhold *et al.*, 1998; Pearson *et al.*, 2004a).

Transitory gap junctions have been demonstrated between RPE cells and dividing retinal neuroblasts, presenting a theoretical pathway for the transfer of cell cycle/cell fate signalling molecules (Hayes, 1976; Hayes, 1977; Townes-Anderson and Raviola, 1981). This relationship has also been demonstrated functionally through the use of fluorescent dye-injections of *in vitro* preparations of the chick retina. By loading RPE cells with a dye that is small enough to pass through gap junctions (e.g. Neurobiotin), patterns of cell coupling can be traced. RPE cells were found to be extensively coupled both to adjacent RPE cells, as well as cells of the NBR (Pearson *et al.*, 2004a). Furthermore, the addition of gap junction blockers led to a reduction in the frequency of Ca+ waves and transients which are thought to play an essential role in the coordination of developmental events (Pearson *et al.*, 2004a).

In vivo data into the role of gap junction communication in eye development is limited. Though a Cx43 double knockout mouse has been generated, studies of its eye have been limited to the development of the lens, and reported findings are largely contradictory (Gao and Spray, 1998; White *et al.*, 2001). However, when gap junction communication was blocked in the chick retina using an antisense gel specific to Cx43, levels of proliferation in the NBL fell significantly and eye growth was retarded (Becker and Mobbs, 1999). Thus gap junctional communication plays a crucial role in regulating the pace of retinal organogenesis.

In view of the fact that the primary defect in retinal development associated with hypopigmentation must ultimately originate in the RPE, a series of studies were undertaken to address the nature of RPE/NBR communication during development.

5.2 Experimental aims

Levels of Cx43 at the RPE/NBR interface were analysed by immunofluorescent labelling coupled with image analysis methods. Differences were detected between pigmented and albino tissue and were focused postnatally. Consequently, the effects of L-DOPA administration on patterns of Cx43 expression were analysed, thus re-addressing the role of L-DOPA in the regulation of retinal development.

Having shown that L-DOPA influences levels of Cx43 in the retina as well as the distribution of cleavage orientations at the VM (chapter 3), the possibility that both parameters are causally linked was explored. Consequently, attempts were made to elevate levels of Cx43 expression in pigmented eye-cup preparations *in vitro* through the application of forskolin (a documented regulator of connexin expression). Finally, the fine structure of the RPE/NBR retina interface was analysed in both pigmented and albino retinae.

5.3 Methods

Cx43 labelling

E13, E15, E18, P1 and P4 pigmented (D.A.) and albino (Wistar) rat retinae were processed and analysed for Cx43 staining. Three eyes (each from a different animal) were examined per time-point/pigmentation type.

Histology and immunohistochemistry

At E18 and earlier stages of development heads were fixed, sliced and processed whole. At later stages the eyes were enucleated and the cornea and lens removed. Tissue was fixed in 4% formalin overnight at room temperature,

cryoprotected in 20% sucrose and bathed in a 2:1 mixture of 20% sucrose/OCT for 30 minutes. Eyecups/embryonic heads were embedded in OCT and quickly frozen by submersion in dry ice. Twenty micron sections were taken in the horizontal sections plane, transferred to poly-lysine coated glass slides (BDH Laboratory Supplies) and left to dry overnight.

To facilitate direct quantitative comparison, all tissue generated from a single experimental run were stained in parallel on the same day. The protocol used was adapted from that described by Becker *et al.* (1995). Slides were defrosted at room temperature, a wax ring was drawn around the sections using a PAP pen and a drop of PBS placed on the sections to rehydrate them. Slides were placed in a humidified chamber and the PBS replaced with a blocking solution of 0.1M lysine, 0.05% Triton X-100 in PBS for 45 minutes. Slides were then incubated with a primary antibody against Cx43 (see below for details) at 37°C for one hour. They were rinsed in PBS (3 x 5 minutes), incubated with a FITC-tagged secondary antibody, (swine anti-rabbit or rabbit anti-mouse; DAKO, 1:200) at 37°C for one hour and mounted in CitiFluor (Canterbury); an anti-fade mounting medium. Three different primary antibodies were used; Gap 15 (rabbit polyclonal, 1:50, (Becker *et al.*, 1995)), Gap 1A (mouse monoclonal, 1:200, (Wright *et al.*, 2001)) and a commercially available rabbit polyclonal anti-Cx43, (1:2000, Sigma). All quantitative analysis was performed on tissue stained with the commercially available antibody.

Image analysis

To quantify levels of Cx43 at the RPE/NBR interface serial sections of the retina exhibiting a C-shape morphology were scanned using a Zeiss lazer scanning confocal microscope. The tissue was excited using an Argon (488nm excitation) and an HeNe1 (543nm excitation) laser. All settings were standardised for the Argon channel, which was set at 52% power, 10% output, detector gain 1000 and offset -0.3. Z-stack images were gathered from the central retina with dimensions of 153.5x153.5x5 μm in the x-, y- and z-planes respectively with inter-z-slice intervals of 0.5 μm, using a x40 objective lens with a 1.5x digital magnification. Z-stack images were then compressed into two dimensional

projections. These were imported into LSM5 Image Examiner from which they were transferred to Photoshop 7.01 as single channel files and subsequently saved in TIFF format. The images were then imported into Image Tool Version 3.0 for analysis. All images were converted into grey-scale representations and thresholded identically at 50 intensity units, (in an 8-bit image intensity values range from 0-255). Using an in-built image processing function the area (in pixels) of individual patches of signal, and the combined total area of signal were calculated, giving an indication of the distribution of plaque sizes as well as the overall level of Cx43 expression. Patches of less than 5 pixels in size were not counted. Five regions were analysed per retina.

Statistical analyses were performed using SPSS 10.1 (SPSS Inc.). The KS-test was used to test for normality. Pair-wise independent samples t-tests were then used to make comparisons between pigmentation types at each developmental stage. Data from L- and D-DOPA treatments were compared independently to the appropriate untreated control, as separate litters were used for each experiment.

DOPA administration

P3.5 albino rats were administered subcutaneous injections of L-DOPA in conjunction with a decarboxylase inhibitor (carbidopa) and D-DOPA at a concentration of 3mM. Eighteen hours later (~P4), the animals were killed and the tissue processed as described above. Three eyes (each from a different animal) were analysed per group.

In vitro treatment of eyecup preparations with forskolin

In an attempt to elevate levels of Cx43 in the developing retina and assess consequent effects on patterns of cell division, forskolin was added to *in vitro* eyecup preparations. Forskolin is a stimulant of the catalytic subunit of adenylate cyclase and a documented regulator of connexin expression. It

thereby promotes transcription of Cx43 mRNA as well as clustering of Cx43 plaques (Wang and Rose, 1995).

P1 pigmented (D.A.) rats were sacrificed and their heads submerged immediately in chilled F-12 minimal essential medium (GIBCO). The eyes were enucleated and the cornea punctured with a fine gauge syringe. The lens was then carefully dissected into small pieces and extracted through a hole in the cornea in an attempt to maintain the structural integrity of the ocular globe. Eye-cups were then incubated in fresh medium for four hours at 37°C/5% CO_2/100% humidity. Two experimental groups were treated with minimal medium that was supplemented with 30µM or 200µM forskolin, (dissolved in Dimethyl sulphoxide (DMSO)). In parallel, retinae were cultured in minimal medium with 1% DMSO (negative control). After the elapsed period, tissue was fixed overnight in 4% formalin, cryoprotected in 20% sucrose and analysed for Cx43 labelling as described above.

Statistical analyses were performed using SPSS 10.1 (SPSS Inc.). Data were tested for normality using the KS-test. Subsequent comparisons between treatment groups were undertaken using an ANOVA test with Tukey HSD *post-hoc* analyis.

Diolistic labelling of the RPE

To examine the anatomy of the RPE/NBR interface, preliminary experiments were undertaken to label RPE cells with lipophilic dyes using a technique known as Diolistic labelling (Gan *et al.*, 2000). Four eyes (each from a different animal) were prepared per pigmentation type.

Bullet preparation

Each dye-coated pellet was initially made up separately so that individual tungsten particles were only coated in a single dye. 2mg, 2.5mg and 4mg of DiI, DiD and DiO respectively were each suspended in 400µl of Dichloromethane

(Methylene Chloride, Sigma Diagnostics) and vortexed. Each dissolved dye was then added to 50 mg of 1.3 μm tungsten particles on non-coated glass slides and spread across the entire surface to form a thin film. These were left to dry for 15 minutes. Particles from all three dye preparations were then scraped from the slide surfaces and fed into a single section of PVP-coated tubing (polyvinyl pyrrolidone, 0.1mg/ml in ethanol; SIGMA) so that each bullet would contain a combination of all three pellet types. The tubing was then shaken to ensure an even distribution of dye-coating, and cut into appropriate lengths using a tube cutter (BioRad). The bullets were stored at 4°C with desiccant pellets.

Tissue preparation

P4 rats of both pigmentation phenotypes (Wistar and D.A.) were sacrificed and their eyes enucleated and stored in 4% formalin. The cornea was then punctured, the lens removed and the neural retina dissected away from the surrounding eye-cup. The eye-cup was then flat-mounted, RPE surface up, on a small circular cover-slip and transferred to a plastic stage. Excess moisture was removed with tissue paper. The preparation was then shot with a combination of DiI, DiD and DiO coated tungsten beads through a thin porous membrane at 100 p.s.i (pounds per square inch) using a gene gun (BioRad). Four to six shots were used per eye depending on penetrance (as gauged by repeated examination under a dissecting microscope with fluorescence unit). Finally, the tissue was stored in PBS for 48 hours to enable the dye to spread and flat-mounted RPE surface up on poly-lysine coated slides. Slides were coverslipped in anti-fade fluorescent mounting medium with added DAPI (DAKO).

Electron microscopy of the RPE/neuroblastic retina interface

To examine the fine structure of the RPE/NBR interface, ultrathin sections of the pigmented and albino retina were examined using a transmission electron microscope. Three eyes were examined per time-point/pigmentation type.

P1 and P4 pigmented (D.A.) and albino (Wistar) rat eyes were fixed in 3%glutaraldehyde/1%paraformaldehyde in 0.08M sodium cacodylate-HCl buffer (pH7.4) overnight. They were then rinsed in PBS (3 x 5 minutes) and immersed in 1% aqueous osmium tetroxide solution for 2 hours at room temperature. Tissue was then rinsed in distilled water (3 x 5 minutes) and subsequently dehydrated by 15 minute incubations in 50%, 70%, 90% and100% ethanol (x3 at 100%), followed by two changes of propylene oxide (20 minutes each). Tissue was infiltrated overnight by a 1:1 mixture of propylene oxide:araldite, and subsequently incubated in pure resin on a rotator for 6 hours before embedding and overnight polymerization at 60°C.

Semithin sections for light microscopy and ultrathin sections for electron microscopy were cut in the horizontal plane using a Leica ultracut S microtome fitted with the appropriate grade of diamond knife. Semithin sections were contrasted with a mixture of 1% borax and 1% toluidine blue in 50% ethanol at 60°C, dried and mounted in DPX. Ultrathin sections on carbon/formvar coated copper slot gids were stained sequentially for 5 minutes with 5% uranyl acetate, 60% ethanol and Reynold's lead citrate. Sections were viewed in a JEOL 1010 TEM, operating at 80kV. Images were recorded onto Kodak 4489 EM film.

5.4 Results

Levels of Cx43 expression in the developing retina; E13 and E15

Patterns of Cx43 expression at the RPE/NBR interface were determined by immunofluorescence detection methods in horizontal sections of E13 and E15, pigmented and albino retinae. In Figure 5.4.1 confocal micrographs of the VM are shown from each pigmentation type and time-point. Sections were stained for Cx43 (green) and counter-stained for nucleic acid (red).

At E13 no label was detected in either the pigmented or the albino at the interface between the RPE and NBR (Figure 5.4.1A&B). Strong labelling at the

apical surface of the lens epithelium and regions of the surface ectoderm provided a reliable positive control (Figure 5.4.1A). In addition, Cx43 was expressed at high levels in the *orra serrata*, a pattern which was retained at later stages (Figure 5.4.2C). By E15, occasional plaques of Cx43 were detected at the RPE/NBR interface (Figure 5.4.1C&D). These were at a low density, and common to both pigmented and albino tissue.

Levels of Cx43 expression in the developing retina, E18-P4

By E18, Cx43 immunofluorescence was detectable as a discrete line of punctuate label between the RPE and NBR in both pigmented and albino eyes (Figure 5.4.2A). Hence, direct quantitative comparison between time-points and pigmentation types could be undertaken. All experimental protocols and methods of analysis were standardised, and conducted in parallel. Data is presented visually as confocal micrographs (Figure 5.4.3). In addition, the following plots are presented as a series of bar charts; the relative area of Cx43 labelling (calculated as the total number of Cx43-positive pixels per unit area; Figure 5.4.4), the relative plaque number (the number of discrete clumps of staining per unit area; Figure 5.4.5A) as well as the relative plaque size (Figure 5.4.5B). All values were normalised to and expressed as a proportion of the E18 albino data-set.

From E18 onwards in the pigmented retina, the level of detectable Cx43 expression fell at each sequential time-point (Figure 5.4.4). This trend could be traced to a concerted drop in the number of Cx43 plaques (Figure 5.4.5A), whilst the size of the plaques themselves remained relatively constant (Figure 5.4.5B). In contrast, in the albino retina, no such trend was discernible. Between E18 and P4 the level of Cx43 expression remained constant (Figure 5.4.4), and though the relative plaque number (Figure 5.4.5A) and plaque size (Figure 5.4.5B) fluctuated between time-points, no clear pattern was discernible. Thus, in the pigmented retina the level of Cx43 expression at the RPE/NBR interface drops from E18 onwards and is manifested as a reduction in the number of

plaques. In the albino however, Cx43 levels remain constant throughout the period examined.

A comparative analysis of Cx43 localisation patterns indicates that at all stages of development studied (E18-P4), levels of the protein detectable were consistently higher in the albino retina (Figure 5.4.4). Thus at E18, the relative area of Cx43 labelling was approximately 50% lower in the pigmented retina. This difference reached a peak at P4, by which time levels in the pigmented retina were around 85% lower than in the albino (Figure 5.4.4). These differences were statistically significant at the 1% level at both P1 and P4, (p=0.004 and 0.006 respectively). Furthermore, these differences were reflected in the relative plaque number and plaque size. At both P1 and P4, Cx43 plaques were significantly larger and more numerous in the albino retina than in the pigmented, (significant at the 1% or 5% level; Figures 5.4.5A & B).

Effects of L- and D-DOPA on patterns of Cx43 expression

Having demonstrated differential patterns of Cx43 expression in the pigmented and albino retina, the effects of L-DOPA on this parameter were examined in early postnatal albino retinae. Thus, P3 albino (Wistar) rats were administered subcutaneous injections of L-DOPA in conjunction with carbidopa, or D-DOPA at a concentration of 3mM. Tissue was then harvested on P4, and analysed as described in the methods section.

Results are presented in the form of a series of bar charts which plot the total area of Cx43 labelling (Figure 5.4.6), the plaque number per unit area (Figure 5.4.7A) as well as the plaque size (Figure 5.4.7B). All data have been normalised to the untreated albino control. For reference, data from the time-matched pigmented control is reproduced in parallel. The introduction of D-DOPA (a negative control) had no effect on patterns of Cx43 expression in the albino retina, as one might expect (Figures 5.4.6 - 5.4.7). In contrast, the introduction of L-DOPA into the bloodstream, led to a decrease in the total level of Cx43 protein detectable (p=0.0110, Figure 5.4.6), as well as the relative size

of individual plaques (p=0.006, Figure 5.4.7B). In addition, the number of plaques was approximately 35% lower in the L-DOPA-treated retinae (relative to the untreated controls). However, this difference was not statistically significant (p=0.161, Figure 5.4.7A), possibly due to a high level of variance in the data.

Thus, the introduction of L-DOPA into the developing albino retina reduced the abnormally high levels of Cx43 expression at the RPE/NBR interface through a reduction in both absolute levels of the protein, as well as the size of individual plaques.

Application of forskolin to pigmented in vitro eye-cup preparations

Pigmented (D.A.) P1 whole eye-cup preparations were incubated for 4 hours in 30μM and 200μM forskolin dissolved in DMSO. After the elapsed period tissue was fixed and processed to analyse patterns of Cx43 protein localisation as described above. Once again, data is presented in the form of a series of bar charts which plot the total area of Cx43 labelling (Figure 5.4.8), the number of plaques per unit area (Figure 5.4.9A), as well as the size of individual plaques, (Figure 5.4.9B). All values were normalised to and expressed as a proportion of the untreated control.

Results clearly show that the addition of forskolin to the medium had no effect on patterns of Cx43 protein localisation. No significant differences could be detected between any of the groups studied with respect to total levels of Cx43 labelling (Figure 5.4.8, p=0.819), the number of Cx43-positive plaques (Figure 5.4.9A, p=0.356) nor the relative size of individual plaques (Figure 5.4.10B, p=0.657). Consequently, the study was taken no further as any secondary effects on patterns of development could not be linked to changes in levels of connexin expression.

Biolistic labelling of the RPE/neural retina interface

Preliminary attempts to label RPE cells in isolated fixed tissue with a combination of lipophilic dyes were highly successful in that individual RPE cells and small clusters (2-4 cells in size) were strongly labelled, and could easily be detected by confocal microscopy (Figure 5.4.10). However, interest in the technique revolved around its potential to explore the nature of RPE/NBR interactions, and more specifically, the structure of processes which might mediate communication between the two tissues.

Attempts were then made to dissect away the surrounding mesenchyme and presumptive sclera from the posterior pole of the optic globe without damaging the RPE or reducing the intraocular pressure. In this way, RPE cells might be shot with tungsten bullets covered in lipophilic dye from the back of the eye, i.e. from the basal surface, without compromising the structural integrity of the RPE/NBR interface. Hence, the fine anatomical relationship underlying these two tissues might be studied.

This approach was eventually abandoned, as dissection of the surrounding mesenchyme from the retina tended to entail damage and/or removal of the RPE. Consequently, an EM project was initiated to examine the fine structure of the RPE/NBR interface, a technique which facilitated the examination of fine structure at a much higher level of resolution without compromising the physical relationship between the two tissues.

EM of the RPE/neural retina interface

The ultrastructure of the RPE/NBR interface was examined in horizontal sections stained with uranyl acetate. P1 and P4 pigmented and albino retinae were studied. N=three retinae (each from a different animal) examined per group.

On a purely qualitative level no fundamental differences could be detected between the ultrastructure of this region as a function of either developmental stage or pigmentation type. No quantitative analysis was undertaken. Consequently, the findings of this study will be discussed *en masse* without the subdivision of sections according to tissue source.

In Figures 5.4.11-5.4.16 EM micrographs are presented, illustrating the salient structural features of the RPE/NBR interface. At the end of the section a schematic representation of this region is provided (Figure 5.4.17). As the area is highly complex and dense in cell processes, it may be of use to consult the schematic diagram initially, or in parallel with the EM micrographs.

Subretinal plexus

The first and most striking finding to come out of this study is that contrary to expectations, mitotic cell division in the NBR did not occur immediately adjacent to the apical surface of the RPE, the two surfaces being separated by a complex plexus of heterogeneous processes (see Figure 5.4.11). This region, (defined as the subretinal plexiform layer (SPL) for the purpose of this thesis), appears as a discrete layer in ultrathin section, several microns in size. It is bounded on one side by the apical surface of the RPE, and on the other, by a band of junctional complexes which define the outer limit of the NBR (Figure 5.4.11A).

The SPL is characterised by several unique features. Firstly, it contains the endfeet of neuroepithelial cell processes (Figure 5.4.11B & 5.4.12). Dividing retinal progenitors undergo a stereotypical pattern of localised migration back and forth across the depth of the retina. Throughout this movement (known as interkinetic nuclear migration), cells retain an apical process which is connected to the ventricular surface. Seen in ultrathin sections, the apical extreme of this process appears as a large bulbous expansion which is densely packed with mitochondria, suggesting an intense level of metabolic activity (Figure 5.4.14). These process endfeet are in close apposition to both adjacent cell endfeet, and the apical surface of the RPE.

Junctional complexes

Highly electron-dense junctional complexes could be detected at all stages examined. These complexes were associated with closely apposed membranes and fell into three distinct categories reflecting the locations in which they were found:

(1) Junctional complex formation between adjacent neuroepithelial cell processes.

Just proximal to the point at which the apical extreme of the neuroepithelial cell process expands to form a bulbous structure, a discrete "collar" of junctional complex forms an intimate association between the cell's membrane and that of adjacent cell processes (Figure 5.4.11B). This was detected in all cell processes that were sectioned in the precise plane and hence could be traced over a distance of 10μm or more. This suggests that the formation of a junctional complex between cell processes is characteristic of retinal neuroepithelial cells that are undergoing interkinetic nuclear migration, and hence, are still in the cell cycle.

(2) Junctional complex formation at the apical surface of an actively dividing cell.

Electron dense junctional complexes were detected at the apical extreme of cells undergoing mitotic division at the VM (Figure 5.4.16). These complexes also appeared to form junctions with adjacent cell processes and were detectable at all stages of the cell cycle, suggesting that the junctions are formed at the apical extreme of a cell's process, and are retained upon migration of the cell body to the VM for the purpose of cell division.

During cytokinesis these junctional complexes might be symmetrically distributed to both daughter cells of the division (Figure 5.4.16C & D). In a snapshot of another division however, the apical daughter cell appeared to have

retained its junctional contact with the VM, whilst the other would seem to migrate away from the VM towards the vitreal surface (Figure 5.4.16E & F). Whether or not this reflects an asymmetric division is unclear, although a more extensive EM study of basal process and apical junction inheritance may complement real-time imaging techniques that are currently being employed to address this issue.

(3) Junctional complex formation between the endfeet of neuropethelial cell processes and the distal extreme of RPE-derived processes.

Junctional complexes similar in appearance to those described above were also observed between the expanded endfeet of neuroepithelial cell processes, and the distal extreme of processes originating from the RPE (Figure 5.4.12C & 5.4.15). These RPE processes seemed to co-localise with regional concentrations of cilia as detected by the characteristic "9+2" arrangement of microtubules in cross-section, (arrows in Figure 5.4.15). In addition, they were of a similar size to the stereotypic cilium (~200-250nm wide), leading to speculation that these RPE-derived processes which form junctional complexes with the endfeet of neuroepithelial cell processes are in fact cilia.

Sites of RPE/neuroblastic retina communication

There were several sites at which the NBR and the RPE came in to close physical contact, and hence, presented potential pathways of non-extracellular communication. First, as described above, electron-dense junctional complexes could be detected between processes arising from the RPE and the endfeet of neuroepithelial cell processes (Figure 5.4.15). These complexes may incorporate connexins, and hence facilitate electrochemical coupling of the two tissues. In addition to these larger RPE-derived processes (potentially composed of cilia), smaller and more abundant processes were found to arise from the apical surface of the RPE and interdigitate between/encapsulate the neuroepithelial process endfeet (Figure 5.4.11A&B). Finally, in sections where the RPE and NBR remained closely apposed during tissue preparation, the neuroepithelial cell endfeet were often found to be in direct contact with the

apical surface of the RPE (Figure 5.4.14). Furthermore, in these instances, electron-dense contributions from both cell membranes could be detected which were characteristic of less complex junctional coupling.

Cx43 localisation, E13 and E15

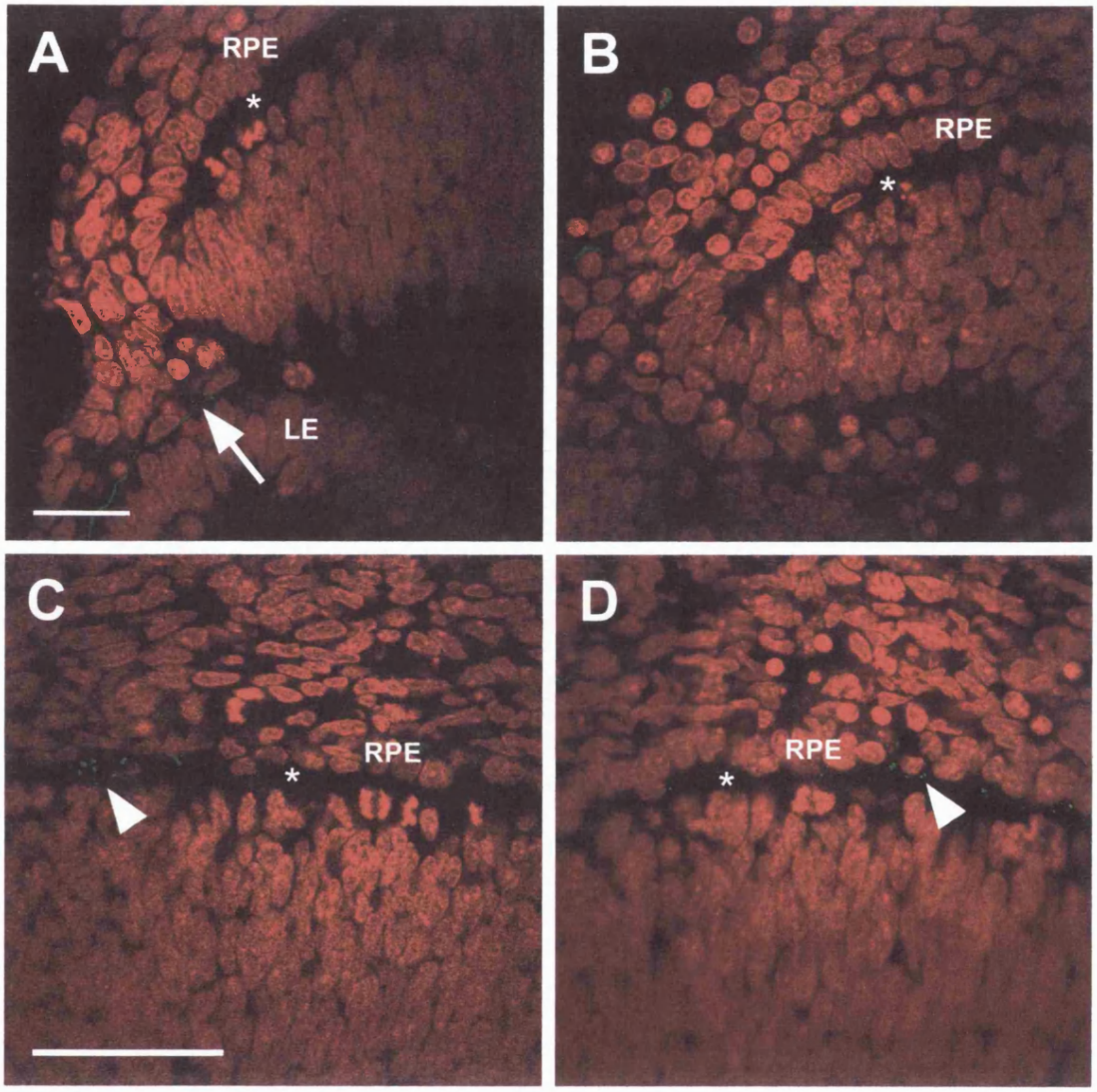

Figure 5.4.1 Patterns of Cx43 labelling in the early developing eye. Retinal sections from the (A) E13 pigmented, (B) E13 albino, (C) E15 pigmented, and (D) E15 albino eye were stained with anti-Cx43 antibodies (green). Nuclei were visualised by counterstaining with DAPI or propidium iodide (red). In the E13 eye Cx43 label was not detected between the RPE and the NBR. In contrast, by E15, punctate labelling could be seen at the RPE/NBR interface in tissue from both pigmented (C) and albino (D) retinae (arrowheads). Labelling was scarce and isolated however. In tissue from both E13 and E15/pigmented and albino retinae, Cx43 was heavily expressed in the apical surface of the lens epithelium (LE), providing an internal positive control; white arrow in (A). Asterisks indicate the position of the VM. RPE = retinal pigment epithelium. Scale bar = 50μm.

Cx43 Localisation, E18-P4

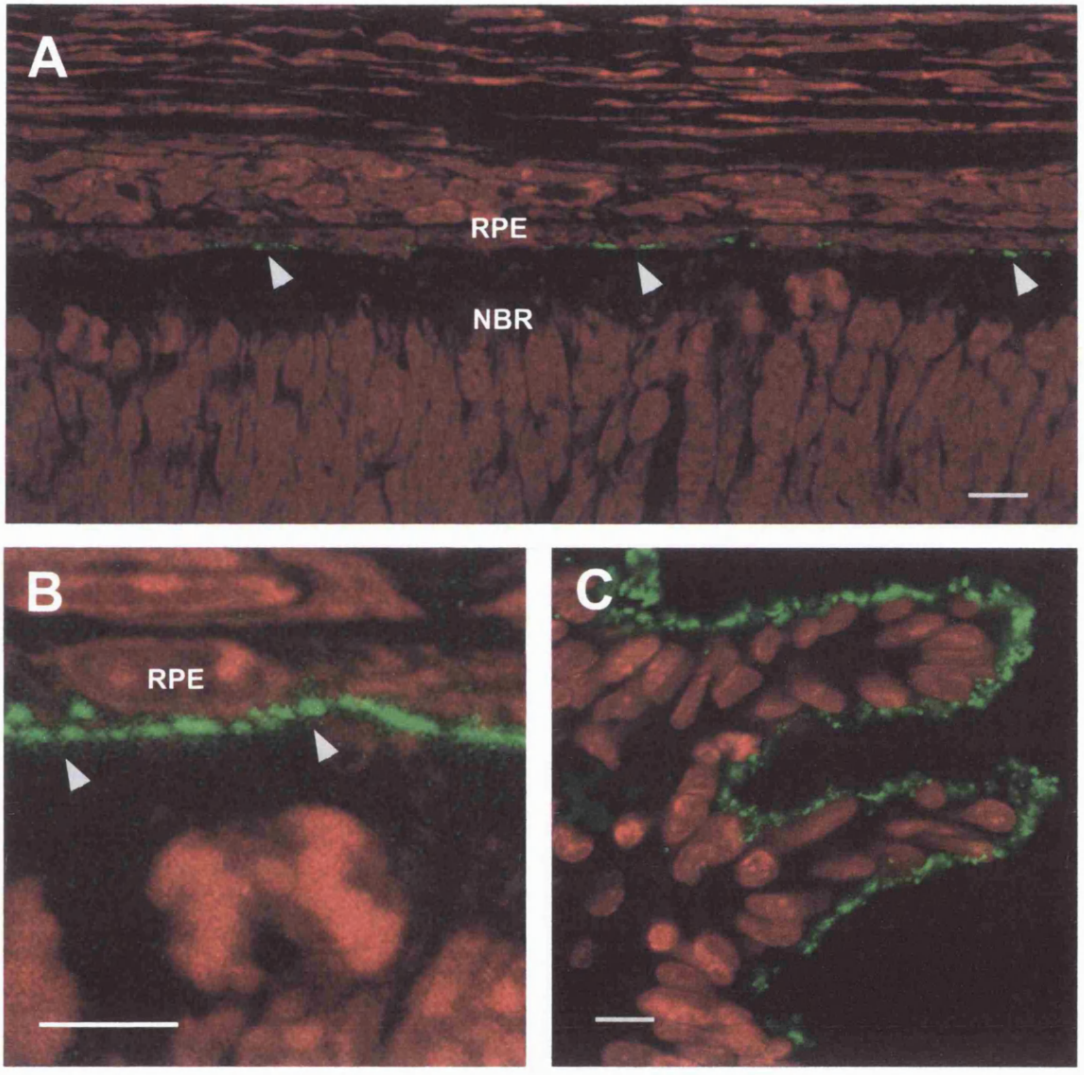

Figure 5.4.2 Pattern of Cx43 expression in the P4 retina. (A) From E18 onwards Cx43 protein could be detected as a line of punctate labelling at the RPE/NBR interface (green). Sections were counterstained with propidium iodide to visualise nucleic acid. In this image a single z-slice is shown. (B) A high magnification image of a mitotic cell from (A) illustrating its relationship with the RPE and associated Cx43 plaques. The image is a two-channel z-stack projection of a section which is several microns in depth. (C) At all stages examined Cx43 was expressed at high levels in the *orra serrata*, providing an internal positive control. Error bars=10μm.

Cx43 levels in the pigmented and albino retina

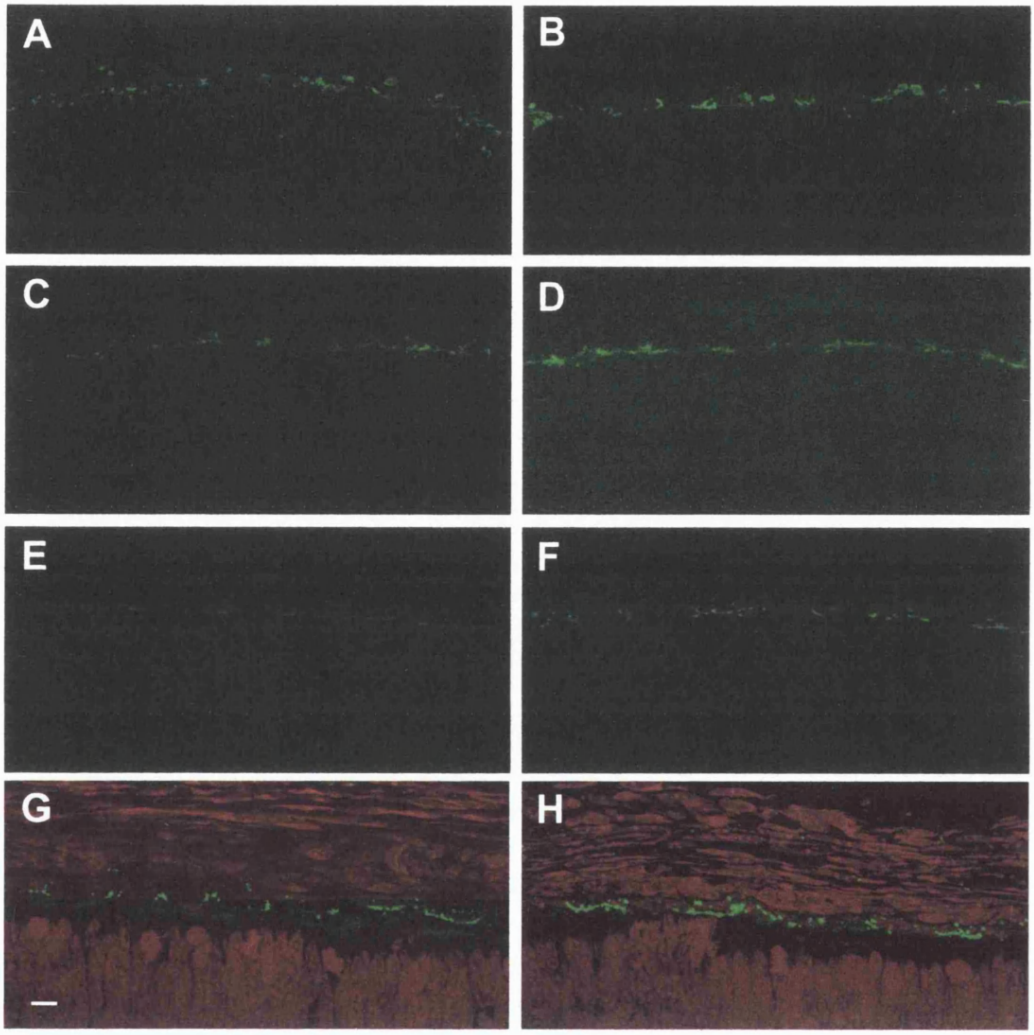

Figure 5.4.3 Patterns of Cx43 expression in the developing pigmented and albino retina, (E18-P4). Confocal micrographs are shown for pigmented (left-hand panels) and albino (right-hand panels) retinae at E18 (A&B), P1 (C&D) and P4 (E&F). Images are single-channel 5μm z-stack projections showing labelling for Cx43 (green). All parameters with respect to tissue staining, imaging and data analysis have been standardised per time-point facilitating direct quantitative comparison between pigmentation types. The area and intensity of staining is greater in the albino retina at P1 and P4. Reference images are shown from P4 pigmented (G) and albino (H) retinae. Tissue has been counterstained with propidium iodide to visualise nucleic acid. Scale bar=10μm and is relevant to all panels.

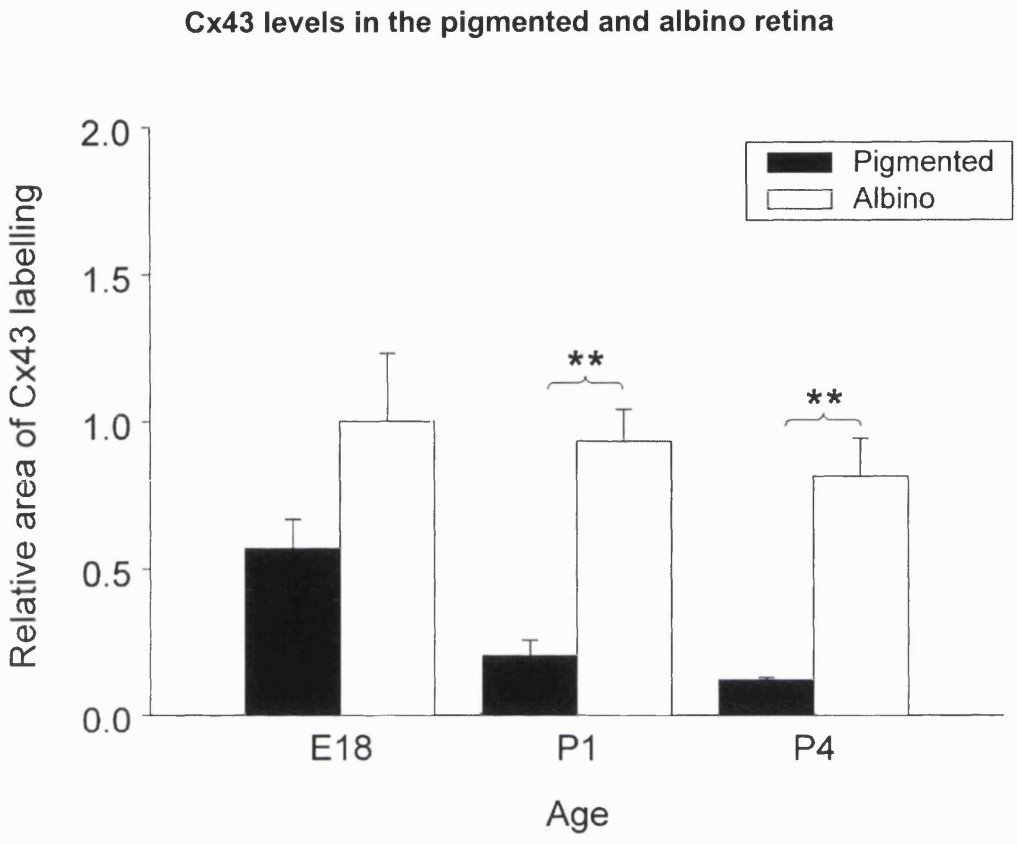

Figure 5.4.4 The relative area of Cx43 labelling is plotted for pigmented (D.A.) and albino (Wistar) rat retinae at E18, P1 and P4. All data are normalised to the E18 albino. Error bars represent the standard error of the mean. All staining, scanning and image analysis protocols were standardised per time-point and performed in parallel facilitating direct quantitative comparison between pigmentation types. Intensity thresholds during image analysis were altered slightly between time-points in order to compensate for differential levels of background signal as a function of age, though settings were maintained between pigmentation types. The total area of Cx43 labelling was consistently higher in the albino tissue at all time-points examined, though it only reached statistical significance at P1 and P4. Three retinae were examined per experimental group and 5 regions were analysed per retina. * $p<0.05$, ** $p<0.01$.

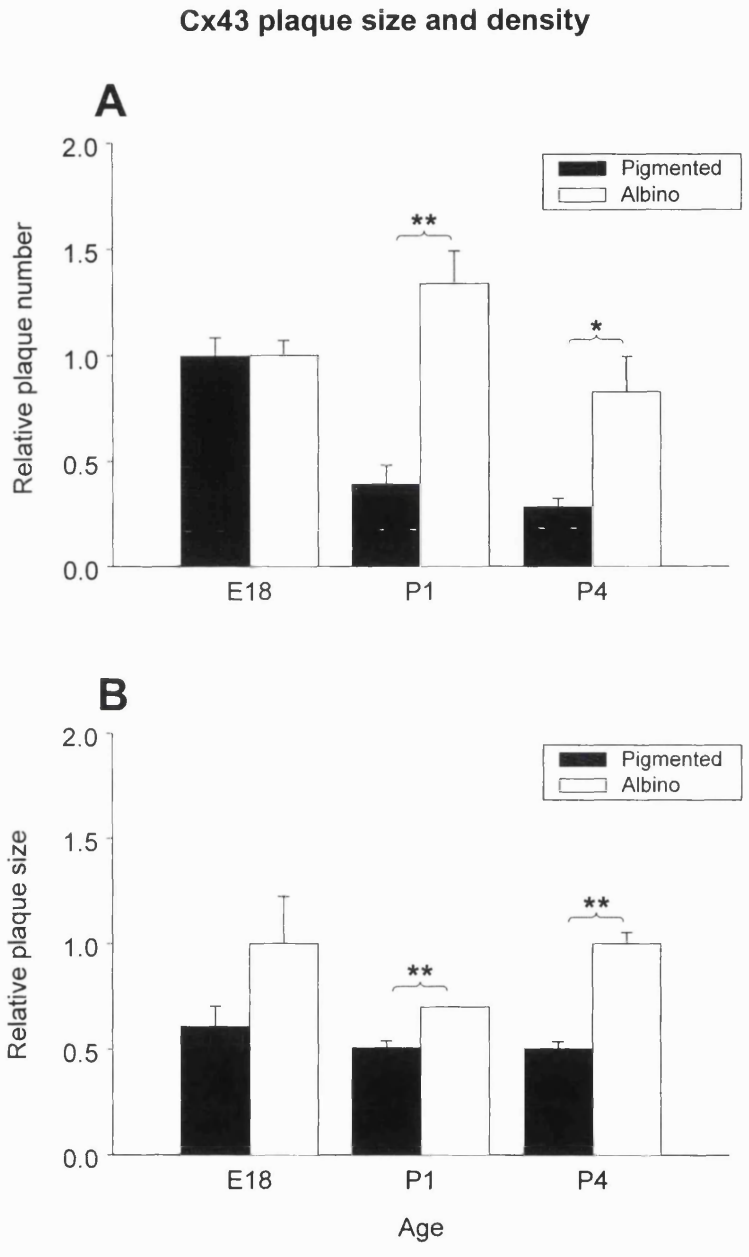

Figure 5.4.5 The relative (A) number and (B) size of Cx43 positive plaques is plotted for pigmented (D.A.) and albino (Wistar) rat retinae at E18, P1 and P4. All data are normalised to the E18 albino. Error bars represent the standard error of the mean. All staining, scanning and image analysis protocols were standardised per time-point and performed in parallel facilitating direct quantitative comparison between pigmentation types. Both the number and size of Cx43 plaques was greater in the albino relative to the pigmented at P1 and P4. No differences could be detected at E18. Three retinae were examined per experimental group and 5 regions were analysed per retina. * $p<0.05$, ** $p<0.01$.

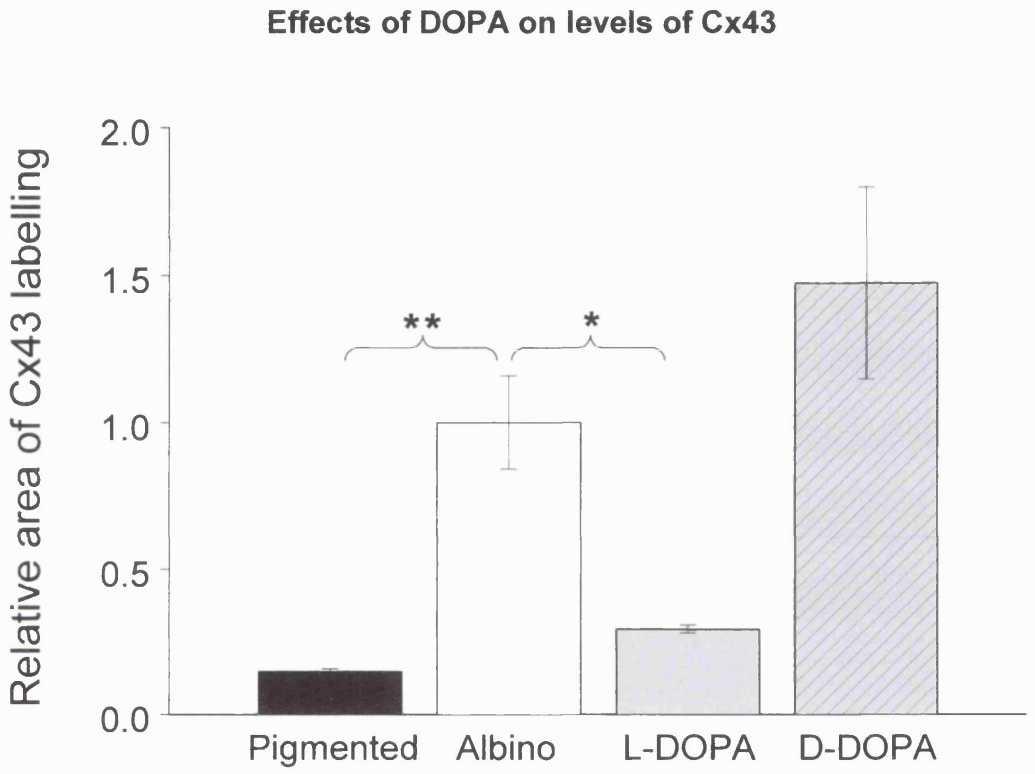

Figure 5.4.6 The relative area of Cx43 labelling is plotted for control, L-DOPA-treated and D-DOPA-treated albino (Wistar) P4 rat retinae. In addition, data from the P4 pigmented tissue is reproduced for comparison. L-DOPA in conjunction with a decarboxylase inhibitor (carbidopa), and D-DOPA were delivered at a concentration of 3mM. All data are normalised to an untreated albino retina. Error bars represent the standard error of the mean. All staining, scanning and image analysis protocols were standardised and performed in parallel for each experimental pair, facilitating direct quantitative comparison. The total area of Cx43 labelling was reduced in the albino retina upon introduction of 3mM L-DOPA to the bloodstream, an effect which was significant at the 5% level. In contrast, D-DOPA had no effects on levels of Cx43 expression. Three retinae were examined per experimental group and 5 regions were analysed per retina. * $p<0.05$, ** $p<0.01$.

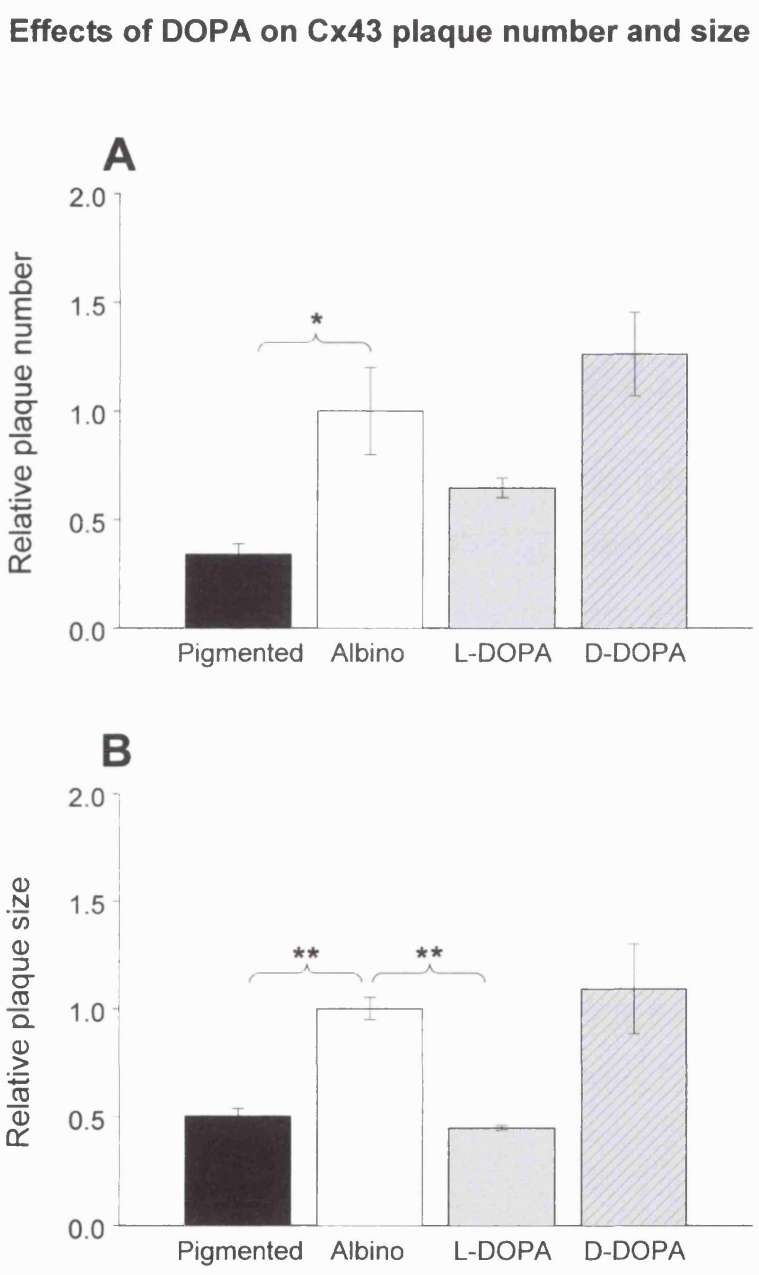

Figure 5.4.7 The relative (A) number and (B) size of Cx43 positive plaques is plotted for control, L-DOPA-treated and D-DOPA-treated P4 albino rat retinae. In addition, data from the P4 pigmented tissue is reproduced for comparison. All data are normalised to the untreated albino retina. Error bars represent the standard error of the mean. All staining, scanning and image analysis protocols were standardised and performed in parallel for each experimental pair, facilitating direct quantitative comparison. Both the number and size of Cx43 plaques was reduced by the introduction of L-DOPA into the retina, although a statistically significant difference was only found with respect to plaque size. Three retinae were examined per treatment group and 5 regions were analysed per retina.

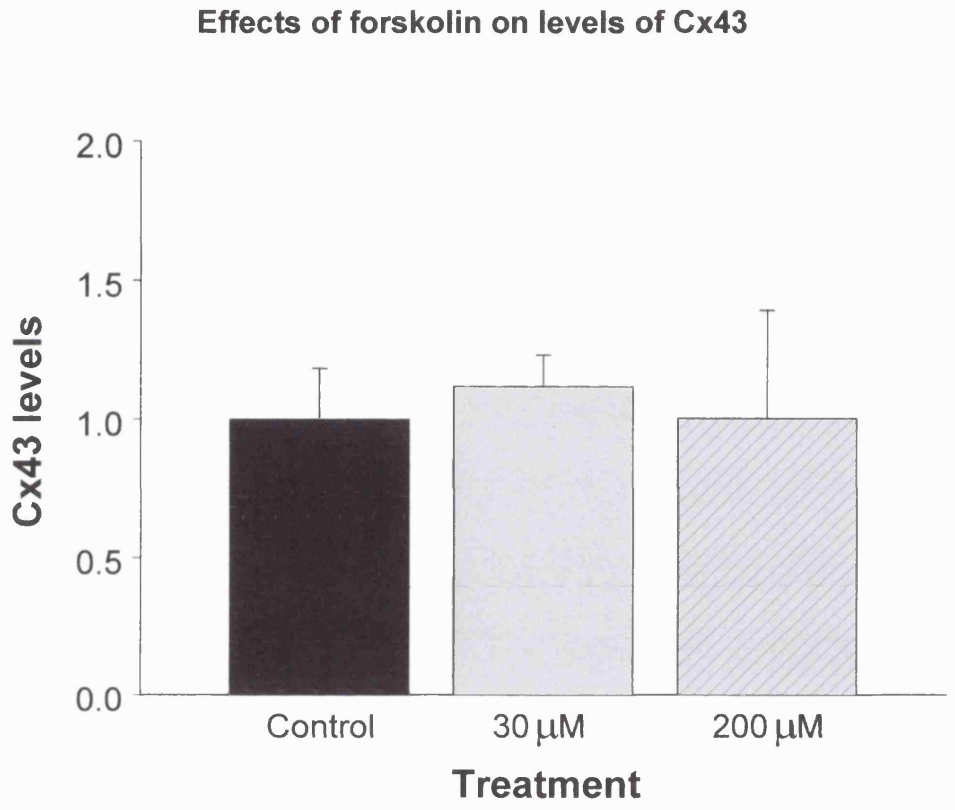

Figure 5.4.8 The relative area of Cx43 labelling is plotted for P1 pigmented (D.A.) rat retinae that were incubated for four hours *in vitro* in minimal medium supplemented with 30μM or 200μM forskolin dissolved in DMSO. All data are normalised to the untreated control. Error bars represent the standard error of the mean. All staining, scanning and image analysis protocols were standardised and performed in parallel facilitating direct quantitative comparison between experimental groups. None of the treatments were found to affect levels of Cx43 labelling (p=0.819). Three retinae were examined per treatment group and 5 regions were analysed per retina.

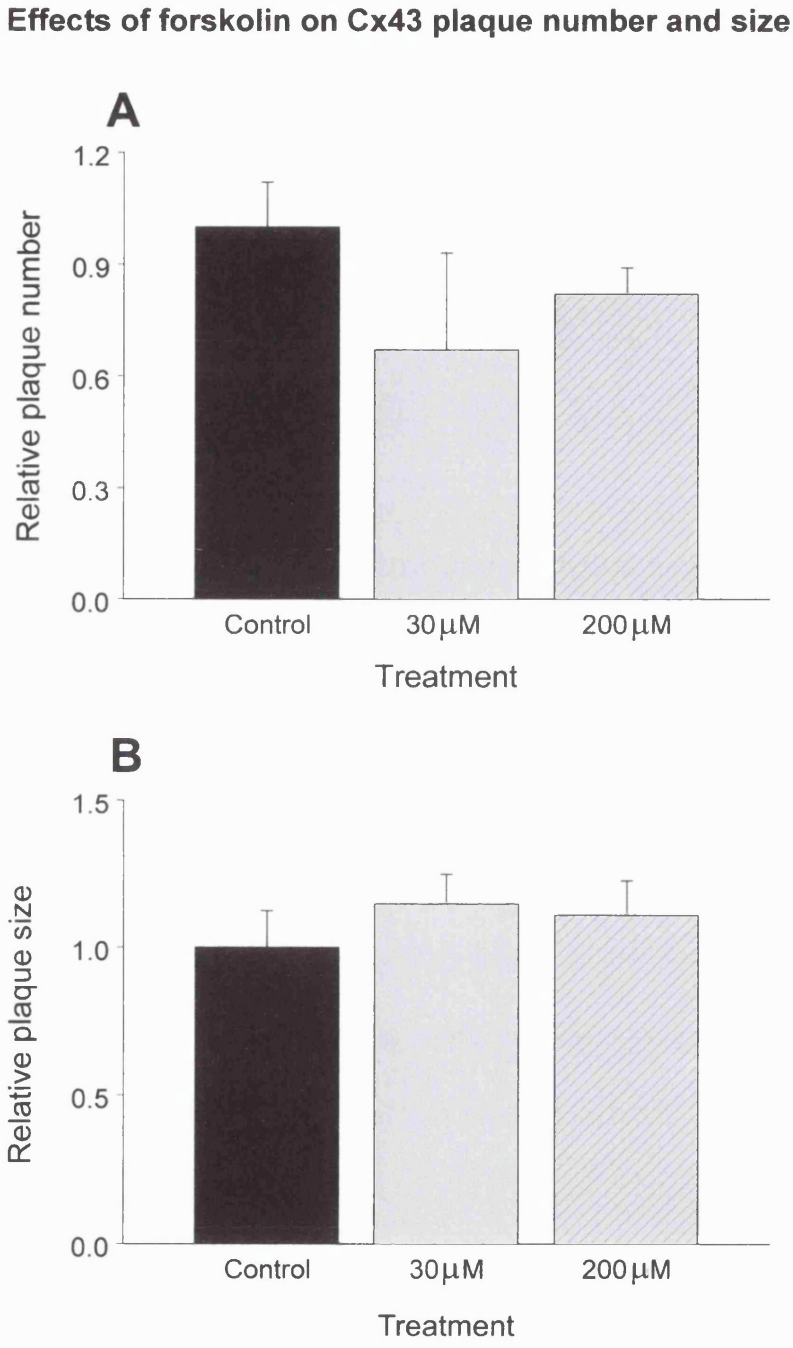

Figure 5.4.9 The relative (A) number and (B) size of Cx43 positive plaques at the RPE/ NBR interface is plotted for P1pigmented (D.A.) rat retinae that were incubated for four hours in minimal medium supplemented with 30μM or 200μM forskolin (dissolved in DMSO). All data are normalised to the untreated pigmented retina. Error bars represent the standard error of the mean. All staining, scanning and image analysis protocols were standardised and performed in parallel facilitating direct quantitative comparison between experimental groups. None of the treatments were found to affect either the number of Cx43 plaques per unit area or the size of individual plaques (p=0.356 and 0.657 respectively). Three retinae were examined per treatment group and 5 regions were analysed per retina.

Diolistic labelling of retinal pigment epithelium cells in fixed tissue

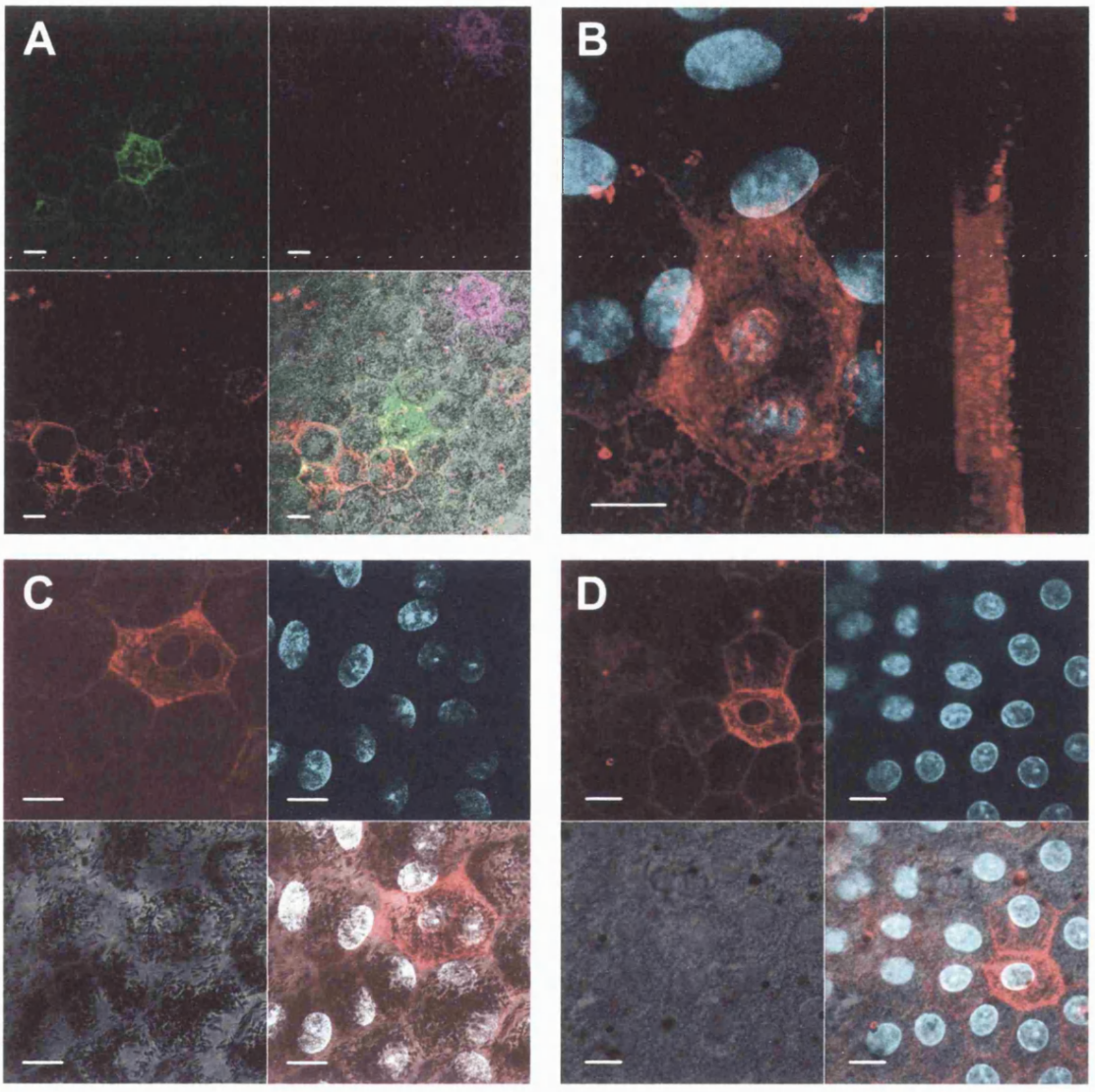

Figure 5.4.10 In order to examine the anatomical structure underlying the interactions between the RPE and NBR during development RPE cells were shot with tungsten beads covered with the lipophilic dyes DiI (red), DiO (green) and DiD (purple); with excitation wavelengths of 568nm, 488nm and 647nm respectively. The tissue was counterstained with DAPI (blue) in order to visualise cell nuclei. (A) P4 pigmented (D.A.) RPE cells labelled with the 3 different dyes, each panel showing a different channel configuration, (clockwise from bottom left; DiI, DiO, DiD and multichannel overlay with DIC). (B) Higher magnification image of an individual RPE cell labelled with DiI and surrounding nuclei. In the right hand panel, the cell has been rotated by 90° about the y-axis. (C) Pigmented (D.A.) and (D) albino (Wistar) rat RPE cells. Individual channels (clockwise from bottom left) represent a DIC image, DiI staining, DAPI labelling and multichannel overlay. Note the binucleate RPE cell in (C). Scale bars=10μM.

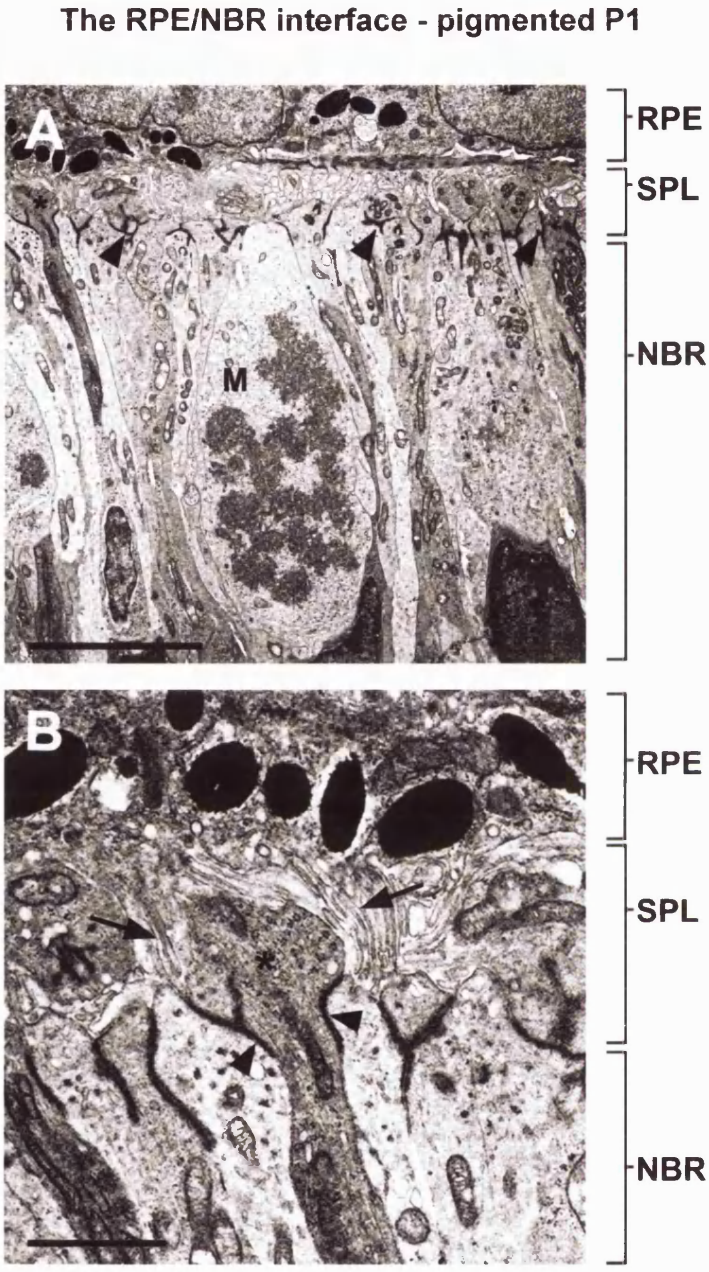

Figure 5.4.11 (A) EM micrograph illustrating the relationship between the RPE and NBR in the P1 pigmented retina. Mitotic cells of the NBR do not sit immediately adjacent to the apical surface of the RPE. The two surfaces are separated by a complex plexus of heterogeneous processes. This subretinal plexiform layer (SPL) is bounded on one side by the apical surface of the RPE, and on the other, by a band of junctional complexes (black arrow-heads) which define the outer limit of the NBR. (B) Higher magnification image of the expanded endfoot (*) of a NBR cell process in the SPL. A collar of junctional complex brings its membrane in to close apposition with adjacent cell processes. A multitude of smaller processes (black arrows) arising from the apical surface of the RPE envelop the process endfoot and interdigitate between adjacent cell processes. Scale bar =5μm in (A) and 1μm in (B).

The RPE/NBR interface - pigmented P4

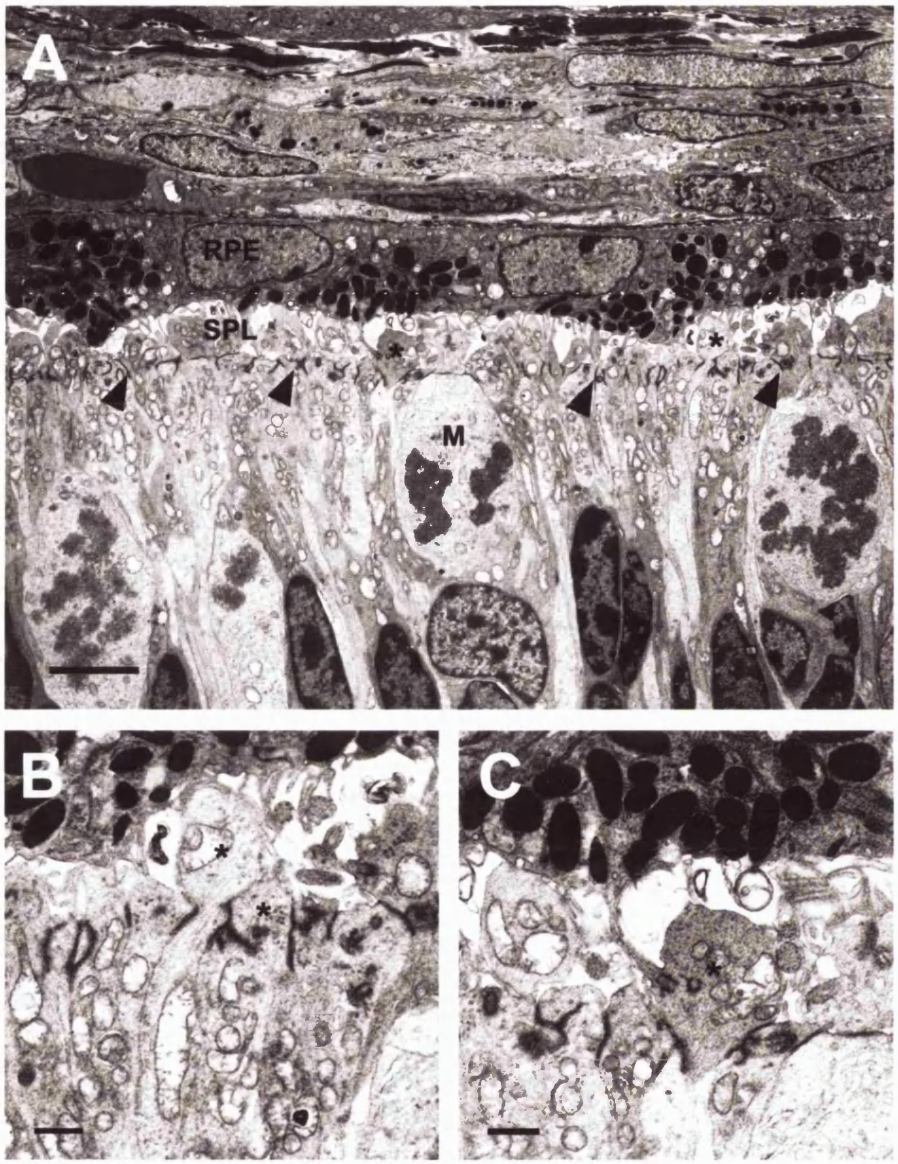

Figure 5.4.12 (A) EM micrograph illustrating the relationship between the RPE and NBR in the P4 pigmented retina. No difference could be detected with respect to the ultrastructure of this region between P1 and P4. The VZ of the NBR was separated from the apical surface of the RPE by a discrete layer of complex and heterogeneous processes arising from both the RPE and NBR. (B) Higher magnification image demonstrating the existence of electron dense junctional complexes between adjacent process endfeet (*). (C) In addition, a similar junctional complex could be detected between the endfeet of retinal neuroblastic cell processes (*) and the distal extreme of processes emanating from the RPE. These latter structures were not homologous with the finer RPE processes described in Figure 5.4.11 and could be distinguished both by size and frequency, being considerably larger and less numerous. Scale bar =5μm in (A) and 1μm in (B&C).

The RPE/NBR interface - pigmented and albino

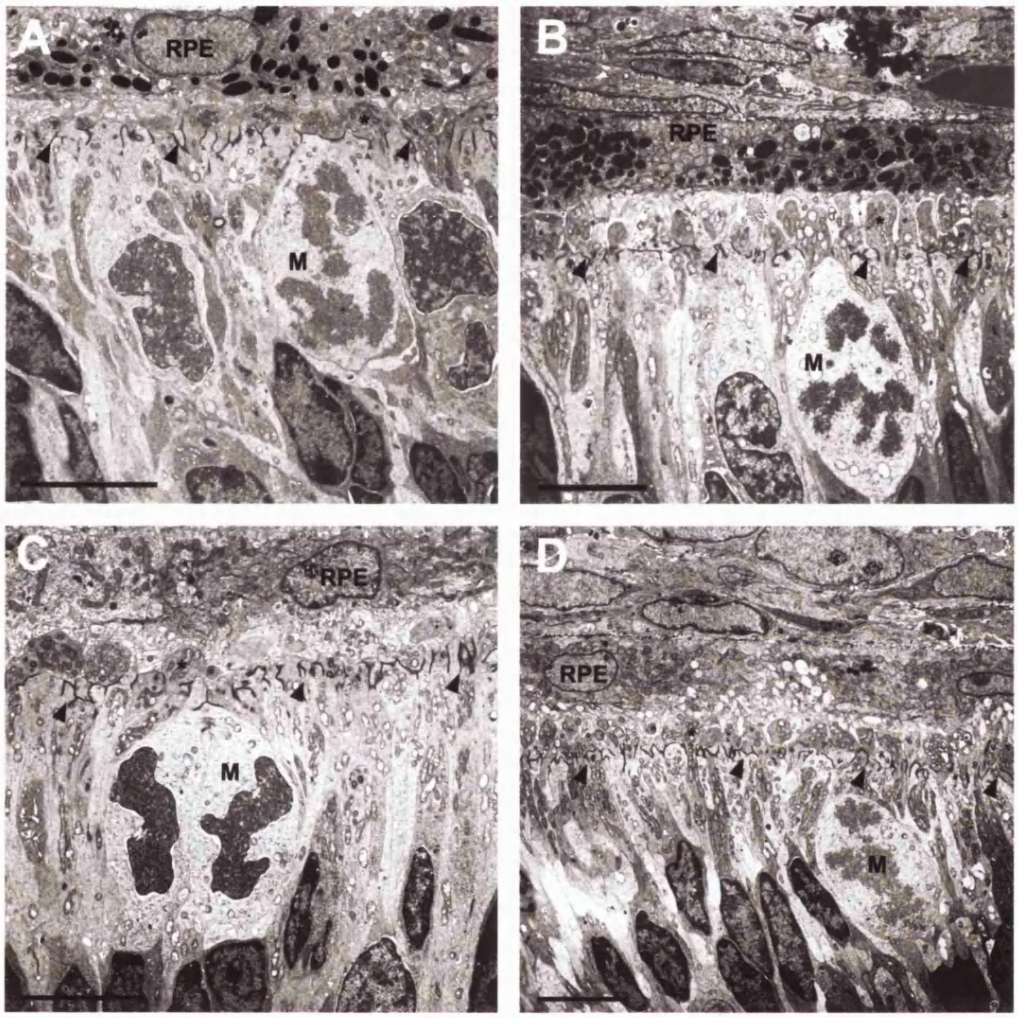

Figure 5.4.13 EM micrographs illustrating the relationship between the RPE and NBR in the (A) pigmented P1, (B) pigmented P4, (C) albino P1and (D) albino P4 rat retina. No difference could be detected with respect to the ultrastructure of this region between developmental time-points or pigmentation types. Black arrowheads indicate the line of electron dense junctional complex which sits at the VM of the NBR. Asterisks denote an example neuroepethalial cell endfoot within the SPL of each image. RPE=retinal pigment epithelium, M=mitotic cell. Scale bar=5μm in all panels.

Putative sites of communication between the RPE and NBR

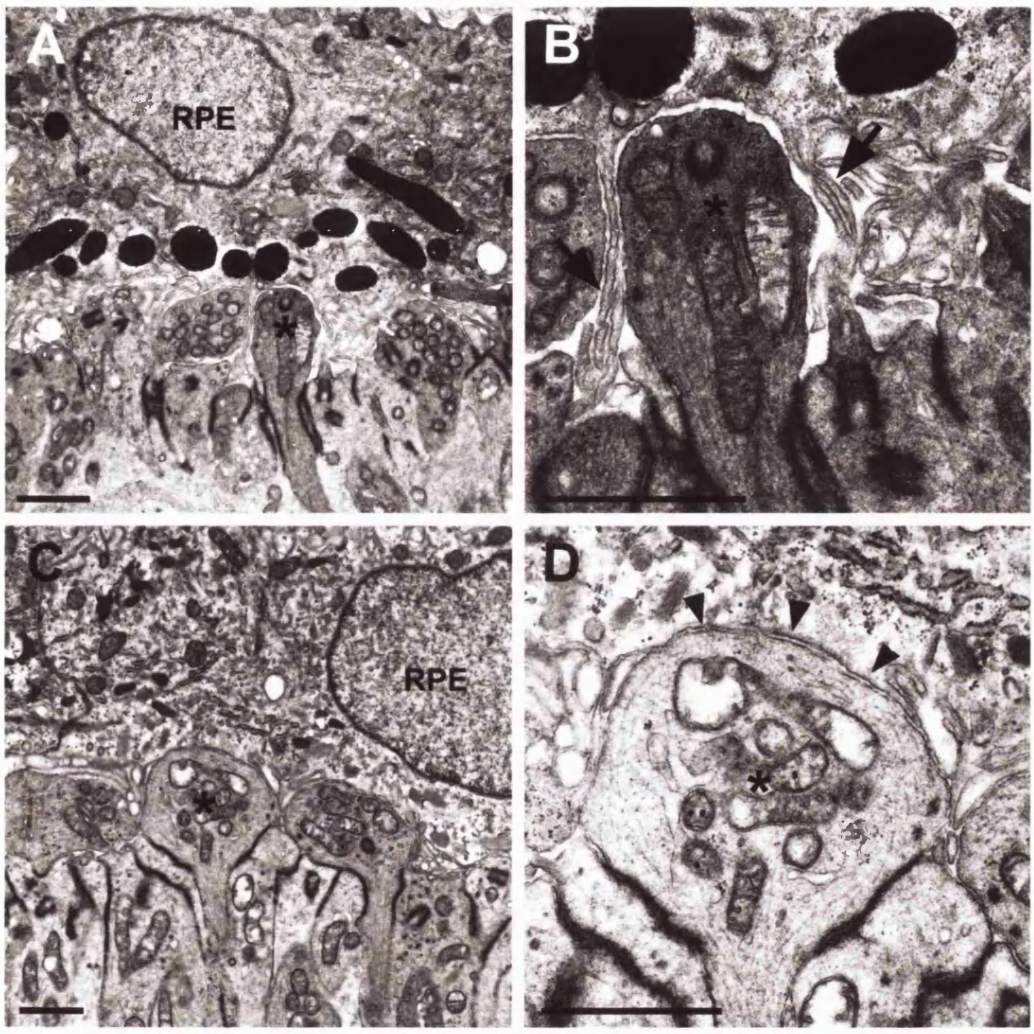

Figure 5.4.14 EM micrographs illustrating the sites at which the RPE and NBR come into close contact. This interaction is mediated by a complex mass of heterogeneous processes. (A&B) Lower and high magnification images (respectively) of a NBR cell process endfoot (*) and its encapsulation by a multitude of RPE cell processes (black arrows). These latter structures are easily visualised when the two tissues become slightly uncoupled during tissue preparation. (C&D) Electron-dense junctions (black arrow-heads) can be detected between the apical surface of the RPE and the endfeet of retinal cell processes (*). Note the density of mitochondria within the endfeet of the neuroblastic cell processes. RPE=retinal pigment epithelium, M=mitotic cell. Scale bar =1μm in all panels.

Cilia arise from the apical surface of the RPE

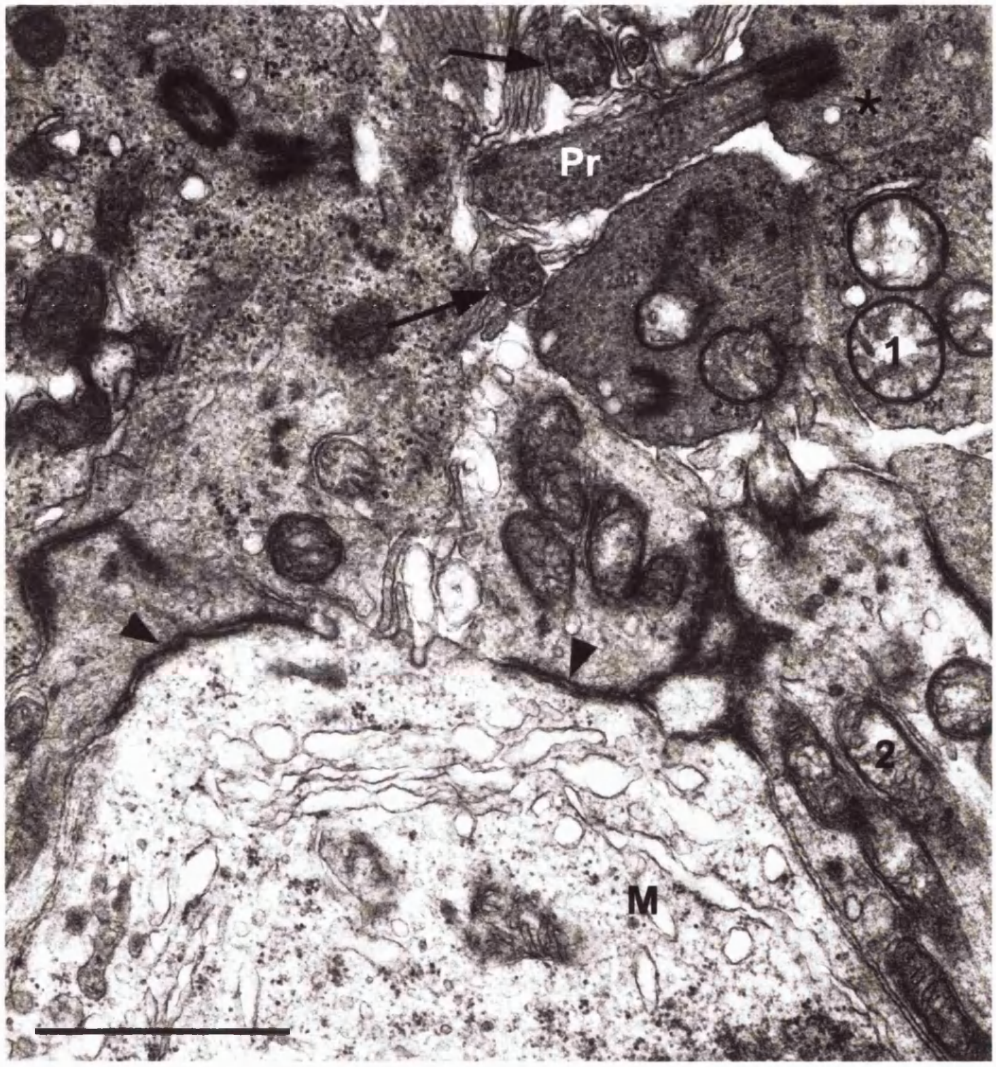

Figure 5.4.15 EM micrograph of the subretinal space in an albino P4 retina. A cellular process similar to that in Figure 5.4.12C arises from the apical surface of the RPE and forms an electron dense junctional complex with the endfoot of a retinal neuroepithelial cell process (*).These RPE cell processes would appear to be associated with localised concentrations of cilia as detected by the characteristic "9+2" arrangement of microtubules in cross-section (black arrows). In addition, they were of a similar thickness to the stereotypical cilium (~200-300nm wide), leading to the speculation that these RPE-derived processes are in fact cilia. Black arrowheads illustrate the junctional complexes which form at the apical membrane of dividing retinal neuroblasts. In higher power images these highly electron-dense structures can be seen to be made up of contributions from both the mitotic cell and adjacent cell processes. Though this particular image is taken from an albino P4 retina it is typical of tissue from each developmental stage and pigmentation type. M=mitotic cell. Pr=RPE cell process. Scale bar =1µm.

Junctional complex at the apical surface of dividing neuroblasts

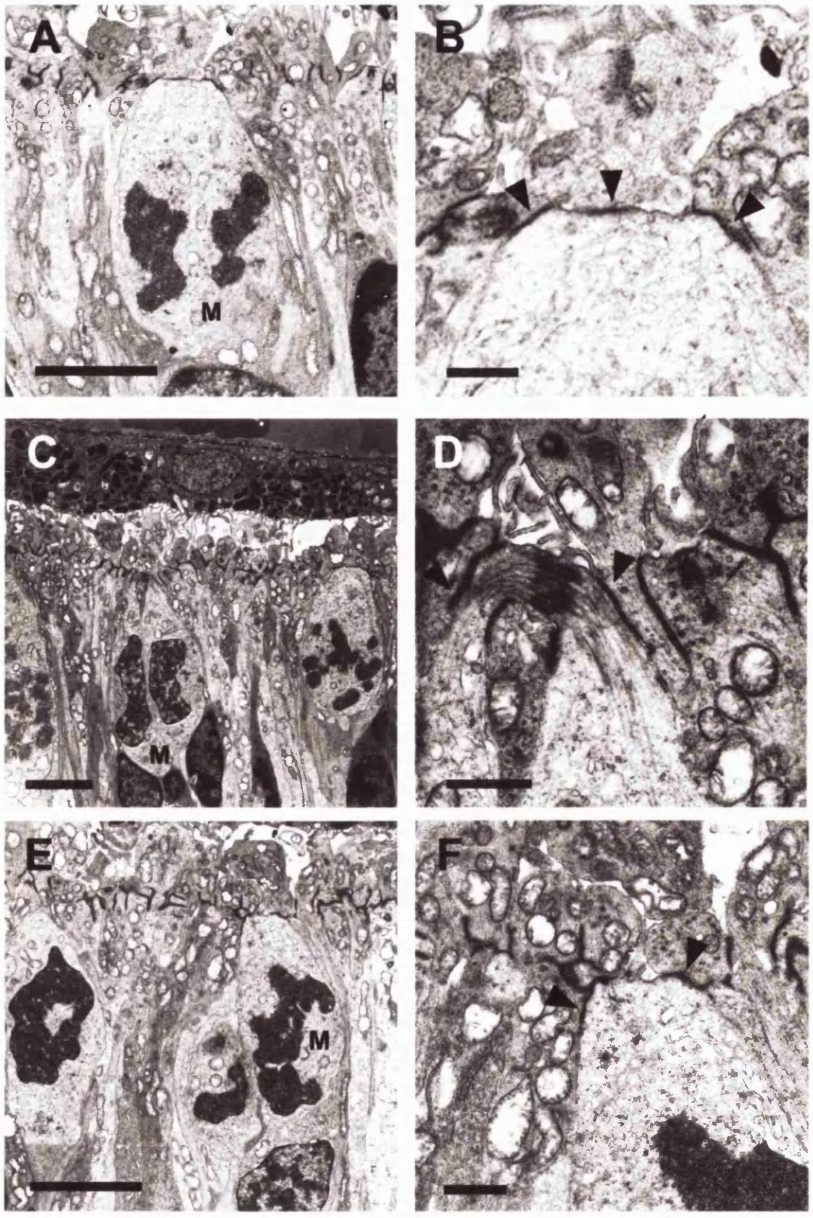

Figure 5.4.16 EM micrographs of actively dividing cells in various stages of mitosis. Electron-dense junctional complexes (black arrow-heads) were detected at the apical membrane of cells undergoing mitotic division, bringing the cell membrane in to close apposition with the endfeet of adjacent cell processes (A&B). These junctions were found in cells in all stages of the cell cycle and would appear to be derived from those found in the endfeet of retinal cell processes. During cytokinesis (as captured in (C) and (D)) they appear to be symmetrically distributed to both daughter cells of the division. In a snapshot of another division however (E&F), the apical daughter cell appears to have retained its junctional contact, whilst the other has broken away from the VM. M=mitotic cell. Scale bars =5μm in left hand panels and 1μm in the right hand panels.

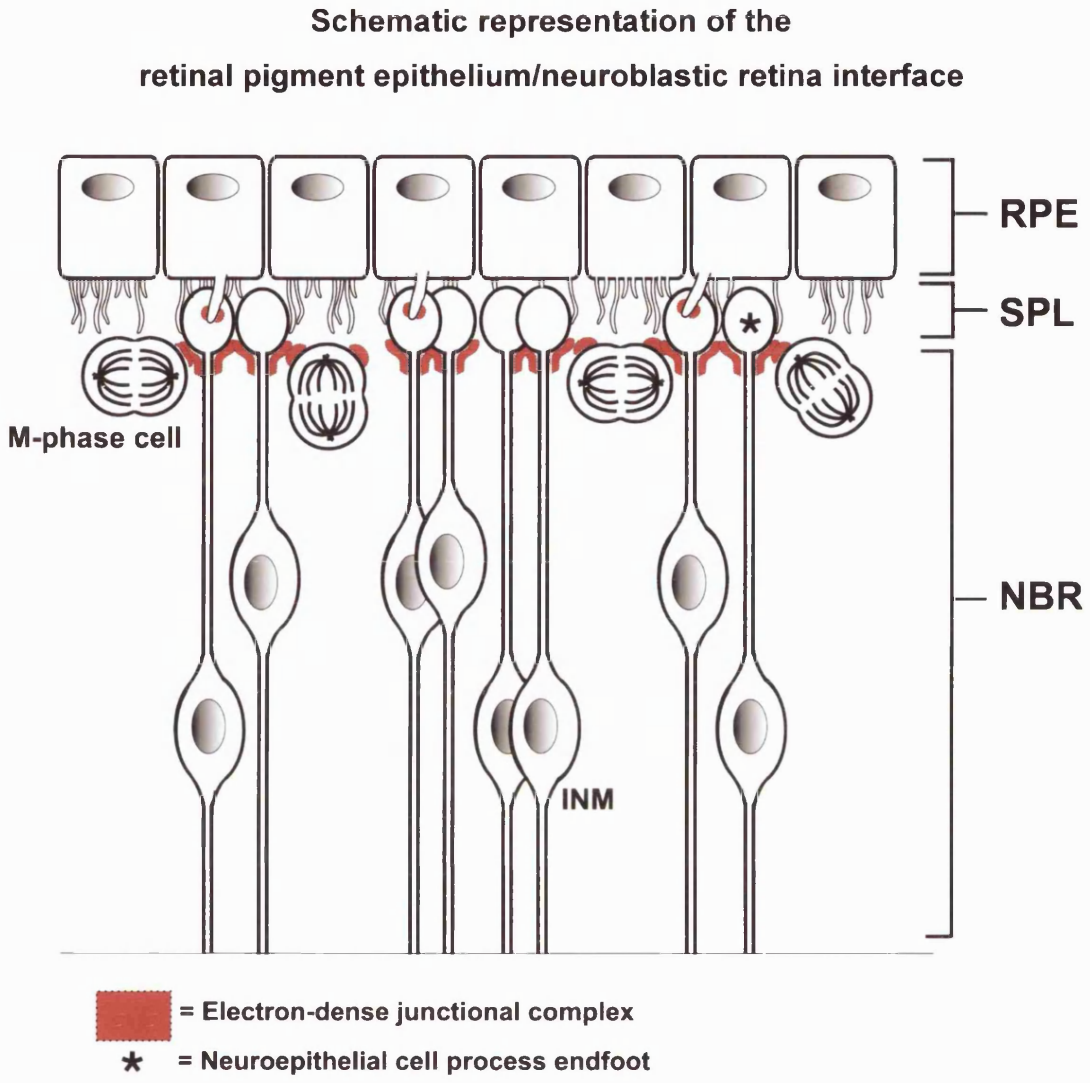

Figure 5.4.17 Between the VM of the neuroblastic retina (NBR) and apical surface of the retinal pigment epithelium (RPE) lies a dense network of complex and heterogeneous processes that would seem to underlie the physical coupling of the NBR and RPE. At the apical surface of the NBR, this zone –which will be referred to as the subretinal plexiform layer (SPL) for the purpose of this thesis- is bounded by a line of electron-dense junctional complex that runs along the VM. This junctional complex was detected at the apical surface of actively dividing (M-phase) cells, and at the interface between the endfeet of processes (*) emanating from cells of the NBR that were undergoing interkinetic nuclear migration (INM). At the apical surface of the RPE, two distinct types of processes were found to emanate from the cell membrane. One was small and resembled the microvillli of the adult RPE, interdigitating between the NBR cell process endfeet. The second was thicker (~200-250nm wide) and less numerous, colocalised with regional concentrations of cilia, and formed junctional complex at its distal extreme with NBR cell endfeet.

5.5 Discussion

The relationship between the RPE and retinal neuroepithelium was examined in developing pigmented and albino tissue using a variety of histological techniques. First, patterns of Cx43 protein localisation -the primary connexin responsible for gap junction mediated electrochemical coupling of the RPE and NBR (Becker *et al.*, 1998; Pearson *et al.*, 2004a)- were analysed by immunofluorescent detection. Tissue from E13 through to P4 was studied; a period encompassing the main window of retinal neurogenesis. Cx43 protein was first detected at the RPE/NBR interface at E15. No differences in either the spatial or temporal patterns of expression could be detected between pigmentation types during the earlier phases of development examined. By P1 however, levels of Cx43 positive labelling were significantly elevated in the albino retina relative to pigmented time-matched controls.

Despite the lack of a physiological correlate to support the differential pattern of Cx43 staining described between pigmentation types, elevated levels of connexin localisation to the RPE/NBR interface are likely to infer a higher level of electrochemical communication between the two tissues (Pearson *et al.*, 2004a). In addition to forming functional gap junctions between the RPE and NBR, Cx43 hemichannels at the apical surface of the RPE present a pathway for the release of regulatory signals into the subretinal space which influence the development of the retinal neuroepithelium (Pearson *et al.*, 2004b).

Thus, levels of RPE-derived regulatory signals reaching the NBR (either by direct transfer or by diffusion across the subretinal space) are likely to differ between the pigmented and albino retina as a consequence of elevations in the level of Cx43 protein. Is it possible that subtle perturbations in the effective concentration of these signals, or alternatively, the temporal window in which they are presented to the retinal neuroepithelium could underlie the many developmental defects that characterise the albino retina? The RPE has been

shown to regulate many processes of retinal development (Raymond and Jackson, 1995; Jablonski *et al.*, 2000; Pinzon-Duarte *et al.*, 2000; Jensen *et al.*, 2001) and gap junctions present the primary means by which signals are propagated between the two tissues during development (Hayes, 1976; Hayes, 1977).

Evidence from an isolated *in vivo* study would suggest that by experimentally inducing a change in levels of gap junction expression in the eye, subtle developmental defects can be induced. When antisense oligodeoxynucleotide gel to Cx43 was applied to the developing chick retina, mitotic levels were reduced and the treated eye was smaller in diameter than the sham-treated control (Becker and Mobbs, 1999). The mechanisms underlying this response may now be understood. In organotypic culture studies of the developing chick retina, ATP released from the RPE via Cx43 hemichannels was found to increase the rate of mitosis in the NBR. Furthermore, the application of a gap junction hemichannel blocker reduced levels of ATP release from the RPE into the subretinal space (Pearson *et al.*, 2004b). Thus, a strong link is made between the expression of gap junctions in the retina during development, and the pace of cell cycle progression. Is it possible that elevated levels of Cx43 expression in the hypopigmented retina induce an increase in levels of mitosis, potentially through an ATP-mediated reduction in cell cycle duration?

There is evidence to suggest that Cx43-based gap junctions in the developing retina play a parallel role in the regulation of programmed cell death, a parameter which is also reportedly elevated in the albino according to one study (Ilia and Jeffery, 1999). Hence, the administration of carbenoxolone to postnatal mouse retinae *in vitro* reduced clustered cell death significantly, (Cusato *et al.*, 2003). Though Cx43 expression could not be detected in the developing retinal neuroepithelium outside the ventricular zone, Becker *et al.* (1998) state in a review of cell coupling in the retina; "whilst connexins can be detected in frozen or vibratome sections....low levels of expression, or subtle changes in distribution, can be missed." Consequently, the possibility that Cx43 labelling in the NBR may have been swamped by background signal can not be ruled out.

In support of this possibility, Cx43 was found to be expressed in the NBL of the chick retina at a much lower level than in the RPE (Pearson *et al.*, 2004a).

Having demonstrated elevated levels of Cx43 in the albino retina, the potential effects of L-DOPA on patterns of its expression were then assessed. Previous studies have shown that the addition of L-DOPA to the developing retinal neuroepithelium influences a range of developmental parameters that are systematically affected by the albino mutation; see chapters 2 and 3 (Akeo *et al.*, 1994; Ilia and Jeffery, 1999). Furthermore, the nature of its action supports the notion of its putative role as an endogenous regulator of retinal development. Results conclusively demonstrate that subcutaneous injections of L-DOPA reduced Cx43 immunolabelling in the albino retina to a level comparable with age-matched pigmented controls. This was manifested as a concerted reduction in the total level of Cx43 immunolabelling, as well as a reduction in the size of individual Cx43 plaques.

Next, attempts were made to ectopically promote connexin expression in the pigmented retina, with a view to examining resulting effects on processes of development, and hence, ascertain whether there is a casual link between elevated levels of Cx43 in the albino retina and other described abnormalities. An issue of particular interest was the potential role of gap junction-mediated communication between the RPE/NBR in the regulation of cleavage orientations. A speculative interpretation of results from chapter 3 and the studies of Cayouette *et al.* (2001) would suggest the existence of an RPE-derived signalling molecule which promotes the adoption of a vertical cleavage orientation around the day of birth, (see chapter 3 discussion). Furthermore, an elevation in availability of the signal to the NBR would be the most parsimonious explanation of abnormal patterns of cleavage orientations in the albino. However, despite the application of forskolin to *in vitro* pigmented eyecup preparations at concentrations as high as 200μM, no changes in patterns/levels of Cx43 protein localisation could be detected.

Forskolin was introduced into the eyecup preparations via supplementation to the culture medium. Though the cornea was pierced and the lens extracted

during tissue preparation, the vitreous may have posed a barrier to the diffusion of medium/forskolin. Consequently, the effective concentration of forskolin which actually reached the retinal neuroepithelium may have been somewhat lower than the calculated concentration. However, after 4 hours of incubation at 4°C the tissue appeared healthy, (as determined by the survival of the GCL and low density of apoptotic profiles), implying that the culture medium had successfully diffused into the eyecup. In addition, the range of forskolin concentrations used throughout this study (30-200μM) were far in excess of the threshold level deemed necessary to induce a change in levels of Cx43 expression.

An alternative explanation for the lack of response to forskolin treatment is that upon piercing the cornea, a reduction in the intraocular pressure may have been induced. As a result, the integrity of the RPE/NBR interface would have been compromised and sections of the two tissues become structurally and physiologically uncoupled. The consequences of mechanically disturbing the RPE/NBR interface during tissue preparation may have swamped, or even defacilitated, by the effects of forskolin treatment. In support of this hypothesis, results indicate that levels of Cx43 in the retina are highly variable within an *in vitro* context, (see standard errors in Figures 5.4.8 & 5.4.9).

Finally, it is possible that subtle differences in gap junction-mediated communication were elicited by the application of forskolin, but simply could not be detected by immunofluorescence methods. Forskolin-induced changes in the phosphorylation state of connexin proteins (Dowling-Warriner and Trosko, 2000) or the clustering pattern of gap junction plaques (Hall and Gourdie, 1995) might alter junctional conductance without altering absolute protein levels. However, in the absence of a functional assay for patterns of cell-cell communication, this line of experimentation was not continued. To address the issue using different methods of analysis, Cx43 levels could be down-regulated in the albino retina using a gap junction blocker such as carbenoxolone (Pearson *et al.*, 2004a), or a connexin anti-sense gel (Becker and Mobbs, 1999). Alternatively, a comparative examination of Cx43 null mice and wildtype controls could be undertaken to search for differential patterns of cell division

and/or cell cycle regulation. Past studies of the Cx43 transgenic mice eye have focused on the development of the cornea as opposed to the retina (Gao and Spray, 1998; White *et al.*, 2001). One potential limitation to this approach is that Cx43 knockout mice typically die at birth[3].

The anatomical structure underlying communication between the RPE and retinal neuroepithelium during development was then examined. Apart from the potential implications of this study on the pathogenesis of albinism, little is known about the fine structure of this region within the wildtype retina. Initial attempts were made to visualise patterns of connectivity using Diolistic labelling methods (Gan *et al.*, 2000). Though preliminary studies were successful, the study was eventually dropped. To maintain the structural integrity of the RPE/NBR interface during tissue preparation proved problematic, particularly since one side of the RPE must be exposed to facilitate labelling of the tissue. Consequently, an EM study of the early postnatal pigmented and albino retina was undertaken.

Upon examination of ultrathin sections using transmission EM, no obvious morphological differences could be detected between the pigmented and albino RPE/NBR interface. Despite obvious differences with respect to ocular pigmentation, all features described in the pigmented animal were also present in the albino. In addition, no differences could be detected in the anatomical structure of the region between the time-points examined. Nevertheless, several interesting findings emerged from the study. In contrast to expectation, retinal neuroblasts undergoing mitosis did not sit immediately adjacent to the apical surface of the RPE. Instead, there was an intervening plexus (dubbed the subretinal plexus, SRP), which was approximately 2-3µm in size within dehydrated ultrathin sections. In the SRP, coupling between retinal neuroepithelium process endfeet, dividing retinal neuroblasts and RPE cells was both extensive and complex; mediated by a dense network of heterogeneous processes and junctional complexes.

---

[3] When the null mutation is embedded in a CD1 background the mice occasionally survive to postnatal day 7 (Naus and Bani-Yaghoub, 1998).

5.6 Conclusions

Patterns of Cx43 protein localisation at the RPE/NBR interface are elevated in the developing albino retina during a window of development that is temporally coincidental with the abnormal patterns of cell proliferation and cell cycle exit, see chapters 2 and 3 (Webster and Rowe, 1991; Ilia and Jeffery, 1999; Ilia and Jeffery, 2000; Donatien and Jeffery, 2002; Gimenez *et al.*, 2004). Furthermore, all of these parameters can be regulated by the introduction of L-DOPA into the bloodstream, a point which strongly implicates its endogenous role in both the regulation of retinal development and the pathogenesis of albinism. Though the effects of gap junction expression on patterns of cell division could not be assessed independently through direct manipulation *in vitro*, both circumstantial and direct evidence from the literature highlights a link between levels of Cx43 expression at the RPE/NBR interface and the regulation of cell proliferation and cell cycle progression (Becker and Mobbs, 1999; Pearson *et al.*, 2002; Pearson *et al.*, 2004a; Pearson *et al.*, 2004b). Finally, no obvious anatomical abnormalities could be detected in the ultrastructure of the RPE/NBR interface of the albino.

Chapter 6:
Planar polarity within the retina

6.1 Introduction

Cells of both developing and adult epithelial tissues may be polarised with respect to multiple axes. In chapter 3, apical-basal polarity and the role it plays in the regulation of asymmetric cell division was addressed. However, many cells are simultaneously polarised with respect to the plane of the tissue, a phenomenon known as planar polarity (Wodarz, 2001). Much of the knowledge of this field has been extrapolated from the study of the invertebrates. The wing hairs, sensory bristles and ommitidia of *Drosophila melanogaster* have traditionally been used as model systems to examine planar polarity, and the role it plays in tissue patterning, (see Adler (2002) for a review).

Recent studies would suggest that the progenitor cells of the developing vertebrate retina are polarised with respect to the plane of the tissue (Das *et al.*, 2003). Furthermore, several mechanisms involved in the specification of retinal polarity may have been conserved throughout the evolution of the vertebrate and invertebrate eye (Neumann and Nuesslein-Volhard, 2000; Zhang and Yang, 2001). (See Wodarz (2001) for a review). In the zebrafish retina, whilst no divisions were found to occur along the apical-basal axis, cleavage orientations within the plane of the tissue were regulated over time (Das *et al.*, 2003). As development progressed, there was a systematic shift from a radial pattern of division to a circumferential pattern. In the rat, a similar pattern was found, with a shift from a random pattern of orientation prenatally, to a pattern similar to that

found late during development in the zebrafish (Das *et al.*, 2003). The authors suggest that this reflects a transition from a symmetric to an asymmetric mode of division. To support this hypothesis they point to the existence of cell fate determinant molecules such as Sonic Hedgehog (Shh), which are expressed in gradients across the plane of the retinal epithelium (Neumann and Nuesslein-Volhard, 2000; Zhang and Yang, 2001). In addition, *sonic you* (*syu*) zebrafish mutants (expressing reduced levels of Shh) exhibit a disruption of cleavage orientations within the plane of the developing retina (Das *et al.*, 2003).

These findings raise the possibility that asymmetric division in the developing vertebrate retina may be simultaneously mediated through the regulation of cleavage orientations in the apical-basal and planar axes. Given that albinos exhibit anatomical defects which could be described as abnormalities in centre-periphery patterning, i.e. an underdevelopment of the central retina (Jeffery and Kinsella, 1992; Donatien *et al.*, 2002); a flattening of the centre-to-periphery gradient in cell density (Jeffery and Kinsella, 1992); a shift in the nasotemporal division (Drager and Olsen, 1980); as well as delays in patterns of layer formation, cell proliferation and cell birth within this axis (Webster and Rowe, 1991; Jeffery and Kinsella, 1992; Ilia and Jeffery, 1996; Ilia and Jeffery, 1999), a comparative study of planar polarity was undertaken within the developing pigmented and albino retina.

6.2 Experimental aims

The orientation of cell division was examined in fixed retinal wholemount preparations using confocal microscopy and Matlab-based image analysis. Studies were initially undertaken in pigmented rat tissue at a range of developmental stages in order to determine the wildtype pattern as a reference with which to compare the albino. However, after having examined both the pigmented and albino retina using two distinct methods of analysis, the findings of Das *et al.* (2003) could not be reproduced. Cellular divisions within the developing rat retina were randomly oriented. Consequently, a study of cleavage orientations within the plane of the chick retinal neuroepithelium was

undertaken. The chick is a highly visual animal with a steep gradient in cell density and a highly specialised central retina. Hence, one might expect planar polarity and tissue patterning to play a more essential role in the development of the chick retina.

6.3 Methods

Retinae were obtained from the following; Dark Agouti (D.A., pigmented) rats at E18, P1 and P4 (N=2/time-point); Wistar (albino) rats at P1 and P4 (N=2/time-point); chicks (Bovans Goldline) at E6, E8 and E11 (N=3/time point). These stages were selected because they span the phase of peak cell production and include the last stages of cell addition. Time-mated female rats of both pigmentation phenotypes were deeply anaesthetised and the foetuses extracted and decapitated. The eyes were removed and placed in 4% buffered formalin. Neonatal rats from time-mated mothers and chick embryos were decapitated and their heads placed in the same fixative. To keep track of retinal orientation a dorso-temporal cut was made and the retina was flat-mounted wet on to a poly-lysine coated slide (BDH Laboratory Supplies, Poole, UK) ventricular surface up. Whole-mounts were washed in PBS, stained for 2.5 minutes with propidium iodide (5μg/ml in PBS), washed in distilled water, and coverslipped in DAKO aqueous mounting medium (Vector Laboratories).

Images were then gathered using a Zeiss laser scanning confocal microscope (LSM 500) using a x40 oil objective lens. Two-dimensional strips (115.2–135.5μm wide) were scanned along radial lines emanating from the centre of the retina by sampling a series of adjacent, non-overlapping areas (2048 x 2048 pixels, 8 bit images) that spanned linearly from the ON to the peripheral retinal margin. Images were then imported into Zeiss Image Examiner Version 2.8 and either analysed directly or exported in TIF format for analysis using Scion Imager (freeware based on NIH image, Scion Corporation). Either every area or every second/third area was analysed depending on the size/age of the retina, so that a sufficiently large data set could be generated. In each area examined, all cells clearly in anaphase were identified and subsequently analysed. As

images were taken in two dimensions (x and y), only divisions occurring within the plane of the tissue (horizontal divisions) were analysed. However, data from chapter 3 and the reported findings of Cayouette *et al.* (2001) have shown that vertical divisions in the postnatal rat retina account for less than 20% of the total. It is therefore unlikely that results will be affected by this sampling bias, though one can not rule out the possibility that horizontally and vertically dividing cells may exhibit distinct patterns of orientation within the plane of the tissue.

The orientations of dividing cells were calculated using two distinct methods which employed custom written MatLab programs, (The MathWorks Inc., Natick, MA). (See appendix 2 for code).The coordinates of each of the anaphase profile poles (white arrowheads in Figure 6.4.1) were used with details of the geographic retinal location of the area to calculate the orientation of the cell relative to the optic nerve head. An angle of 0^{o} represents a division occurring along the radial axis (a radial division), and an angle of 90^{o} represents a division occurring perpendicular to a radial line emanating from the ON (a circumferential division), see Figure 6.4.1 legend. For the rat, n=486, 619 and 587 cells analysed at E18, P1 and P4 respectively; for the chick, n=1234, 1912 and 194 at E6, E8 and E11 respectively.

The second method of analysis calculates the orientation of all anaphase cells in a defined area relative to a randomly selected neighbour. An orientation of 0^{o} represents a division occurring parallel to its neighbour's axis of division, whereas 90^{o} represents a division occurring perpendicular to its neighbour's axis of division. By analysing the orientation of dividing cells relative to a randomly selected neighbour as well as the optic nerve head, the possibility that dividing cells may be aligned to some other structure or retinal location was examined. For the pigmented rat, n=169, 182 and 162 cells analysed (at E18, P1 and P4 respectively); for the albino rat, n=151 and 159 cell analysed (at P1 and P4 respectively). For the chick, n=257, 296 and 151 cells analysed (at E6, E8 and E11). Data were then plotted in the form of cumulative frequency distributions in Axum 5.0 (Mathsoft, Cambridge, MA). (See Tibber *et al.* (2004)

and appendix 2 for a more detailed explanation of the image analysis techniques developed and an explanation of the MatLab code).

Statistical analyses were performed using SPPSS 10.1 (SPSS Inc., CA). Intra-group comparisons were made between distributions of cell orientations from distinct retinal quadrants. Where no statistical differences were found, data were then pooled and comparisons made between time-points. Non-parametric Mann-Whitney and Kruskal-Wallis tests were used (when two, or more than two groups respectively were compared), as the data were non-normally distributed, (as determined by the KS-test). Differences were considered significant at the 5% level. Regression analyses were performed using Excel (Microsoft Corporation).

6.4 Results

Anaphase orientations in the pigmented rat retina

In retinal whole-mounts, anaphase profiles could be identified across the retinal surface at the level of the ventricular zone. In pigmented animals the orientation of anaphase profiles from all four retinal quadrants (dorsal, temporal, ventral and nasal) were plotted in relation to the optic nerve head, at three different time points during the main period of retinal cell production (E18, P1 and P4). Data is presented in the form of sample images taken at random from each time-point/retinal quadrant (Figure 6.4.2), as well as a series of cumulative frequency distributions which describe the distribution of cleavage orientations relative to the optic nerve head (Figures 6.4.3-6.4.5, panel A).

A close observation of Figure 6.4.2 suggests that multiple anaphase cells in the same reference area are oriented randomly with respect to the dorsal axis and surrounding neighbours, independent of developmental stage and retinal region. This is confirmed by quantitative analysis as shown in the scatter plots of Figures 6.4.3-6.4.5, panel A. At all stages/retinal locations, the data exhibits a

tight linear relationship, (R^2 values >0.98, regression analysis), implying a random distribution. Furthermore, statistical analyses showed that the distribution of orientations did not differ significantly between the four quadrants (p=0.59, 0.98, 0.28 at E18, P1 and P4 respectively), nor between the time points studied (p=0.65).

To be sure that there was no trend in the data at specific retinal eccentricities which may have been overlooked as a result of pooling data, anaphase orientations at each stage of development were then plotted against retinal eccentricity (Figures 6.4.3. - 6.4.5, panel B). Again, no trend was evident at any retinal location, and a continuous spread of orientations was found across the entire retina. This suggests that anaphase profiles were randomly orientated relative to the optic nerve, and irrespective of retinal location and stage of development.

It is possible that anaphase orientations could be organised relative to a retinal location other than the optic nerve head, although it is unlikely this would generate the close correlations seen in Figures 6.4.3 - 6.4.5, panel B. Nevertheless, data were reanalysed by calculating the orientation of defined anaphase profiles relative to the orientation of a randomly selected dividing neighbour in the same area. Analyses were therefore independent of retinal location, (Figure 6.4.6A). Once again, the cumulative frequency plots follow a tight linear relationship (R^2 values >0.99, regression analysis) and the distribution of orientations did not differ significantly between time-points studied (p=0.81). This would suggest that the cleavage orientation of a neuroblastic cell in the pigmented rat retina is randomly oriented relative to both the optic nerve head and its surrounding neighbours.

Anaphase orientations in the albino rat retina

Given that no evidence of planar polarity could be detected in the wildtype pigmented retina, it is unlikely that one would be found in the albino. Consequently, a less comprehensive study was undertaken of the albino retina

at P1 and P4. Cell orientations were analysed relative to the orientation of surrounding neighbours, Figure 6.4.6B. This period of development represents that in which one would expect to find an emerging pattern of regulated cleavage orientations based on the results reported by Das *et al.* (2003). However, in support of findings in the pigmented rat retina, cleavage orientations were randomly oriented in the albino. The cumulative frequency plots were linear (R^2 values >0.99, regression analysis) indicating random orientation, and the distribution of orientations did not differ significantly between time-points studied (p=0.44).

Anaphase orientations in the chick retina

Cleavage orientations were analysed in the E6, E8 and E11 chick retina, a period spanning the peak in cell generation through to the last stages of cell proliferation. By E11, all of the primary cell layers are present (ONL, INL and GCL) though not fully differentiated. In the far periphery at the apical extreme of the presumptive neural retina a subset of non-differentiated cells remained proliferative.

Cleavage orientations in the chick were analysed as per rat retinae, using both techniques outlined; calculating orientations relative to both the pecten (Figures 6.4.8-6.4.10, panel A), as well as the orientation of a dividing neighbour (Figure 6.4.11). Two quadrants (dorsal and nasal) were investigated at each of the three stages. The pattern found in the chick was similar to that in the rat. Once again, cleavage orientations were randomly oriented with respect to the optic nerve head; the cumulative frequency plots were linear (R^2 values >0.99, regression analysis) and no significant differences were found between the distribution of orientations from distinct retinal quadrants (p=0.88, 0.51, 0.94 at E6, E8 and E11 respectively) nor between time points (p=0.54). Similarly, there was no relationship between the orientation at anaphase and retinal eccentricity of a cell (Figures 6.4.8 - 6.4.10, panel B). Data for the E11 retina is clumped in three distinct bands, reflecting slight variations in the developmental maturity of

the individual, size of the retina and/or variations in the way the retinae opened up upon dissection.

Finally, cleavage orientations were plotted relative to the orientation of a dividing neighbour (Figure 6.4.11). Again, no discernable pattern was evident; the cumulative frequency plots wee linear (R^2 values >0.99, regression analysis) indicating a random orientation, and the distribution of orientations did not differ significantly between time-points studied (p= 0.5). Hence, anaphase profiles in the chick retina were randomly oriented with respect to both the optic nerve head and their surrounding neighbours, irrespective of retinal eccentricity and developmental stage.

Calculating cleavage orientations within the plane of the tissue

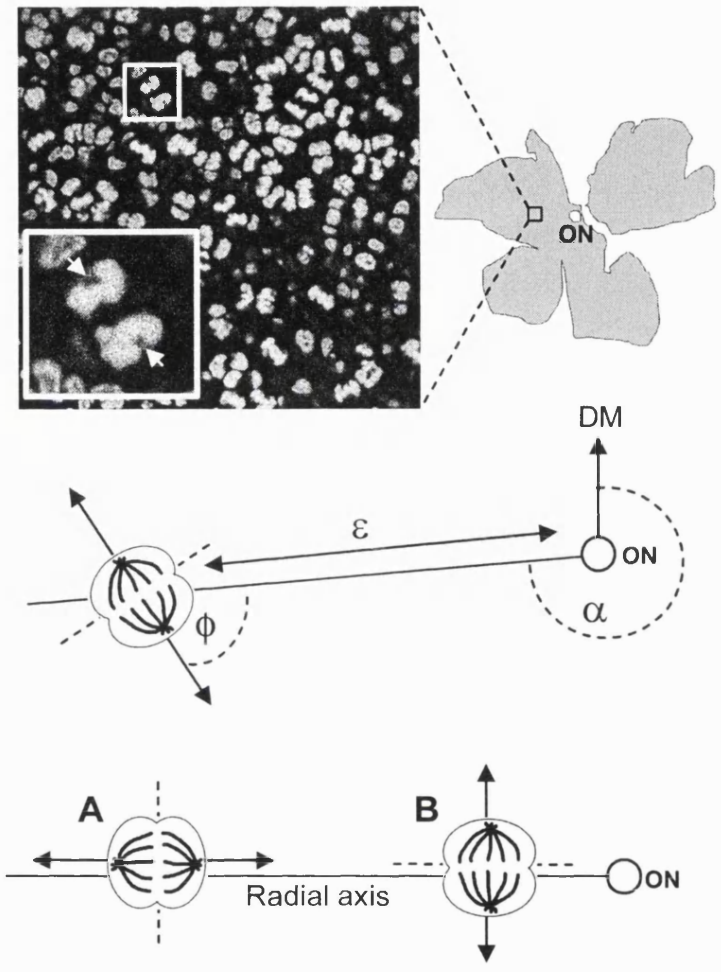

Figure 6.4.1 The coordinates of a cell's anaphase poles (indicated by the white arrowheads) were used to calculate ϕ, the cell's orientation relative to a radial axis emanating from the optic nerve head (ON); ε, the eccentricity of the cell from the ON; and α, the cell's polar angle (measured from the dorsal meridian). To determine ϕ, a Matlab program was used to calculate the angle of intersection between two lines, the first passing between the two anaphase poles (parallel to the mitotic spindle and perpendicular to the cleavage plane), and a second connecting the optic nerve to the central point of the cell. An orientation of 0°, a radial division (A), is a division in which the mitotic spindle is aligned along a radial axis. An orientation of 90°, a circumferential division (B), is a division in which the mitotic spindle is aligned perpendicular to a radial axis emanating from the optic nerve head.

Cleavage orientations within the plane of the pigmented rat neuroepithelium

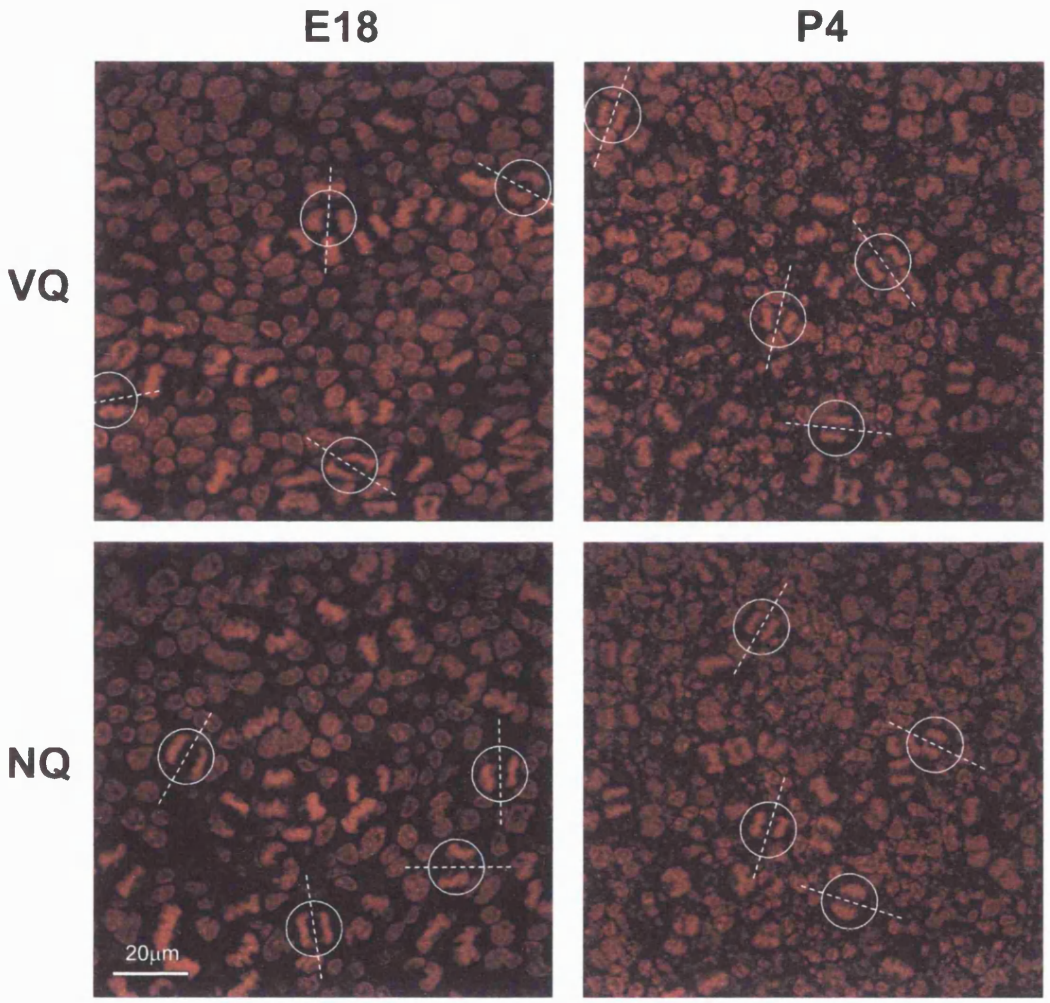

Figure 6.4.2 Pigmented rat retinae were fixed at E18, P1 and P4, stained with propidium idodie (red) to visualise the chromatin, and whole-mounted on to glass slides GCL down. The tissue was then imaged using a laser scanning confocal microscope. Ventral (VQ), nasal (NQ), temporal (TQ) and dorsal (DQ) quadrants of the retina were scanned, and the orientation of anaphase profiles calculated. A randomly chosen selection of images taken from ventral and nasal quadrants of the E18 and P4 retina are presented. A number of anaphase profiles are encircled in white; dotted lines represent the cleavage plane, which is perpendicular to the mitotic spindle axis. Multiple cells exhibiting distinct cleavage orientations can be seen with the same retinal region, a result which is supported by quantitative analysis. Dorsal is up.

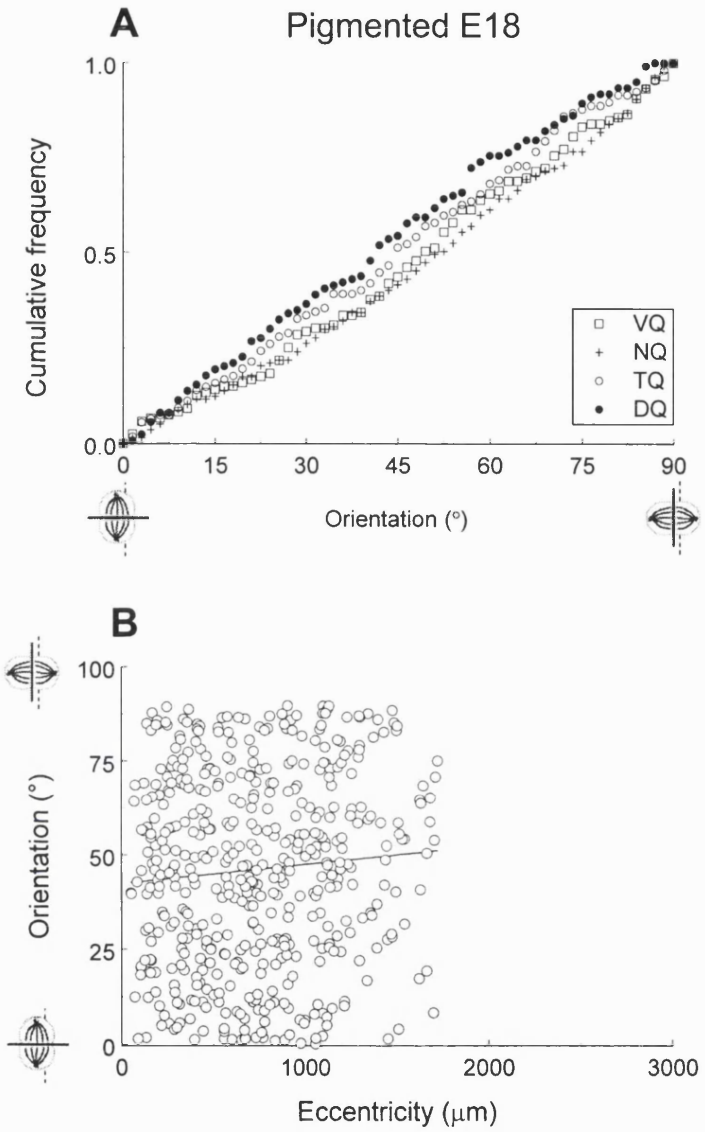

Figure 6.4.3 Distribution of anaphase cell orientations and the relationship between cell orientation and retinal eccentricity in the pigmented E18 rat retina. (A) Anaphase orientations relative to the optic nerve head are shown in the form of a cumulative frequency distribution. 0 ° represents a radial division, whereas 90 ° represents a circumferential division. Linear regression analyses show that for each quadrant R^2 values are >0.98, indicating a random distribution. Statistical analysis indicates that there are no significant differences between the distribution of orientations between quadrants (p=0.59). (B) Scatter plot showing the relationship between the eccentricity of a cell and its orientation relative to the ON. Clearly there is no relationship between the two parameters, and all orientations between 0° and 90° are found with equal frequencies across the central/peripheral axis. N=2 retinae per time-point, n=486 cells analysed. VQ = Ventral quadrant; NQ = nasal quadrant; TQ = temporal quadrant; DQ = dorsal quadrant.

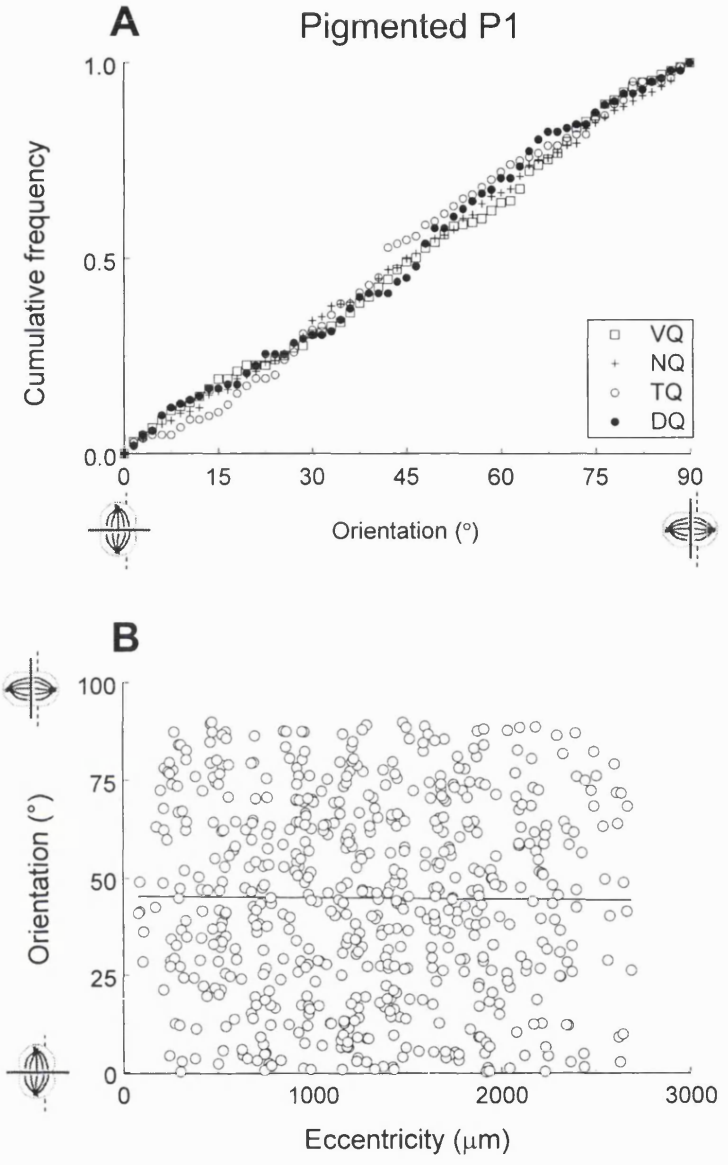

Figure 6.4.4 Distribution of anaphase cell orientations and the relationship between cell orientation and retinal eccentricity in the pigmented P1 rat retina. (A) Anaphase orientations relative to the optic nerve head are shown in the form of a cumulative frequency distribution. 0^{o} represents a radial division, whereas 90^{o} represents a circumferential division. Linear regression analyses show that for each quadrant R^2 values are >0.98, indicating a random distribution. Statistical analysis indicates that there are no significant differences between the distribution of orientations between quadrants (p=0.98). (B) Scatter plot showing the relationship between the eccentricity of a cell and its orientation relative to the ON. Clearly there is no relationship between the two parameters, and all orientations between 0^{o} and 90^{o} are found with equal frequencies across the central/peripheral axis. N=2 retinae per time-point, n=619 cells analysed. VQ = Ventral quadrant; NQ = nasal quadrant; TQ = temporal quadrant; DQ = dorsal quadrant.

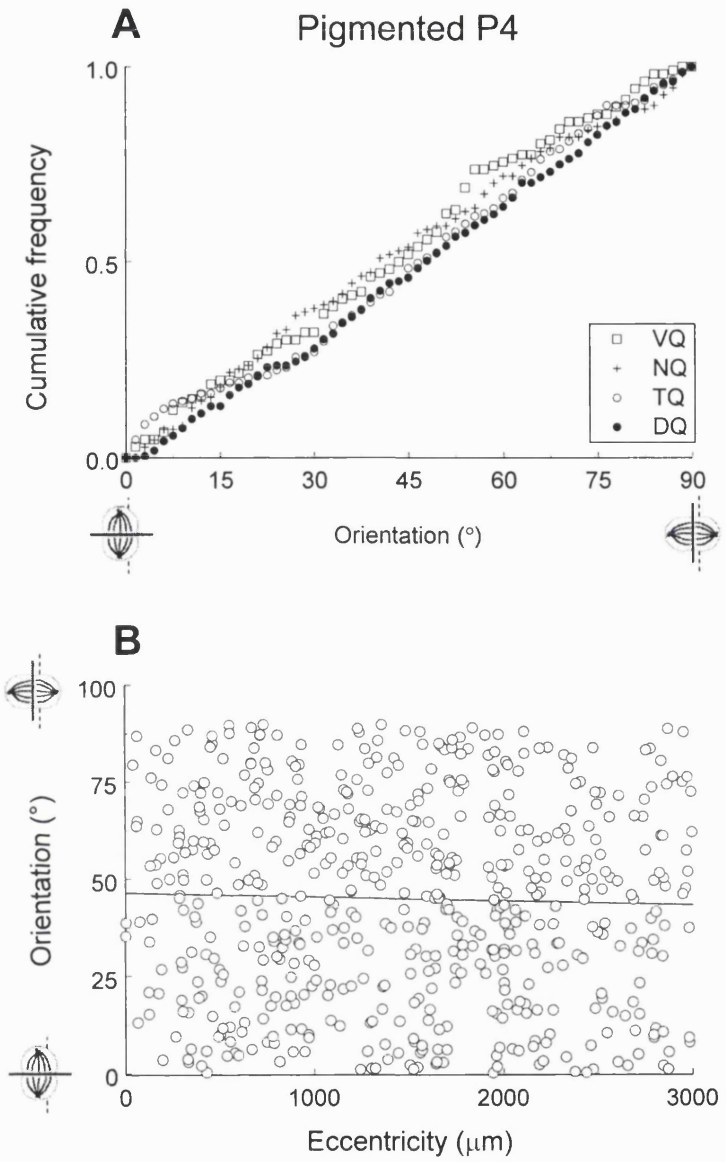

Figure 6.4.5 Distribution of anaphase cell orientations and the relationship between cell orientation and retinal eccentricity in the pigmented P4 rat retina. (A) Anaphase orientations relative to the optic nerve head are shown in the form of a cumulative frequency distribution. 0^{o} represents a radial division, whereas 90^{o} represents a circumferential division. Linear regression analyses show that for each quadrant R^2 squared values are >0.98, indicating a random distribution. Statistical analysis indicates that there are no significant differences between the distribution of orientations between quadrants (p=0.28). (B) Scatter plot showing the relationship between the eccentricity of a cell and its orientation relative to the ON. Clearly there is no relationship between the two parameters, and all orientations between 0^{o} and 90^{o} are found with equal frequencies across the central/peripheral axis. N=2 retinae per-time point, n=578 cells analysed. VQ = Ventral quadrant; NQ = nasal quadrant; TQ = temporal quadrant; DQ = dorsal quadrant.

The distribution of cleavage orientations relative to a randomly selected neighbour in pigmented and albino rat retinae

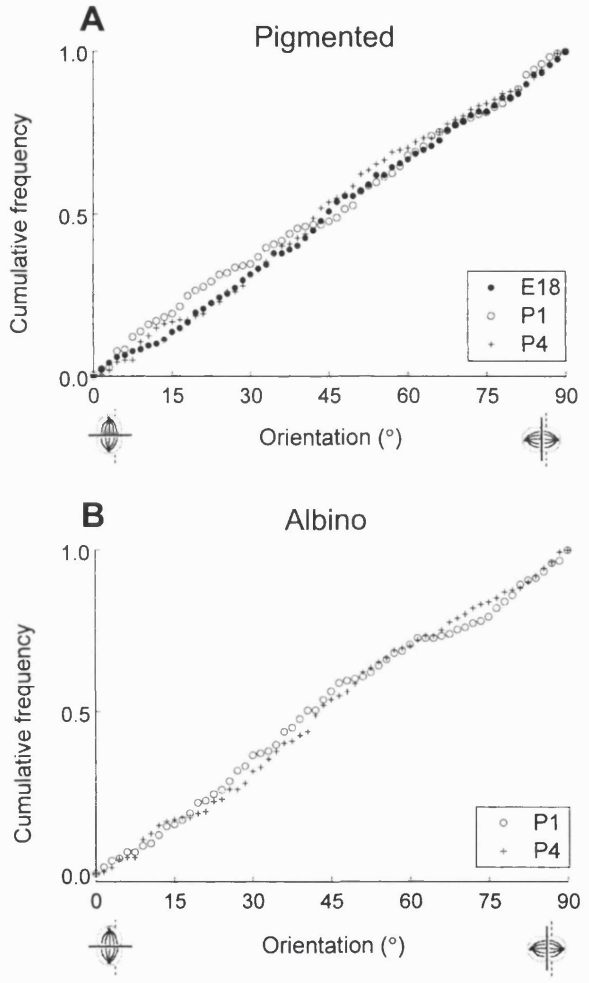

Figure 6.4.6 The distribution of anaphase orientations are presented for the (A) pigmented rat and (B) albino rat retina in the form of cumulative frequency distributions. For the pigmented rat three time-points were analysed; E18, P1 and P4. For the albino rat, data were only analysed at P1 and P4. 0^{o} represents a division occurring parallel to a randomly selected neighbour, whereas 90^{o} represents a division occurring perpendicular to its neighbour. R^2 values for all quadrants were >0.99, indicating a random distribution. No significant differences were found between the distribution of orientations at each time-point, (p=0.81 and 0.44 in the pigmented and albino rat respectively). For the pigmented rat n=169, 182 and 162 cells analysed at E18, P1 and P4 respectively; for the albino rat n=151 and 159 cells analysed at P1 and P4 respectively).

Cleavage orientations within the plane of the chick retinal neuroepithelium

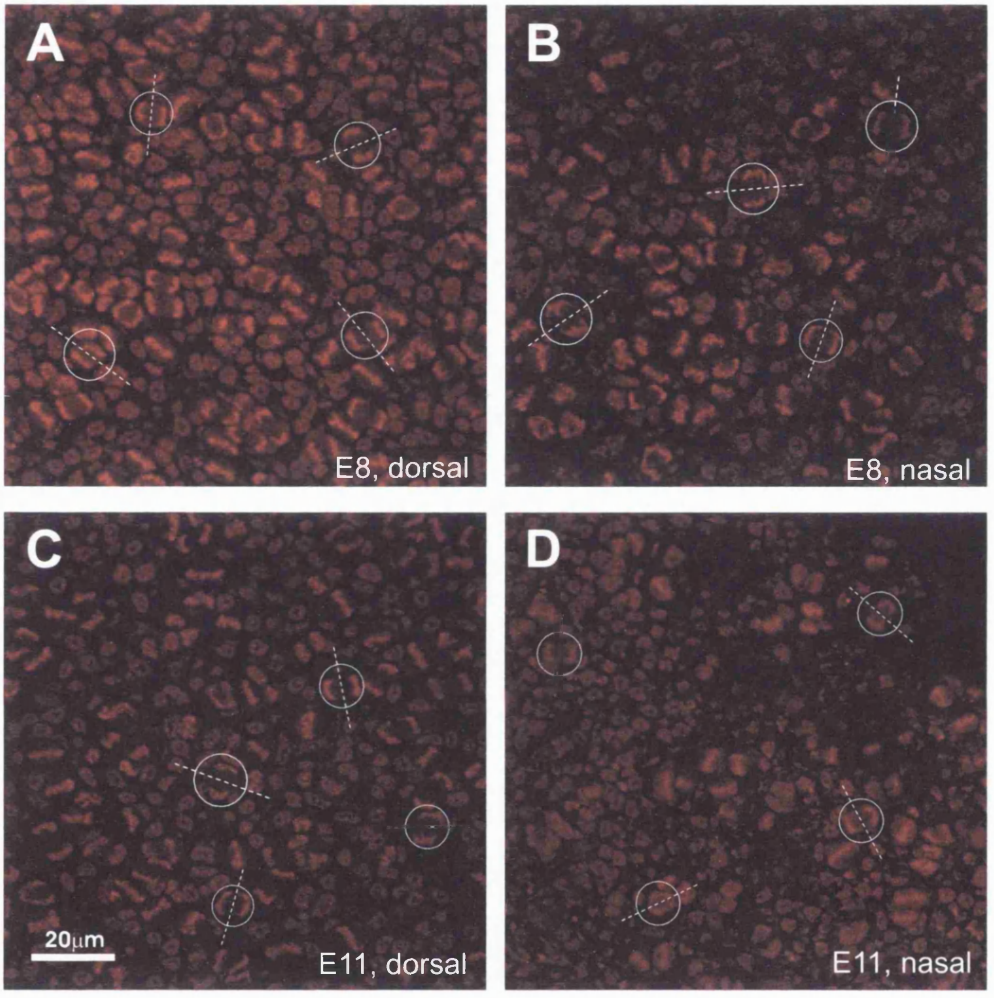

Figure 6.4.7 Chick retinae were fixed at E6, E8 and E11, stained with propidium idodie (red) to visualise the chromatin, and whole-mounted on to glass slides GCL down. The tissue was then imaged using a laser scanning confocal microscope. Dorsal and nasal quadrants of the retina were scanned, and the orientation of anaphase profiles calculated relative to the optic nerve head as well as a randomly selected dividing neighbour. A randomly chosen selection of images taken from E6 and E11 retinae are presented. Multiple cells exhibiting distinct cleavage orientations can be seen within the same retinal region, a result which is supported by quantitative analysis. Dorsal is up.

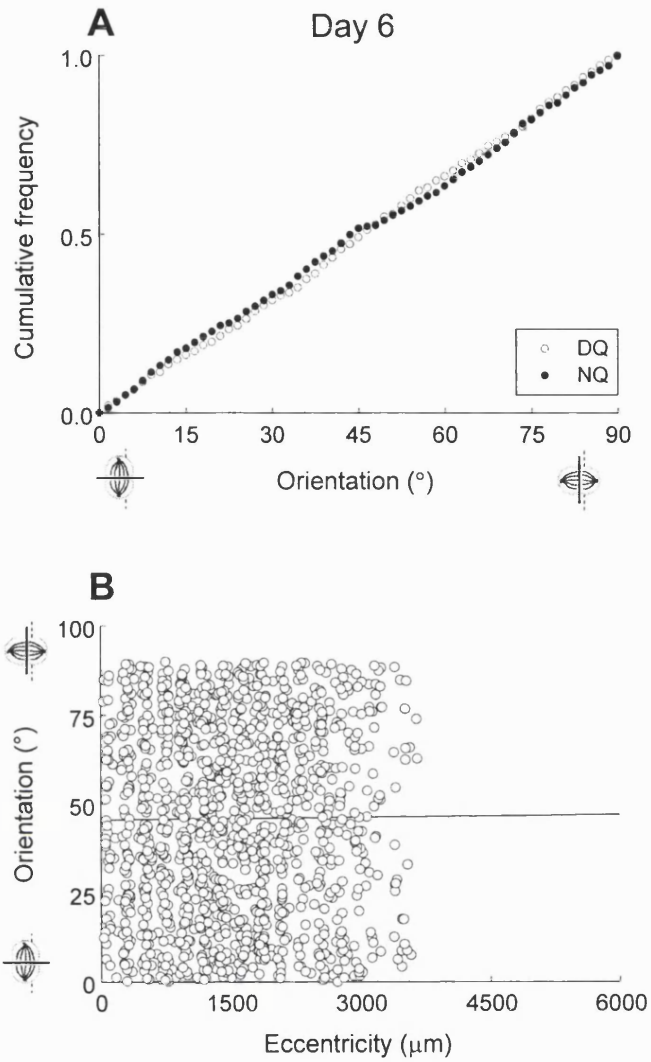

Figure 6.4.8 Distribution of anaphase cell orientations and the relationship between cell orientation and retinal eccentricity in the day 6 chick retina. (A) Anaphase orientations relative to the optic nerve head are shown in the form of a cumulative frequency distribution. 0^{o} represents a radial division, whereas 90^{o} represents a circumferential division, (see Methods for a definition of modes of division). Linear regression analyses show that for each quadrant R^2 values are >0.99, indicating a random distribution. Statistical analysis indicates that there are no significant differences between the distribution of orientations between quadrants (p=0.88). (B) Scatter plot showing the relationship between the eccentricity of a cell and its orientation relative to the optic nerve. Clearly there is no relationship between the two parameters, and all orientations between 0^{o} and 90^{o} are found with equal frequencies across the central/peripheral axis. N=3 retinae per time-point, n=1234 cells analysed. DQ = dorsal quadrant, NQ. = nasal quadrant.

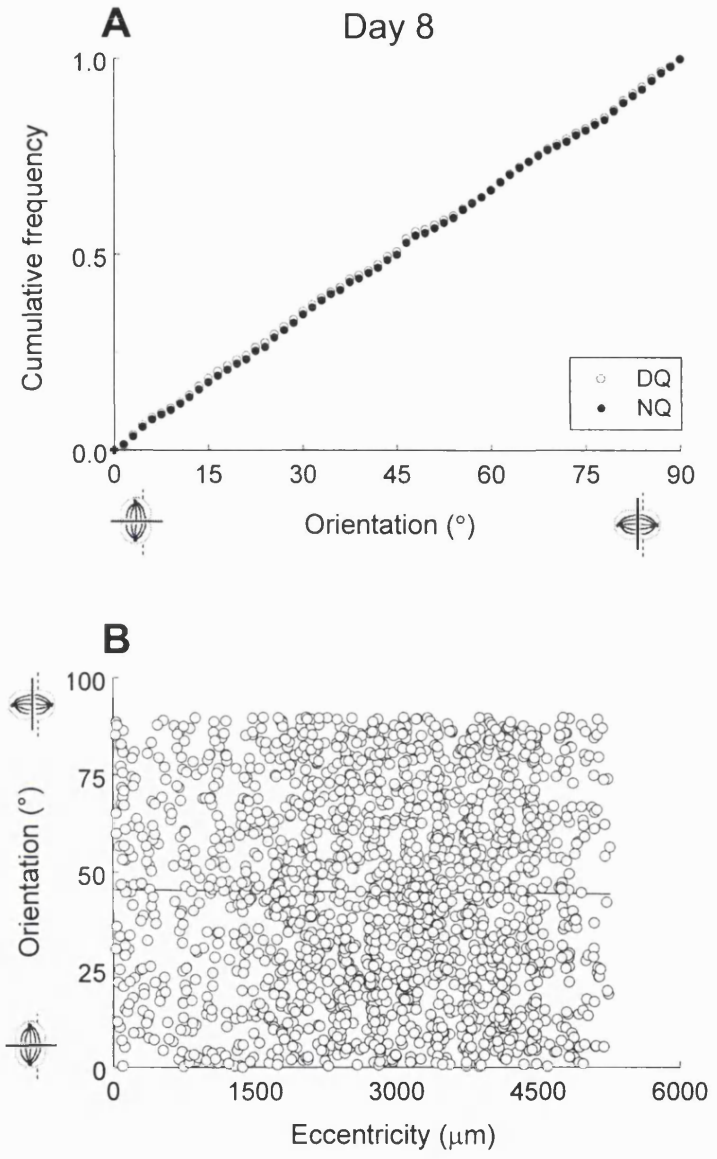

Figure 6.4.9 Distribution of anaphase cell orientations and the relationship between cell orientation and retinal eccentricity in the day 8 chick retina (A) Anaphase orientations relative to the optic nerve head are shown in the form of a cumulative frequency distribution. 0° represents a radial division, whereas 90° represents a circumferential division, (see Methods for a definition of modes of division). Linear regression analyses show that for each quadrant R^2 values are >0.99, indicating a random distribution. Statistical analysis indicates that there are no significant differences between the distribution of orientations between quadrants, (p=0.51). (B) Scatter plot showing the relationship between the eccentricity of a cell and its orientation relative to the optic nerve head. Clearly there is no relationship between the two parameters, and all orientations between 0° and 90° are found with equal frequencies across the central/peripheral axis. N=3 retinae per time-point, n=1912 cells analysed. DQ = dorsal quadrant, NQ. = nasal quadrant.

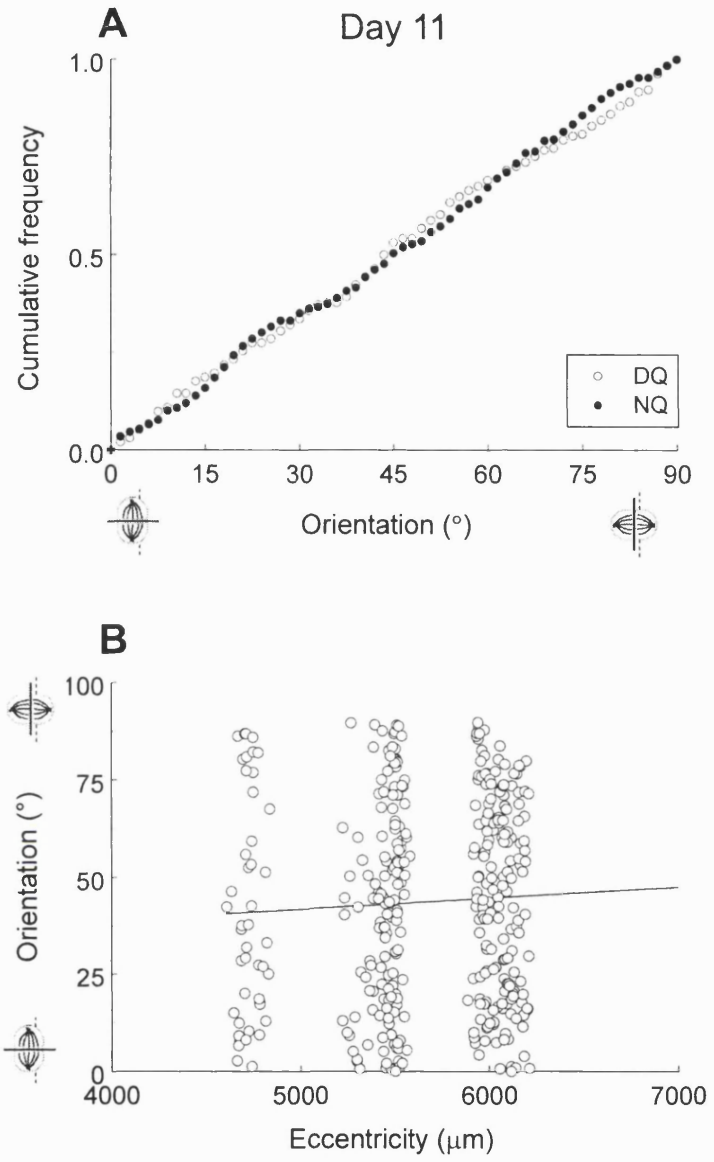

Figure 6.4.10 Distribution of anaphase cell orientations and the relationship between cell orientation and retinal eccentricity in the day 11 chick retina. (A) Anaphase orientations relative to the optic nerve head are shown in the form of a cumulative frequency distribution. 0° represents a radial division, whereas 90° represents a circumferential division. Linear regression analyses show that for each quadrant R^2 values are >0.99, indicating a random distribution. Statistical analysis indicates that there are no significant differences between the distribution of orientations between quadrants (p=0.94). (B) Scatter plot showing the relationship between the eccentricity of a cell and its orientation relative to the optic nerve head. Clearly there is no relationship between the two parameters. By this stage of development dividing cells were limited to the peripheral margin of the retina. N=3 retinae per time-point, n=194 cells analysed. DQ = dorsal quadrant, NQ. = nasal quadrant.

The distribution of cleavage orientations relative to a randomly selected neighbour in the chick retina

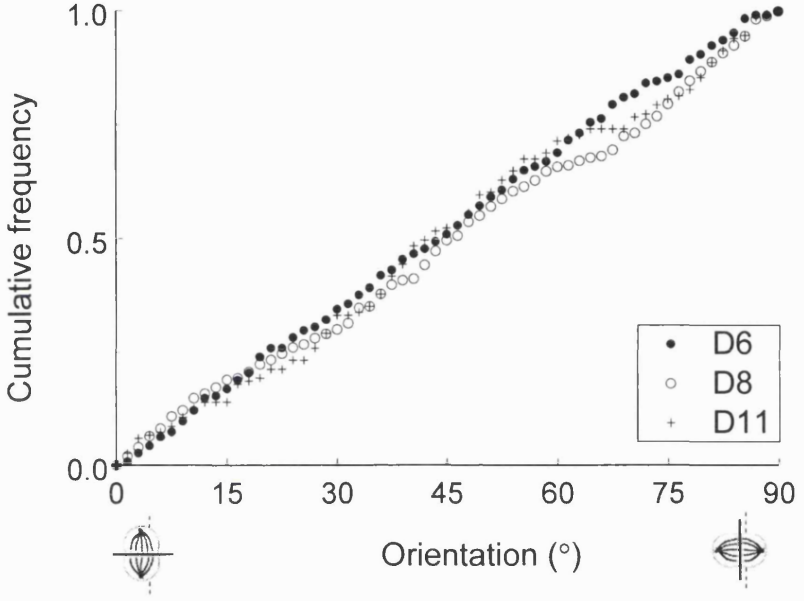

Figure 6.4.11 Distribution of anaphase cell orientations relative to a randomly selected neighbour in the chick retinal neuroepithelium. The distribution of anaphase orientations are presented for the D6, D8 and D11 chick retina in the form of cumulative frequency distributions. 0^{o} represents a division occurring parallel to a randomly selected neighbour, whereas 90^{o} represents a division occurring perpendicular to its neighbour. R^2 values for all quadrants were >0.99, indicating a random distribution. No significant differences were found between the distribution of orientations at each time-point (p=0.5). N=3 retinae per time-point and n=257, 296 and 151 cells analysed at E6, E8 and E11 respectively.

6.5 Discussion

The orientation of anaphase profiles was analysed in the pigmented and albino rat, and in the chick, over a window of development that incorporates the period of peak cell production through to the tail-off of retinal proliferation (E18 to P4 in the rat, and E6 to E11 in the chick). The studies incorporated the analysis of over 5000 cells in total, using two distinct methods of analysis; anaphase orientations were plotted relative to both the optic nerve head as well as the orientation of a randomly selected neighbour. Throughout the entire study, no evidence was found to suggest that the distribution of anaphase orientations was anything but random, irrespective of retinal eccentricity, developmental stage and pigmentation phenotype.

These findings with respect to planar polarity in the developing rat retina are in contrast to those previously reported by Das *et al.* (2003); they described randomly oriented anaphase profiles at E6 and P0, but a circumferential pattern of alignment by P4. In contrast, results from live-imaging studies of the Sprague-Dawley strain of rat (Tibber *et al.*, 2004) -as used by Das *et al.* (2003)- support the findings of this thesis. Orientations at metaphase entry were found to be randomly distributed. In addition, the angle at metaphase entry was strongly correlated to the angle adopted at anaphase, the average difference being19^{o} (±17^{o}), thus ruling out the possibility that strain variance or subtle differences in developmental timing could underlie the discrepancy between results. However, it is difficult to make direct comparisons with the results of Das *et al.* (2003) as they provide no statistical information for the rat data, and the cumulative frequency distribution for P0 is not presented. Consequently, there was no evidence to suggest that cleavage orientations within the plane of the developing retinal neuroepithelium were regulated in the chick or the rat.

These findings were also supported by live-imaging data on the dynamics of metaphase rotations in the developing rat retina (Tibber *et al.*, 2004).

Documented movements were generally small, bidirectional and oscillatory about a fixed orientation that would finally be adopted during anaphase. This fixed orientation seemed to be random, and perhaps more a product of the orientation at which metaphase was initiated than any other factor. The rotations observed were similar to a subset of those described by Haydar *et al.* (2003) in a time-lapse confocal imaging study of the developing mouse telencephalon. Though rotations were followed within the apical-basal plane, the study suggested that metaphase rotations fell into two distinct categories of behavioural patterns that predicted the symmetry and final orientation of a division. Metaphase rotations in the plane of the rat retina were similar to Haydar's 'default' symmetrical divisions both in terms of metaphase duration and the dynamics of the rotation. This is consistent with a lack of planar polarity in the rat retinal neuroblasts, as prolonged and more extensive metaphase rotations incorporating several 'mode switches' (movements exceeding 45°) seemed to be characteristic of a division in which a specific cleavage orientation other than the default was regulated and sought.

Patterns of cell division within the plane of the developing rat and chick retina also differed from those reported in the zebrafish retina (Das *et al.*, 2003); a systematic shift from a radial to a circumferential pattern of division occurred over a 15 hour time-period. Why would such a fundamental mechanism of development be present in the zebrafish retina, but not in the rat and chick? One possibility is that planar polarity in the zebrafish retina may be involved in the process of asymmetric division as it is in the invertebrate nervous system. Indeed, in contrast to the rat and the chick, no apical-basal divisions have been found in the zebrafish retina (Cayouette *et al.*, 2001; Silva *et al.*, 2002; Das *et al.*, 2003). Thus, while asymmetric division in the zebrafish retina may be mediated through the control of cleavage orientation and cell fate determinant localisation within the planar axes, this system may be confined to the apical/basal plane in the rat and chick retina.

The findings of this study add further support to a growing body of evidence that suggests that whilst cleavage orientation and asymmetric division play an intricate role in the development of the vertebrate nervous system, the precise

mechanisms of this process are considerably more complex than in the invertebrates. Furthermore, though much of the machinery for its regulation has been evolutionarily conserved amongst the vertebrates, there is considerable divergence between species in its operation.

6.6 Conclusions

Studies of planar polarity in the developing vertebrate retina were initially undertaken due to its potential role in the pathogenesis of albinism. Having demonstrated defects in apical-basal polarity associated with hypopigmentation as well as abnormalities in the timing of processes with respect to the centre-to-periphery gradient of development, the possibility that planar polarity is simultaneously disrupted in the albino was addressed. However, the results reported by Das *et al.* (2003) could not be reproduced, and no evidence of planar polarity was found in either the pigmented or albino rat, conclusions which were supported by live-imaging studies undertaken by a collaborating laboratory. Consequently, we were drawn further in to the issue of planar polarity and the role it plays in vertebrate retinogenesis than initially intended and undertook a similar study of the chick retina. Once again, the results were clear and reproducible; cells were randomly oriented with respect to the plane of the tissue.

Chapter 7:
The effects of dopamine on retinal development

7.1 Introduction

A growing body of evidence would suggest that L-DOPA has an endogenous function as a neurotransmitter and/or neuromodulator, which is independent of its role as a precursor in the biosynthesis of catecholamines and the melanins (Opacka-Juffry and Brooks, 1995; Hornykiewicz, 2002). Immunocytological studies have shown that several nuclei of the central nervous system produce L-DOPA as an end-product. These putative DOPA-releasing cells are immunopositively labelled for DOPA and TH, but do not express DDC, (see Smeets and Gonzalez (2000) for a comprehensive review). Furthermore, both *in vivo* and *in vitro* studies have shown that L-DOPA influences a wide range of developmental processes including; levels of proliferation and apoptosis (Wick, 1977; Wick, 1980; Ilia and Jeffery, 1999), patterns of cleavage orientation (chapter 3) and cell birth/retinal lamination (chapter 2), as well as rates of cell cycle progression (Akeo *et al.*, 1994), and has been implicated in the regulation of Schlemm's canal formation (Libby *et al.*, 2003). These findings raise the possibility that L-DOPA represents a fundamental neurotransmitter/neuroregulator of both the adult and developing central nervous system. However, receptors exhibiting L-DOPA specificity have not been identified to date.

A parallel theory which does not conflict with the putative role of L-DOPA as an independent neurotransmitter/neuromodulator posits that tyrosinase in the RPE provides a non-TH mediated source of L-DOPA for catecholamine synthesis by the neural retina (see Figure 7.1.1). Incubation of chick retinal segment explants in L-DOPA led to an accumulation of DA, and an increase in cyclic AMP (cAMP) levels (a measure of dopaminergic stimulation via D_1-like DA receptors) (Kubrusly *et al.*, 2003). In support of a role for DA during early development of the retina, dopaminergic receptors and DDC are both expressed in the chick NBR prior to the formation of dopaminergic synapses and the expression of TH (Lankford *et al.*, 1988; Gardino *et al.*, 1993; Kubrusly *et al.*, 2003). Furthermore, DA influences a variety of developmental processes (Lankford *et al.*, 1988; Varella *et al.*, 1999; Guimaraes *et al.*, 2001), and has been shown to mimic the anti-tumour effects of L-DOPA *in vitro* (Wick, 1978; Wick, 1980).

Consequently, the potential effects of DA on the processes of retinal development were ascertained to examine a potential link between levels of tyrosinase activity and the dopaminergic system during development, (see Figure 7.1.1). More specifically, a series of studies was undertaken to determine whether the addition of DA to the developing retina mimics the reported effects of L-DOPA. If the latter hypothesis were correct, developmental abnormalities of the albino visual system that have hitherto been directly attributed to a shortage of L-DOPA, may in fact be a reflection of secondary consequences on levels of retinal DA.

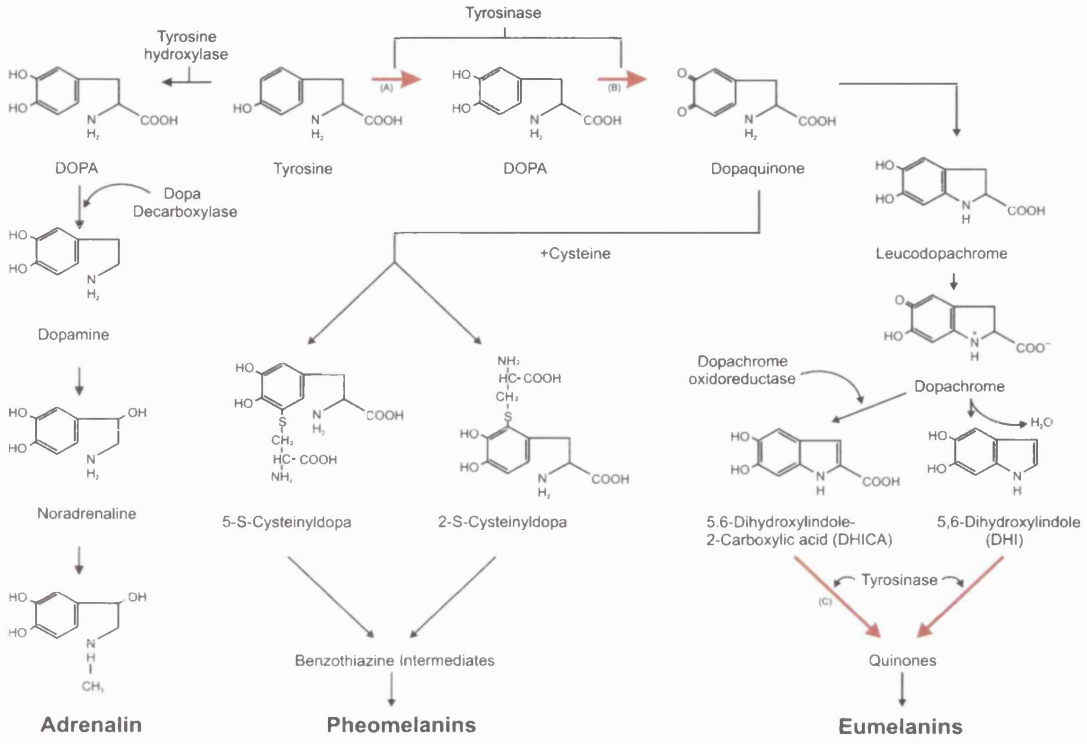

Figure 7.3.1 Catecholamine and melanin synthesis pathways. The first step in the biosynthesis of the melanins and the catecholamines involves the hydroxylation of tyrosine to form DOPA. Traditionally, this step of the pathway is thought to be catalysed by tyrosinase in the melanocytes, and tyrosine hydroxylase (TH) in the brain. Recent studies have challenged this paradigm, suggesting that tyrosinase-mediated DOPA synthesis in the RPE may provide the neural retina with a substrate for catecholamine synthesis prior to the expression of TH. Stages of the pathway which are catalysed by tyrosinase are indicated by red arrows. The figure has been adapted from King and Summers (1988).

7.2 Experimental aims

The effects of DA application on the processes of retinal development were examined in the early postnatal (P0-P3) rat to facilitate comparison with results from the *in vivo* studies into the effects of L-DOPA administration (chapters 2 and 3). However, as a result of the inability of DA to cross the blood-retinal barrier, intravenous delivery methods were inappropriate. Two alternative assays were used; DA was administered to *in vitro* organotypic culture preparations of pigmented and albino retinae, and in parallel, by intraocular injection of albino pups *in vivo*. The effects of the treatment on patterns of cell division, levels of proliferation and Cx43 expression were then examined using confocal microscopy of both fixed and live tissue.

7.3 Methods

Intraocular injection of Dopamine

For the *in vivo* studies, only albino (Wistar) rats were used. P3 pups were each administered a single intraocular injection of ~0.4µl of DA with ascorbate (1:1) dissolved in 1% DMSO in PBS (100µM and 1mM solutions). The second eye was left untreated, thus presenting a negative control. As a second control, animals were administered a sham intraocular injection of 1% DMSO. Animals were then killed by decapitation 6 hours later and the eyes submerged in 4% formalin over night. They were then washed in PBS, cryoprotected overnight in 20% sucrose and subsequently embedded in OCT. The cornea and lens were removed and the tissue bathed in a 2:1 mixture of 20% sucrose/OCT for 30 minutes. Eyecups were embedded in OCT and quickly frozen by submersion in dry ice. Four retinae (each from a different animal) were examined per treatment group.

Live-imaging and tissue culture

P0-P1 albino (Sprague-Dawley) and pigmented (D.A.) rats were decapitated and their eyes removed and placed in cold artificial cerebro-spinal fluid (ACSF) containing (mM); 119 NaCl, 26.2 $NaHCO_3$, 2.5 KCl, 1 KH_2PO_4, 1.3 $MgCl_2$, 2.5 $CaCl_2$ and 11 glucose, (Sigma-Aldrich; BDH). The solution was maintained at pH 7.4 by gassing with 95% O_2 and 5% CO_2. Neural retinae were dissected from the eye-cups and kept in ACSF at room temperature prior to, and during staining. The vital chromatin dye Hoechst 33342 (5 μM, Molecular probes) was used to label cells. Retinae were stained for ten minutes and then transferred to a heated (37°C) perfusion chamber on the stage of an inverted confocal microscope (Zeiss LSM510) with the ventricular surface facing the microscope objective, (x63 water immersion).

The tissue was kept flat by means of a platinum 'harp' with nylon strings. During imaging, retinae were continuously superfused with gassed (95% O_2, 5% CO_2) ACSF containing Hoechst 33342 (2 μM). Twelve-bit Images (512x512 pixels) were acquired every 30 seconds over a 2 hour period using the 350nm line of a UV laser. Images were analysed using Metamorph (Universal Imaging Corporation). For each cell the times of transition between stages of the cell cycle and angular displacements of the metaphase plate during mitosis were noted.

Statistical analyses were performed using SPSS 10.1 (SPSS Inc.). Data were tested for normality (KS-test). The duration of mitosis and each of its composite phases in control and DA-treated tissue were compared using an independent samples t-test. Following imaging all the tissue were collected and prepared for histological examination using the methods outlined above. In brief, retinae were fixed in 4% formalin and cryoprotected in 20% sucrose before being embedded and frozen in OCT. Four retinae (each from a different animal) were examined per treatment group.

Quantifying levels of proliferation and cleavage orientation

Tissue from both *in vitro* and *in vivo* experiments were subjected to the same methods of preparation and analysis once embedded in OCT. Twenty micron sections were taken in the horizontal plane, transferred to poly-lysine coated glass slides (BDH Laboratory Supplies) and left to adhere overnight. Slides were then rinsed for 60 seconds in distilled water, washed in PBS and coverslipped in DAKO fluorescent mounting medium with added DAPI.

Images were gathered using the 543nm line of a Zeiss laser scanning confocal microscope (LSM 500) using a x60 oil objective lens. Eight-bit z-stack images were generated with dimensions of approximately 146.2x98x10μm in the x-, y- and z-planes respectively. From these, the cleavage orientations of dividing retinal neurobalsts were calculated using a technique outlined in the methods section of chapter 4 and described by Haydar *et al.* (2003). In addition, levels of proliferation were calculated by performing mitotic cell counts from a slice mid-way through the z-stack. These were then standardised per mm of retina. Mitotic figures were easily recognisable as localised condensations of chromatin lying adjacent to the VM.

Statistical analyses were performed using SPSS 10.1 (SPSS Inc.). Data were tested for normality and homogeneity of variance using the KS-test and Levene test respectively. For the *in vitro* data, levels of proliferation and the proportion of vertical divisions were compared between control and DA-treated retinae using an independent samples t-test and chi-squared test respectively. For the intraocular data (3 independent groups), means were compared using a oneway ANOVA test with Tukey HSD *post-hoc* analysis.

Quantifying levels of Cx43 labelling

In addition to analysing patterns of cleavage orientation and proliferation, tissue from the *in vivo* studies were analysed for Cx43 expression. Tissue was stained using a protocol adapted from that described by Becker *et al.* (1995). A full

description of methods of tissue labelling and image acquisition/analysis can be found in the methods section of chapter 5.

Five regions were analysed per retina (n=5), and 4 retinae were studied per treatment group (N=4). Statistical analyses were performed using SPSS 10.1 (SPSS Inc.). Data were tested for normality using the KS- test. Levels of Cx43 expression were then compared between control and treatment groups using an oneway ANOVA test with Tukey *post-hoc* analysis.

7.4 Results

Intraocular injection of dopamine

Levels of proliferation

Levels of proliferation were examined in P3 albino retinae 6 hours after administration of intra-ocular injections of DA with ascorbate. As negative controls, intraocular injections of DMSO were made in parallel, and additionally, untreated eyes were analysed. Data is presented in the form of a series of histograms (Figure 7.4.1) in which the plot represents the average number of mitotic cells per mm, and the error bar represents the standard error of the mean. Data is presented from two separate experimental runs in which different concentrations of DA were used; 100μM (Figure 7.4.1A) and 1mM (Figure 7.4.1B). Data is shown from counts made at both central and peripheral retinal locations.

In both experiments, levels of proliferation were elevated in the peripheral retina relative to the centre, reflecting the centre-to-periphery gradient of development that as been discussed in previous chapters. Intraocular injections of DA and DMSO were consistently found to reduce levels of proliferation by ~20%, irrespective of retinal location. This effect only reached statistical significance in the peripheral retina of the second experimental run, i.e. at a higher

concentration of DA (Figure 7.4.1B). Though the reduction in mitotic levels induced by the introduction of DA to the retina exceeded the effect of the DMSO injection (reflected in a lower *p* value; 0.049 compared to 0.006 respectively) this difference was not in itself significant, nor was it consistent between experiments. Consequently, there was no evidence to suggest that DA reduced levels of proliferation *in vivo* beyond the general effects induced by the carrier alone.

Cleavage orientation

The distribution of cleavage orientations for control (untreated), DMSO-treated and DA-treated albino retinae are shown in Figures 7.4.2A-D in a series of frequency distributions. The data have been grouped into 10^{o} bins ranging from 0^{o} to 90^{o}, (representing horizontal and vertical divisions respectively). In addition, superimposed are pie-charts, indicating the proportion of divisions that are aligned horizontally (dark grey), and vertically (light grey). Horizontal and vertical divisions were defined as divisions occurring at an angle of $<45^{o}$ or $\geq 45^{o}$ relative to the VM respectively.

As described previously (chapter 3), cleavage orientations in the developing retinal neuroepithelium exhibit a unimodal distribution. The majority of cells are horizontally aligned relative to the plane of the tissue. This is true of both control and treated retinae (Figure 7.4.2A-D). Eight percent of all divisions in the P3 control retina were found to be vertically orientated (Figure 7.4.2A). In the DMSO-treated retinae 7% of all mitotic cells examined were vertically aligned, Figure 7.4.2B. In the DA-treated retinae, the proportion of vertical divisions was halved to 4%, irrespective of the concentration of DA used, Figure 7.4.2C&D. This effect approached statistical significance when comparing DA-treated and untreated retinae directly using a chi-squared test, (p=0.056 and 0.066 at concentrations of 100µM and 1mM respectively). However, when the proportion of vertical divisions in the DA-treated retinae were compared with the sham-treated eyes, the effects were not statistically significant. This lack of significance was supported by comparing the mean frequency of vertical divisions between groups using an ANOVA test. Consequently, though the

proportion of vertical divisions was reduced in DA-treated tissue from two independent experiments, the effect was not statistically significant.

Patterns of Cx43 labelling

Patterns of Cx43 labelling were quantified in control, DMSO-treated and DA-treated albino P3 retinae using simple image analysis techniques. This was possible as Cx43 labelling was clearly detectable as a series of discrete plaques lying at the interface between the RPE and NBR (Figure 7.4.3). Data is presented in the form of a series of histograms that plot (A) the total area of Cx43 labelling (calculated as the total number of positive pixels per unit area), as well as (B) the plaque density, (calculated as the frequency of Cx43 plaques per unit area). All data were then normalised to the albino control, so that both indexes of Cx43 labelling were expressed as relative proportions. Data is presented for two separate experimental runs. In the first (Figure 7.4.4), DA was delivered to the eye at a concentration of 100μM. In the second (Figure 7.4.5), a higher concentration of 1mM was used.

In the first experiment, the total level of Cx43 labelling was significantly reduced in the DA-treated retinae relative to both the control and DMSO-treated retinae, (p= 0.004 and 0.044 respectively; Figure 7.4.4A). However, DA had no effect on the density of Cx43 plaques (Figure 7.4.4B), suggesting that changes in levels of Cx43 were mediated by changes in plaque size rather than plaque number.

Surprisingly, when DA was introduced at a higher concentration (1mM), there was no detectable effect on the total area of Cx43 labelling, nor on the density of Cx43 plaques, (Figure 7.4.5A&B). Though this may reflect a concentration dependency with respect to the action of DA in the retina, it is equally likely to be due to experimental error, (see discussion).

The effects of dopamine in vitro

Levels of proliferation

Patterns of proliferation in P0-P1 retinae were analysed in histological section following live-imaging over a 2 hour period. Both pigmented (D.A.) and albino (Lister Hooded) rat retinae treated with 100μM DA/ascorbate were analysed and compared with time-matched controls, (for which the medium was not supplemented with DA). Data is presented in the form of a frequency histogram (Figure 7.4.6) which plots the mean number of mitotic cells per mm of retina for each experimental group. Error bars represent the standard error of the mean.

The data illustrates that the application of 100μM DA has a differential effect on the pigmented and albino retina *in vitro* (Figure 7.4.6). Thus, in the pigmented retina, levels of proliferation are indistinguishable between control and treated groups. In contrast, DA reduced levels of proliferation in the albino retina by approximately 50%; an effect which was significant at the 5% level (p= 0.049).

Patterns of cleavage orientation

The distribution of cleavage orientations in control and DA-treated retinae are shown for both pigmented (Figure 7.4.7) and albino (Figure 7.4.8) tissue. Data is presented in the same form as Figure 7.4.2. A series of frequency distributions are shown for which data have been grouped into 10° bins ranging from 0° to 90°. In addition, superimposed are pie-charts, indicating the proportion of horizontal (dark grey) to vertical (light grey) divisions. Horizontal and vertical divisions were defined as divisions occurring at an angle of <45° or ≥45° relative to the VM respectively.

DA was found to have no effect on cleavage orientations *in vitro.* In all experimental and control groups studied, data followed a unimodal distribution such that nearly 60% of all divisions were aligned within 10° of the horizontal, (defined by the plane of the developing neuroepithelium). Indeed, outside the

context of the entire eye, the proportion of vertical divisions would seem to drop to a base-line minimum of ~4%. This finding supports those reported by Cayouette *et al.* (2001) who suggest that the presence of the RPE is instrumental in/conducive to the adoption of a vertical cleavage orientation.

Rates of mitosis and its composite phases

Prior to histological analysis pigmented and albino retinal neuroepithelia were flat-mounted ventricular surface up and live-imaged over a two hour period with and without DA in the culture medium. The duration of mitosis and its composite phases were calculated by tracing changes in the state of cellular chromatin (Figure 7.4.9). Data is presented in two distinct forms. In Figure 7.4.10 the mean duration of M-phase (prophase, metaphase, anaphase and telophase combined) is plotted for each experimental group. In Figure 7.4.11 the mean duration of each composite phase is plotted for both pigmented (Figure 7.4.11 A) and albino (Figure 7.4.11 B) retinae.

Considering the whole of M-phase first, its duration did not differ between the pigmented and albino tissue, lasting approximately 60 minutes irrespective of pigmentation type. However, the addition of DA had a differential effect on the pigmented and albino retina. In the pigmented DA-treated tissue, M-phase duration was slightly shorter than in time-matched pigmented controls. In contrast, DA addition elongated M-phase in the albino retina by approximately 50%, an effect which was significant at the 5% level.

In Figure 7.4.10 these changes in M-phase duration can be traced back to alterations in one or more of its composite phases. Thus, in the albino retina, the effects of DA on M-phase duration were mediated by a selective elongation of prophase and metaphase, though this effect was only found to be statistically significant with respect to the latter (at the 5% level). In the pigmented retina, though no significant effect on M-phase duration was induced by the addition of DA to the culture medium, all of the composite phases examined were slightly shorter in the DA-treated retinae. This even reached statistical significance with

respect to anaphase and telophase durations. However, it is important to note that multiple pair-wise statistical comparisons are susceptible to false positives.

The effects of dopamine on levels of proliferation *in vivo*

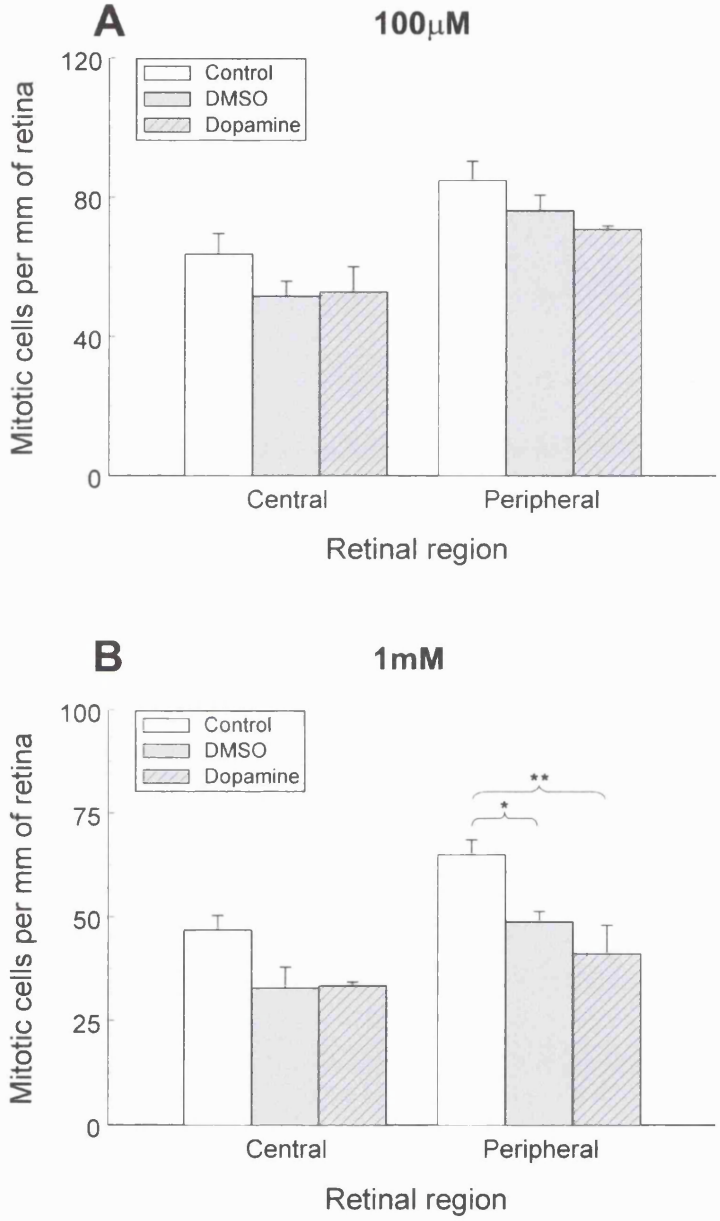

Figure 7.4.1 The mitotic index (number of dividing cells per mm of retina) is shown for control (untreated), DMSO-injected and DA-treated albino (Wistar) rat retinae. DA was delivered by intraocular injection at a concentration of (A) 100μM, and (B) 1mM. Tissue was analysed 6 hours post-injection. Error bars represent the standard error of the mean. Though levels of proliferation were consistently lower in the treated retinae relative to the untreated controls, the difference was only significant in the peripheral retina (1mM). No differences were found between DMSO-injected and DA-treated retinae. Four retinae were examined per experimental group. 12 regions were sampled per retina. * $p<0.05$, ** $p<0.01$.

The effects of dopamine on cleavage orientations *in vivo*

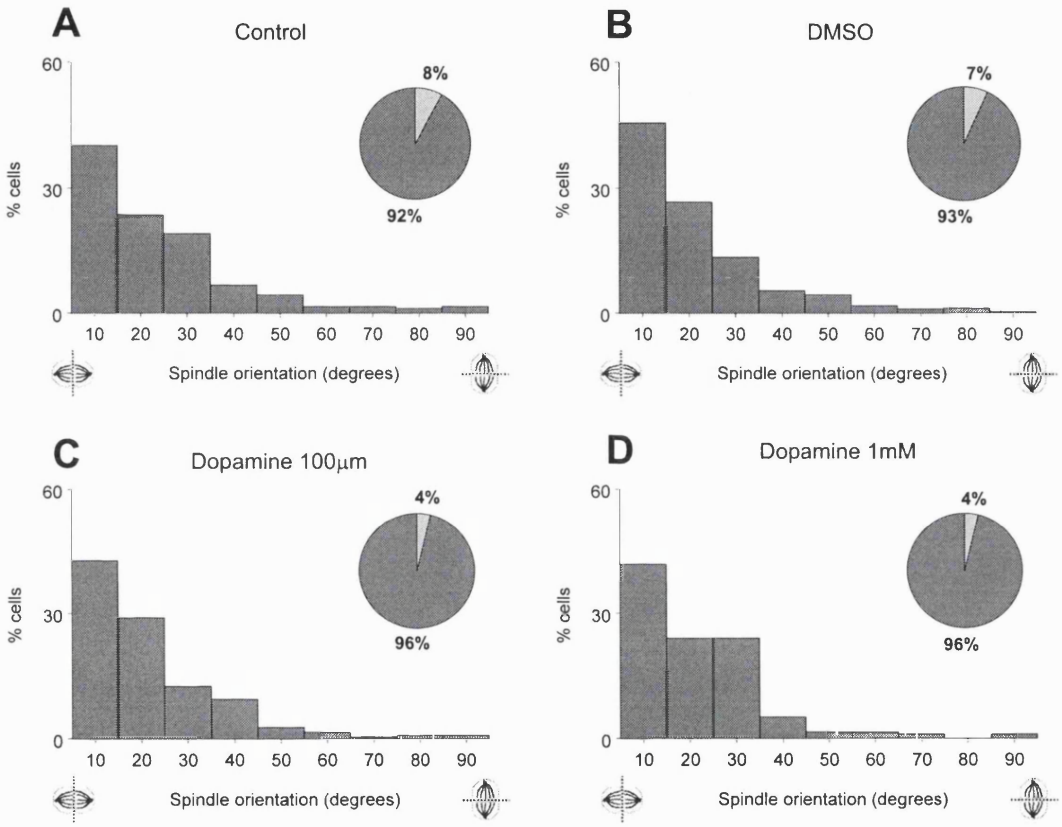

Figure 7.4.2 Frequency histograms of the distribution of cleavage orientations relative to the VM are presented for (A) control; (B) DMSO-treated; and (C-D) DA-treated P3 albino retinae (at concentrations of 100μM and 1mM respectively). Superimposed are pie-charts describing the relative proportion of horizontal (dark grey) to vertical (light grey) divisions. Though the proportion of vertical divisions was reduced in the DA-treated retinae relative to both untreated and DMSO-treated controls, the difference did not reach statistical significance at the 5% level. (p=0.056 and 0.066 comparing the 100μM and 1mM DA-treated retinae to untreated controls; chi-squared test). The number of retinae examined and cells analysed for each group= control (8, 537); DMSO-treated (8, 498); 100μM DA-treated (4, 255); 1mM DA-treated (4, 196).

The effects of 100μM dopamine on levels of Cx43 *in vivo*

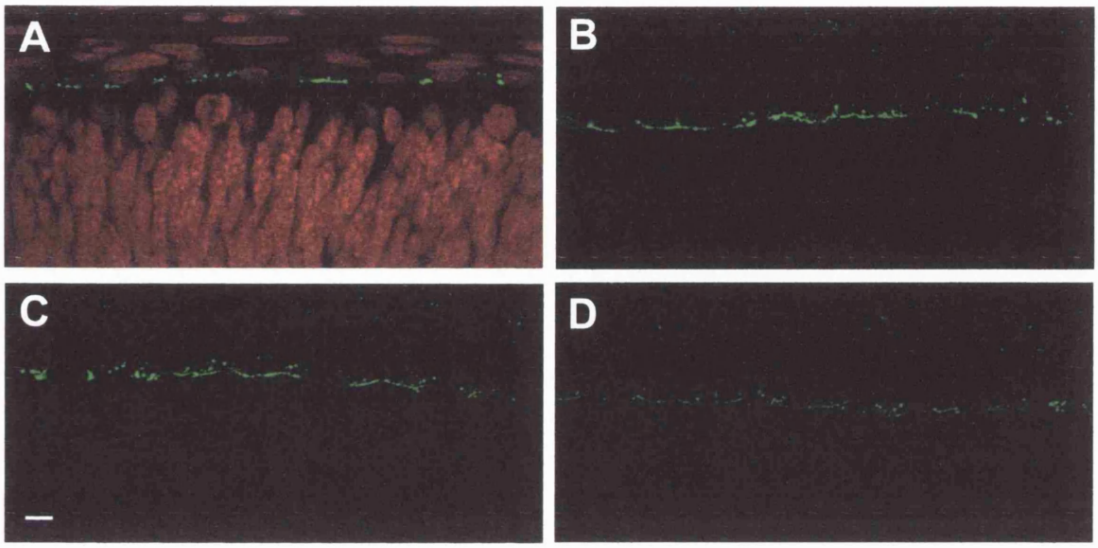

Figure 7.4.3 Patterns of Cx43 localisation in the P3 albino retina following intraocular injection of 100μM dopamine. (A) A reference image of the untreated albino retina shows a punctate distribution of labelling at the interface between the RPE and NBR. Tissue was stained with an antibody against Cx43 (green) and counterstained with propidium iodide to visualise nucleic acid. The other images are single-channel 5μm z-stack projections of the (B) untreated control, (C) DMSO-treated and (D) DA-treated albino retina. All staining, imaging and data analysis protocols were standardised, facilitating direct quantitative comparison between treatment groups. The relative area of Cx43 labelling was significantly reduced upon treatment with DA. However, when a higher concentration of DA was used (1mM), no effect could be detected. Scale bar=10μm.

The effects of 100μM dopamine on levels of Cx43 *in vivo*

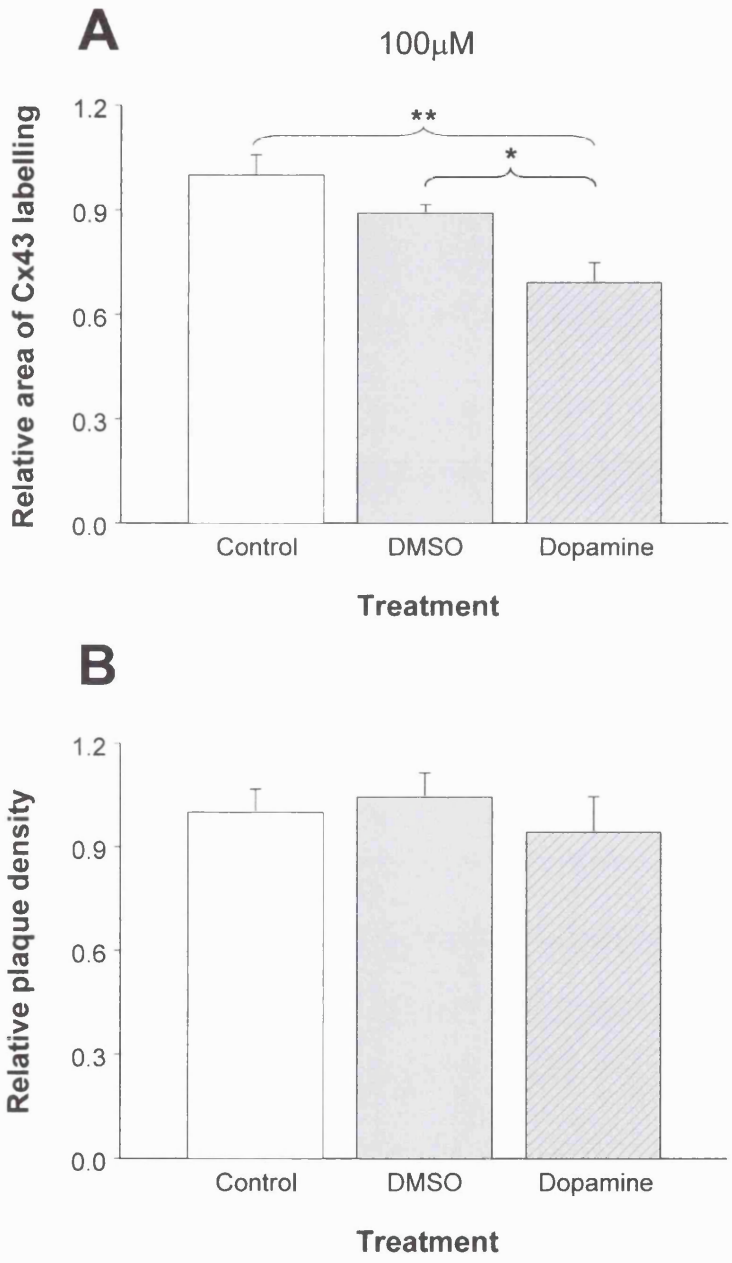

Figure 7.4.4 (A) The relative area of Cx43 labelling and (B) the relative density of Cx43 plaques (calculated as frequency per unit area) are plotted for control, DMSO-treated and DA-treated albino retinae. All data are normalised to the untreated control to facilitate direct comparison with further treatments. The total area of Cx43 labelling was significantly reduced by treatment with 100μM DA relative to both the untreated and DMSO-treated tissue. In contrast, neither of the treatments had any effect on the relative plaque density (frequency per unit area). Four retinae were examined per experimental group and 5 regions were analysed per retina. * $p<0.05$, ** $p<0.01$.

The effects of 1mM dopamine on levels of Cx43 *in vivo*

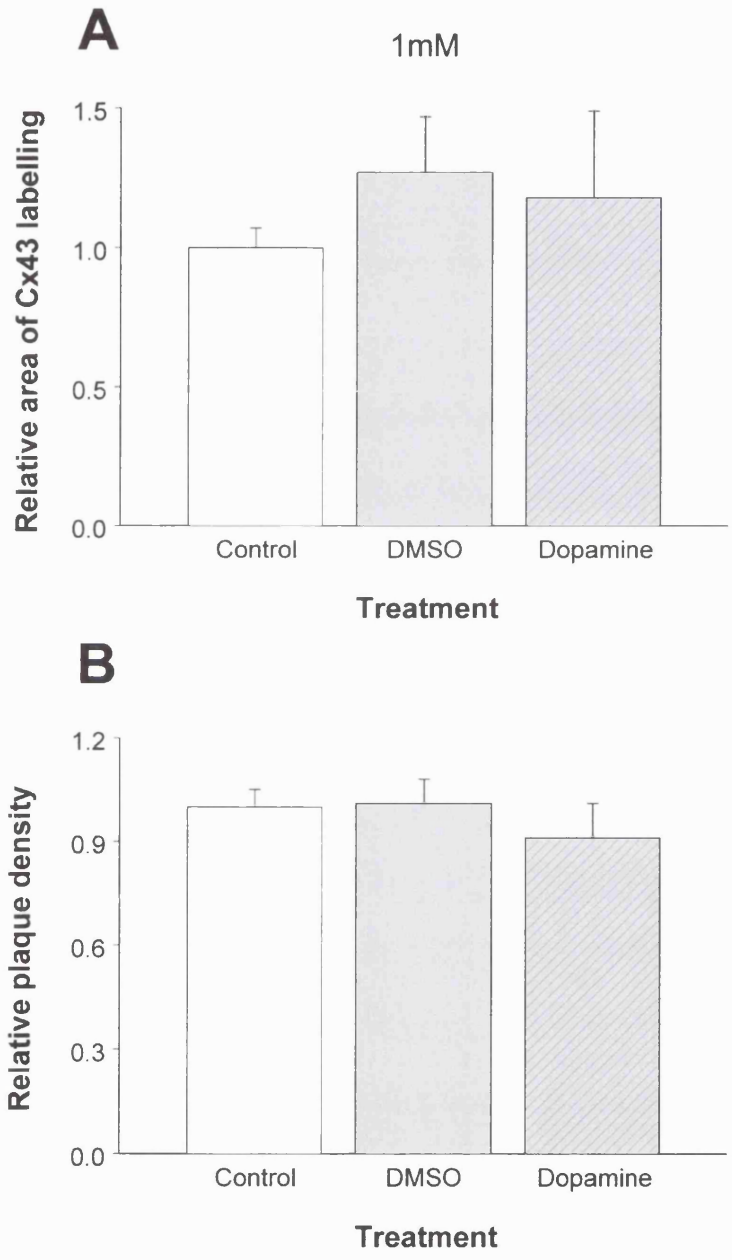

Figure 7.4.5 (A) The relative area of Cx43 labelling and (B) the relative density of Cx43 plaques (calculated as frequency per unit area) are plotted for control, DMSO-treated and DA-treated retinae. All data are normalised to the untreated control. Neither the total area of Cx43 labelling, nor the relative plaque density were affected by treatment with 1mM DA or DMSO. Four retinae were examined per experimental group and 5 regions were analysed per retina.

The effects of 100μM dopamine on levels of proliferation *in vitro*

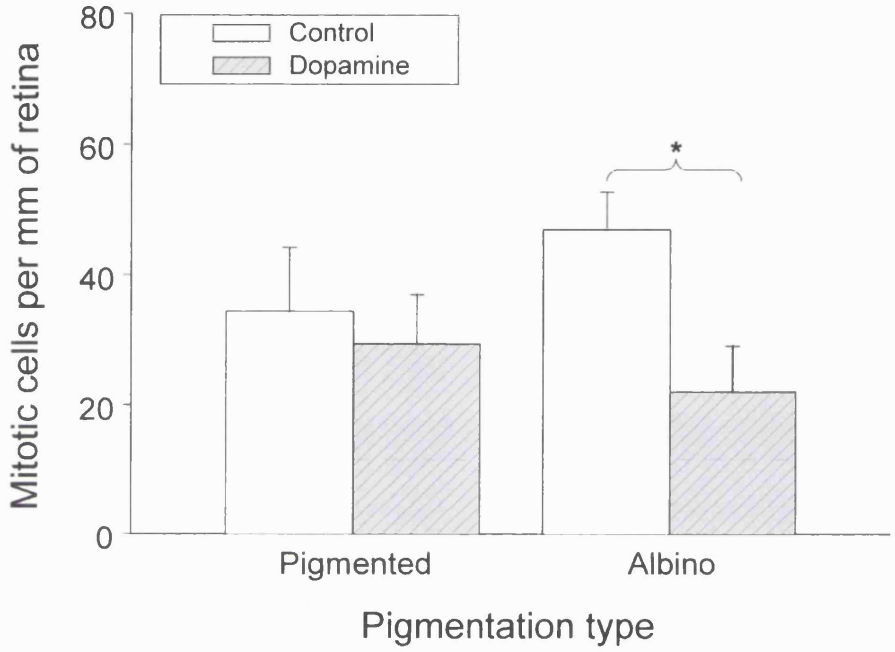

Figure 7.4.6 The mitotic index (number of dividing cells per mm of retina) is shown for control and DA-treated pigmented and albino retinal neuroepithelia following 2 hours of live-imaging. Once the imaging period had elapsed the tissue was fixed in 4% formalin and prepared for histological analysis. Four retinae were examined per experimental group, except for the albino control (N=3). 10 regions were sampled per retina. Levels of proliferation were significantly reduced in the DA-treated albino retina. * $p<0.05$.

Cleavage orientations in the *in vitro* pigmented retina following treatment with 100μM dopamine

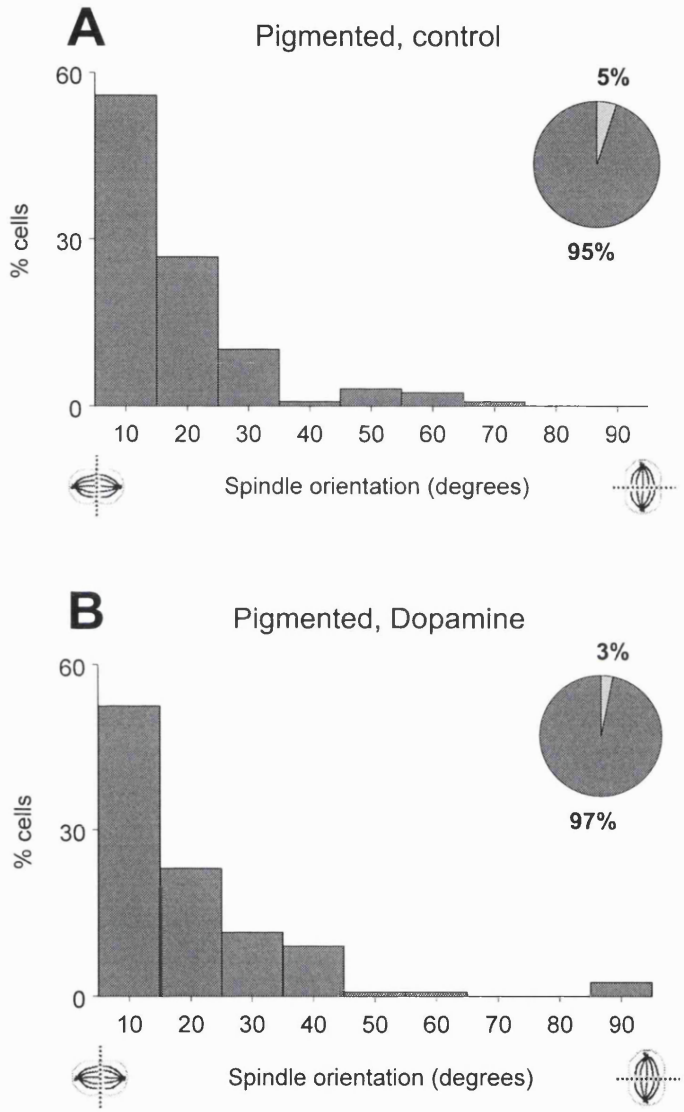

Figure 7.4.7 Frequency histograms of the distribution of cleavage orientations relative to the VM are presented for (A) control and (B) DA-treated pigmented retinal neuroepithelia following a 2 hour live-imaging period. Superimposed are pie-charts describing the relative proportion of horizontal (dark grey) to vertical (light grey) divisions. DA had no effect on patterns of cleavage orientation *in vitro*. Three retinae were analysed per experimental group, and n=127 and 122 cells analysed for the control and DA-treated retinae respectively.

Cleavage orientations in the *in vitro* albino retina following treatment with 100μM dopamine

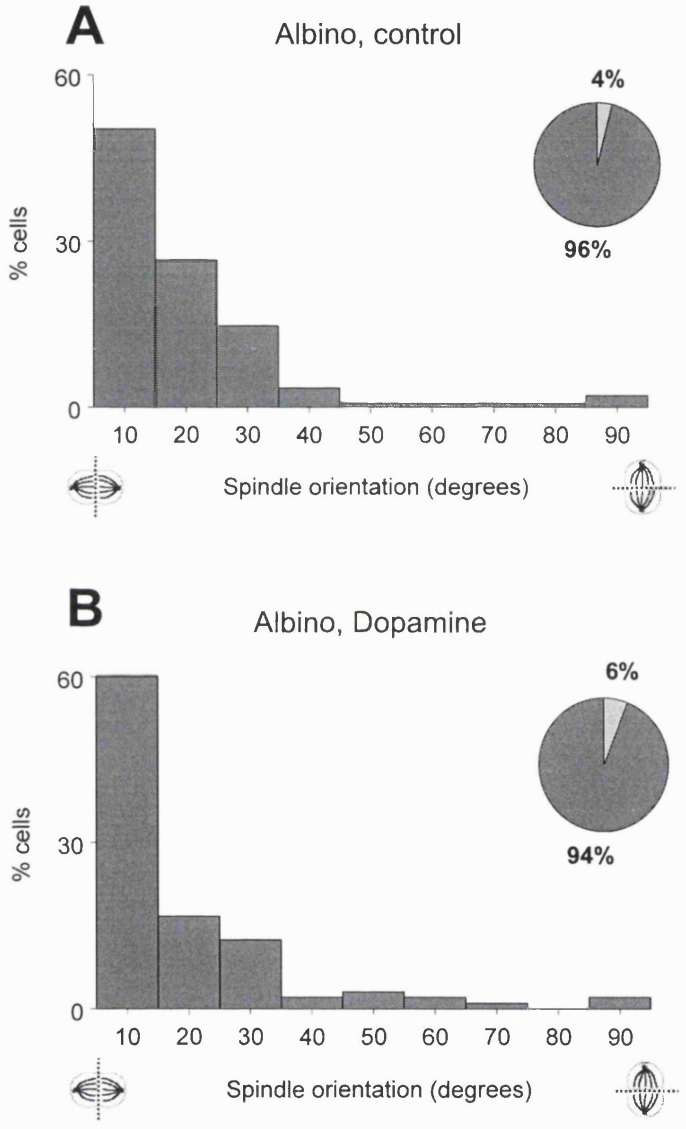

Figure 7.4.8 Frequency histograms of the distribution of cleavage orientations relative to the VM are presented for (A) control and (B) DA-treated albino retinal neuroepithelia following a 2 hour live-imaging period. Superimposed are pie-charts describing the relative proportion of horizontal (dark grey) to vertical (light grey) divisions. DA had no effect on patterns of cleavage orientation *in vitro*. Three retinae were analysed per experimental group. n=143 and 96 cells analysed for the control and DA-treated retinae respectively.

Live-imaging of mitotic cell division in the retinal neuroepithelium

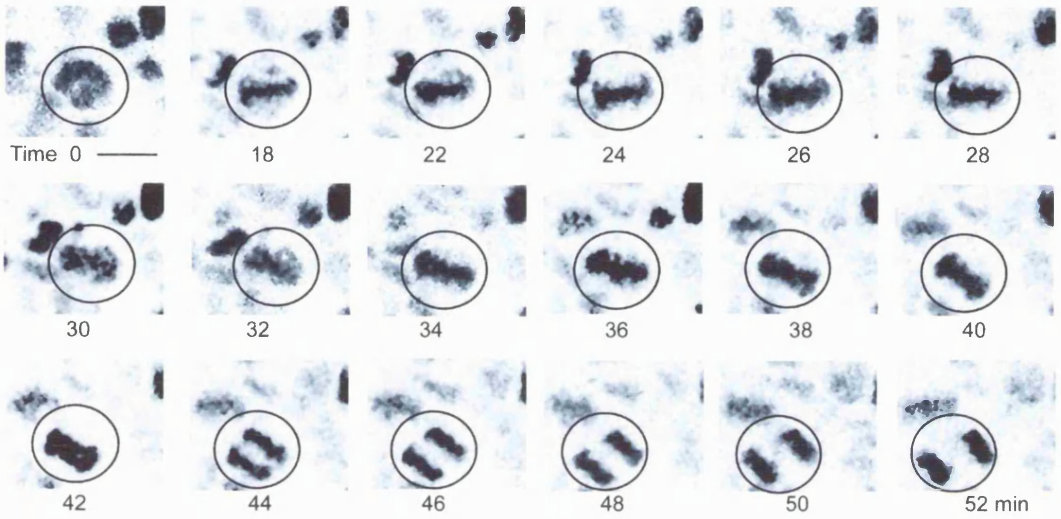

Figure 7.4.9 Retinae from P0-P1 albino (Sprague-Dawley) and pigmented (D.A.) rats were flat-mounted ventricular surface up on a heated perfusion chamber on an inverted confocal microscope (Zeiss LSM510). Chromatin was labelled with the vital chromatin dye Hoechst 33342 and individual dividing cells tracked as they passed through the various phases of the cell cycle. Following imaging, all the tissue were collected and prepared for histological examination. In the example above, the cell entered metaphase at time zero, and anaphase at time 42 (42 minutes later). Scale bar=10μm. Image has been reproduced from Tibber *et al.* (2004).

M-phase duration in the *in vitro* pigmented and albino retina following treatment with 100μM dopamine

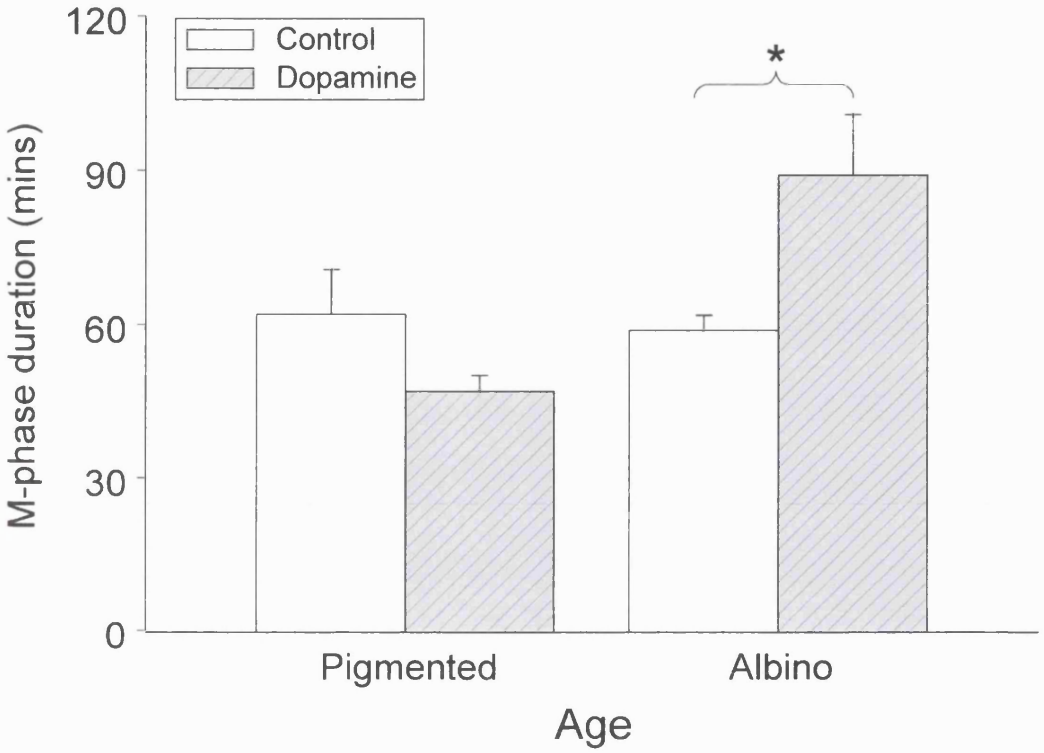

Figure 7.4.10 The entire duration of M-phase (prophase, metaphase, anaphase and telophase combined) in the developing pigmented and albino retinal neuroepithelium following treatment with 100μM DA *in vitro*. Data has been gathered from the live-imaging of tissue over a 2 hour period. Error bars represent the standard error of the mean. DA was found to act differentially on the two pigmentation phenotypes. In the albino retina M-phase duration was significantly lengthened by the addition of DA to the medium. In contrast, the duration of M-phase was shorter in the DA-treated pigmented tissue (relative to time-matched controls), though this difference was not statistically significant. Four retinae were analysed per experimental group, and the number of cells analysed for each group=pigmented control (103), DA-treated pigmented (117), albino control (91) and DA-treated albino (30). * $p<0.05$.

Duration of cell cycle phases *in vitro* following treatment with dopamine

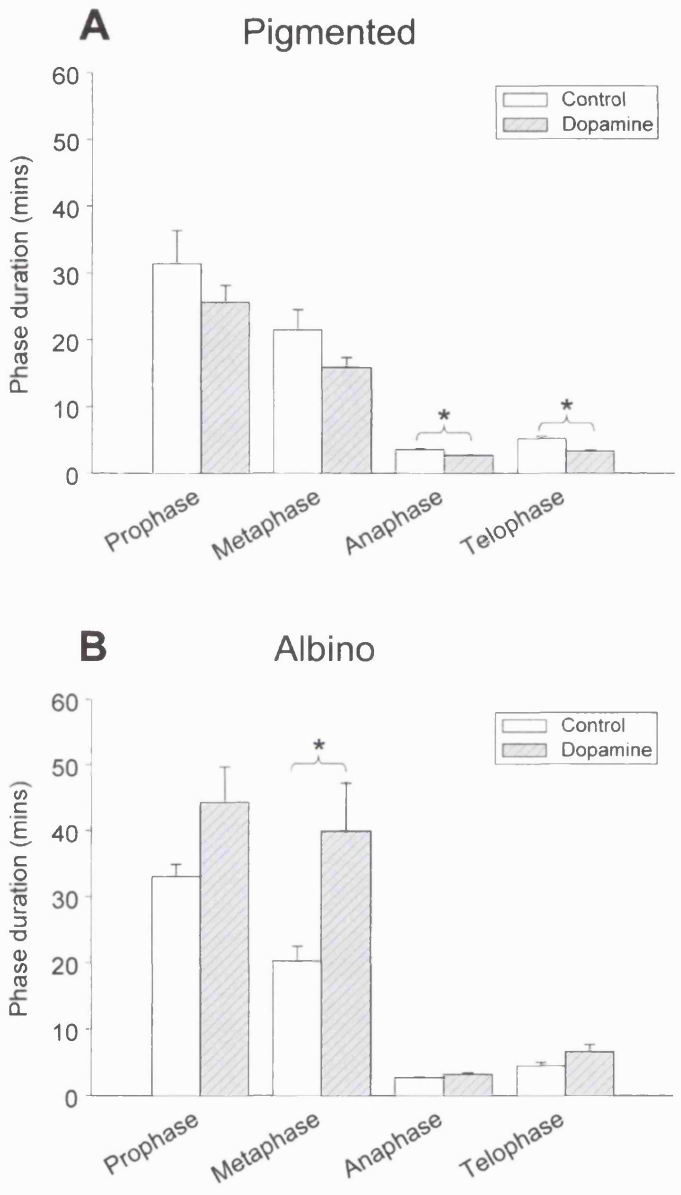

Figure 7.4.11 Data has been gathered from the live-imaging of retinal neuroepithelia over a 2 hour period. Error bars represent the standard error of the mean. DA was found to acted differentially on the two pigmentation types. In the DA-treated pigmented tissue all phases were slightly prolonged relative to age-matched controls, although this difference was only significant with respect to anaphase and telophase. In the albino retina, the lengthening of M-phase as a result of DA treatment (see figure 7.4.10), was primarily due to an increase in the duration of metaphase. 4 retinae were analysed per experimental group. The number of cells traced through prophase, metaphase, anaphase and telophase respectively = (112, 136, 132, 129) in the pigmented control; (121, 176, 174, 173) in the DA-treated pigmented; (106, 149, 143, 139) in the albino control; and (31, 82, 54, 50) in the DA-treated albino. * $p<0.05$.

7.5 Discussion

Studies were undertaken to assess the potential effects of DA on the processes of retinal development and determine whether they mimic the documented response patterns upon application of L-DOPA (Wick, 1977; Akeo *et al.*, 1994; Ilia and Jeffery, 1999). The working hypothesis posited that reduced levels of L-DOPA in the albino retina might lead to a defect in dopaminergic stimulation during development. There are two potential pathways by which this hypothetical link could be manifest. First, L-DOPA might function independently as a neurotransmitter and/or neuromodulator with dopaminergic receptor binding affinity (Misu *et al.*, 2002). Alternatively, tyrosinase-mediated L-DOPA generation in the RPE might present an early substrate for catecholamine synthesis to the NBR (Kubrusly *et al.*, 2003). If the latter were correct, previous reports into the effects of L-DOPA on retinal development may in fact be due to its conversion into DA.

To address these issues, DA was administered to postnatal developing retinae. However, in contrast to L-DOPA, DA does not cross the blood-retinal barrier, and consequently, could not be delivered to the retina by introduction into the blood stream. The effects of DA on development were thus explored using two alternatives techniques, both of which have their inherent though distinct sets of limitations. First, the effects were explored *in vivo* by intraocular injection. In this way the effects of DA on retinal development could be assessed within the context of the surrounding tissues. However, the downside of this technique was that precise dosages were difficult to regulate and subsequent ocular damage varied between replicates.

In parallel, the short-term effects of DA were studied *in vitro* using organ culture methods. The advantage of this technique was that dosages could be administered with a high degree of precision, and delivered directly to the ventricular surface. However, by studying development of the NBR *in vitro* the regulatory effects of the RPE and surrounding tissues were lost. This was

particularly relevant with respect to cleavage orientations, which were severely affected by the loss of environmental context, a finding which supports a previous study into the regulatory role of the RPE (Cayouette *et al.*, 2001).

Results from the *in vivo* studies indicate that the very act of piercing the cornea and penetrating the optic cup induced subtle perturbations in all parameters examined. This was most probably due to a loss of intraocular pressure as a consequence of the puncture, and subsequent localised separations of the RPE/NBR. Whilst levels of proliferation were reduced in the DA-treated retinae, the effect was merely comparable to that induced by sham-treatment with DMSO.

There was some evidence to suggest that patterns of cleavage orientation were shifted by the addition of DA. DA addition reduced the proportion of vertical divisions by approximately 50%, and in this respect mimicked the effects of L-DOPA (see chapter 3). Though results were consistent at both concentrations of DA used, on neither occasion were they statistically significant. It is unclear whether the ambiguity of this result was due to a low sample size. Though the number of cells sampled was high (between 196 and 537 cells per group), only 4 retinae were examined at each concentration of DA. In view of the difficulties involved in regulating precise dosages it is possible that a larger sample size may clarify this issue.

The only DA-specific effect which was found to be statistically significant was with respect to patterns of Cx43 localisation. DA reduced the overall level of Cx43 labelling, though no change in plaque number could be detected, (thus mimicking the effects of L-DOPA; chapter 5). Unfortunately, this effect was not reproduced when a higher concentration of DA was used. This discrepancy between data-sets may reflect true dose-dependency. Alternatively, the discrepancy may be due to experimental error.

There are two lines of evidence to suggest that the conflicting data was indeed due to experimental error. First, when the higher concentration of DA was delivered, it was noted that several of the eyes were extremely inflamed as a

result of the treatment, more so than during previous experimental runs. Second, by comparing Figure 7.4.4A with Figure 7.4.5A it is clear that whilst the level of variability in the data is comparable/minimal in the untreated control eyes of both experiments, the standard error of the mean is greatly elevated in the data from the treated eyes of the second experiment. Furthermore, this increase in variability can not be a specific response to DA-treatment as it is also evident in the data from the DMSO-treated tissue. It would thus seem likely that either the retinae were directly damaged by the mechanical stress of piercing the eye, or alternatively, that the integrity of the RPE/NBR interface was compromised by a drop in the level of intraocular pressure.

Data gathered from the *in vitro* studies also led to several interesting findings. First, when maintained *in vitro* the proportion of vertical divisions within the retinal neuroepithelium dropped to a base-line of approximately 4%. This was independent of pigmentation type. Thus, outside the context of the entire eye, patterns of cleavage orientation did not differ between the pigmented and the albino retina. This reinforces the fact that abnormal patterns of cleavage orientation in the albino retina (chapter 3) are due to specific defects in the operation/regulation of this system, rather than a generalised disruption of retinal structure/cell localisation. Consequently, the effects of DA on patterns of cleavage orientation could not be analysed using the organotypic *in vitro* system employed. Perhaps a more complex *in vitro* methodology in which the RPE is either retained or co-cultured may provide a more physiologically relevant set of results.

In contrast to patterns of cleavage orientation, DA was found to elicit significant effects on levels of proliferation and cell cycle progression *in vitro*. Furthermore, there was a differential response in the pigmented and albino tissue. Thus, in the albino retina, DA led to a concerted reduction in the level of proliferation and a lengthening of the duration of mitosis; both by a factor of ~50%. This was primarily due to a selective elongation of metaphase/prophase. In the pigmented retina however, DA had no significant effect on either of these parameters, though mitosis and all of its composite phases were slightly elongated in DA-treated pigmented retinae.

These findings provide the first evidence to suggest that retinal progenitors of pigmented and albino retinae are intrinsically distinct if only in their capacity to respond to local environmental cues. Though a subset of pigmented and albino retinal explants from the ventrotemporal retina have been shown to exhibit differential growth patterns *in vitro* when presented with a chiasmatic substrate (Marcus *et al.*, 1996), the study examined the growth of ganglion cell axons, i.e. cells that had already exited the cell cycle, (and hence adopted a specific spatial/physiological identity). The results described here suggest that even prior to cell cycle exit, cells of the pigmented and albino retina have adopted a distinct intrinsic program which is retained (at least for a short period) upon separation from the RPE and surrounding tissues. Though one could argue that diffusible signals from the RPE could have been transferred along with the retinal explants, it seems unlikely that this could account for the prolonged differential response patterns. Tissue was washed prior to imaging and continuously superfused with medium throughout the two hour imaging period.

Perhaps pigmented and albino retinae exhibit differential response patterns to DA as a result of a distinct history of exposure to the neurotransmitter. If the RPE does indeed provide the NBR with an early source of L-DOPA for catecholamine synthesis -as a recent paper posits (Kubrusly *et al.*, 2003)- one would expect DA levels to be lower in the albino retina from approximately E10-E11 onwards, i.e. when tyrosinase is first expressed (Beermann *et al.*, 1992; Gimenez *et al.*, 2003). Consequently, there may be an up-regulation of DA receptors or a shift in receptor kinetics in the albino retina to compensate for this substrate. D_1 receptors have been detected throughout the neuroblastic layer of the late prenatal and early postnatal rat using mRNA localisation and histochemical detection methods (Schambra *et al.*, 1994; Koulen, 1999). Furthermore, this precedes the lamina-specific clustered expression pattern typical of their role in synaptic neurotransmission (Koulen, 1999). A comparative analysis of D_1 receptor localisation and retinal DA concentrations in the pigmented and albino retina throughout development may therefore cast some light on the putative link between levels of tyrosinase expression/activity and DA receptor activity.

7.6 Conclusions

Results from *in vitro* and *in vivo* experiments into the effects of DA on retinal development were not entirely consistent and did not always reach statistical significance. Consequently, the results were inconclusive. Irrespective, several general points can be made. First, exogenously introduced DA was biologically active in the early postnatal rodent retina. Though not always statistically significant, the effects of DA on patterns of cell proliferation, cleavage orientation and Cx43 labelling mimicked L-DOPA with respect to the direction of their action. Thus, both chemicals reduced levels of proliferation, Cx43 expression and the proportion of vertical divisions in the developing retinal neuroepithelium.

Second, DA had a differential effect on the pigmented and albino retina *in vitro*. This would suggest that pigmented and albino retinal progenitors are inherently distinct prior to cell cycle exit. Furthermore, it provides circumstantial evidence of a link between the melanin synthesis pathway and the dopaminergic system. However, if the nature of this putative link is to be elucidated, a more comprehensive set of studies must be undertaken in which the effects of L-DOPA and DA are ascertained in parallel using identical methodology, (see future studies proposed, chapter 8).

Chapter 8:
Conclusions

8.1 Summary

The foundations of this thesis rested on a series of studies performed by Ilia and Jeffery (Ilia and Jeffery, 1996; Ilia and Jeffery, 1999; Ilia and Jeffery, 2000). The fundamental observation described therein is that levels of proliferation in the developing albino retina are severely elevated relative to pigmented time-matched controls. Furthermore, this abnormality can be corrected by the introduction of L-DOPA into *in vitro* albino eyecup preparations (Ilia and Jeffery, 1999). The working hypothesis of this laboratory –outlined in an early review (Jeffery *et al.*, 1997)- posited that reduced levels of L-DOPA in the albino retina implies an absence of critical regulatory control, which is manifested as an excess of cell proliferation and a delay in the maturational gradient. Consequently, the retina becomes abnormally thickened and hypoxic (Semo *et al.*, 2001), resulting in a wave of excessive cell death (Ilia and Jeffery, 1999) which culminates in a selective depletion of the rod photoreceptor population.

From this starting point, a series of experiments was undertaken to examine patterns of cell division in the albino retina and the putative role of L-DOPA in the regulation of retinal development, using an *in vivo* model; the tyrosinase-negative Wistar rat. In support of previous findings, levels of proliferation were elevated in the albino retina, and furthermore, could be temporally correlated with an excess of cells in the cell cycle, as well as a delay in the process of retinal lamination/tissue differentiation (chapter 2). However, in contrast to these reports, developmental abnormalities observed in the albino were heavily

focused towards the latter periods of neurogenesis, only reaching statistical significance between P1 and P4.

Having demonstrated abnormalities in patterns of cell proliferation, cell cycle exit and retinal lamination in the albino retina, the orientation of dividing retinal neuroblasts was examined, recent studies having implicated the role of this parameter in the process of cell fate determination within the vertebrate retina (Cayouette *et al.*, 2001; Cayouette and Raff, 2003). Whilst no evidence was found to suggest that cleavage orientations within the plane of the developing neuroepithelium were regulated over time (Tibber *et al.*, 2004), the distribution of cleavage orientations within the apical-basal plane was both qualitatively and quantitatively disrupted in the albino (chapter 3). The precise implications of this finding are unclear, though current models would predict a shift in the relative proportion of cell types born during the later phases of neurogenesis, i.e. rod photoreceptors, bipolar cells and/or Müller glia (Cayouette and Raff, 2003). Data from chapter 3 would suggest that the Müller cell population does not differ between pigmentation types.

Upon analysis of RPE/NBR interactions in the developing pigmented and albino retina, Cx43 levels were found to be significantly elevated in the albino at P1 and P4 (chapter 5). This presents a potential mechanistic pathway which may underlie the broad spectrum of developmental abnormalities that have been described in the hypopigmented retina. Thus, Cx43-based gap junctional communication represents the primary channel for communication between the RPE and NBR (Becker *et al.*, 1998; Janssen-Bienhold *et al.*, 1998; Pearson *et al.*, 2004a), and the RPE/factors derived from the RPE are known to play a critical role in the regulation of; cleavage orientation (Cayouette *et al.*, 2001), levels of proliferation (Becker and Mobbs, 1999), the pace of cell cycle progression (Pearson *et al.*, 2004b), as well as the process of retinal lamination (Jensen *et al.*, 2001).

For all but one parameter found to be disrupted in the albino retina throughout the course of these studies, data has simultaneously shown that they can either be corrected, or at least regulated (i.e. shifted towards the wildtype state), by

the introduction of L-DOPA through intravenous *in vivo* methods. Thus, the administration of L-DOPA to the developing albino retinal neuroepithelium was found to induce the following responses:

1. A reduction in levels of proliferation.
2. A promotion of retinal lamina differentiation.
3. A promotion of horizontal cleavage orientations and/or inhibition of vertical cleavage orientations.
4. A reduction in levels of Cx43 localisation at the RPE/NBR interface.

Finally, attempts were made to unravel the mechanisms by which L-DOPA mediates this wide range of regulatory effects (chapter 7). Encouraged by a series of recent publications that highlighted the potential role of tyrosinase-mediated L-DOPA production in the dopamine synthesis pathway (Eisenhofer *et al.*, 2003; Kubrusly *et al.*, 2003), a preliminary study was undertaken to examine the effects of DA on the developing retina. Though the experimental protocols used were not ideal, and results were not conclusive, preliminary evidence from both *in vitro* and *in vivo* studies would suggest that DA may be capable of inducing effects (1), (4) and possibly (3) from the list above.

8.2 Revised model of the later stages of albino retinal development

Based on the evidence gathered during the course of this thesis, a speculative revision of the model of albino retinal development (Jeffery, 1997) can be drawn:

During the development of the early postnatal albino retina a lack of RPE-derived regulatory control (mediated by L-DOPA or one of its metabolites in the wildtype retina), results in a failure of cells to exit the cell cycle. Consequently, the period of retinal proliferation is extended and the transition to a state of histological differentiation is delayed. Either as a consequence of abnormal thickening of the retina and tissue hypoxia, or alternatively, an anachronistic

local environment, levels of cell death within the population of newborn cells becomes elevated, resulting in translaminar cell deficits in the adult. In parallel, low levels of L-DOPA -or one of its metabolites- fail to regulate the formation of Cx43 plaques at the apical surface of the RPE, such that an excess of regulatory signals are released into the subretinal space. The potential implications of this are manifold, one of which is the prolongation/ augmentation of a putative signal from the RPE which is conducive to the adoption of a vertical cleavage orientation. This may in turn influence the relative proportion of rod photoreceptors to bipolar cells generated, and hence, the relative size of these cell populations in the adult retina.

8.3 Future studies proposed

(1) The effects of longitudinal administration of L-DOPA on the adult anatomy/physiology of the retina.

Having demonstrated the effects of L-DOPA administration on the developing postnatal albino retina, it would be of great interest to determine the long-term consequences of its re-introduction. Furthermore, the effects of L-DOPA on the developing pigmented retina could be traced in parallel in order to characterise differential response patterns. Due to its capacity to cross both the blood-retinal and placental barrier (Merchant *et al.*, 1995), L-DOPA could be delivered to embryos from the earliest stages of development through to weaning, via introduction to the mother's feed. Individual pups from each litter would then be sacrificed and the eyes tested for concentrations of L-DOPA (using high performance liquid chromatography) to ensure that its delivery had been successful.

Once the animals reach adulthood they would be tested electrophysiologically and subsequently fixed for histological analysis. All analyses would be performed on and referred back to untreated age-matched pigmented and albino controls. Visual evoked potential (VEP) responses would be recorded to assess decussation patterns at the optic chiasm. Animals would then be

sacrificed and resin sections generated in order to examine the thickness of each nuclear and plexiform layer, as well as the absolute size/dimensions of the eye and retina. In addition, rod counts and ganglion cell counts would be undertaken and anterograde labelling of the optic disc used to assess decussation patterns at the chiasm anatomically.

(2) The role of DA during retinal development and its relevance to the pathogenesis of albinism.

In chapter 7, a preliminary study using both *in vivo* and *in vitro* experimental methods was undertaken in an attempt to address this issue. However, a more comprehensive set of experiments must be undertaken in which the effects of L-DOPA and DA on retinal development are examined in parallel. Precisely the same experimental methods must be used, so that variables are minimised and direct quantitative comparisons can be made. A standardised *in vitro* protocol in which the RPE is cultured for several days in the presence of the NBR (facilitating the formation of functional junctions and connections) would enable various factors to be introduced into the medium and resulting effects to be analysed by immunohistological methods. The following combinations of factors should be applied to both pigmentation types: L-DOPA with a DDC inhibitor; L-DOPA with a DDC inhibitor and DA receptor blockers; DA and DA with DA-receptor-subtype blockers. Following the period of incubation the tissue would be analysed for levels of proliferation, cell death, the proportion of cells in the cell cycle as well as the extent of lamina differentiation.

In parallel a comparative analysis of pigmented and albino retinae *in vivo* would be undertaken on embryos ranging from E11 to P6. Tissue would be processed to determine relative levels of endogenous ocular L-DOPA and DA (measured using HPLC), as well as the spatial and temporal pattern of DA receptor subtype localisation, (analysed by simple immunohistological detection).

Appendices

Appendix 1;
Cell cycle rates in an albino mouse model

A1.1 Introduction

At the start of this thesis several experiments were initiated using an hypopigmented Balb/c mouse model of albinism. These included a comparative study of cell cycle rates in pigmented and albino retinae, as well as an analysis of the long-term consequences (both behavioural and anatomical) of prolonged L-DOPA administration during development. However, at a later stage, these studies were dropped and the line of investigation transferred to rat models of albinism.

An examination of cell cycle rates was undertaken in the neonatal pigmented and albino mouse retina, as previous studies highlighted aberrant patterns of cell proliferation in the albino (Webster and Rowe, 1991; Ilia and Jeffery, 1999; Donatien and Jeffery, 2002) that might be linked to defects in cell cycle progression; see discussion section of Ilia and Jeffery (1999). Furthermore, abnormal levels of mitosis in the albino retina could be regulated *in vitro* through the re-introduction of L-DOPA (Ilia and Jeffery, 1999), a melanin precursor which selectively arrests cell cycle progression in S-phase (Wick, 1977; Wick, 1979; Wick, 1980; Akeo *et al.*, 1992).

To examine the duration of the mitotic cell cycle and each of its composite phases in the developing pigmented and albino mouse retina, a BrdU-labelling study was undertaken. The technique employed was adapted from thymidine-labelling protocols that have previously been employed in the retina (Denham, 1967; Young, 1985).

A1.2 Methods

Pigmented (C57B1/6J) and albino (Balb/c) pure-bred mice litters were used, ranging from 6-12 pups in size. All animals were time-mated. Day 0 was considered to be the first 24 hours following observation of a plug. Exceptionally small animals were discarded from the experiment. A total of 36 pigmented and 35 albino mouse pups were analysed, (see Table A1.2.1).

Injection of BrdU

Subcutaneous injections of BrdU were administered to P0 mice. Each injection contained 600μg of BrdU (Sigma) dissolved in 50μl PBS. The time of administration was designated as time zero. Animals were then sacrificed by decapitation at regular intervals of no less than 30 minutes over a 32 hour period. The number of animals used and mitotic cells counted at each stage are shown in Table A1.2.1.

Histology and immunohistochemistry

Following decapitation the tissue was fixed in 4% paraformaldehyde overnight and washed in PBS. Surrounding tissue was dissected from around the eyes, leaving them attached to the upper jaw via the lower orbit. The tissue was then dehydrated through a series of alcohol washes of increasing concentration (30 minutes each in 50%, 70%, 80%, 90% and 100% ethanol), and finally replaced by iso-propyl alcohol due its paraffin-miscible properties. The tissue was then bathed in two changes of paraffin at 60°C for a total duration of 4 hours, before being orientated and left to set at room temperature.

Four-micron sections were taken in the horizontal plane, transferred to poly-lysine coated glass slides (BDH Laboratory Supplies) and melted on overnight. After removal of the paraffin with xylene, the slides were passed through to distilled water via a series of alcohol washes of decreasing concentrations (5

minutes each in 100%, 90%, 80%, 70% and 50% ethanol). The tissue was then pre-treated with a 2 Normal solution of hydrochloric acid for 30 minutes at 37°C, and washed before being exposed to a second step of pre-treatment. The slides were submerged in a 1:10 dilution of trypsin in PBS-T (phosphate buffer saline with triton) for 22 minutes at 37°C.

Epitopes were blocked in normal horse serum for 30 minutes and incubated with mouse IgG1 isotype monoclonal anti-BrdU (1:1000, Sigma) overnight at room temperature. The slides were then washed in PBS and incubated in fluorescein conjugated antimouse IgG (1:100, Vector Laboratories) for 2 hours. Finally, following a series of washes in PBS the tissue was counter-stained with propidium idodide (5μg/ml in PBS) for 3 minutes and coverslipped in Vectashield fluorescent mounting medium (Vector laboratories).

Imaging and analysis

Sections were studied using an upright Olympus light microscope with a fluorescent unit at x400 magnification (x40 objective with a x10 eye-piece). Only sections which exhibited a clear C-shape morphology were used to gather data. Tissue from every third section was analysed to avoid multiple counts of the same cells. Data were gathered from both central and peripheral retinal regions. All cells undergoing mitosis at the VM were scored as being either single-labelled (with propidium iodide) or double-labelled (positive for both propidium iodide and BrdU). Cells undergoing mitosis could be identified by their circular cell morphology, condensed chromatin, and an encompassing ring free of stain (Figure A1.3.1).

Scatter plots were generated in Axum 5.0 tracing the change in percentage of dividing cells at the VM that were BrdU positive over time, (see Figure A1.3.2). A line of best fit was then added using a WLS (locally Weighted Least Squares) smoothing function designed to describe trends in non-parametric data sets. These were then used to calculate the duration of each phase of the cell cycle using a technique described by Young (1985), which is outlined below.

Calculation of cell cycle phase duration

At time zero none of the dividing cells are labelled with BrdU as it is only incorporated during S-phase. After around 1.5 hours however, BrdU-positive cells begin to appear at the ventricular margin (VM) and undergo mitosis. This period provides an estimation of the **minimum duration of G2-phase**, as it is the time taken for the first cells that were in S-phase at the time of injection to traverse G2-phase, migrate from the inner region of the neuroblastic layer to the VM and undergo mitosis. The actual length of G2–phase however is calculated as a mean of the time of initial BrdU detection at the VM, and the time at which 50% of the dividing cells are BrdU-positive.

The first increase in proportion of double labelled cells is steep as the cohort of cells that incorporate the BrdU are initially synchronised with respect to their cell cycle. Any inherent variation in their rates of progression will not have had time to take effect. The interval between the time of injection (designated time zero) and the peak in proportion of BrdU-positive cells gives an indication of the **maximum length of G2-phase and mitosis** combined. It represents the time taken for all the cells that had just traversed the S/G2-phase boundary at time zero (and hence did not incorporate the BrdU) to pass through G2-phase and M-phase, enter G1-phase and migrate away from the VM.

Once the curve reaches its peak there is a stable plateau that persists for around 12 hours, as the labelled cells undergo mitosis. At around 17 hours post-injection (hpi) the curve begins to drop, as cells that were at the end of G1-phase at time zero (and hence did not incorporate the BrdU) begin to enter the ventricular zone, having passed through S-phase and G2-phase in the meantime. This elapsed period therefore represents the **minimum duration of S-phase and G2-phase** combined. A **mean value for S-phase** is calculated as the interval between the times at which 50% of the cells are double labelled (on the first ascending and first descending limbs of the curve, corresponding to approximately 2.5hpi and 20hpi respectively).

At around 25hpi the curve begins to rise again. By this time, the cohort of cells that incorporated BrdU during S-phase have undergone an entire round of replication. They have migrated to the VM (during G2-phase), divided (M-phase), returned to the inner most region of the neuroblastic layer (during G1-phase) and undergone DNA replication (S-phase) before having migrated back to the ventricular margin (during G2-phase) to undergo a second division. However, the gradient of this section of the curve is much lower than the first, as variance in cell cycle lengths between labelled cells begins to take affect. From this section of the curve both the **minimum generation time** and **the mean generation time** can de extrapolated. The former is estimated as the time elapsed between the first rise and second rise in percentage of double labelled cells. The mean generation time however is taken to be the interval between the points at which 50% of dividing cells are double labelled on the first and second ascending limbs of the curve. Finally, given that the maximum duration of G2-phase and mitosis combined can be calculated, as well as the mean duration of S-phase and the mean generation time, an approximation of G1-phase duration can be calculated by a simple process of subtraction.

Time (hpi)	*Pigmented (C57B1/6J)*			*Albino (Balb/c)*		
	N	n	%BrdU+	N	n	%BrdU+
1	1	43	0	3	106	0
1.5	1	173	0	1	173	0
2	1	214	93	1	127	13
3	1	225	99	1	73	85
4	1	467	99	1	283	97
5	1	154	100	1	387	99
6	1	202	100	1	268	99
7	0	-	-	1	345	98
8	0	-	-	-	-	-
9	0	-	-	1	81	94
10	0	-	-	-	-	-
11	0	-	-	-	-	-
12	1	135	99	1	457	100
13	0	-	-	-	-	-
14	0	-	-	-	-	-
15	0	-	-	-	-	-
16	1	581	100	1	681	98
17	1	193	100	1	192	98
18	1	295	95	1	177	92
19	1	581	85	1	250	76
19.5	0	-	-	1	620	80
20	2	404	68	1	34	50
21	2	369	47	1	318	19
22	2	290	32	1	84	14
23	3	109	3	1	366	7
24	2	502	6	2	293	3
25	2	431	6	2	418	0
26	2	225	9	1	117	0
27	3	450	12	2	581	3
28	1	358	22	2	113	19
29	1	928	42	1	51	18
30	1	224	40	2	432	26
31	2	391	48	1	363	33
32	1	136	55	1	117	52

Table A1.2.1 Sample sizes and raw data. The number of animals used (N) and mitotic cells scored (n) per time-point (hours post-injection; hpi) are shown for pigmented (C57B1/6J) and albino (Balb/c) P0 mouse retinae. In addition, the percentage of mitotic cells at the VM which were BrdU-positive is presented for each time-point.

A1.3 Results

The percentage of dividing cells at the VM that were BrdU-positive was calculated for retinal tissue that had been collected at sequential time-points over a 32 hour period following administration of a BrdU pulse (Figure A1.3.2). In addition, scatter plots are presented for the latter portion of the study (25hpi to 32hpi). By this stage, subtle variations in the cell cycle can be detected (Figure A1.3.3). Finally, Figure A1.3.4 presents a series of pie-charts in which the slices are proportional to the relative duration of the phases of the cell cycle, and the absolute size of the pie chart is proportional to the relative generation time (G_T). The two panels on the left represent the data from the pigmented (C57B1/6J) tissue, and is separated into central and peripheral groups. Similarly, the panels on the right show the data from the central and peripheral albino (Balb/c) retina.

Only two phases of the cell cycle were found to vary in length between all of the groups studied. These were G1- and S-phase, with the greatest variation existing in the former. S-phase only varied from 17 to 19.5 hours across all the groups studied, whereas estimations of the duration of G1-phase spread between 4.75 and 9.75 hours. Elongation of the cell cycle in post-embryonic tissue is known to be mediated through the lengthening of G1-phase exclusively. This is in contrast to the embryonic process of cell cycle elongation with time, which is achieved through the lengthening of all phases of the cell cycle in concert (Alexiades and Cepko, 1996).

If the pigmented data is considered first, the mean generation time is approximately 0.5 hours longer in the central retina than it is in the peripheral retina, (29.75 hours and 29.25 hours respectively). This is indicative of the fact that as development progresses the generation time increases. In addition, the mammalian retina develops along a centre-to-periphery gradient, so that at any defined time-point the central areas of the retina are developmentally more mature than the periphery. Consequently, the cell cycle length will be slightly shorter in the peripheral retina relative to more central regions.

In the albino retina, a centre-to-periphery gradient is also evident with a mean generation time that is approximately 1.5 hours longer in the central retina than in the periphery, (31.75 hours compared to 29.25 hours). This is primarily due to changes in the duration of G1-phase. Comparing albino and pigmented data, the mean generation time is 2 hours longer in the central albino retina than it is in the pigmented, whilst data from the peripheral retina of both phenotypes is indistinguishable.

Finally, a linear curve-fit was applied to the data from 25hpi to 32hpi (Figure A1.3.3). This corresponds to the second rise in BrdU-positive cells at the VM, when the labelled cohort of cells have passed through an entire round of replication and re-enter M-phase for a second division. It is over this later period that variability in cell cycle rates becomes evident. Considering the pigmented data (Figure A1.3.3A), the linear plots are essentially identical for central and peripheral regions, except that they are out of phase by approximately 0.5 hours. This is indicative of the fact that the cell cycle is slightly longer in the central retina as a result of its relative developmental maturity (see above for explanation). R^2 values are high (0.88 and 0.9 for central and peripheral data respectively), suggesting that there is little variability in the generation time of cells within BrdU-labelled cohorts.

In contrast, the scatter plots for the albino retina do not fit the linear model so closely. This is reflected in lower R^2 values (0.67 and 0.82 in the central and peripheral retina respectively), suggesting that there is more inherent variation in cell cycle length amongst the animals used. In addition, a lower gradient is evident in the central albino retina relative to the pigmented (4.7 in contrast to 7.5). If all the cells within a defined zone were temporally synchronised and did not vary with respect to the length of their cell cycle, the second rise in BrdU positively labelled cells at the VM would be as steep as the initial rise. Instead, as time progresses, variation in the cell cycle length of individual cells begins to take effect. The cells become asynchronous, and their progression through the cell cycle drifts out of phase. Thus, the gradient of the second rise in labelling is

inversely proportional to the level of variation in cell cycle lengths within a zone; a low gradient being indicative of high variation.

This implies that the generation time of individual cells within the central albino retina is highly variable. Is it possible that this is further indication of a lower level of regulatory control in the albino retina and a disruption of the centre-to-periphery gradient of development? Without tight control and coordination of cell cycle progression and exit variation in cell cycle lengths will begin to desynchronise cells, a phenomenon which would be maximal in older tissue.

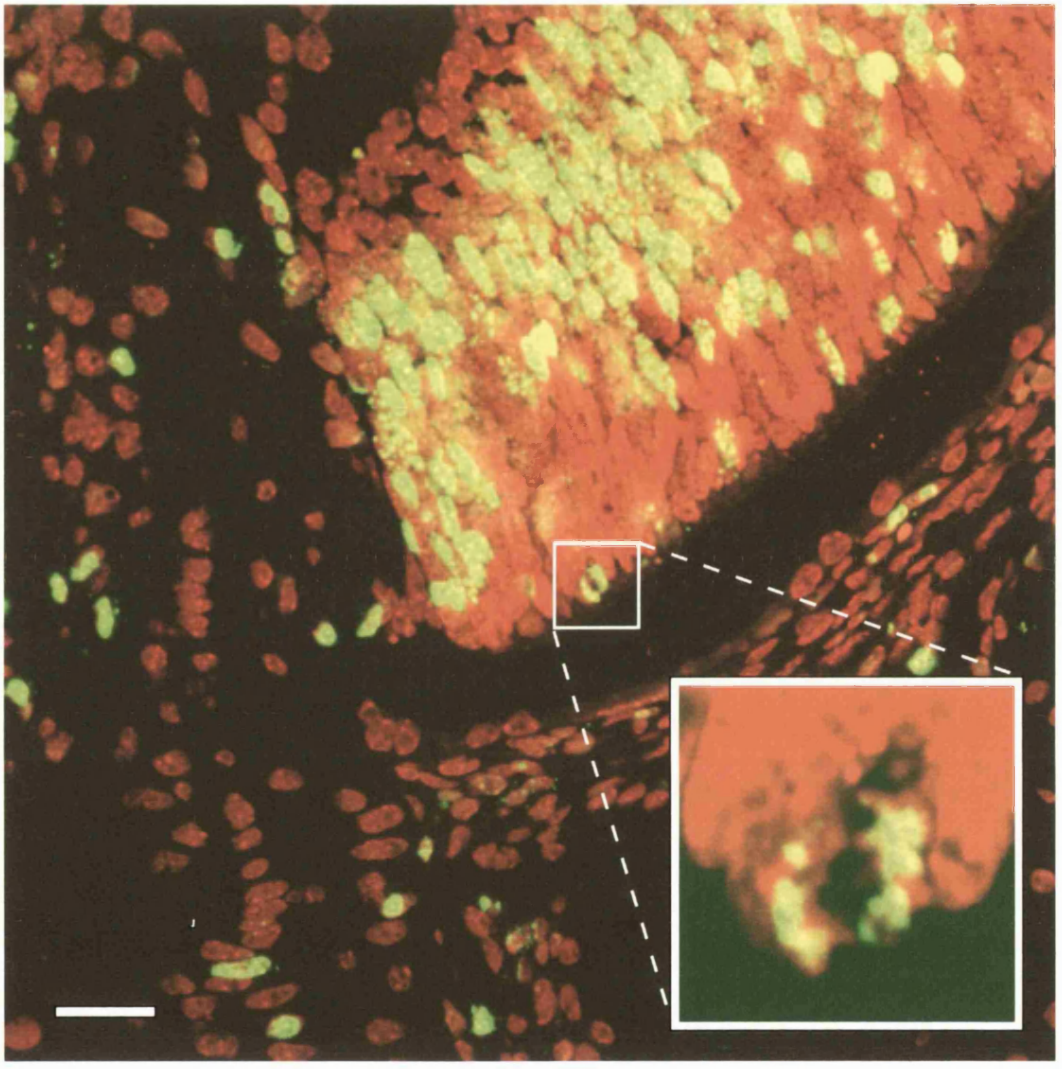

Figure A1.3.1 Cell cycle rates and the duration of its composite phases were calculated in pigmented and albino mice retinae using a technique described by Young (1985). BrdU (a base analogue) is delivered to the eye by subcutaneous injection and is incorporated into DNA exclusively during the period of DNA synthesis (S-phase). This enables a temporally synchronised cohort of cells to be traced as they progress through the layers of the retina and distinct phases of the cell cycle, a process known as interkinetic nuclear migration. Tissue is stained for BrdU (green/yellow) and counter-stained with propidium iodide to visualise nucleic acid. Inset is an higher magnification image of an actively dividing cell that has incorporated the BrdU. Scale bar=20μm.

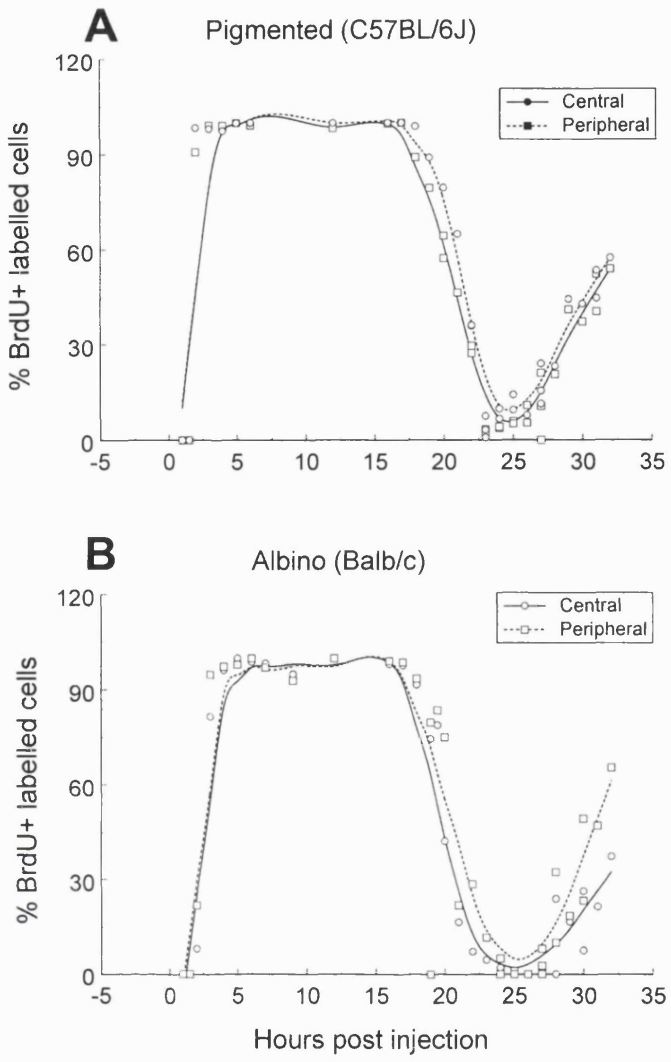

Figure A1.3.2 BrdU study of the pigmented and albino mouse retina at P0. Newborn pigmented and albino mice litters were given intraperitoneal pulses of BrdU and subsequently killed at regular intervals over the following 32 hours. The tissue was then sectioned, stained and the proportion of dividing cells at the VM that were BrdU-positive counted. Data is presented for (A) pigmented and (B) albino mouse tissue at P0 in a series of scatter plots with fitted curves, calculated using a weighted least squares (WLS) smoothing function. The plots reflect the idealised movements of a synchronised cohort of cells as they progress through the various phases of the cell cycle and undergo interkinetic nuclear migration. The first rise in the curve reflects the initial arrival of BrdU-labelled cells at the ventricular zone (VZ) to undergo cellular division. They then traverse G1-, S-, and G2-phases before returning to the VZ for a second round of division (detected as the second rise in the curve). For all groups studied, curves were tightly in phase for the first 18hrs as labelled cells were initially synchronised, differences beginning to show 25hours post-injection as variations in cycle rates began to take effect. From these plots the duration of each phase of the cell cycle can be derived (see Methods section).

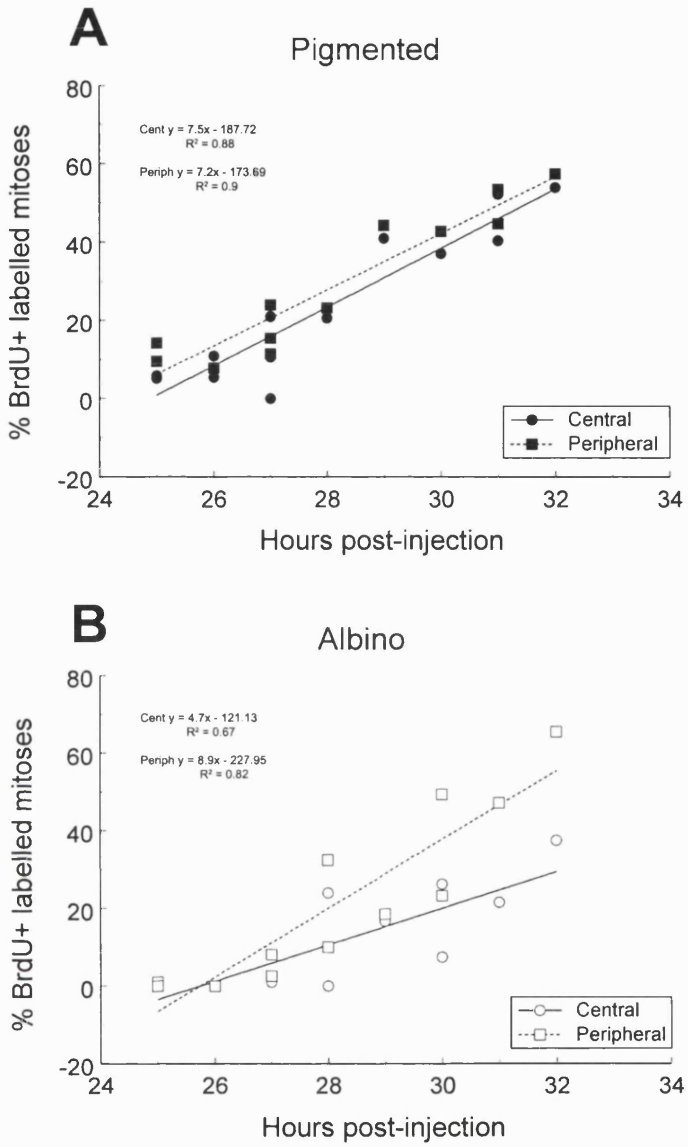

Figure A1.3.3 Differences in the cell cycle length of the pigmented and albino mouse retina. The proportion of dividing cells that were BrdU-positive are shown from 25hpi to 32hpi for the (A) pigmented and (B) albino mouse retina. Data is presented for both central and peripheral regions in the form of scatter plots with linear curve fits. Linear equations and R^2 values are superimposed. By this stage, variations in the cell cycle can be detected both between pigmentation types and retinal regions. In the pigmented retina linear plots are out of phase by approximately 0.5 hours, which is indicative of a longer cell cycle duration in the central retina relative to the periphery. R^2 values are high (0.88 and 0.9). In the albino retina there is more inherent variation in cell cycle length amongst the animals used (i.e. between replicates) which is reflected in lower R^2 values (0.67 and 0.82), and amongst individual cells within labelled cohorts of the central retina, which is reflected in a reduced gradient.

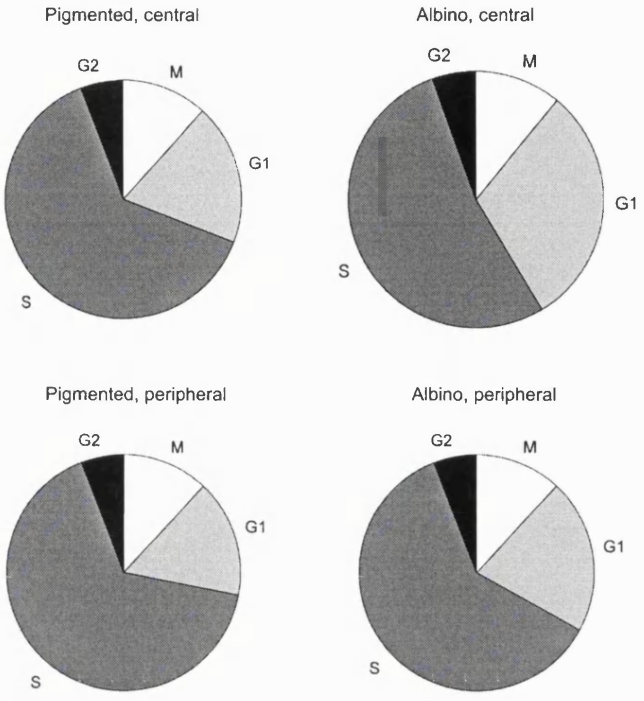

Cell cycle phase	*Pigmented*		*Albino*	
	Central	Peripheral	Central	Peripheral
M	3.5	3.5	3.5	3.5
G1	5.75	4.75	9.75	6.25
S	19	19.5	17	18
G2	1.75	1.75	1.75	1.75
Generation time	29.75	29.25	31.75	29.25

Figure A1.3.4 Relative duration of the cell cycle and its composite phases. The relative duration of the cell cycle and each of its composite phases are shown for the pigmented and albino mouse in both central and peripheral retina in the form of a series of pie-charts. The relative duration of the whole cell cycle (the generation time) is represented by the relative size of the entire pie-chart. In addition, the absolute duration (in hours) of each phase is presented in a table below. In both pigmented and albino tissue the cell cycle is slightly longer in the central retina relative to the periphery (0.5hrs and 1.5hrs respectively). As development progresses, the generation time lengthens and is reflected in differences between the developmentally more mature central retina and the periphery. Any variations in the generation time are primarily due to differences in the duration of G1-phase exclusively.

A1.4 Conclusions

The length of the cell cycle and each of its composite phases was calculated in the newborn mouse retina. The findings of this experiment would suggest that despite the reported delays in maturational gradients and abnormalities in patterns of cell generation, the length of the cell cycle and its composite phases are relatively robust in the albino. Not only is the length of the entire cell cycle comparable to the pigmented, but albino retinal progenitors exhibit the usual lengthening of the cell cycle across the maturational gradient (with a longer cell cycle duration in the central retina) as well as the regulation of this process through the selective elongation of G1- phase (Young, 1985).

Cell cycle studies of the developing albino retina have also been undertaken at earlier developmental time-points. In a study of the albino mouse, flow cytometric methods of analysis performed on dissociated retinal cells stained with propidium iodide revealed no differences in cell cycle parameters at E13 (Rachel *et al.*, 2002). Similarly, no differences in cell cycle length were detected in the E11.5 mouse (Ben Reese, unpublished observations). In view of these findings it would seem unlikely that differences in cell cycle length could account for the abnormalities that have been described in the albino retina. However, until a comprehensive analysis of cell cycle rates is undertaken over a broader window of development one cannot exclude the possibility that subtle variations in cell cycle length may play a role in the albino condition.

Appendix 3:
Matlab code – Planar polarity

```
% Purpose; calculates the cleavage orientation of a cell relative to a
radial line emanating from a reference point, (the optic nerve (ON),
or absolute origin).

clear;
close all;

% Clears all variables from previous sessions and closes all images
and plots.

question = {'X1:','Y1:','X2:','Y2:','X screen displacements:','Y
screen displacements:','No. of pixels per screen in x plane:','No. of
pixels per screen in y plane:','X pixel size in microns:','Y pixel
size in microns:','Plot data?:'};

def = {'','','','','','0','1024','1024','0.11','0.11','Y'};
title = 'Input parameters';
answer = inputdlg(question,title,1,def);

Dx=str2num(answer{5});
Dy= str2num(answer{6});

% Creates a dialogue box which allows input of the displacement
scalar, (i.e. the number of screen displacements from the ON in the x
and y planes; conventional monitor notation used).

if Dx>=0 & Dy>=0
  quadrant=1
elseif Dx<0 & Dy>=0
    quadrant=2
```

```
elseif Dx<0 & Dy<0
  quadrant=3
elseif Dx>=0 & Dy<0
    quadrant=4
end

% Calculates which quadrant of the retina the area of interest (aoi)
is in on the basis of the sign (+/-) of each component of the
displacement scalar.

XPixels= str2num(answer{7});
Xscreen_displace = Dx*XPixels;

YPixels= str2num(answer{8});
Yscreen_displace = Dy*YPixels;

% Calculates the distance (in pixels) of the roi from the ON.

x1= str2num(answer{1});
y1= str2num(answer{2});
x2= str2num(answer{3});
y2= str2num(answer{4});

if y1<=y2
        Cx1=x1
        Cy1=y1
        Cx2=x2
        Cy2=y2
elseif y1>y2
        Cx1=x2
        Cy1=y2
        Cx2=x1
        Cy2=y1
end

% Loads in the coordinates of the cell poles and defines (x1, y1) as
the pole closest to the ventricular margin, VM.

Cx3=(Cx1+Cx2)/2;
Cy3=(Cy1+Cy2)/2;
```

```
% Calculates the coordinates of the cell's hypothetical mid-point
(Cx3, Cy3).

xps= str2num(answer{9});
yps= str2num(answer{10});

Cx1=Cx1*xps;
Cx2=Cx2*xps;
Cx3=Cx3*xps;
Xscreen_displace=Xscreen_displace*xps;

Cy1=Cy1*yps;
Cy2=Cy2*yps;
Cy3=Cy3*yps;
Yscreen_displace=Yscreen_displace*yps;

% Converts all distances into absolute distances, i.e. from pixels
into microns.

        ACx1=Xscreen_displace+Cx1;
        ACy1=Yscreen_displace+Cy1;

        ACx2=Xscreen_displace+Cx2;
        ACy2=Yscreen_displace+Cy2;

        ACx3=Xscreen_displace+Cx3;
        ACy3=Yscreen_displace+Cy3;

% Converts the coordinates so that they are defined relative to the
absolute origin (ON) rather than the origin of the roi.

if quadrant==1

        if Cx2>Cx3
            theta=atan2((ACy3),(ACx3));
            alpha=atan2((Cy2-Cy3),(Cx2-Cx3));
            DEV = (alpha - theta)*180/pi;
        elseif Cx2<Cx3
            theta=atan2((ACy3),(ACx3));
            alpha=atan2((Cy2-Cy3),(Cx3-Cx2));
            DEV = (alpha+theta)*180/pi;
```

```
        else
            theta=atan2((ACy3),(ACx3));
            DEV = ((pi/2)-theta)*180/pi;
        end

        Cell_Eccentricity= sqrt(((ACx3)^2)+((ACy3)^2))
        theta_polar=(pi/2)+theta;
        Polar_Angle=theta_polar*180/pi

elseif quadrant==2

       if Cx3<Cx2
            theta=atan2((ACy3),(-ACx3));
            alpha=atan2((Cy2-Cy3),(Cx2-Cx3));
            DEV = (theta+alpha)*180/pi;
        elseif Cx3>Cx2
            theta=atan2((ACy3),(-ACx3));
            alpha=atan2((Cy2-Cy3),(Cx3-Cx2));
            DEV = (alpha-theta)*180/pi;
        else
            theta=atan2((ACy3),(-ACx3));
            DEV = ((pi/2)-theta)*180/pi;

        end
        Cell_Eccentricity= sqrt(((-ACx3)^2)+((ACy3)^2))
        theta_polar=(3*pi/2)-theta;
        Polar_Angle=theta_polar*180/pi

elseif quadrant==3

        if Cx3>Cx2
            theta=atan2((-ACy3),(-ACx3));
            alpha=atan2((Cy2-Cy3),(Cx3-Cx2));
            DEV = (pi-(theta+alpha))*180/pi;
        elseif Cx3<Cx2
            theta=atan2((-ACy3),(-ACx3));
            alpha=atan2((Cy2-Cy3),(Cx2-Cx3));
            DEV = (theta-alpha)*180/pi;
        elseif Cx3==Cx2
            theta=atan2((-ACy3),(-ACx3));
            DEV = ((pi/2)-theta)*180/pi;
```

```
        end
        Cell_Eccentricity=sqrt(((-ACx3)^2)+((-ACy3)^2))
        theta_polar=(3*pi/2)+theta;
        Polar_Angle=theta_polar*180/pi

elseif quadrant==4

        if Cx3<Cx2
            theta=atan2((-ACy3),(ACx3));
            alpha=atan2((Cy2-Cy3),(Cx2-Cx3));
            DEV = (theta+alpha)*180/pi;
        elseif Cx3>Cx2
            theta=atan2((-ACy3),(ACx3));
            alpha=atan2((Cy2-Cy3),(Cx3-Cx2));
            DEV = (alpha-theta)*180/pi;
        elseif Cx3==Cx2
            theta=atan2((-ACy3),(ACx3));
            DEV = ((pi/2)-theta)*180/pi;
        end
         Cell_Eccentricity= sqrt(((ACx3)^2)+((-ACy3)^2))
         theta_polar=pi/2-theta;
         Polar_Angle=theta_polar*180/pi

end

if DEV>90;
    DEV=180-DEV
else
    DEV=DEV
end

Intercentrosomal_distance=sqrt(((Cx2-Cx1)^2)+((Cy1-Cy2)^2))

% Using simple trigonometry the following is calculated:
% THETA; the angle of a line connecting the ON to the cell's midpoint,
(relative to the horizontal meridian).
% ALPHA; the angle of a line connecting the two cell poles,(relative
to the horizontal meridian).
% DEV; the deviation of the mitotic spindle axis from the radial axis.
% Results are then converted into radians (*180/pi).
```

```
graph=(answer{11});
if graph=='Y'|graph=='y'

figure(1);
a=[ACx1,ACx2];
b=[ACy1,ACy2];
plot(ACx1,ACy1,'o',ACx2,ACy2,'o');
```

% Creates a plot area and plots the position of the cell's poles.

```
axis xy;
axis([(ACx3-15),(ACx3+15),(ACy3-15),(ACy3+15)])

    if quadrant==1
        view(0,270);
    elseif quadrant==2
        view(0,270);
    elseif quadrant==3
        view(0,270);
    elseif quadrant==4
        view(0,270);
        end
```

% Scales the plot relative to the distance between the cell poles and orientates the graph such that the dorsal meridian is localised to the top of the screen, (absolute north).

```
hold on;
plot(a,b,'r--')
```

% Plots a line connecting the two cell poles, (perpendicular to the assumed cleavage plane).

```
hold on;

c=[0,ACx3];
d=[0,ACy3];
plot(c,d,'b--');
```

% Plots a line connecting the cell's hypothetical midpoint to the absolute origin, (ON).

```
figure(2);
polar(theta_polar,Cell_Eccentricity,'o');
view(90,270);

end

% Creates a polar plot indicating the distance of the cell's midpoint
from the absolute origin.
```

Appendix 4:
Matlab code – Distance from VM

```
% Purpose; calculates the distance of a cell from the ventricular
margin, defined by a reference plane which runs along the outer limit
of the NBR.
% Adapted from a program written by Dr. A.V. Whitmore.

clear;
close all;

% Clears all variables from previous sessions and closes all images
and plots.

question = {'Reference plane coordinates:','x1:','y1:','x2:','y2:','x
pixel size in microns:','y pixel size in microns:'};
def = {'tissue.dat','','','','','0.11','0.11'};
title = 'Input parameters';
answer = inputdlg(question,title,1,def);

% Creates a dialogue box which facilitates input of the following; x
and y coordinates of the centrosome pair of a cell of interest and the
pixel size in microns for both the x and y axes. In addition it loads
a data file entitled 'tissue.dat' in which the coordinates of a range
of points lying along the VM have been pre-stored.

Edge_Data=load(answer{1});
ex=Edge_Data(:,1)
ey=Edge_Data(:,2)

% Assigns x coordinates to a variable ex, and y coordinates to a
variable ey.
```

```
[p,S]=polyfit(ex,ey,1)

% Calculates the regression co-efficients of a line of best fit to
data (ex, ey). In addition, it defines the polynomial as first order
only, and hence calculates a straight line.
% Variable p now holds the coefficients of the first order polynomial;
i.e. if p=3,2 then the equation of the straight line which best fits
the data is y=3x+2.

x1= str2num(answer{2});
y1= str2num(answer{3});
x2= str2num(answer{4});
y2= str2num(answer{5});

xps= str2num(answer{6});
yps= str2num(answer{7});

x1=x1*xps;
x2=x2*xps;

y1=y1*yps;
y2=y2*yps;

% Converts coordinate system from pixels into vector distances
(microns).

x3=(x1+x2)/2;
y3=(y1+y2)/2;

% Calculates the midpoint of the cell.

b=(x3*p(:,1)+p(:,2))
b=b*yps;

% Calculates a point on the regression line that shares the same x
value as the midpoint of the cell of interest.
% In order to do so, it retrieves (b) the y value for the value of x
which is equal to the x coordinate of the cell's midpoint.
% p(:,1) represents the first regression coefficient, p(:,2)
represents the second, i.e. m and c respectively for the equation of a
line y=mx+c.
```

```
h=b-y3
h=abs(h)

% Calculates the distance from the midpoint of the cell to the
regression line (h).

theta=atan(p(:,1))
theta=abs(theta)

% Calculates the orientation of the regression line to the horizontal,
(and converts from radians into degrees).
% The first coefficient of the polynomial equals the gradient of the
line; the difference in y over the difference in x, or
opposite/adjacent. The angle of the line to the horizontal
is therefore the inverse tan of the first coefficient.

        if p(:,1)>0

           d=sin((pi/2)-theta)*h

       elseif p(:,1)<0

           d=sin((pi/2)-theta)*h

        else

            d=h

        end

% Calculates the shortest distance (d) from the cell midpoint to the
regression line, (to which it lies normal).
```

References

Adams RJ. 1996. Metaphase spindles rotate in the neuroepithelium of rat cerebral cortex. J Neurosci 16:7610-7618.

Adler PN. 2002. Planar signaling and morphogenesis in Drosophila. Dev Cell 2:525-535.

Akeo K, Tanaka Y, Okisaka S. 1994. A comparison between melanotic and amelanotic retinal pigment epithelial cells in vitro concerning the effects of L-dopa and oxygen on cell cycle. Pigment Cell Res 7:145-151.

Akeo K, Ueno N, Dorey CK. 1992. The effect of oxygen on melanin precursors released from retinal pigment epithelial cells in vitro. Pigment Cell Res 5:379-386.

Alberts B, Bray D, Lewis J, Raff M, Roberts K, Watson JD. 1994. Molecular biology of the cell. Garland Publishing, Inc.:958-961.

Alexiades MR, Cepko C. 1996. Quantitative analysis of proliferation and cell cycle length during development of the rat retina. Dev Dyn 205:293-307.

Alexiades MR, Cepko CL. 1997. Subsets of retinal progenitors display temporally regulated and distinct biases in the fates of their progeny. Development 124:1119-1131.

Ault SJ, Leventhal AG, Vitek DJ, Creel DJ. 1995. Abnormal ipsilateral visual field representation in areas 17 and 18 of hypopigmented cats. J Comp Neurol 354:181-192.

Austin CP, Feldman DE, Ida JA, Jr., Cepko CL. 1995. Vertebrate retinal ganglion cells are selected from competent progenitors by the action of Notch. Development 121:3637-3650.

Baker NE, Yu SY. 2001. The EGF receptor defines domains of cell cycle progression and survival to regulate cell number in the developing Drosophila eye. Cell 104:699-708.

Balkema GW, Drager UC. 1990. Origins of uncrossed retinofugal projections in normal and hypopigmented mice. Vis Neurosci 4:595-604.

Bardin AJ, Le Borgne R, Schweisguth F. 2004. Asymmetric localization and function of cell-fate determinants: a fly's view. Curr Opin Neurobiol 14:6-14.

Barishak YR. 1992. Embryology of the eye and its adnexae. Dev Ophthalmol 24:1-142.

Beazley LD, Perry VH, Baker B, Darby JE. 1987. An investigation into the role of ganglion cells in the regulation of division and death of other retinal cells. Brain Res 430:169-184.

Becker D, Bonness VV, Mobbs P. 1998. Cell Coupling in the Retina: Patterns and Purpose. Cell Biol Int 22:781-792.

Becker DL. 2003. Unpublished observations.

Becker DL, Evans WH, Green CR, Warner A. 1995. Functional analysis of amino acid sequences in connexin43 involved in intercellular communication through gap junctions. J Cell Sci 108 (Pt 4):1455-1467.

Becker DL, Mobbs P. 1999. Connexin alpha1 and cell proliferation in the developing chick retina. Exp Neurol 156:326-332.

Beermann F, Schmid E, Schutz G. 1992. Expression of the mouse tyrosinase gene during embryonic development: recapitulation of the temporal regulation in transgenic mice. Proc Natl Acad Sci U S A 89:2809-2813.

Belliveau MJ, Young TL, Cepko CL. 2000. Late retinal progenitor cells show intrinsic limitations in the production of cell types and the kinetics of opsin synthesis. J Neurosci 20:2247-2254.

Blaszczyk WM, Straub H, Distler C. 2004. GABA content in the retina of pigmented and albino rats. Neuroreport 15:1141-1144.

Borgens RB, Shi R. 1995. Uncoupling histogenesis from morphogenesis in the vertebrate embryo by collapse of the transneural tube potential. Dev Dyn 203:456-467.

Brilliant MH. 2001. The mouse p (pink-eyed dilution) and human P genes, oculocutaneous albinism type 2 (OCA2), and melanosomal pH. Pigment Cell Res 14:86-93.

Buescher M, Yeo SL, Udolph G, Zavortink M, Yang X, Tear G, Chia W. 1998. Binary sibling neuronal cell fate decisions in the Drosophila embryonic central nervous system are nonstochastic and require inscuteable-mediated asymmetry of ganglion mother cells. Genes Dev 12:1858-1870.

Caffe AR, Visser H, Jansen HG, Sanyal S. 1989. Histotypic differentiation of neonatal mouse retina in organ culture. Curr Eye Res 8:1083-1092.

Carter-Dawson LD, LaVail MM. 1979. Rods and cones in the mouse retina. II. Autoradiographic analysis of cell generation using tritiated thymidine. J Comp Neurol 188:263-272.

Cayouette M. 2003. Email to author.13th May.

Cayouette M, Raff M. 2002. Asymmetric segregation of Numb: a mechanism for neural specification from Drosophila to mammals. Nat Neurosci 5:1265-1269.

Cayouette M, Raff M. 2003. The orientation of cell division influences cell-fate choice in the developing mammalian retina. Development 130:2329-2339.

Cayouette M, Whitmore AV, Jeffery G, Raff M. 2001. Asymmetric segregation of Numb in retinal development and the influence of the pigmented epithelium. J Neurosci 21:5643-5651.

Cepko CL. 1993. Retinal Cell Fate Determination. In: Progress in Retinal Research. Pergamon Press Ltd. p 1-13.

Cepko CL, Austin CP, Yang X, Alexiades M, Ezzeddine D. 1996. Cell fate determination in the vertebrate retina. Proc Natl Acad Sci U S A 93:589-595.

Chan SO, Baker GE, Guillery RW. 1993. Differential action of the albino mutation on two components of the rat's uncrossed retinofugal pathway. J Comp Neurol 336:362-377.

Chenn A, McConnell SK. 1995. Cleavage orientation and the asymmetric inheritance of Notch1 immunoreactivity in mammalian neurogenesis. Cell 82:631-641.

Chiang M, Robinson KR, Vanable JW, Jr. 1992. Electrical fields in the vicinity of epithelial wounds in the isolated bovine eye. Exp Eye Res 54:999-1003.

Chow RL, Lang RA. 2001. Early eye development in vertebrates. Annu Rev Cell Dev Biol 17:255-296.

Cooper MS, Keller RE. 1984. Perpendicular orientation and directional migration of amphibian neural crest cells in dc electrical fields. Proc Natl Acad Sci U S A 81:160-164.

Cooper MS, Schliwa M. 1985. Electrical and ionic controls of tissue cell locomotion in DC electric fields. J Neurosci Res 13:223-244.

Creel D, O'Donnell FE, Jr., Witkop CJ, Jr. 1978. Visual system anomalies in human ocular albinos. Science 201:931-933.

Cronin CA, Ryan AB, Talley EM, Scrable H. 2003. Tyrosinase expression during neuroblast divisions affects later pathfinding by retinal ganglion cells. J Neurosci 23:11692-11697.

Cusato K, Bosco A, Rozental R, Guimaraes CA, Reese BE, Linden R, Spray DC. 2003. Gap junctions mediate bystander cell death in developing retina. J Neurosci 23:6413-6422.

Cusato K, Stagg SB, Reese BE. 2001. Two phases of increased cell death in the inner retina following early elimination of the ganglion cell population. J Comp Neurol 439:440-449.

Das T, Payer B, Cayouette M, Harris WA. 2003. In vivo time-lapse imaging of cell divisions during neurogenesis in the developing zebrafish retina. Neuron 37:597-609.

Denham S. 1967. A cell proliferation study of the neural retina in the two-day rat. J Embryol Exp Morphol 18:53-66.

Donatien P, Aigner B, Jeffery G. 2002. Variations in cell density in the ganglion cell layer of the retina as a function of ocular pigmentation. Eur J Neurosci 15:1597-1602.

Donatien P, Jeffery G. 2002. Correlation between rod photoreceptor numbers and levels of ocular pigmentation. Invest Ophthalmol Vis Sci 43:1198-1203.

Dooley CM, James J, Jane McGlade C, Ahmad I. 2003. Involvement of numb in vertebrate retinal development: Evidence for multiple roles of numb in neural differentiation and maturation. J Neurobiol 54:313-325.

Dowling-Warriner CV, Trosko JE. 2000. Induction of gap junctional intercellular communication, connexin43 expression, and subsequent differentiation in human fetal neuronal cells by stimulation of the cyclic AMP pathway. Neuroscience 95:859-868.

Drager UC. 1985. Calcium binding in pigmented and albino eyes. Proc Natl Acad Sci U S A 82:6716-6720.

Drager UC, Balkema GW. 1987. Does melanin do more than protect from light? Neurosci Res Suppl 6:S75-86.

Drager UC, Olsen JF. 1980. Origins of crossed and uncrossed retinal projections in pigmented and albino mice. J Comp Neurol 191:383-412.

Dreher Z, Robinson SR, Distler C. 1992. Muller cells in vascular and avascular retinae: a survey of seven mammals. J Comp Neurol 323:59-80.

Dyer MA, Cepko CL. 2000. p57(Kip2) regulates progenitor cell proliferation and amacrine interneuron development in the mouse retina. Development 127:3593-3605.

Dyer MA, Cepko CL. 2001a. p27Kip1 and p57Kip2 regulate proliferation in distinct retinal progenitor cell populations. J Neurosci 21:4259-4271.

Dyer MA, Cepko CL. 2001b. Regulating proliferation during retinal development. Nat Rev Neurosci 2:333-342.

Edlund T, Jessell TM. 1999. Progression from extrinsic to intrinsic signaling in cell fate specification: a view from the nervous system. Cell 96:211-224.

Eisenhofer G, Tian H, Holmes C, Matsunaga J, Roffler-Tarlov S, Hearing VJ. 2003. Tyrosinase: a developmentally specific major determinant of peripheral dopamine. Faseb J 17:1248-1255.

Elschnig A. 1913. Zur Anatomie des menschlichen albinoauges. Graefe's Arch. Clin. Ophthalmol. 84:401-419.

Esteve JV, Jeffery G. 1998. Reduced retinal deficits in an albino mammal with a cone rich retina: a study of the ganglion cell layer at the area centralis of pigmented and albino grey squirrels. Vision Res 38:937-940.

Estivill-Torrus G, Pearson H, van Heyningen V, Price DJ, Rashbass P. 2002. Pax6 is required to regulate the cell cycle and the rate of progression from symmetrical to asymmetrical division in mammalian cortical progenitors. Development 129:455-466.

Ezzeddine ZD, Yang X, DeChiara T, Yancopoulos G, Cepko CL. 1997. Postmitotic cells fated to become rod photoreceptors can be respecified by CNTF treatment of the retina. Development 124:1055-1067.

Furukawa T, Mukherjee S, Bao ZZ, Morrow EM, Cepko CL. 2000. rax, Hes1, and notch1 promote the formation of Muller glia by postnatal retinal progenitor cells. Neuron 26:383-394.

Gabriel R, Wilhelm M, Straznicky C. 1993. Morphology and distribution of Muller cells in the retina of the toad Bufo marinus. Cell Tissue Res 272:183-192.

Galderisi U, Jori FP, Giordano A. 2003. Cell cycle regulation and neural differentiation. Oncogene 22:5208-5219.

Gan WB, Grutzendler J, Wong WT, Wong RO, Lichtman JW. 2000. Multicolor "DiOlistic" labeling of the nervous system using lipophilic dye combinations. Neuron 27:219-225.

Gao Y, Spray DC. 1998. Structural changes in lenses of mice lacking the gap junction protein connexin43. Invest Ophthalmol Vis Sci 39:1198-1209.

Gardino PF, dos Santos RM, Hokoc JN. 1993. Histogenesis and topographical distribution of tyrosine hydroxylase immunoreactive amacrine cells in the developing chick retina. Brain Res Dev Brain Res 72:226-236.

Gaudin D, Fellman JH. 1967. The biosynthesis of DOPA in albino skin. Biochim Biophys Acta 141:64-70.

Gaur VP, Eldred W, Sarthy PV. 1988. Distribution of Muller cells in the turtle retina: an immunocytochemical study. J Neurocytol 17:683-692.

Gerdes J, Lemke H, Baisch H, Wacker HH, Schwab U, Stein H. 1984. Cell cycle analysis of a cell proliferation-associated human nuclear antigen defined by the monoclonal antibody Ki-67. J Immunol 133:1710-1715.

Gimenez E, Lavado A, Giraldo P, Montoliu L. 2003. Tyrosinase gene expression is not detected in mouse brain outside the retinal pigment epithelium cells. Eur J Neurosci 18:2673-2676.

Gimenez E, Lavado A, Jeffery G, Montoliu L. 2004. Regional abnormalities in retinal development are associated with local ocular hypopigmentation. Eur J Neurosci Under review.

Gonzalez-Hoyuela M, Barbas JA, Rodriguez-Tebar A. 2001. The autoregulation of retinal ganglion cell number. Development 128:117-124.

Grant S, Patel NN, Philp AR, Grey CN, Lucas RD, Foster RG, Bowmaker JK, Jeffery G. 2001. Rod photopigment deficits in albinos are specific to mammals and arise during retinal development. Vis Neurosci 18:245-251.

Gregor Z. 1978. The perifoveal vasculature in albinism. Br J Ophthalmol 62:554-557.

Guillery RW. 1986. Neural abnormalities of albinos. TINS:364-367.

Guillery RW, Hickey TL, Kaas JH, Felleman DJ, Debruyn EJ, Sparks DL. 1984. Abnormal central visual pathways in the brain of an albino green monkey (Cercopithecus aethiops). J Comp Neurol 226:165-183.

Guillery RW, Updyke BV. 1976. Retinofugal pathways in normal and albino axolotls. Brain Res 109:235-244.

Guimaraes MZ, Hokoc JN, Duvoisin R, Reis RA, De Mello FG. 2001. Dopaminergic retinal cell differentiation in culture: modulation by forskolin and dopamine. Eur J Neurosci 13:1931-1937.

Guo M, Jan LY, Jan YN. 1996. Control of daughter cell fates during asymmetric division: interaction of Numb and Notch. Neuron 17:27-41.

Halaban R, Cheng E, Svedine S, Aron R, Hebert DN. 2001. Proper folding and endoplasmic reticulum to golgi transport of tyrosinase are induced by its substrates, DOPA and tyrosine. J Biol Chem 276:11933-11938.

Hall JE, Gourdie RG. 1995. Spatial organization of cardiac gap junctions can affect access resistance. Microsc Res Tech 31:446-451.

Hasanee K, Ahmed IIK. 2001. Albinism. http://www.emedicine.com/oph/topic315.htm.

Haydar TF, Ang E, Jr., Rakic P. 2003. Mitotic spindle rotation and mode of cell division in the developing telencephalon. Proc Natl Acad Sci U S A 100:2890-2895.

Haydar TF, Wang F, Schwartz ML, Rakic P. 2000. Differential modulation of proliferation in the neocortical ventricular and subventricular zones. J Neurosci 20:5764-5774.

Hayes BP. 1976. The distribution of intercellular gap junctions in the developing retina and pigment epithelium of Xenopus laevis. Anat Embryol (Berl) 150:99-111.

Hayes BP. 1977. Intercellular gap junctions in the developing retina and pigment epithelium of the chick. Anat Embryol (Berl) 151:325-333.

Hinkle L, McCaig CD, Robinson KR. 1981. The direction of growth of differentiating neurones and myoblasts from frog embryos in an applied electric field. J Physiol 314:121-135.

Hoffmann MB, Tolhurst DJ, Moore AT, Morland AB. 2003. Organization of the visual cortex in human albinism. J Neurosci 23:8921-8930.

Hojo M, Ohtsuka T, Hashimoto N, Gradwohl G, Guillemot F, Kageyama R. 2000. Glial cell fate specification modulated by the bHLH gene Hes5 in mouse retina. Development 127:2515-2522.

Hornykiewicz O. 2002. L-DOPA: from a biologically inactive amino acid to a successful therapeutic agent. Amino Acids 23:65-70.

Horsburgh GM, Sefton AJ. 1987. Cellular degeneration and synaptogenesis in the developing retina of the rat. J Comp Neurol 263:553-566.

Hotary KB, Robinson KR. 1990. Endogenous electrical currents and the resultant voltage gradients in the chick embryo. Dev Biol 140:149-160.

Hotary KB, Robinson KR. 1992. Evidence of a role for endogenous electrical fields in chick embryo development. Development 114:985-996.

Ilia M, Jeffery G. 1996. Delayed neurogenesis in the albino retina: evidence of a role for melanin in regulating the pace of cell generation. Brain Res Dev Brain Res 95:176-183.

Ilia M, Jeffery G. 1999. Retinal mitosis is regulated by dopa, a melanin precursor that may influence the time at which cells exit the cell cycle: analysis of patterns of cell production in pigmented and albino retinae. J Comp Neurol 405:394-405.

Ilia M, Jeffery G. 2000. Retinal cell addition and rod production depend on early stages of ocular melanin synthesis. J Comp Neurol 420:437-444.

Jablonski MM, Tombran-Tink J, Mrazek DA, Iannaccone A. 2000. Pigment epithelium-derived factor supports normal development of photoreceptor neurons and opsin expression after retinal pigment epithelium removal. J Neurosci 20:7149-7157.

Jaffe LF, Stern CD. 1979. Strong electrical currents leave the primitive streak of chick embryos. Science 206:569-571.

Janssen-Bienhold U, Dermietzel R, Weiler R. 1998. Distribution of connexin43 immunoreactivity in the retinas of different vertebrates. J Comp Neurol 396:310-321.

Jeffery G. 1984. Retinal ganglion cell death and terminal field retraction in the developing rodent visual system. Brain Res 315:81-96.

Jeffery G. 1997. The albino retina: an abnormality that provides insight into normal retinal development. Trends Neurosci 20:165-169.

Jeffery G. 2001. Architecture of the optic chiasm and the mechanisms that sculpt its development. Physiol Rev 81:1393-1414.

Jeffery G, Brem G, Montoliu L. 1997. Correction of retinal abnormalities found in albinism by introduction of a functional tyrosinase gene in transgenic mice and rabbits. Brain Res Dev Brain Res 99:95-102.

Jeffery G, Darling K, Whitmore A. 1994. Melanin and the regulation of mammalian photoreceptor topography. Eur J Neurosci 6:657-667.

Jeffery G, Kinsella B. 1992. Translaminar deficits in the retinae of albinos. J Comp Neurol 326:637-644.

Jeffery G, Williams A. 1994. Is abnormal retinal development in albinism only a mammalian problem? Normality of a hypopigmented avian retina. Exp Brain Res 100:47-57.

Jensen AM, Walker C, Westerfield M. 2001. mosaic eyes: a zebrafish gene required in pigmented epithelium for apical localization of retinal cell division and lamination. Development 128:95-105.

Jeon CJ, Strettoi E, Masland RH. 1998. The major cell populations of the mouse retina. J Neurosci 18:8936-8946.

Jimbow K, Park JS, Kato F, Hirosaki K, Toyofuku K, Hua C, Yamashita T. 2000. Assembly, target-signaling and intracellular transport of tyrosinase gene family proteins in the initial stage of melanosome biogenesis. Pigment Cell Res 13:222-229.

King RA, Olds DP, Townsend D. 1988. Mechanisms of hypopigmentation in human oculocutaneous albinism. Prog Clin Biol Res 256:183-191.

King RA, Summers CG. 1988. Albinism. Dermatol Clin 6:217-228.

Kinnear PE, Jay B, Witkop CJ, Jr. 1985. Albinism. Surv Ophthalmol 30:75-101.

Kliot M, Shatz CJ. 1985. Abnormal development of the retinogeniculate projection in Siamese cats. J Neurosci 5:2641-2653.

Knoblich JA. 2001. Asymmetric cell division during animal development. Nat Rev Mol Cell Biol 2:11-20.

Kornack DR, Rakic P. 1995. Radial and horizontal deployment of clonally related cells in the primate neocortex: relationship to distinct mitotic lineages. Neuron 15:311-321.

Koulen P. 1999. Postnatal development of dopamine D1 receptor immunoreactivity in the rat retina. J Neurosci Res 56:397-404.

Kubrusly RC, Guimaraes MZ, Vieira AP, Hokoc JN, Casarini DE, De Mello MC, De Mello FG. 2003. l-DOPA supply to the neuro retina activates dopaminergic communication at the early stages of embryonic development. J Neurochem 86:45-54.

Lankford KL, DeMello FG, Klein WL. 1988. D1-type dopamine receptors inhibit growth cone motility in cultured retina neurons: evidence that neurotransmitters act as morphogenic growth regulators in the developing central nervous system. Proc Natl Acad Sci U S A 85:4567-4571.

LaVail JH, Nixon RA, Sidman RL. 1978. Genetic control of retinal ganglion cell projections. J Comp Neurol 182:399-421.

Libby RT, Smith RS, Savinova OV, Zabaleta A, Martin JE, Gonzalez FJ, John SW. 2003. Modification of ocular defects in mouse developmental glaucoma models by tyrosinase. Science 299:1578-1581.

Lin H, Schagat T. 1997. Neuroblasts: a model for the asymmetric division of stem cells. Trends Genet 13:33-39.

Linden R. 2000. The anti-death league: associative control of apoptosis in developing retinal tissue. Brain Res Brain Res Rev 32:146-158.

Lu B, Jan L, Jan YN. 2000. Control of cell divisions in the nervous system: symmetry and asymmetry. Annu Rev Neurosci 23:531-556.

Luther PW, Peng HB, Lin JJ. 1983. Changes in cell shape and actin distribution induced by constant electric fields. Nature 303:61-64.

Marcus RC, Wang LC, Mason CA. 1996. Retinal axon divergence in the optic chiasm: midline cells are unaffected by the albino mutation. Development 122:859-868.

McCaig CD, Allan DW, Erskine L, Rajnicek AM, Stewart R. 1994. Growing nerves in an electric field. Neuroprotocols 4:134-141.

McCaig CD, Zhao M. 1997. Physiological electrical fields modify cell behaviour. Bioessays 19:819-826.

Merchant CA, Cohen G, Mytilineou C, DiRocco A, Moros D, Molinari S, Yahr MD. 1995. Human transplacental transfer of carbidopa/levodopa. J Neural Transm Park Dis Dement Sect 9:239-242.

Misu Y, Goshima Y, Miyamae T. 2002. Is DOPA a neurotransmitter? Trends Pharmacol Sci 23:262-268.

Mitchell CH. 2001. Release of ATP by a human retinal pigment epithelial cell line: potential for autocrine stimulation through subretinal space. J Physiol 534:193-202.

Mitrofanis J, Stone J. 1988. Distribution of cholinergic amacrine cells in the retinas of normally pigmented and hypopigmented strains of rat and cat. Vis Neurosci 1:367-376.

Montoliu L. 2004. Email to author.:2nd May.

Morgan JE, Henderson Z, Thompson ID. 1987. Retinal decussation patterns in pigmented and albino ferrets. Neuroscience 20:519-535.

Morland AB, Hoffmann MB, Neveu M, Holder GE. 2002. Abnormal visual projection in a human albino studied with functional magnetic resonance imaging and visual evoked potentials. J Neurol Neurosurg Psychiatry 72:523-526.

Morrison SJ, Perez SE, Qiao Z, Verdi JM, Hicks C, Weinmaster G, Anderson DJ. 2000. Transient Notch activation initiates an irreversible switch from neurogenesis to gliogenesis by neural crest stem cells. Cell 101:499-510.

Murciano A, Zamora J, Lopez-Sanchez J, Frade JM. 2002. Interkinetic nuclear movement may provide spatial clues to the regulation of neurogenesis. Mol Cell Neurosci 21:285-300.

Naus CC, Bani-Yaghoub M. 1998. Gap junctional communication in the developing central nervous system. Cell Biol Int 22:751-763.

Neumann CJ, Nuesslein-Volhard C. 2000. Patterning of the zebrafish retina by a wave of sonic hedgehog activity. Science 289:2137-2139.

Oetting WS. 2000. The tyrosinase gene and oculocutaneous albinism type 1 (OCA1): A model for understanding the molecular biology of melanin formation. Pigment Cell Res 13:320-325.

Oetting WS. 2002. New insights into ocular albinism type 1 (OA1): Mutations and polymorphisms of the OA1 gene. Hum Mutat 19:85-92.

Oetting WS, Bennett DC. 2004. International Albinsim Center. www.cbc.umn.edu/tad/genes.htm.

Oetting WS, Fryer JP, Shriram S, King RA. 2003. Oculocutaneous albinism type 1: the last 100 years. Pigment Cell Res 16:307-311.

Ohnuma S, Hopper S, Wang KC, Philpott A, Harris WA. 2002. Co-ordinating retinal histogenesis: early cell cycle exit enhances early cell fate determination in the Xenopus retina. Development 129:2435-2446.

Ohnuma S, Philpott A, Wang K, Holt CE, Harris WA. 1999. p27Xic1, a Cdk inhibitor, promotes the determination of glial cells in Xenopus retina. Cell 99:499-510.

Opacka-Juffry J, Brooks DJ. 1995. L-dihydroxyphenylalanine and its decarboxylase: new ideas on their neuroregulatory roles. Mov Disord 10:241-249.

Orida N, Feldman JD. 1982. Directional protrusive pseudopodial activity and motility in macrophages induced by extracellular electric fields. Cell Motil 2:243-255.

Pearson R, Catsicas M, Becker D, Mobbs P. 2002. Purinergic and muscarinic modulation of the cell cycle and calcium signaling in the chick retinal ventricular zone. J Neurosci 22:7569-7579.

Pearson RA, Catsicas M, Becker DL, Bayley P, Luneborg NL, Mobbs P. 2004a. Ca(2+) signalling and gap junction coupling within and between pigment epithelium and neural retina in the developing chick. Eur J Neurosci 19:2435-2445.

Pearson RA, Dale N, Llaudet E, Mobbs P. 2004b. Regulation of neural retinal progenitor proliferation by ATP released from the retinal pigment epithelium. Under review.

Perron M, Kanekar S, Vetter ML, Harris WA. 1998. The genetic sequence of retinal development in the ciliary margin of the Xenopus eye. Dev Biol 199:185-200.

Pinzon-Duarte G, Kohler K, Arango-Gonzalez B, Guenther E. 2000. Cell differentiation, synaptogenesis, and influence of the retinal pigment epithelium in a rat neonatal organotypic retina culture. Vision Res 40:3455-3465.

Provis JM, Diaz CM, Dreher B. 1998. Ontogeny of the primate fovea: a central issue in retinal development. Prog Neurobiol 54:549-580.

Rachel RA, Dolen G, Hayes NL, Lu A, Erskine L, Nowakowski RS, Mason CA. 2002. Spatiotemporal features of early neuronogenesis differ in wild-type and albino mouse retina. J Neurosci 22:4249-4263.

Raymond SM, Jackson IJ. 1995. The retinal pigmented epithelium is required for development and maintenance of the mouse neural retina. Curr Biol 5:1286-1295.

Reichenbach A, Schnitzer J, Friedrich A, Knothe AK, Henke A. 1991. Development of the rabbit retina: II. Muller cells. J Comp Neurol 311:33-44.

Rhyu MS, Jan LY, Jan YN. 1994. Asymmetric distribution of numb protein during division of the sensory organ precursor cell confers distinct fates to daughter cells. Cell 76:477-491.

Rice DS, Goldowitz D, Williams RW, Hamre K, Johnson PT, Tan SS, Reese BE. 1999. Extrinsic modulation of retinal ganglion cell projections: analysis of the albino mutation in pigmentation mosaic mice. Dev Biol 216:41-56.

Robinson KR. 1985. The responses of cells to electrical fields: a review. J Cell Biol 101:2023-2027.

Robinson SR. 1987. Ontogeny of the area centralis in the cat. J Comp Neurol 255:50-67.

Robinson SR, Dreher Z. 1990. Muller cells in adult rabbit retinae: morphology, distribution and implications for function and development. J Comp Neurol 292:178-192.

Robinson SR, Rapaport DH, Stone J. 1985. Cell division in the developing cat retina occurs in two zones. Brain Res 351:101-109.

Salceda R, Sanchez-Chavez G. 2000. Calcium uptake, release and ryanodine binding in melanosomes from retinal pigment epithelium. Cell Calcium 27:223-229.

Schambra UB, Duncan GE, Breese GR, Fornaretto MG, Caron MG, Fremeau RT, Jr. 1994. Ontogeny of D1A and D2 dopamine receptor subtypes in rat brain using in situ hybridization and receptor binding. Neuroscience 62:65-85.

Semo M, Bryce J, Jeffery G. 2001. Oxygen modulates cell death in the proliferating retina. Eur J Neurosci 13:1257-1260.

Shen Q, Zhong W, Jan YN, Temple S. 2002. Asymmetric Numb distribution is critical for asymmetric cell division of mouse cerebral cortical stem cells and neuroblasts. Development 129:4843-4853.

Shi R, Borgens RB. 1995. Three-dimensional gradients of voltage during development of the nervous system as invisible coordinates for the establishment of embryonic pattern. Dev Dyn 202:101-114.

Shulman JM, Perrimon N, Axelrod JD. 1998. Frizzled signaling and the developmental control of cell polarity. Trends Genet 14:452-458.

Silva AO, Ercole CE, McLoon SC. 2002. Plane of Cell Cleavage and Numb Distribution during Cell Division Relative to Cell Differentiation in the Developing Retina. J Neurosci 22:7518-7525.

Silva AO, Ercole CE, McLoon SC. 2003. Regulation of ganglion cell production by Notch signaling during retinal development. J Neurobiol 54:511-524.

Smeets WJ, Gonzalez A. 2000. Catecholamine systems in the brain of vertebrates: new perspectives through a comparative approach. Brain Res Brain Res Rev 33:308-379.

Smith PR, Benos DJ. 1991. Epithelial Na+ channels. Annu Rev Physiol 53:509-530.

Song B, Zhao M, Forrester JV, McCaig CD. 2002. Electrical cues regulate the orientation and frequency of cell division and the rate of wound healing invivo. Proc Natl Acad Sci U S A 99:13577-13582.

Spana EP, Doe CQ. 1996. Numb antagonizes Notch signaling to specify sibling neuron cell fates. Neuron 17:21-26.

Spedick MJ, Beauchamp GR. 1986. Retinal vascular and optic nerve abnormalities in albinism. J Pediatr Ophthalmol Strabismus 23:58-63.

Spencer F, Green, Howes, Jakobiec, Zimmerman. 1985. Opthalmic Pathology. In: Opthalmic Pathology. W.B. Saunders Co. p 607-613.

Stone J, Rowe MH, Campion JE. 1978. Retinal abnormalities in the Siamese cat. J Comp Neurol 180:773-782.

Takahashi T, Nowakowski RS, Caviness VS, Jr. 1996. The leaving or Q fraction of the murine cerebral proliferative epithelium: a general model of neocortical neuronogenesis. J Neurosci 16:6183-6196.

Tibber MS, Kralj-Hans I, Savage J, Mobbs PG, Jeffery G. 2004. The orientation and dynamics of cell division within the plane of the developing vertebrate retina. Eur J Neurosci 19:497-504.

Tombran-Tink J, Chader GG, Johnson LV. 1991. PEDF: a pigment epithelium-derived factor with potent neuronal differentiative activity. Exp Eye Res 53:411-414.

Townes-Anderson E, Raviola G. 1981. The formation and distribution of intercellular junctions in the rhesus monkey optic cup: the early development of the cilio-iridic and sensory retinas. Dev Biol 85:209-232.

Turner DL, Cepko CL. 1987. A common progenitor for neurons and glia persists in rat retina late in development. Nature 328:131-136.

Turner DL, Snyder EY, Cepko CL. 1990. Lineage-independent determination of cell type in the embryonic mouse retina. Neuron 4:833-845.

Uemura T, Shepherd S, Ackerman L, Jan LY, Jan YN. 1989. numb, a gene required in determination of cell fate during sensory organ formation in Drosophila embryos. Cell 58:349-360.

Varella MH, de Mello FG, Linden R. 1999. Evidence for an antiapoptotic role of dopamine in developing retinal tissue. J Neurochem 73:485-492.

Voyvodic JT, Burne JF, Raff MC. 1995. Quantification of normal cell death in the rat retina: implications for clone composition in cell lineage analysis. Eur J Neurosci 7:2469-2478.

Waid DK, McLoon SC. 1995. Immediate differentiation of ganglion cells following mitosis in the developing retina. Neuron 14:117-124.

Wakamatsu Y, Maynard TM, Jones SU, Weston JA. 1999. NUMB localizes in the basal cortex of mitotic avian neuroepithelial cells and modulates neuronal differentiation by binding to NOTCH-1. Neuron 23:71-81.

Wang Y, Rose B. 1995. Clustering of Cx43 cell-to-cell channels into gap junction plaques: regulation by cAMP and microfilaments. J Cell Sci 108 (Pt 11):3501-3508.

Watanabe T, Raff MC. 1990. Rod photoreceptor development in vitro: intrinsic properties of proliferating neuroepithelial cells change as development proceeds in the rat retina. Neuron 4:461-467.

Webster MJ, Rowe MH. 1991. Disruption of developmental timing in the albino rat retina. J Comp Neurol 307:460-474.

Wetts R, Fraser SE. 1988. Multipotent precursors can give rise to all major cell types of the frog retina. Science 239:1142-1145.

White TW, Sellitto C, Paul DL, Goodenough DA. 2001. Prenatal lens development in connexin43 and connexin50 double knockout mice. Invest Ophthalmol Vis Sci 42:2916-2923.

Wick MM. 1977. l-Dopa methyl ester as a new antitumour agent. Nature 269:512-513.

Wick MM. 1978. Dopamine: a novel antitumor agent active against B-16 melanoma in vivo. J Invest Dermatol 71:163-164.

Wick MM. 1979. Levodopa and dopamine analogs: melanin precursors as antitumor agents in experimental human and murine leukemia. Cancer Treat Rep 63:991-997.

Wick MM. 1980. Levodopa and dopamine analogs as DNA polymerase inhibitors and antitumor agents in human melanoma. Cancer Res 40:1414-1418.

Wodarz A. 2001. Cell polarity: no need to reinvent the wheel. Curr Biol 11:R975-978.

Wright CS, Becker DL, Lin JS, Warner AE, Hardy K. 2001. Stage-specific and differential expression of gap junctions in the mouse ovary: connexin-specific roles in follicular regulation. Reproduction 121:77-88.

Young RW. 1983. The ninth Frederick H. Verhoeff lecture. The life history of retinal cells. Trans Am Ophthalmol Soc 81:193-228.

Young RW. 1985. Cell proliferation during postnatal development of the retina in the mouse. Brain Res 353:229-239.

Zhang XM, Yang XJ. 2001. Regulation of retinal ganglion cell production by Sonic hedgehog. Development 128:943-957.

Zhao M, Agius-Fernandez A, Forrester JV, McCaig CD. 1996. Orientation and directed migration of cultured corneal epithelial cells in small electric fields are serum dependent. J Cell Sci 109 (Pt 6):1405-1414.

Zhao M, Forrester JV, McCaig CD. 1999. A small, physiological electric field orients cell division. Proc Natl Acad Sci U S A 96:4942-4946.

Zhao M, McCaig CD, Agius-Fernandez A, Forrester JV, Araki-Sasaki K. 1997. Human corneal epithelial cells reorient and migrate cathodally in a small applied electric field. Curr Eye Res 16:973-984.

Zhao M, Pu J, Forrester JV, McCaig CD. 2002. Membrane lipids, EGF receptors, and intracellular signals colocalize and are polarized in epithelial cells moving directionally in a physiological electric field. Faseb J 16:857-859.

Zhong W. 2003. Diversifying neural cells through order of birth and asymmetry of division. Neuron 37:11-14.

Zhong W, Feder JN, Jiang MM, Jan LY, Jan YN. 1996. Asymmetric localization of a mammalian numb homolog during mouse cortical neurogenesis. Neuron 17:43-53.